AD-A140 196 A VECTOR SPACE APPROACH TO TIME-VARIANT ENERGY SPECTRAL ANALYSIS(U) ROME AIR DEVELOPMENT CENTER GRIFFISS AFB NY J E ROACH DEC 83 RADC-TR-83-270 1/3

UNCLASSIFIED NL

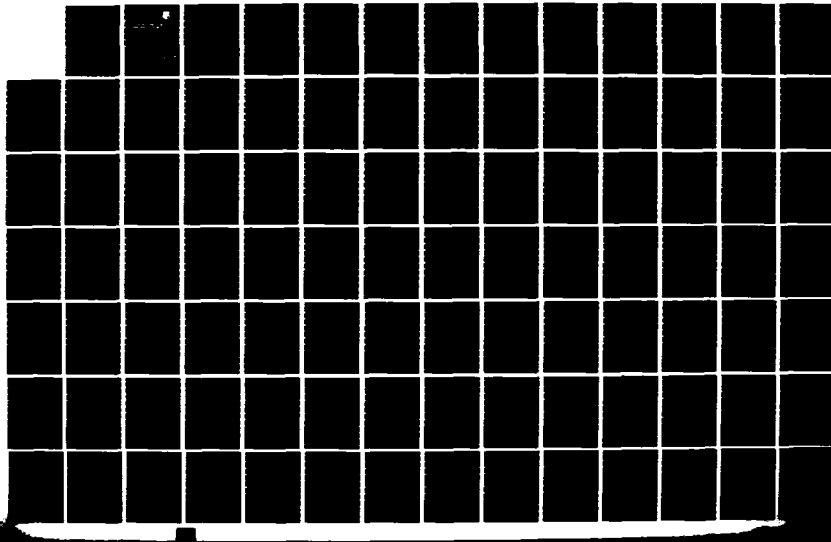

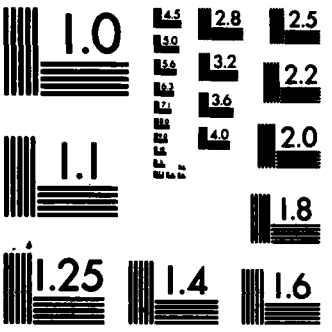

RADC-TR-83-270
In-House Report
December 1983

A VECTOR SPACE APPROACH TO TIME-VARIANT ENERGY SPECTRAL ANALYSIS

James E. Roach

ROME AIR DEVELOPMENT CENTER
Air Force Systems Command
Griffiss Air Force Base, NY 13441

This report has been reviewed by the RADC Public Affairs Office (PA) and is releasable to the National Technical Information Service (NTIS). At NTIS it will be releasable to the general public, including foreign nations.

RADC-TR-83-270 has been reviewed and is approved for publication.

APPROVED:

HENRY J. RUSH, Assistant Chief
Communications Transmission Branch
Communications Division

APPROVED:

BRUNO BEEK, Technical Director
Communications Division

FOR THE COMMANDER:

JOHN A. RITZ
Acting Chief, Plans Office

If your address has changed or if you wish to be removed from the RADC mailing list, or if the addressee is no longer employed by your organization, please notify RADC (DCCL) Griffiss AFB NY 13441. This will assist us in maintaining a current mailing list.

Do not return copies of this report unless contractual obligations or notices on a specific document requires that it be returned.

UNCLASSIFIED

SECURITY CLASSIFICATION OF THIS PAGE (When Data Entered)

REPORT DOCUMENTATION PAGE		READ INSTRUCTIONS BEFORE COMPLETING FORM
1. REPORT NUMBER RADC-TR-83-270	2. GOVT ACCESSION NO. AD-A140196	3. RECIPIENT'S CATALOG NUMBER
4. TITLE (and Subtitle) A VECTOR SPACE APPROACH TO TIME-VARIANT ENERGY SPECTRAL ANALYSIS		5. TYPE OF REPORT & PERIOD COVERED In-House Report 6. PERFORMING ORG. REPORT NUMBER N/A
7. AUTHOR(s) James E. Roach		8. CONTRACT OR GRANT NUMBER(s) N/A
9. PERFORMING ORGANIZATION NAME AND ADDRESS Rome Air Development Center (DCCL) Griffiss AFB NY 13441		10. PROGRAM ELEMENT, PROJECT, TASK AREA & WORK UNIT NUMBERS 62702F 4519PROJ
11. CONTROLLING OFFICE NAME AND ADDRESS Rome Air Development Center (DCCL) Griffiss AFB NY 13441		12. REPORT DATE December 1983 13. NUMBER OF PAGES 258
14. MONITORING AGENCY NAME & ADDRESS(if different from Controlling Office) Same		15. SECURITY CLASS. (of this report) UNCLASSIFIED 15a. DECLASSIFICATION/DOWNGRADING SCHEDULE N/A

16. DISTRIBUTION STATEMENT (of this Report)

Approved for public release; distribution unlimited

17. DISTRIBUTION STATEMENT (of the abstract entered in Block 20, if different from Report)

Same

18. SUPPLEMENTARY NOTES

None

19. KEY WORDS (Continue on reverse side if necessary and identify by block number)

Spectral Analysis
Identification Techniques
Vector Space Formulation
Time Variant Spectra

20. ABSTRACT (Continue on reverse side if necessary and identify by block number)

When analyzing signals, it is natural and useful to think of them in terms of an energy distribution, which is a function of frequency, evolving with time. Although traditionally used for spectral analysis, the Fourier Transform is inadequate for describing a time evolving spectrum. There are approaches, with appropriate theoretical justification, that attempt to describe the time-variant spectrum. An investigation of these approaches indicates serious difficulties of interpretation and→(over)

DD FORM 1 JAN 73 1473 EDITION OF 1 NOV 65 IS OBSOLETE

UNCLASSIFIED

SECURITY CLASSIFICATION OF THIS PAGE (When Data Entered)

implementation. A more practical and successful approach is a piecewise Fourier Transform. This in-house report provides the theoretical justification, lacking in the open literature, for the piecewise approach. Also included is a useful framework for applying "weighting" windows to time-frequency energy spectral analysis.

ACKNOWLEDGEMENT

I wish to acknowledge my Savior, the Lord Jesus Christ, for His kindness in allowing me to write this dissertation. Without Him, none of this would have been possible. Any errors that may be found herein are solely my responsibility but any good that may result from this work should not be credited to me but to the Person Who changed my life. I also wish to thank Ed Cossette and John Entzminger of Rome Air Development Center for their encouragement and support. Dr. Donald Weiner, my advisor, helped me continually over the five years of research. Dr. Nathan Schwartz was kind enough to be the reader for the dissertation and to encourage me in the final month. Dr. Guenter Salter, Dean of the College of Arts and Science at Bob Jones University, encouraged me greatly and provided valuable support.

The drawings in this dissertation were very nicely done by my good friend and fellow electrical engineer, Brent Reed. Special thanks are due to Mrs. Andy George who typed in three weeks what actually needed two months. Many dear Christian brothers and sisters prayed for me that this work would be successfully completed and it was. Finally, my wife Barb and our three children, Becky, Jeff, and Joy, stood behind me every step of the way, giving me encouragement and love.

TABLE OF CONTENTS

TABLE OF CONTENTS (Continued)

LIST OF FIGURES

Chapter 1

INTRODUCTION

An important part of the analysis of signals is the determination of energy as a function of frequency. The usual approach to this task is to calculate the classical Fourier Transform of the signal and to investigate the square of its magnitude. This approach has been used for years to analyze all kinds of signals. Yet, for most of those who do energy spectral analysis, something is lacking. It is natural to think of the frequency distribution of energy as a changing function of time. Our perception of speech, communications signals, physiological signals, and, in fact, all continuous information-bearing signals prompts this interpretation. There is a process taking place within the signal; energy within the signal is sensed to be distributing itself over different frequencies as time goes on. The Fourier Transform, however, cannot provide the information for such a time-frequency energy distribution. By its very definition, the Fourier Transformation uses the entire signal and permits analysis of only the frequency distribution of energy of the signal as a whole. To solve this problem, many who do spectral analysis have taken a "piecewise" approach; the signal is broken up into contiguous pieces and each piece is separately Fourier Transformed. The resulting family of Fourier Transformations is then treated as if it were the basis for a joint time-frequency energy distribution. Despite this practice, a theoretical justification for

this approach cannot be found in the literature. On the other hand, there are some interesting approaches which do have some theoretical justification but they suffer from serious difficulties of interpretation and implementation.

The main contribution of this work consists of showing that

(1) There <u>is</u> a theoretical justification for treating the piecewise Fourier Transform approach as a valid basis for joint time-frequency energy analysis, and

(2) there is a general family of "windowed" Fourier Series expansions which provides a useful framework for applying "weighting" windows to time-frequency energy spectral analysis.

In addition, this work provides a sound justification for using windows with the Finite Fourier Transformation along with some of their limitations. A new perspective on signals is also given through the concept of a signal vector moving through a vector space whose basis vectors provide measurements of signal energy in time and frequency.

In order to standardize notation and clarify assumptions, the following explanations are given. All signals discussed are assumed to be complex and square integrable. That is, the signal x(t) is assumed to have finite energy E given by

$$E = \int_{-\infty}^{\infty} |x(t)|^2 \, dt < \infty \, . \qquad (1\text{-}1)$$

Observations are assumed to be made of the signal beginning at a finite

start time, t_A, and ending at a finite stop time, t_B. Outside of the time interval $[t_A, t_B]$, the signal is assumed unknown. Furthermore, x(t) is assumed to be "piecewise smooth," meaning the signal x(t) and its first derivative dx(t)/dt are both piecewise continuous. This is not an overly restrictive requirement; most real-world, physical signals are piecewise smooth. The Fourier Transform of the signal x(t) is defined as

$$X(\omega) = \int_{-\infty}^{\infty} x(t)\ e^{-j\omega t}\ dt \qquad (1\text{-}2)$$

where the radian frequency, ω, is related to the cyclical frequency, f, by the expression

$$\omega = 2\pi f\ . \qquad (1\text{-}3)$$

Alternatively the Fourier Transform is frequently written as

$$X(f) = \int_{-\infty}^{\infty} x(t)\ e^{-j2\pi ft}\ dt. \qquad (1\text{-}4)$$

Since the right sides of (1-2) and (1-4) are identical, X(f) and $X(\omega)$ represent identical quantities. Furthermore, the transform in (1-4) should be denoted by $X(2\pi f)$ in order to be consistent with $X(\omega)$ defined in (1-2). However following common practice, the notation $X(\omega)$ and X(f) will be used for convenience. Strictly speaking, $X(\omega)$ and X(f) are two different functions, the difference being a scale factor

in the independent variable. The term "energy spectrum" will denote the squared magnitude of either X(f) or X(ω), depending upon the context. Although use of the Inverse Fourier Transform will <u>not</u> be made in the discussion, it is defined for a signal x(t) as

$$x(t) = \int_{-\infty}^{\infty} X(f)\ e^{j2\pi ft}\ df \qquad (1\text{-}5)$$

or by

$$x(t) = \frac{1}{2\pi} \int_{-\infty}^{\infty} X(\omega)\ e^{j\omega t}\ d\omega\ . \qquad (1\text{-}6)$$

An important result is Parseval's Formula given by

$$\int_{-\infty}^{\infty} |x(t)|^2\ dt = \frac{1}{2\pi} \int_{-\infty}^{\infty} |X(\omega)|^2\ d\omega \qquad (1\text{-}7)$$

or by

$$\int_{-\infty}^{\infty} |x(t)|^2\ dt = \int_{-\infty}^{\infty} |X(f)|^2\ df\ . \qquad (1\text{-}8)$$

This relationship is the basis for the interpretation of $|X(\omega)|^2$ or $|X(f)|^2$ as the frequency distribution of energy or as the energy "density" in frequency of the signal x(t). Since the Dirac Delta function is often used in this context, it is defined here by its familiar integral property. Specifically, the Dirac Delta function of time, δ(t), is defined by

$$\int_{-\infty}^{\infty} x(t)\ \ \delta(t-t_o)\ dt = x(t_o)\ . \qquad (1\text{-}9)$$

When the limits of integration are finite, there results

$$\int_{t_A}^{t_B} x(t)\delta(t-t_o)\,dt = \begin{cases} x(t_o) \;;\; t_A < t_o < t_B \\ \tfrac{1}{2}\, x(t_o^{+}) \;:\; t_o = t_A \\ \tfrac{1}{2}\, x(t_o^{-}) \;;\; t_o = t_B \\ 0 \;;\; t_o < t_A \text{ or } t_o > t_B, \end{cases} \tag{1-10}$$

where it is assumed that $t_A < t_B$ and the notations t_o^{+} and t_o^{-} denote the limit at t_o taken from the right and left, respectively. A counterpart to the Dirac Delta function used with discrete functions is the Kronecker Delta, δ_{km}, defined by

$$\delta_{km} = \begin{cases} 1 \;;\; k = m \\ 0 \;;\; k \neq m \end{cases} \tag{1-11}$$

Both of these functions will appear in the discussions. Finally, it is useful to define the rectangle function, $\text{Rect}(\frac{t}{T})$, as

$$\text{Rect}(\tfrac{t}{T}) = \begin{cases} 1 \;;\; |t| \leq \frac{T}{2} \\ 0 \;;\; |t| > \frac{T}{2} \quad . \end{cases} \tag{1-12}$$

The Fourier Transform of this function is often known as the "sinc" function of cyclical frequency f. In particular, its definition is

$$\text{sinc}(fT) = \frac{\sin(\pi fT)}{(\pi fT)} \tag{1-13}$$

$$= \int_{-\infty}^{\infty} \text{Rect}\left(\frac{t}{T}\right) e^{-j2\pi ft}\, dt \; . \tag{1-14}$$

A sketch of the $\text{Rect}(\frac{t}{T})$ and its Fourier Transform is given in Figure 1-1.

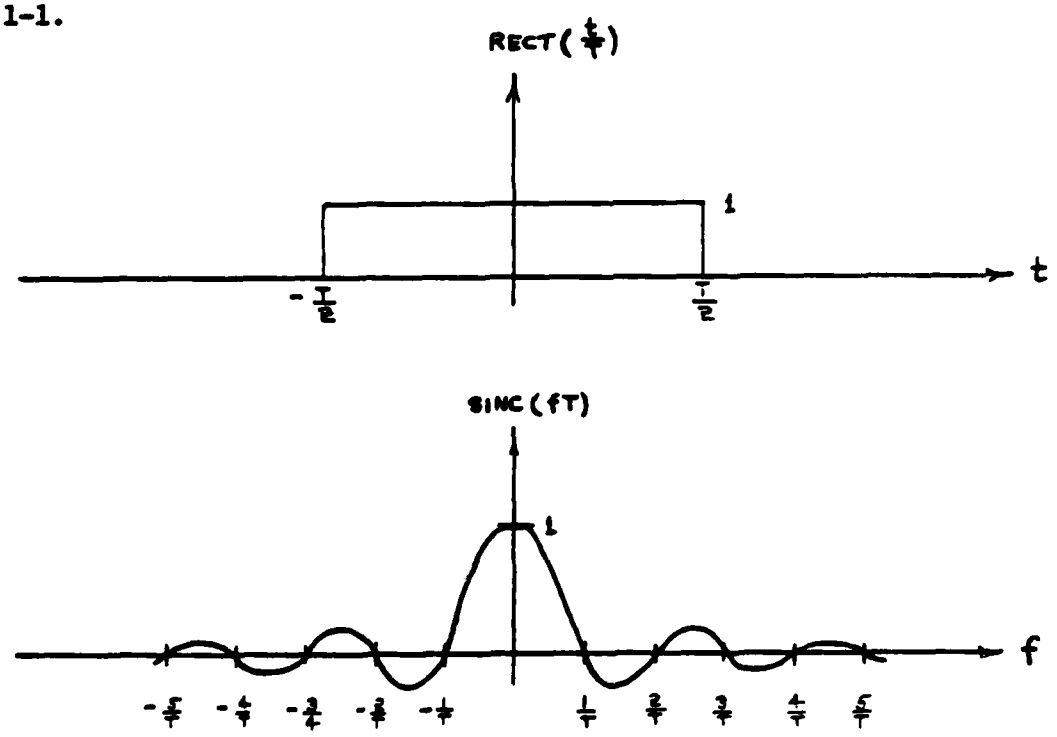

FIG. 1-1 RECT $(\frac{t}{T})$ AND ITS FOURIER TRANSFORM, SINC(fT)

In terms of the radian frequency ω, the Fourier Transform of the rectangle function is

$$\int_{-\infty}^{\infty} \text{Rect}\left(\frac{t}{T}\right) e^{-j\omega t}\, dt = \frac{\sin(\omega T/2)}{\omega\, T/2} \; . \tag{1-15}$$

With this as background, a brief outline of the dissertation is given next. Chapter 2 discusses the approaches that have been proposed in the past for time-variant energy spectral analysis. The original approach was proposed by Gabor [1] in 1946. Although many concepts were proposed over the years, it seems that only one took hold, the "piecewise" Fourier Transform approach. Five significant questions are posed in Chapter 2 which reveal the inadequate theoretical development of this popular approach. Chapter 3 presents the proposed vector space interpretation of time-variant energy spectral analysis. A clear, useful concept is presented which nicely lends itself to a theoretical justification of the "piecewise" Fourier Transform approach. In addition, a family of windows is shown to be useful in providing "sharp" spectral representions of signals. Finally the five questions from the end of Chapter 2 are answered. Chapter 4 considers problems arising in practical applications of the approach proposed in Chapter 3. A summary and recommendation for future work is given in Chapter 5. Lastly, the appendix lists the computer programs used in Chapters 3 and 4.

Chapter 2

PREVIOUS APPROACHES TO TIME-VARIANT SPECTRAL ANALYSIS

In this chapter the previous approaches to the problem of time-variant energy spectral analysis are described. By time-variant energy spectral analysis is meant the process of describing the energy of a given time function x(t) by a two dimensional distribution over time and frequency. From this point of view, the ordinary concept of the frequency spectrum of a signal, expressed in terms of its Fourier Transform, is not adequate to describe the time-varying behavior of signal energy. An example is the acoustic signal generated by a musician on his instrument. Here the signal consists of a time sequence of musical "notes," each "note" being an acoustical vibration of prescribed intensity and frequency and lasting only a short time. An observer interested in what is happening <u>within</u> this signal gathers very little information from an ordinary Fourier frequency spectrum which is based on the entire history of the signal. This inadequacy of the ordinary Fourier spectrum motivated researchers to look for ways to construct an "energy spectrum" which changes as the signal changes.

The concepts presented in this chapter will be shown to have serious difficulties of interpretation. The main emphasis of this chapter will be to show these difficulties and to set the stage for the proposed approach which is discussed in Chapter 3. The work of Gabor [1], who developed a representation of a signal in terms of a fundamental building

block in the time-frequency plane called the logon, is first discussed. The significant further work, based upon Gabor, done by Bastiaans [2] and Lerner [3] is also pointed out. Fallacies associated with Gabor's concepts are shown and the difficulties with implementing his representation are explained. The works of Page [4], Levin [5], and Rihaczek [6] to establish a two dimensional "instantaneous" energy spectrum are then discussed. Problems that arise with the interpretation and implementation of these concepts are also shown. Finally, the popular Discrete Fourier Transform approach to time-variant spectral analysis is discussed and the recently-developed Wigner Distribution [7, 8, 9, 10] approach is presented.

2.1 Gabor's Logon Concept

In 1946 Gabor published a landmark paper, "Theory of Communication" [1] in which he sought to represent time signals in two dimensions, with time and frequency being coordinates. He pointed out that our own physical perception of sound corresponds to a two dimensional function of time and frequency even though, strictly speaking, the acoustical vibration detected by the human ear is a function of time alone. Gabor defined an "elementary signal" as

$$\psi_e(t;\, t_o,\, f_o) = e^{-\alpha^2(t-t_o)^2}\, e^{j(2\pi f_o t + \theta)} \qquad (2\text{-}1\text{-}1)$$

and its Fourier Transform, $\Psi_e(f;\, t_o,\, f_o)$, as

$$\Psi_e(f;\, t_o,\, f_o) = \int_{-\infty}^{\infty} \psi_e(t;\, t_o,\, f_o)\, e^{-j2\pi ft}\, dt \qquad (2\text{-}1\text{-}2)$$

$$= \frac{\sqrt{\pi}}{\alpha}\, e^{-(\pi^2/\alpha^2)(f-f_o)^2}\, e^{-j2\pi f t_o}\, e^{j(2\pi f_o t_o + \theta)}. \qquad (2\text{-}1\text{-}3)$$

This elementary signal is just a complex cisoidal function of frequency f_o and phase θ which is modulated by a Gaussian function centered at time t_o. (See Figure 2-1-1a and Figure 2-1-1b.)

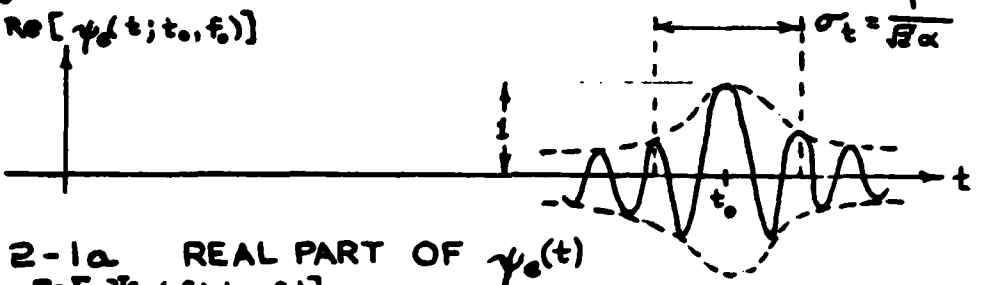

FIG. 2-1a REAL PART OF $\psi_e(t)$

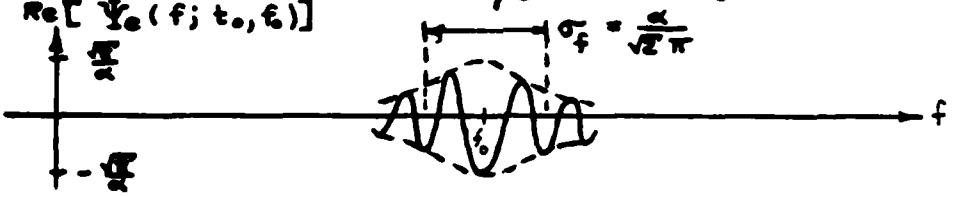

FIG. 2-1b REAL PART OF $\Psi_e(f)$

The spread of each function is defined by its standard deviation. The property of "reciprocal spreading" is noted, specifically,

$$\sigma_t = \frac{1}{2\pi} \frac{1}{\sigma_f} , \qquad (2\text{-}1\text{-}4)$$

where σ_t and σ_f are the standard deviations of their respective Gaussian envelope functions in (2-1-1) and (2-1-3).

Gabor chose this "elementary signal" as a foundation on which to construct an approximation for an arbitrary physical signal. His choice was evidently influenced by the fact that this function has a unique property. Of all well-behaved, physically meaningful functions, this is the only function for which the product of "effective duration" Δt, and "effective bandwidth," Δf, which are defined below, takes on its minimum value of ½. These "effective" terms are essentially

measures of the mean square deviation from time and frequency center-points, respectively. Specifically, for an arbitrary complex signal x(t) with Fourier Transform X(f) and finite total energy E given by

$$E = \int_{-\infty}^{\infty} |x(t)|^2 \, dt \,, \tag{2-1-5}$$

the effective duration Δt is defined by

$$\Delta t = \left[\frac{2\pi}{E} \int_{-\infty}^{\infty} (t-\bar{t})^2 \, |x(t)|^2 \, dt \right]^{\frac{1}{2}} \tag{2-1-6}$$

while the effective bandwidth Δf is given by

$$\Delta f = \left[\frac{2\pi}{E} \int_{-\infty}^{\infty} (f-\bar{f})^2 \, |X(f)|^2 \, df \right]^{\frac{1}{2}} \tag{2-1-7}$$

where

$$\bar{t} = \frac{1}{E} \int_{-\infty}^{\infty} t \, |x(t)|^2 \, dt \tag{2-1-8}$$

and

$$\bar{f} = \frac{1}{E} \int_{-\infty}^{\infty} f \, |X(f)|^2 \, df \,. \tag{2-1-9}$$

The quantities $\bar{t}$ and $\bar{f}$ are the assumed time and frequency "center-points," respectively. Using the Schwarz inequality, Gabor showed that the product $\Delta t \Delta f$ is always larger than or equal to ½ for arbitrary functions. However, only when the "elementary signal" is substituted

for x(t) in (2-1-6) and (2-1-7) is it found that $\bar{t} = t_o$, $\bar{f} = f_o$, and $\Delta t \Delta f = \frac{1}{2}$ exactly. This property evidently suggested that the elementary signal would make a good basis for building a two-dimensional time-frequency analysis. Gabor's development built upon this fact as follows. First, the elementary signal, $\psi_e(t; t_o, f_o)$, was called the $(0, 0)^{th}$ element and the generalized elementary signal, $\psi_e(t; t_k, f_\ell)$, was called the $(k, \ell)^{th}$ element. (Notation will be simplified here by writing $\psi_{k\ell}(t)$ instead of $\psi_e(t; t_k, f_\ell)$.) It is seen that for $\psi_{k\ell}(t)$, $\bar{t} = t_k$, $\bar{f} = f_\ell$, and $\Delta t \Delta f = \frac{1}{2}$, as before. Next, Gabor defined a two-dimensional grid called the logon grid by partitioning the time-frequency plane into rectangular cells, the cell centered at (t_k, f_ℓ) being associated with the $(k, \ell)^{th}$ elementary signal. Each cell has sides Δt and Δf, found from (2-1-6) and (2-1-7) with $\psi_{k\ell}(t)$ substituted for x(t). Specifically,

$$\Delta t = \sqrt{\frac{\pi}{2}} \frac{1}{\alpha} \qquad (2\text{-}1\text{-}10)$$

and

$$\Delta f = \frac{\alpha}{\sqrt{2\pi}} \quad . \qquad (2\text{-}1\text{-}11)$$

The area of each cell is therefore $\Delta t \Delta f = \frac{1}{2}$. The $(k, \ell)^{th}$ cell, along with its associated weight, $a_{k\ell}$, is called the $(k, \ell)^{th}$ <u>logon</u> and it corresponds to the weighted elementary signal given by

$$a_{k\ell}\psi_{k\ell}(t) = a_{k\ell}\, e^{-\alpha^2(t-t_k)^2} e^{j(2\pi f_\ell t + \theta)} \; . \qquad (2\text{-}1\text{-}12)$$

A sketch of the logon grid is given in Figure 2-2, where the shading indicates the value of weight for each logon.

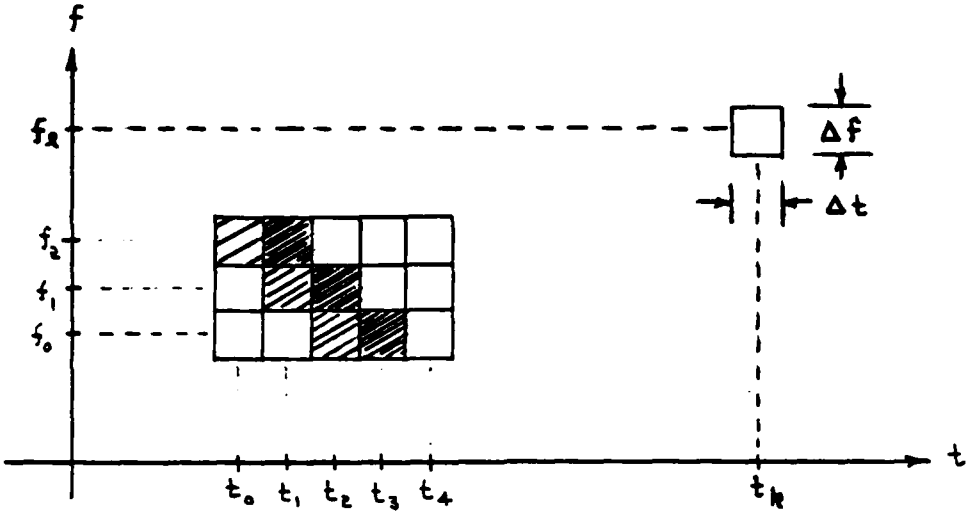

FIG. 2-2 THE LOGON GRID

In essence then, the logon grid lends itself to approximating an arbitrary signal x(t) by the approximation $\hat{x}(t)$, where

$$\hat{x}(t) = \sum_{k=-\infty}^{\infty} \sum_{\ell=-\infty}^{\infty} a_{k\ell}\psi_{k\ell}(t) \quad . \tag{2-1-13}$$

It is important to note that $\psi_{k\ell}(t)$ is <u>not</u> truncated in time and frequency as is its associated logon at $t = t_k$ and $f = f_\ell$.

It would be expected that, if $\hat{x}(t)$ is a "good" approximation in some sense, then this grid of logons should give a good indication of where significant amounts of energy lie in the time-frequency plane as the signal unfolds in time. It will be shown later that this is not the case; in fact the approximation of a signal by the sum of elementary signals in (2-1-13) actually <u>obscures</u> the contribution made by the signal in a finite length subinterval to the time-variant distribution of signal

energy. Before the fallacies of the logon concept are shown, the problem of making x(t) a "good" approximation is first discussed.

2.1.1. Completeness of the Set of Elementary Signals

The function $\hat{x}(t)$ should meet certain conditions to be considered a good approximation. The usual criterion is that the integrated squared representation error, ε, be minimized. By definition,

$$\varepsilon = \int_{-\infty}^{\infty} |x(t) - \hat{x}(t)|^2 \, dt \, . \qquad (2\text{-}1\text{-}14)$$

Substituting the expression for $\hat{x}(t)$ from (2-1-13), it is found that

$$\varepsilon = \int_{-\infty}^{\infty} |x(t)|^2 \, dt - 2RE \left[\sum_{k=-\infty}^{\infty} \sum_{\ell=-\infty}^{\infty} a_{k\ell} \int_{-\infty}^{\infty} x^*(t) \psi_{k\ell}(t) dt \right]$$

$$+ \sum_{k=-\infty}^{\infty} \sum_{\ell=-\infty}^{\infty} \sum_{m=-\infty}^{\infty} \sum_{n=-\infty}^{\infty} a_{k\ell} a_{mn}^* \int_{-\infty}^{\infty} \psi_{k\ell}(t) \psi_{mn}^*(t) dt, \qquad (2\text{-}1\text{-}15)$$

where the order of integration and summation has been interchanged assuming the series to be uniformly convergent. In order to minimize ε it is necessary to choose the $a_{k\ell}$ appropriately. This means that ε is a function of the complex variable $a_{k\ell}$ and optimization theory can be applied to minimize ε $[\{a_{k\ell}\}]$. It is found immediately that, because the set of $\psi_{k\ell}(t)$ functions are not orthogonal, serious difficulties arise. The minimization process results in a large number of simultaneous linear equations for the $a_{k\ell}$. In general, this system of equations cannot be readily solved.

Interestingly enough, Gabor proposed an approach for determining a set of coefficients $a_{k\ell}$ that does not explicitly account for the representation error. He determined a set of $a_{k\ell}$ by using a technique of successive approximations over finite intervals of x(t). The approach starts by considering a representation of x(t) about the point t_N in an interval of width Δt. Within this interval, it was assumed, as a first approximation, that there were no contributions from neighboring elementary signals outside this interval. In effect, the approximation of (2-1-13) was expressed as

$$\hat{x}(t) = \sum_{k=-\infty}^{\infty} \sum_{\ell=-\infty}^{\infty} a_{k\ell}\psi_{k\ell}(t) \qquad (2\text{-}1\text{-}16)$$

$$= e^{j\theta} \sum_{k=-\infty}^{\infty} \sum_{\ell=-\infty}^{\infty} a_{k\ell}\, e^{-\alpha^2(t-t_k)^2} e^{j2\pi f_\ell t} \qquad (2\text{-}1\text{-}17)$$

$$= e^{j\theta} \sum_{k=-\infty}^{\infty} e^{-\alpha^2(t-t_k)^2} \sum_{\ell=-\infty}^{\infty} a_{k\ell} e^{j2\pi f_\ell t} \qquad (2\text{-}1\text{-}18)$$

and the first approximation, $\hat{x}_1(t)$, was defined as

$$\hat{x}_1(t) = e^{j\theta}\, e^{-\alpha^2(t-t_N)^2} \sum_{\ell=-\infty}^{\infty} a_{N\ell} e^{j2\pi f_\ell t}\,,$$

$$t_N - \frac{\Delta t}{2} < t < t_N + \frac{\Delta t}{2} \quad (N=0, \pm 1, \pm 2, \ldots). \qquad (2\text{-}1\text{-}19)$$

It is noted that the elements in the sum of (2-1-18) for which $k \neq N$ are ignored in the first approximation $\hat{x}_1(t)$ in accordance with Gabor's assumption. Next, recognizing that he needed to deal with only the function $\hat{x}_1(t)\, e^{+\alpha^2(t-t_N)^2}$ when $t_N - \frac{\Delta t}{2} < t < t_N + \frac{\Delta t}{2}$, Gabor made

the approximation

$$x(t)\, e^{+\alpha(t-t_N)^2} \approx \hat{x}_1(t)\, e^{+\alpha^2(t-t_N)^2}$$

$$= e^{j\theta} \sum_{\ell=-\infty}^{\infty} a_{N\ell}\, e^{j2\pi f_\ell t}, \qquad (2\text{-}1\text{-}20)$$

$$t_N - \frac{\Delta t}{2} < t < t_N + \frac{\Delta t}{2}.$$

Therefore, an approximate Fourier Series representation for $x(t)\, e^{+\alpha(t-t_N)^2}$ was obtained in the specified interval centered at t_N. The constants $a_{N\ell}$ could then be found by the usual procedure for determining Fourier coefficients. At this point, Gabor had an exact representation for $\hat{x}_1(t)\, e^{+\alpha^2(t-t_N)^2}$ over the specified interval under the assumption of no overlap from neighboring elementary signals. However, it is realized that when the coefficients $a_{N\ell}$ are obtained in this way, the representation for x(t) would in fact have error due to overlap from neighboring elementary signals. To deal with this problem, Gabor presented a heuristic argument for iteratively processing the error so as to converge on a set of coefficients $a_{k\ell}$ which would yield a close approximation. However, he did not justify in any detail the convergence of the iterative process nor did he discuss its representation error.

It was not until 1980 that the open literature provided a key to the situation. Martin Bastiaans [2], using a set of functions which were found to be "bi-orthogonal" to the Gabor elementary signals, was able to find a set of $a_{k\ell}$ for Gabor's expansion. But he, too, failed

to discuss the representation error for his $a_{k\ell}$. In the following development it is shown that Bastiaans' choice of $a_{k\ell}$ gives the best set of coefficients in the sense of minimizing $\varepsilon\ [[a_{k\ell}]]$, and in addition, establishes the completeness of Gabor's set of elementary signals. Completeness is important because it guarantees that the representation error converges to zero for a sufficiently large number of basis functions in the expansion. It is completeness that allows us to control the representation error in any given case and to achieve whatever accuracy is desired for the approximation.

Bastiaans first changed Gabor's notation, defining a function $g_{k\ell}(t)$ in place of $\psi_{k\ell}(t)$. Specifically,

$$g_{k\ell}(t) = \left(\frac{2}{\sigma}\right)^{\frac{1}{4}} e^{\frac{-\pi}{\sigma}(t-kT)^2}\ e^{\frac{j2\pi\ell t}{T}}\ e^{-j\pi k\ell} \qquad (2\text{-}1\text{-}21)$$

is used instead of $\psi_{k\ell}(t)$, where

$$\psi_{k\ell}(t) = e^{-\alpha(t-t_k)^2}\ e^{j2\pi f_\ell t}\ e^{j\theta}\ . \qquad (2\text{-}1\text{-}22)$$

To make the transition in notation, it is noted that Bastiaans substitutes

$$\begin{array}{lll} \sqrt{\frac{\pi}{\sigma}} & \text{for} & \alpha \\ kT & \text{for} & t_k \\ \frac{\ell}{T} & \text{for} & f_\ell \end{array} \qquad (2\text{-}1\text{-}23)$$

and

$$-\pi k\ell \quad \text{for} \quad \theta\ .$$

In addition, he sets $T = \sqrt{\sigma}$ and multiplies his Gaussian modulated cisoidal function by a factor of $(\frac{2}{\sigma})^{\frac{1}{4}}$. This is done so that

$$\int_{-\infty}^{\infty} |g_{k\ell}(t)|^2 \, dt = 1. \tag{2-1-24}$$

Therefore each elementary signal $g_{k\ell}(t)$ has unit energy.

Bastiaan's significant findings are:

A. There exists a discrete set of functions, $\gamma_{k\ell}(t)$, which are "bi-orthogonal" to the $g_{k\ell}(t)$ and exhibit a closure relation with $g_{k\ell}(t)$. Specifically,

$$\int_{-\infty}^{\infty} g_{k\ell}(t)\gamma^*_{mn}(t) \, dt = \delta_{mk} \, \delta_{n\ell} \, , \tag{2-1-25}$$

where δ_{mk} is the Kronecker delta function defined by

$$\delta_{mk} = \begin{cases} 1 \, , & m = k \\ 0 \, , & m \neq k \, , \end{cases} \tag{2-1-26}$$

and

$$\sum_{k=-\infty}^{\infty} \sum_{\ell=-\infty}^{\infty} g_{k\ell}^{*}(t_1) \, \gamma_{k\ell}(t_2) = \delta(t_1-t_2) \, , \tag{2-1-27}$$

where $\delta(t)$ is the Dirac delta function defined by

$$\int_{-\infty}^{\infty} x(t) \, \delta(t-t_o)dt = x(t_o). \tag{2-1-28}$$

B. The $\gamma_{k\ell}(t)$ are the Gaussian-modulated cisoidal functions given by

$$\gamma_{k\ell}(t) = \left(\frac{2}{\sigma}\right)^{\frac{1}{4}} \left(\frac{\pi}{K_o}\right)^{\frac{3}{2}} e^{-\frac{\pi}{\sigma}(t-kT)^2} e^{\frac{j2\pi\ell t}{T}} e^{-j\pi k\ell} \sum_{m > \left(\frac{t}{T} - k - \frac{1}{2}\right)} (-1)^m e^{-\pi(m+\frac{1}{2})^2}, \tag{2-1-29}$$

where the constant $K_o = 1.85407468...$ is the complete elliptic integral for the modulus $\frac{1}{\sqrt{2}}$.

C. The Gabor coefficients $a_{k\ell}$ are given by

$$a_{k\ell} = \int_{-\infty}^{\infty} x(t)\gamma_{k\ell}^{*}(t)\, dt\,, \tag{2-1-30}$$

where $x(t)$ is the signal to be expanded into the discrete set of $g_{k\ell}(t)$.

In his paper, Bastiaans does not explain in what sense this choice of coefficients results in a "good" representation. Consequently, this set of $a_{k\ell}$ is now examined to determine the representation error achieved.

First, $g_{k\ell}(t)$ is written in place of $\psi_{k\ell}(t)$ in the expression for the error function $\varepsilon\,[\{a_{k\ell}\}]$ in (2-1-15) to obtain

$$\varepsilon\,[\{a_{k\ell}\}] = \int_{-\infty}^{\infty} |x(t)|^2\, dt - 2\mathrm{RE}\left\{\sum_{k,\ell=-\infty}^{\infty} a_{k\ell} \int_{-\infty}^{\infty} x^{*}(t) g_{k\ell}(t)dt\right\}$$

$$+ \sum_{k,\ell,m,n=-\infty}^{\infty} a_{k\ell}\, a_{mn}^{*} \int_{-\infty}^{\infty} g_{k\ell}(t) g_{mn}^{*}(t)dt. \tag{2-1-31}$$

Again it is noted that the $g_{k\ell}(t)$ are not orthogonal as was also the case for the $\psi_{k\ell}(t)$. Bastiaans' expression for the $a_{k\ell}$ in (2-1-30) is now substituted into $\varepsilon\,[\{a_{k\ell}\}]$ to obtain

$$\varepsilon\ [\{a_{k\ell}\}] = \int_{-\infty}^{\infty}|x(t)|^2\,dt$$

$$- 2\mathrm{RE}\ \{\sum_{k,\ell=-\infty}^{\infty}\sum \iint_{-\infty}^{\infty} x(t_2)\gamma_{k\ell}^*(t_2)x^*(t_1)g_{k\ell}(t_1)\,dt_1\,dt_2\}$$

$$+ \sum_{k,\ell,m,n=-\infty}^{\infty}\sum\sum\sum \iiint_{-\infty}^{\infty} x(t_2)\gamma_{k\ell}^*(t_2)x^*(t_1)\gamma_{mn}(t_1)g_{k\ell}(t_3)g_{mn}^*(t_3)dt_1dt_2dt_3. \qquad (2\text{-}1\text{-}32)$$

Using Bastiaans' expression in (2-1-27), there results

$$\varepsilon\ [\{a_{k\ell}\}] = \int_{-\infty}^{\infty}|x(t)|^2dt - 2\mathrm{RE}\ \{\iint_{-\infty}^{\infty} x(t_2)\delta(t_1-t_2)x^*(t_1)dt\,dt_2\}$$

$$+ \iiint_{-\infty}^{\infty} x(t_2)\left[\sum_{k,\ell=-\infty}^{\infty}\sum g_{k\ell}(t_3)\gamma_{k\ell}^*(t_2)\right]\left[\sum_{m,n=-\infty}^{\infty}\sum g_{mn}^*(t_3)\gamma_{mn}(t_1)\right]$$

$$x^*(t_1)\,dt_1dt_2dt_3 \qquad (2\text{-}1\text{-}33)$$

$$= \int_{-\infty}^{\infty}|x(t)|^2\,dt - 2\mathrm{RE}\ \{\int_{-\infty}^{\infty} x(t_2)x^*(t_2)dt_2\}$$

$$+ \iiint_{-\infty}^{\infty} x(t_2)\ \delta(t_3-t_2)\delta(t_3-t_1)x^*(t_1)dt_1dt_2dt_3 \qquad (2\text{-}1\text{-}34)$$

$$= \int_{-\infty}^{\infty} |x(t)|^2 \, dt - 2RE \left\{ \int_{-\infty}^{\infty} |x(t)|^2 \, dt \right\} + \int_{-\infty}^{\infty} |x(t)|^2 \, dt \tag{2-1-35}$$

$$= 0! \tag{2-1-36}$$

This shows that the representation error is zero for Bastiaans' choice of $\{a_{k\ell}\}$ provided that an infinite number of functions $g_{k\ell}(t)$ are used in the expansion. Since $\varepsilon\,[\{a_{k\ell}\}]$ is by definition nonnegative, a true minimum for the representation error has been obtained. In addition, this shows that the set of functions $g_{k\ell}(t)$ are complete because

$$\varepsilon\,[\{a_{k\ell}\}] = 0 \tag{2-1-37}$$

for an infinite number of coefficients in the doubly-indexed set of $\{a_{k\ell}\}$.

It should also be pointed out that if x(t) is known <u>only</u> over a finite representation interval $[t_A, t_B]$, the Gabor elementary functions are still complete in terms of the Bastiaans development over this finite interval. To see this, $a_{k\ell}$ is modified by defining the coefficient $a'_{k\ell}$, where

$$a'_{k\ell} = \int_{t_A}^{t_B} x(t) \gamma^*_{k\ell}(t) \, dt. \tag{2-1-38}$$

The representation error is also modified by defining $\varepsilon'[\{a'_{k\ell}\}]$, as

$$\varepsilon'[\{a'_{k\ell}\}] = \int_{t_A}^{t_B} |x(t) - \sum_{k,\ell=-\infty}^{\infty} a'_{k\ell}\, g_{k\ell}(t)|^2\, dt. \qquad (2\text{-}1\text{-}39)$$

Substituting (2-1-38) into (2-1-39), it follows that

$$\varepsilon'[\{a'_{k\ell}\}] = \int_{t_A}^{t_B} |x(t)|^2 dt$$

$$-2\mathrm{RE}\left\{\sum_{k,\ell=-\infty}^{\infty} \iint_{t_A}^{t_B} x(t_1)\gamma^*_{k\ell}(t_1)x^*(t_2)g_{k\ell}(t_2)dt_1dt_2\right\}$$

$$+\sum_{k,\ell,m,n=-\infty}^{\infty}\sum\sum \iiint_{t_A}^{t_B} x(t_1)\gamma^*_{k\ell}(t_1)x^*(t_2)\gamma_{mn}(t_2)g_{k\ell}(t_3)g^*_{mn}(t_3)dt_1dt_2dt_3.$$

(2-1-40)

By inserting (2-1-27) into this expression, there results

$$\varepsilon'[\{a_{k\ell}{}'\}] = 0\,, \qquad (2\text{-}1\text{-}41)$$

for the infinite set of coefficients $\{a_{k\ell}\}$.

This discussion shows that the Gabor representation is complete over the finite interval as well as the infinite interval, with the only requirement that

$$\int_{-\infty}^{\infty} |x(t)|^2\, dt < \infty\,. \qquad (2\text{-}1\text{-}42)$$

Physically real signals are therefore representable in terms of the Gabor elementary signals. It should be noted that this representation

is valid only for Bastiaans' choice of the parameters in (2-1-23). Specifically,

$$t_k = kT \tag{2-1-43}$$

and

$$f_\ell = \frac{\ell}{T} \tag{2-1-44}$$

are noted. These conditions give $g_{k\ell}(t)$ as defined in (2-1-21).

2.1.2. The Fallacy of the Logon Concept

One of the benefits expected from the Gabor representation for x(t) was that the rectangular cell, or logon, associated with its elementary signal, would tell where significant amounts of energy are distributed in the time-frequency plane. This concept is now investigated.

It is important to note that the representation of a signal's energy spectral density, as the signal changes in time within the observation interval, is of interest. One attempt at analyzing this is to compare the energy spectrum corresponding to one subinterval during the observation with the energy spectra of neighboring subintervals. Hopefully this will give a picture of how the signal's energy redistributes itself along the frequency axis as variations unfold within the time domain signal. Gabor's logon grid is expected to provide a convenient description of this energy distribution over time and frequency.

In order to study time-variant energy, a finite length observation interval is defined to be $[t_A, t_B]$. As shown previously, the Gabor elementary signals are complete over this interval. Within this interval, it is desired to analyze the progression of energy spectra for a number of subintervals; for example, the three subintervals shown in Figure 2-3.

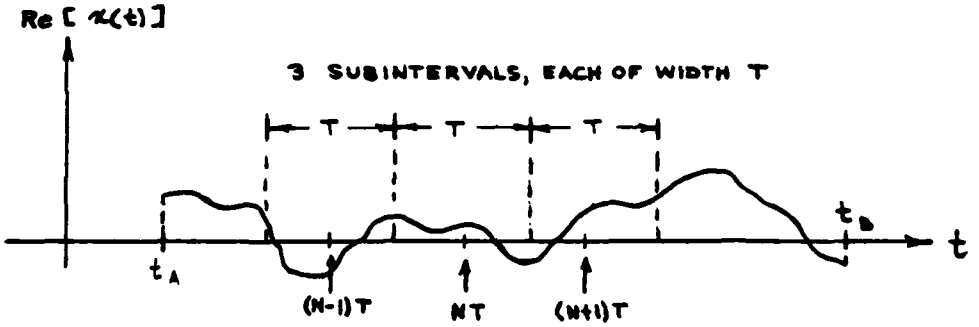

FIG. 2-3 SUBINTERVALS WITHIN THE OBSERVATION

The total energy within the subinterval centered at t = NT is

$$\int_{NT-\frac{T}{2}}^{NT+\frac{T}{2}} |x(t)|^2 \, dt. \qquad (2\text{-}1\text{-}45)$$

Using Parseval's Energy Theorem,

$$\int_{NT-\frac{T}{2}}^{NT+\frac{T}{2}} |x(t)|^2 \, dt = \int_{-\infty}^{\infty} \left| \int_{NT-\frac{T}{2}}^{NT+\frac{T}{2}} x(t) \, e^{-j2\pi ft} dt \right|^2 df, \qquad (2\text{-}1\text{-}46)$$

where the quantity

$$\left| \int_{NT-\frac{T}{2}}^{NT+\frac{T}{2}} x(t) \, e^{-j2\pi ft} dt \right|^2 \qquad (2\text{-}1\text{-}47)$$

is recognized as an energy spectral density and will hencefo th be

denoted by $|X(NT, f, T)|^2$. Specifically,

$$X(NT, f, T) = \int_{NT-\frac{T}{2}}^{NT+\frac{T}{2}} x(t)\, e^{-j2\pi ft}\, dt. \qquad (2\text{-}1\text{-}48)$$

It is hoped that, whatever the representation for x(t), the resulting form for $|X(NT, f, T)|^2$ should clearly show the distribution of energy in frequency due <u>solely</u> to the sighal's variations within the subinterval centered at NT. For example, if the subinterval under consideration contained a pure sinisoid of frequency 10 Hertz, we would hope that the expression for $|X(NT, f, T)|^2$ would have a significant magnitude primarily near f = 10 Hertz.

Now $|X(NT, f, T)|^2$ is evaluated for the case where x(t) is represented by $\hat{x}(t)$ over $[t_A, t_B]$. In particular

$$\hat{x}(t) = \sum_{k,\ell=-\infty}^{\infty} a_{k\ell}'\, g_{k\ell}(t), \qquad (2\text{-}1\text{-}49)$$

where

$$a_{k\ell}' = \int_{t_A}^{t_B} x(t)\gamma_{k\ell}^*(t)\, dt, \qquad (2\text{-}1\text{-}50)$$

and

$$g_{k\ell}(t) = \left(\frac{2}{\sigma}\right)^{\frac{1}{4}} e^{-\frac{\pi}{\sigma}(t-kT)^2}\, e^{j\frac{2\pi\ell t}{T}}\, e^{-j\pi k\ell}. \qquad (2\text{-}1\text{-}51)$$

The function $g_{k\ell}(t)$ is recognized as the Gabor elementary signal from (2-1-21) and $\gamma_{k\ell}(t)$ is as stated in (2-1-29). It is recalled from

Section 2.1.1. that these functions are complete over $[t_A, t_B]$. Substituting $\hat{x}(t)$ for $x(t)$ in (2-1-48), there results

$$X(NT, f, T) = \int_{NT-\frac{T}{2}}^{NT+\frac{T}{2}} \hat{x}(t)\, e^{-j2\pi ft}\, dt \qquad (2\text{-}1\text{-}52)$$

$$= \sum_{k,\ell=-\infty}^{\infty} \sum a_{k\ell}' \int_{NT-\frac{T}{2}}^{NT+\frac{T}{2}} g_{k\ell}(t)\, e^{-j2\pi ft}\, dt, \qquad (2\text{-}1\text{-}53)$$

where interchange of summation and integration was assumed permissible. Similar to the definition of $X(NT, f, T)$, the function $G_{k\ell}(NT, f, T)$ is defined as

$$G_{k\ell}(NT, f, T) = \int_{NT-\frac{T}{2}}^{NT+\frac{T}{2}} g_{k\ell}(t)\, e^{-j2\pi ft}\, dt\ , \qquad (2\text{-}1\text{-}54)$$

which is recognized as an integral over a finite section of a Gaussian-enveloped function. Inspection of (2-1-54) reveals that $G_{k\ell}(NT, f, T)$ becomes smaller and smaller as the quantity $|k-N|$ becomes larger and larger because, for $|k| >> N$, the integration limits lie very far out on the "tail" of a Gaussian-enveloped cisoidal function. Using (2-1-54) in (2-1-53), it follows that

$$X(NT, f, T) = \sum_{k,\ell=-\infty}^{\infty} \sum a_{k\ell}'\, G_{k\ell}(NT, f, T), \qquad (2\text{-}1\text{-}55)$$

where $a_{k\ell}'$ is the weighting associated with the logon centered at $t = kT$ and $f = \frac{\ell}{T}$. It will now be shown that the energy spectral density

$|X(NT, f, T)|^2$ is <u>not</u> clearly identified by the logons along the line $t = NT$ as had been hoped. These logons are shown in Figure 2-4.

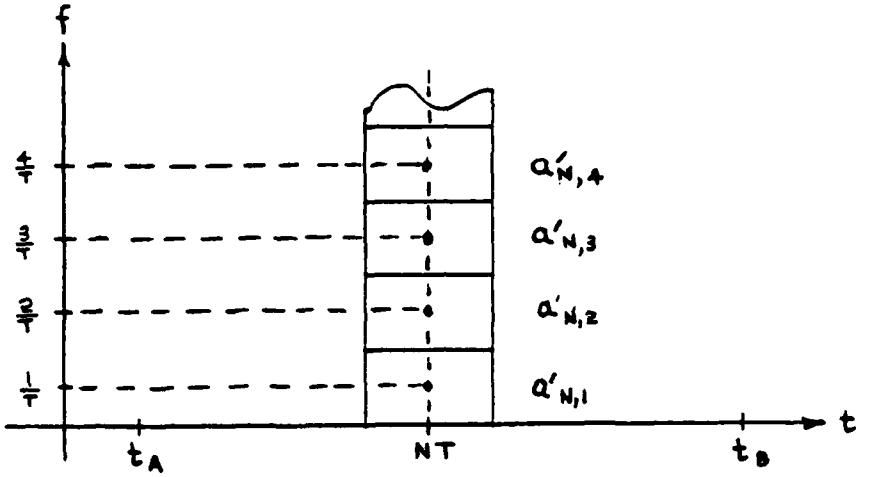

FIG. 2-4 LOGONS ALONG THE LINE $t = NT$ WITH THE ASSOCIATED WEIGHTS $\alpha'_{N,\ell}$

Using (2-1-55), the energy spectral density becomes

$$|X(NT, f, T)|^2 = \left| \sum_{k,\ell=-\infty}^{\infty} a_{k\ell}' G_{k\ell}(NT, f, T) \right|^2 \qquad (2\text{-}1\text{-}56)$$

$$= \sum_{k,\ell=-\infty}^{\infty} |a_{k\ell}'|^2 \, |G_{k\ell}(NT, f, T)|^2$$

$$+ \sum_{\substack{k,\ell,m,n=-\infty \\ (k\neq m \text{ or } \ell\neq m)}}^{\infty} a_{k\ell}' a_{mn}'^{*} G_{k\ell}(NT, f, T) G_{mn}^{*}(NT, f, T). \qquad (2\text{-}1\text{-}57)$$

It is important to notice that $G_{k\ell}(NT, f, T)$, as defined in (2-1-54), is not related to the signal $x(t)$ whereas $a_{k\ell}'$ is dependent upon the signal throughout the <u>entire</u> observation interval as indicated in (2-1-50).

Hopefully, $|G_{k\ell}(NT, f, T)|$ will be small for $k \neq N$ so that the major contributions to $|X(NT, f, T)|^2$ can be identified as just the logons along the line $t = NT$ in Figure 2-4. But this is <u>not the case in general</u> as shown next.

Substituting the form for $g_{k\ell}(t)$ from (2-1-51) into (2-1-54) there results

$$G_{k\ell}(NT, f, T) = (\frac{2}{\sigma})^{\frac{1}{4}} e^{-j\pi k\ell} \int_{NT-\frac{T}{2}}^{NT+\frac{T}{2}} e^{-\frac{\pi}{\sigma}(t-kT)^2} e^{j\frac{2\pi}{T}\ell t} e^{-j2\pi ft} dt \quad (2\text{-}1\text{-}58)$$

$$= (\frac{2}{\sigma})^{\frac{1}{4}} e^{j\pi k\ell} e^{-j2\pi fkT} \int_{(N-k)T-\frac{T}{2}}^{(N-k)T+\frac{T}{2}} e^{-\frac{\pi}{\sigma}y^2} e^{-j2\pi(f-\frac{\ell}{T})y} dy, \quad (2\text{-}1\text{-}59)$$

where the change of variable $y = t - kT$ was made. For simplicity, let $f = \frac{M}{T}$ where M is an integer. Specifically,

$$G_{k\ell}(NT, \tfrac{M}{T}, T) = (\frac{2}{\sigma})^{\frac{1}{4}} e^{j\pi k\ell} \int_{(N-k)T-\frac{T}{2}}^{(N-k)T+\frac{T}{2}} e^{-\frac{\pi}{\sigma}y^2} e^{-j\frac{2\pi}{T}(M-\ell)y} dy. \quad (2\text{-}1\text{-}60)$$

Setting $f = \frac{M}{T}$ means that attention is being focused on the function

$$|X(NT, f, T)|^2\Big|_{f=\frac{M}{T}} = |X(NT, \tfrac{M}{T}, T)|^2 \quad (2\text{-}1\text{-}61)$$

$$= |\sum_{k,\ell=-\infty}^{\infty} a_{k\ell}' G_{k\ell}(NT, \tfrac{M}{T}, T)|^2 \quad (2\text{-}1\text{-}62)$$

which is the energy density at the specific frequency $\frac{M}{T}$ due to the signal within the time interval of width T centered at NT. By substituting (2-1-60) into (2-1-62), it is noticed that all the logons along the line t = NT for which $\ell \neq M$ will influence the calculation of energy spectral density at $f = \frac{M}{T}$ and, in addition, the logons away from the line t = NT (for which $k \neq N$) will also contribute to the spectral density. The latter contribution is more troublesome because it indicates that logons along the lines t = (N ± 1)T, (N ± 2)T,..., etc. "leak" their associated weights $a'_{N\pm1,\ell}$, $a'_{N\pm2,\ell}$,...etc. into the measurement of spectral density of the (N, M)th cell in the time-frequency plane. To study the magnitude of this "leakage," consider Figure 2-5 in which several logons along the line $f = \frac{M}{T}$ are shaded. The cell of interest is the (N,M)th cell as shown.

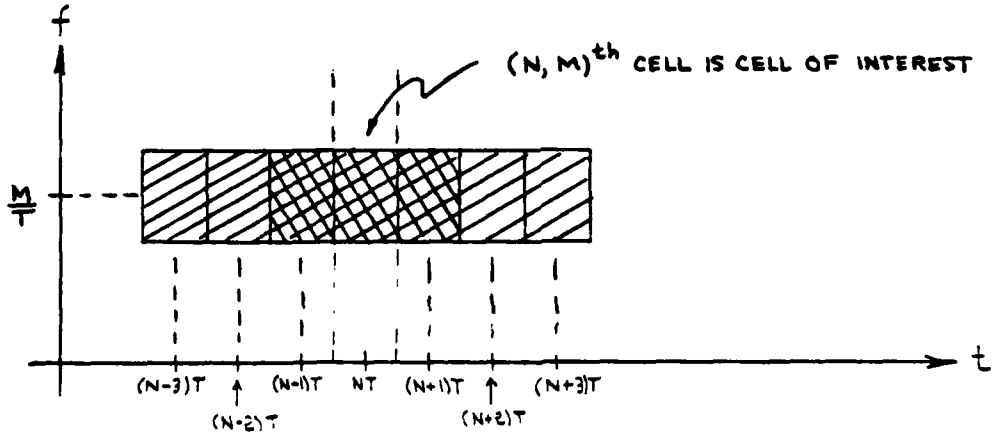

FIG. 2-5 NEIGHBORING LOGONS ALONG $f = \frac{M}{T}$

For the cells along the line $f = \frac{M}{T}$, the frequency index $\ell = M$ while the time index k = N, N±1, N±2,..., etc. With $\ell = M$, (2-1-60) becomes

$$G_{kM}(NT, \frac{M}{T}, T) = (\frac{2}{\sigma})^{\frac{1}{4}} e^{j\pi kM} \int_{(N-k)T-\frac{T}{2}}^{(N-k)T+\frac{T}{2}} e^{-\frac{\pi}{\sigma}y^2} dy \qquad (2\text{-}1\text{-}63)$$

which is a real quantity because $e^{j\pi kM} = (-1)^{kM}$. Using the Gaussian error function erf(t), defined as

$$\text{erf}(t) = \frac{1}{\sqrt{2\pi}} \int_0^t e^{-z^2/2}\, dz, \qquad (2\text{-}1\text{-}64)$$

and making the change of variable $z = \sqrt{\frac{2\pi}{\sigma}}\, y$, (2-1-63) can be written

$$G_{kM}(NT, \tfrac{M}{T}, T) = (2\sigma)^{\frac{1}{4}} \frac{(-1)^{kM}}{\sqrt{2\pi}} \int_{\sqrt{\frac{2\pi}{\sigma}}[(N-k)T - \frac{T}{2}]}^{\sqrt{\frac{2\pi}{\sigma}}[(N-k)T + \frac{T}{2}]} e^{-z^2/2}\, dz \qquad (2\text{-}1\text{-}65)$$

$$= (2\sigma)^{\frac{1}{4}} (-1)^{kM} \{\text{erf}\, [\sqrt{\tfrac{2\pi}{\sigma}}(N-k+\tfrac{1}{2})T] - \text{erf}\, [\sqrt{\tfrac{2\pi}{\sigma}}(N-k-\tfrac{1}{2})T]\}. \qquad (2\text{-}1\text{-}66)$$

Recalling that Bastiaans set $T = \sqrt{\sigma}$, it follows that

$$G_{kM}(NT, \tfrac{M}{T}, T) = (2\sigma)^{\frac{1}{4}} (-1)^{kM} \{\text{erf}\, [\sqrt{2\pi}\,(N-k+\tfrac{1}{2})] - \text{erf}\, [\sqrt{2\pi}\,(N-k-\tfrac{1}{2})]\}. \qquad (2\text{-}1\text{-}67)$$

Table 2-1 presents the values of $(2\sigma)^{\frac{1}{4}} (-1)^{kM} G_{kM}(NT, \frac{M}{T}, T)$ in actual magnitude and in decibels relative to the value at k = N. (Values of erf(t) were found in Feller [13], page 167, and the decibels column was calculated by the expression $10 \log_{10}(G_{kM}/G_{NM})$.

TABLE 2-1

MAGNITUDES FOR FACTORS ALONG THE LINE $f = \frac{M}{T}$

$(2\sigma)^{\frac{1}{2}}(-1)^{kM} G_{kM}(NT, \frac{M}{T}, T)$

k	ACTUAL MAGNITUDE	dB RELATIVE TO k=N VALUE
N	0.7893	0.0
N ± 1	0.1052	-8.75
N ± 2	8.642×10^{-5}	-39.61
N ± 3	$< 10^{-6}$	< 58.9
⋮	⋮	⋮
⋮	⋮	⋮

The values in the table show that there are three significant $G_{kM}(NT, \frac{M}{T}, T)$ functions. These functions are those for which k = N ± 1 and k = N and they multiply their associated $a_{k\ell}'$ coefficients in (2-1-62). These associated $a_{k\ell}'$ coefficients correspond to the logons shown doubly shaded in Figure 2-5. Depending upon the coefficients $a_{k\ell}'$, the other four shaded logons may also contribute significantly. This is a serious situation because it runs counter to our expectation that only logons along the line t = NT should represent the energy spectral density of the time interval centered at NT. Herein lies the

fallacy of the Gabor logon: what Gabor offered as a conceptually convenient tool is not convenient for analyzing and isolating energy densities from individual subintervals. The logon grid misleads one into thinking that there are distinct, continuous blocks in the time-frequency plane where the signal energy is concentrated. Not only are the individual energy densities not concentrated in their respective logons, but they are also "smeared out" by the expression in (2-1-62) involving the logon grid weights $a_{k\ell}'$. At the root of this problem is the fact that the logon grid is just not a legitimate description of a signal being approximated by a sum of Gaussian-enveloped cisoidal basis functions. The concept of the logon grid is, by its very definition, a two-dimensional "map" of contiguous blocks, each block having a weight $a_{k\ell}'$ indicating the strength of a corresponding basis function $g_{k\ell}(t)$. It attempts to localize the influence of individual basis functions to individual cells of finite width in time and frequency. However, because the basis functions are not strictly limited to their individual cells, there may be severe leakage effects caused by large weighting coefficients $a_{k\ell}'$, thus invalidating the interpretation of where signal energy is truly concentrated. The logon grid is therefore not a reliable tool for determining signal energy nor for representing the approximation

$$\hat{x}(t) = \sum_{k,\ell=-\infty}^{\infty} a_{k\ell}' \, g_{k\ell}(t). \qquad (2\text{-}1\text{-}68)$$

2.1.3. Lerner's Elementary Functions

In his publication of 1961, Robert Lerner [3] generalized the Gabor approach to the logon grid by extending the signal representation to more general elementary signals. He allowed the elementary signal to have the general form $v_{k\ell}(t)$, where

$$v_{k\ell}(t) = v(t - kT)e^{j\frac{2\pi}{T}\ell t}, \qquad (2\text{-}1\text{-}69)$$

v(t) being a "convenient" finite energy function whose energy is concentrated near t = 0 and whose energy spectrum $|V(f)|^2$ is concentrated near f = 0. This is quite similar to Gabor's elementary signal with its Gaussian envelope function multiplying a cisoidal pulse. Lerner approximated a given signal x(t) with the function $\hat{x}(t)$, where

$$\hat{x}(t) = \sum_{k,\ell=-\infty}^{\infty} a_{k\ell}' v_{k\ell}(t). \qquad (2\text{-}1\text{-}70)$$

Although he gave arguments to support his claim that the set of $v_{k\ell}(t)$ is complete for practically all well-behaved v(t) with small time-bandwidth product, Lerner did not establish that his grid of $a_{k\ell}'$ weights provides any better analysis of energy than Gabor's. If, once again, attention is focused on x(t) in the subinterval $[NT - \frac{T}{2}, NT + \frac{T}{2}]$ and $v_{k\ell}(t)$ is substituted for $g_{k\ell}(t)$ in (2-1-53), the Fourier Transform of the signal in that subinterval is

$$X(NT, f, T) = \sum_{k,\ell=-\infty}^{\infty} a'_{k\ell} \int_{NT-\frac{T}{2}}^{NT+\frac{T}{2}} v_{k\ell}(t)\, e^{-j2\pi ft}\, dt. \qquad (2\text{-}1\text{-}71)$$

Let $V_{k\ell}(NT, f, T)$ be defined, as was $G_{k\ell}(NT, f, T)$ in (2-1-54); that is

$$V_{k\ell}(NT, f, T) = \int_{NT-\frac{T}{2}}^{NT+\frac{T}{2}} v_{k\ell}(t)\, e^{-j2\pi ft}\, dt. \qquad (2\text{-}1\text{-}72)$$

It follows that $|X(NT, f, T)|^2$ may be expressed as

$$|X(NT, f, T)|^2 = \Big| \sum_{k,\ell=-\infty}^{\infty} a'_{k\ell}\, V_{k\ell}(NT, f, T) \Big|^2$$

$$= \sum_{k,\ell=-\infty}^{\infty} |a'_{k\ell}|^2\, |V_{k\ell}(NT, f, T)|^2$$

$$+ \sum_{\substack{k,\ell,m,n=-\infty \\ (k\neq m \text{ or } \ell\neq m)}}^{\infty} a'_{k\ell}\, a'^{*}_{mn}\, V_{k\ell}(NT, f, T)\, V^{*}_{mn}(NT, f, T). \qquad (2\text{-}1\text{-}73)$$

Since Lerner did not consider signal energy in his work, he failed to require the energy spectrum of a finite length subinterval, here given by $|X(NT, f, T)|^2$, to have a clear relationship to the signal in the corresponding subinterval. When this is desirable, the $v_{k\ell}(t)$ should be chosen to yield this property, yet Lerner neglected this issue.

It will be shown in Chapter 3 that this property is achieved by defining the $v_{k\ell}(t)$ to be time-limited. It will be emphasized there that this property clarifies the relationship between the individual subinterval and its energy spectrum. It is sufficient to say here that

Lerner did not go into the issue of time-variant energy spectra, nor did he indicate concern for the possible misconceptions arising from a grid-type of representation in the time-frequency plane.

2.2 Page's Instantaneous Power Spectrum

In 1952, C. H. Page [4] attempted to express the intuitive concept of a time-variant energy spectrum. He approached the definition of an energy density distributed in time and frequency by considering the properties which that energy density should satisfy. The difficiency of the ordinary Fourier energy spectrum, determined by the entire history of the signal from $t=-\infty$ to $t=\infty$, was very evident to him. He pointed out that, when a man and woman sing alternate verses of a song, our intuition predicts that the energy spectrum should change with frequency as time goes on. Yet the ordinary Fourier energy spectrum "averages out" the energy spectra over consecutive, finite-length time intervals. With this in mind, it was postulated that there must be some two-dimensional function of time and frequency which becomes progressively more similar to the ordinary Fourier spectrum as more and more of the signal's history is included in the observation interval.

Page defined an energy density $\rho(t,f)$ in the time-frequency plane such that the total energy in the signal from $t=-\infty$ to $t=T$ is

$$\int_{-\infty}^{T}\int_{-\infty}^{\infty}\rho(t,f)\,dfdt. \qquad (2\text{-}2\text{-}1)$$

The rate of change of total energy with time T is the instantaneous power (as a function of T) and is given by

$$\frac{\partial}{\partial T}\int_{-\infty}^{T}\int_{-\infty}^{\infty}\rho(t,f)\ dfdt = \int_{-\infty}^{\infty}\rho(T,f)df \qquad (2\text{-}2\text{-}2)$$

which shows that $\rho(t,f)$ can be viewed as an instantaneous power spectrum at the time t=T. To represent $\rho(T,f)$ in terms of the given signal x(t), it is noted by Parseval's Theorem that the total energy up to time T is

$$\int_{-\infty}^{T}|x(t)|^2\ dt = \int_{-\infty}^{\infty}\left|\int_{-\infty}^{\infty}x(t)\ e^{-j2\pi ft}dt\right|^2\ df. \qquad (2\text{-}2\text{-}3)$$

Since (2-2-1) expresses the same total energy from $t=-\infty$ to t=T, then

$$\int_{-\infty}^{T}\int_{-\infty}^{\infty}\rho(t,f)\ dfdt = \int_{-\infty}^{\infty}\left|\int_{-\infty}^{T}x(t)\ e^{-j2\pi ft}dt\right|^2\ df. \qquad (2\text{-}2\text{-}4)$$

Differentiating both sides of this equation with respect to T produces the result

$$\int_{-\infty}^{\infty}\rho(T,f)\ df = \frac{\partial}{\partial T}\int_{-\infty}^{\infty}\left|\int_{-\infty}^{T}x(t)\ e^{-j2\pi ft}dt\right|^2\ df. \qquad (2\text{-}2\text{-}5)$$

With the total energy being finite, the integral on the right hand side exists. Furthermore, the partial derivative of the integrand on the right side is seen to be a continuous function of T and f. Specifically,

$$\frac{\partial}{\partial T}\left|\int_{-\infty}^{T}x(t)\ e^{-j2\pi ft}dt\right|^2 = 2RE\left\{x(T)e^{-j2\pi fT}\int_{-\infty}^{T}x^*(t)e^{+j2\pi ft}dt\right\}. \qquad (2\text{-}2\text{-}6)$$

Therefore the partial derivative may be taken within the integral on the right side of (2-2-5), giving

$$\frac{\partial}{\partial T} \int_{-\infty}^{\infty} \left| \int_{-\infty}^{T} x(t)\ e^{-j2\pi ft} dt \right|^2 df$$

$$= \int_{-\infty}^{\infty} \frac{\partial}{\partial T} \left| \int_{-\infty}^{T} x(t)\ e^{-j2\pi ft} dt \right|^2 df. \qquad (2\text{-}2\text{-}7)$$

Using (2-2-5), it follows that

$$\int_{-\infty}^{\infty} \rho(T,f)\ df = \int_{-\infty}^{\infty} \frac{\partial}{\partial T} \left| \int_{-\infty}^{T} x(t)\ e^{-j2\pi ft} dt \right|^2 df \qquad (2\text{-}2\text{-}8)$$

which Page considered a <u>sufficient</u> condition to determine $\rho(T,f)$. In particular,

$$\rho(T,f) = \frac{\partial}{\partial T} \left| \int_{-\infty}^{T} x(t)\ e^{-j2\pi ft} dt \right|^2$$

$$= 2RE \left\{ x(T)\ e^{-j2\pi fT} \int_{-\infty}^{T} x^*(t)\ e^{+j2\pi ft} dt \right\}. \qquad (2\text{-}2\text{-}9)$$

Strictly speaking, (2-2-8) is an equality only between integrals and not, in general, between integrands. Nevertheless, Page treated (2-2-9) as a useful expression for $\rho(T,f)$.

An interesting modification of this concept was presented by Morris Levin [5] in 1964. Levin defined the "running Fourier Transforms"

$$X_T^-(f) = \int_{-\infty}^{T} x(t)\ e^{-j2\pi ft}dt \qquad (2\text{-}2\text{-}10)$$

and

$$X_T^+(f) = \int_{T}^{\infty} x(t)\ e^{-j2\pi ft}dt. \qquad (2\text{-}2\text{-}11)$$

Just as Page identified the expression

$$\frac{\partial}{\partial T}\left|\int_{-\infty}^{T} x(t)\ e^{-j2\pi ft}dt\right|^2 \qquad (2\text{-}2\text{-}12)$$

with the instantaneous power spectrum of the signal in the interval $(-\infty,T)$, Levin identified the expression

$$\frac{\partial}{\partial T}\left|\int_{T}^{\infty} x(t)\ e^{-j2\pi ft}dt\right|^2 \qquad (2\text{-}2\text{-}13)$$

with the instantaneous power spectrum of the signal in the interval (T,∞). Using (2-2-10) and (2-2-11), he defined

$$\frac{\partial}{\partial T}\left|X_T^-(f)\right|^2 \qquad (2\text{-}2\text{-}14)$$

and

$$\frac{\partial}{\partial T}\left|X_T^+(f)\right|^2 \qquad (2\text{-}2\text{-}15)$$

as the instantaneous power spectra for the intervals $(-\infty,T)$ and (T,∞), respectively. Past and future values of the signal x(t) can then be treated symmetrically by defining the new instantaneous power spectrum $\rho'(T,f)$ as

$$\rho'(T,f) = \tfrac{1}{2}\left[\frac{\partial}{\partial T}\,|X_T^-(f)|^2 - \frac{\partial}{\partial T}\,|X_T^+(f)|^2\right] . \qquad (2\text{-}2\text{-}16)$$

This gives the mathematically pleasing result that

$$\rho'(T,f) = RE\,\{x(T)e^{-j2\pi fT}\int_{-\infty}^{\infty} x^*(t)\; e^{+j2\pi ft}\,dt\}$$

$$= RE\,\{x(T)e^{-j2\pi fT}X^*(f)\}, \qquad (2\text{-}2\text{-}17)$$

where X(f) is the ordinary Fourier Transform of x(t) taken from $t=-\infty$ to $t=+\infty$. Levin then showed that $\rho'(T,f)$ had the following desirable properties:

$$\int_{-\infty}^{\infty} \rho'(T,f)\; df = |x(T)|^2 , \qquad (2\text{-}2\text{-}18)$$

$$\int_{-\infty}^{\infty} \rho'(T,f)\; dT = |X(f)|^2 \qquad (2\text{-}2\text{-}19)$$

and

$$\int_{-\infty}^{\infty}\int_{-\infty}^{\infty} \rho'(T,f)\; dT\; df = \int_{-\infty}^{\infty} |x(t)|^2\; dt. \qquad (2\text{-}2\text{-}20)$$

This last property suggests that $\rho'(T,f)$ may be used as an energy density. All of these properties, while mathematically pleasing, still do not justify the assumption by Page that the integrands on both sides of (2-2-8) are equal.

In order to put this instantaneous spectrum concept on a firmer footing, August Rihaczek [6] developed a different approach to $\rho'(T,f)$. He considered a complex signal within a time interval ΔT centered at $t=t_o$. Based on this time interval, the total complex energy E_c within a frequency band ΔB centered at f_o was defined as

$$E_c = \tfrac{1}{2} \int_{t_o - \frac{\Delta T}{2}}^{t_o + \frac{\Delta T}{2}} x(t)\, y^*(t)\, dt \qquad (2\text{-}2\text{-}21)$$

where

$$y(t) = \mathcal{F}^{-1} \{ \text{Rect} \left[\frac{f-fo}{\Delta B} \right] X(f) \} \qquad (2\text{-}2\text{-}22)$$

and

$$\text{Rect} \left[\frac{f-fo}{\Delta B} \right] = \begin{cases} 1, & |f-f_o| < \frac{\Delta B}{2} \\ 0, & |f-f_o| > \frac{\Delta B}{2} \end{cases} . \qquad (2\text{-}2\text{-}23)$$

It is noted that $y(t)$ is the Inverse Fourier Transform of only that part of the signal's transform within the frequency band of interest. Rihaczek allowed the band ΔB to be chosen so small that $X(f)$ did not change over it. Specifically,

$$y(t) = X(fo)\ \mathcal{F}^{-1}\ \{\text{Rect}\left[\frac{f-fo}{\Delta B}\right]\}$$

$$= X(fo)\ e^{+j2\pi f_o t}\ \Delta B\ \text{sinc}\ (t\Delta B). \qquad (2\text{-}2\text{-}24)$$

Furthermore, ΔB was allowed to become the infinitesimally small quantity δB so that

$$\Delta B\ \text{sinc}\ (T\Delta B) = \delta B. \qquad (2\text{-}2\text{-}25)$$

Using this in (2-2-24), there results.

$$y(t) = X(f_o)\ \delta B\ e^{+j2\pi f_o t}\ . \qquad (2\text{-}2\text{-}26)$$

Substituting this expression for y(t) into (2-2-21) gives

$$E_c = \tfrac{1}{2}\ X^*(f_o)\ \delta B \int_{t_o - \frac{\Delta T}{2}}^{t_o + \frac{\Delta T}{2}} x(t)\ e^{-j2\pi f_o t}\ dt. \qquad (2\text{-}2\text{-}27)$$

Rihaczek assumed next that ΔT is so small that x(t) does not change its value within it, so that

$$E_c = \tfrac{1}{2}\ x(t_o)X^*(f_o)\ \delta B \int_{t_o - \frac{\Delta T}{2}}^{t_o + \frac{\Delta T}{2}} e^{-j2\pi f_o t}\ dt. \qquad (2\text{-}2\text{-}28)$$

$$= \tfrac{1}{2}\ x\ (t_o)\ X^*(f_o)\ \delta B\ [\Delta T\ e^{-j2\pi f_o t_o}\ \text{sinc}\ (f\Delta T)]. \qquad (2\text{-}2\text{-}29)$$

Letting ΔT become the infinitesimally small quantity δT, there results

$$\Delta T \text{ sinc } (f\Delta T) = \delta T. \qquad (2\text{-}2\text{-}30)$$

Using this in (2-2-29), the final result is

$$E_c = \tfrac{1}{2} x(t_o)\, X^*(f_o)\, e^{-j2\pi f_o t_o}\, \delta B\, \delta T. \qquad (2\text{-}2\text{-}31)$$

Inspecting this expression, the energy density at the point (t_o, f_o) is defined to be

$$x(t_o)\, X^*(f_o)\, e^{-j2\pi f_o t_o}\,, \qquad (2\text{-}2\text{-}32)$$

the product $\delta B \delta T$ being the elementary cell area in the time-frequency plane and the factor of $\frac{1}{2}$ being due to the complex notation. It is interesting that this energy density is the complex version of Levin's expression for the energy density (or instantaneous power spectrum) $\rho'(t,f)$ in (2-2-17).

Although these attempts to define a useful, intuitively pleasing energy density over the time-frequency plane may have established some interesting properties, they fall far short of providing a useful tool for time-variant energy spectral analysis. The reason for this is that no satisfactory explanation can be given for the fact that the "energy density" in (2-2-17) and (2-2-32) can become negative. Rihaczek alluded to this fact when he stated that (2-2-32) is not really a measure of the energy distribution at (t_o, f_o). He admitted that positive values of his energy density may be offset by negative values at neighboring points, so that very little energy may actually be concentrated where the energy density has large values. Consequently, it was concluded that the energy density must be integrated over a time-frequency <u>cell</u> chosen

large enough to prevent significant interaction or "leakage" from adjacent cells. This would hopefully yield a positive energy for each cell. There is a similarity here to the problem of neighboring cell "leakage" on the Gabor logon grid. Unfortunately, knowledge of the proper cell size requires fine-grained knowledge of the signal's characteristics in time and frequency which are unknown in many real problems. Furthermore, the requirement to furnish the proper cell size for integration of the energy density demands some of the very information that one would use time-variant energy spectral analysis to determine!

Another major difficulty lies in the implementation of (2-2-17) and (2-2-32). Those expressions require the signal's Fourier Transform, X(f), to be accurately known. However, X(f) relies upon knowledge of the signal x(t) over the infinite time interval $(-\infty,\infty)$. When x(t) is very long it is not easy to calculate X(f) with the precision desired for fine-grained analysis of the energy density of (2-2-17) or (2-2-32).

2.3 The Wigner Distribution

A recent discovery [7, 8, 9] of some importance is that a certain integral expression related to the Ambiguity function has interesting properties when used for time-variant spectral analysis. This integral expression is called the Wigner distribution after the man who introduced it in the context of quantum mechanics. The cross Wigner distribution of two signals x(t) and y(t) is defined by

$$W_{x,y}(t,\omega) = \int_{-\infty}^{\infty} x(t + \tfrac{\tau}{2})\, y^{*}(t - \tfrac{\tau}{2})\, e^{-j\omega\tau}\, d\tau \qquad (2\text{-}3\text{-}1)$$

where $\omega = 2\pi f$ is the radian frequency. The auto-Wigner distribution of the signal x(t) is then

$$W_x(t,\omega) = \int_{-\infty}^{\infty} x(t + \tfrac{\tau}{2})\, x^*(t - \tfrac{\tau}{2})\, e^{-j\omega\tau}\, d\tau \qquad (2\text{-}3\text{-}2)$$

which is similar to the Ambiguity function $A_x(t,\omega)$ given by

$$A_x(t,\omega) = \int_{-\infty}^{\infty} x(\tau + \tfrac{t}{2})\, x^*(\tau - \tfrac{t}{2})\, e^{-j\omega\tau}\, d\tau. \qquad (2\text{-}3\text{-}3)$$

It is noted that the roles of t and τ are interchanged in (2-3-2) and (2-3-3) but the interchange only affects the arguments of the signal. It is interesting that (2-3-2) and (2-3-3) are in general <u>different</u> representations. However, when the signal is real and symmetric (even or odd), that is,

$$x(t) = \pm\, x(-t) \qquad (2\text{-}3\text{-}4)$$

then

$$W_x(t,\omega) = \pm\, 2A_x(2t,\, 2\omega). \qquad (2\text{-}3\text{-}5)$$

Some of the advantages of using the auto Wigner distribution (WD) for signal representation instead of the ambiguity function (AF) are the following.

1. The WD of any (real or complex) signal is real while the AF is in general complex.
2. The WD of a real signal is an even function of frequency while the AF in general is not.

3. The effect of a time shift t_o on the signal is to shift the time argument of the WD by t_o while the effect on the AF is to add a linear term, $-\omega t_o$, to the phase angle.

4. The effect of a frequency shift ω_o on the signal (or equivalently multiplication by $e^{j\omega_o t}$) is to shift the frequency argument of the WD by ω_o while the effect on the AF is to add a linear term, $\omega_o t$, to the phase angle.

5. The properties of a joint time-frequency density function given in (2-2-18), (2-2-19) and (2-2-20) are satisfied by the WD but not in general by the AF. However, for real signals, the AF satisfies similar relationships. Specifically, given a signal with total energy E,

$$\frac{1}{2\pi} \int\int_{-\infty}^{\infty} W_x(t,\omega)\, dt\, d\omega = E, \tag{2-3-6}$$

$$\frac{1}{2\pi} \int_{-\infty}^{\infty} W_x(t_o, \omega)\, d\omega = |x(t_o)|^2, \tag{2-3-7}$$

and

$$\int_{-\infty}^{\infty} W_x(t,\omega_o)\, dt = |X(\omega_o)|^2. \tag{2-3-8}$$

On the other hand, only for a <u>real</u> signal with total energy E there results

$$\frac{1}{2\pi} \int\int_{-\infty}^{\infty} A_x(t,\omega)\, dt\, d\omega = 2E, \tag{2-3-9}$$

$$\frac{1}{2\pi}\int_{-\infty}^{\infty} A_x(t_o,\omega)\, d\omega = x^2(\frac{t_o}{2}), \qquad (2\text{-}3\text{-}10)$$

and

$$\int_{-\infty}^{\infty} A_x(t,\omega_o)\, dt = |X(\frac{\omega_o}{2})|^2. \qquad (2\text{-}3\text{-}11)$$

This shows that the WD is the more convenient choice when density-function properties are desirable.

6. The WD of a signal timelimited to a certain interval will itself be timelimited to the same interval whereas the AF does not in general exhibit this property. Specifically, if

$$x(t) = 0\ ,\ t < t_a \text{ and } t > t_b\ , \qquad (2\text{-}3\text{-}12)$$

then

$$W_x(t,\omega) = 0\ ,\ t < t_a \text{ and } t > t_b. \qquad (2\text{-}3\text{-}13)$$

7. The WD of a signal bandlimited to a certain frequency interval will itself be bandlimited to the same interval whereas the AF does not in general exhibit this property. Specifically, if

$$X(\omega) = 0\ ,\ \omega < \omega_a \text{ and } \omega > \omega_b, \qquad (2\text{-}3\text{-}14)$$

then

$$W_x(t,\omega) = 0 \ , \ \omega < \omega_a \text{ and } \omega > \omega_b. \qquad (2\text{-}3\text{-}15)$$

8. The instantaneous frequency $\Omega_x(t)$ of a <u>complex</u> signal can be found by determining the average frequency of the WD. Specifically, the average frequency of the WD is

$$\frac{\int_{-\infty}^{\infty} \omega \, W_x(t,\omega) \, d\omega}{\int_{-\infty}^{\infty} W_x(t,\omega) \, d\omega} = IM \{\frac{d}{dt} \ln x(t)\} = \Omega_x(t) \qquad (2\text{-}3\text{-}16)$$

This property is not exhibited by the AF.

The preceding properties are very useful in describing signal characteristics which vary in time and frequency. However, a crucial point is reached when considering the Wigner distribution as an energy density. The problem is again that this "density function" is not in general positive. This poses great difficulties of interpretation. For example, it may be asked, "What does a negative value for energy density physically mean?" or "What is the significance of a negative value for the integration of the density over a finite region in the time-frequency plane?" Evidently those who introduced the Wigner distribution as a tool for time-variant spectral analysis have not found answers to these questions [7, 8, 9, 10]. It might be suggested that the absolute value or the squared value of the Wigner distribution be used. However, a very significant insight gained by these researchers is that the imposition of a positivity requirement on <u>any</u> time-fequency energy density function prevents it from satisfying most of the properties listed above.

> "On the other hand it was shown that positivity of such a representation excludes it from having properties that are desirable for the extraction of instantaneous information like the instantaneous power, instantaneous frequency, and the finite support property. If such instantaneous characteristics should be obtainable from such a time-frequency representation, then we have to accept negative values for it. This seems to be the only way to accommodate Heisenberg's uncertainty relation."[9]

The meaning of the Heisenberg uncertainty relation in this context is that an arbitrarily sharp frequency representation is impossible when analyzing arbitrarily short time intervals. It is interesting that the authors of the paper quoted above felt they were forced to accept negative values for an energy density. It will be shown in Chapter 3 that a different approach to time-variant energy avoids this problem.

Another noteworthy fact pointed out by these same researchers is that the Wigner distribution belongs to a class of related time-frequency representations among which are the ambiguity function and the representation of Page and Rihaczek. The relationship between them is nicely developed but here, again, the interpretation of negative energy density is the main stumbling block to satisfactory application.

2.4 Conventional Discrete Fourier Transform Techniques

The most common technique in use today for time-variant energy spectral analysis involves the Finite Fourier Transform [14], $X_{FT}(f)$, defined by

$$X_{FT}(f) = \int_0^T x(t)\ e^{-j2\pi ft}\ dt. \qquad (2\text{-}4\text{-}1)$$

Its sampled version, the Discrete Fourier Transform, $X_{DFT}(f_\ell)$, is given by

$$X_{DFT}(f_\ell) = \sum_{n=0}^{N-1} x(t_n) e^{-j2\pi f_\ell t_n} , \qquad (2\text{-}4\text{-}2)$$

where $\ell = 0, 1, \ldots, N-1$ (2-4-3)

and $f_\ell = \frac{\ell}{T}$ (2-4-4)

Since the discovery of computer algorithms for the rapid calculation of (2-4-2), the popularity of the DFT for all kinds of spectral analysis has grown enormously. In a typical application, the signal x(t) is first sampled at an appropriate rate. The magnitude squared of $X_{DFT}(f_\ell)$ is then determined as an approximation to the energy spectral density $|X_{FT}(f)|^2$ evaluated at the specific frequencies $f = f_\ell$. This result is then interpreted as the sampled version of the energy spectral density for the signal in the finite-length observation interval [o,T]. However, in applications to time-variant energy spectral analysis, the procedure commonly used is to partition the entire observation interval into subintervals, as was done in Figure 2-3. For each subinterval centered at t_k and having width T, the time-indexed version of (2-4-1) is approximated. This time-indexed version, $X_{FT}(f; t_k)$, is defined as

$$X_{FT}(f; t_k) = \int_{t_k - \frac{T}{2}}^{t_k + \frac{T}{2}} x(t)\, e^{-j2\pi f t} dt, \qquad (2\text{-}4\text{-}5)$$

and it is approximated by the time-indexed version of (2-4-2), $X_{DFT}(f_\ell; t_k)$, given by

$$X_{DFT}(f_\ell; t_k) = \sum_{n=k-\frac{N}{2}}^{n=k+\frac{N}{2}-1} x(t_n)\, e^{-j2\pi f_\ell t_n} , \qquad (2\text{-}4\text{-}6)$$

where

$$\ell = 0, 1, \ldots, N-1, \tag{2-4-7}$$

$$f_\ell = \frac{\ell}{T} , \tag{2-4-8}$$

and

$$t_{n+1} - t_n = \frac{T}{N} , \tag{2-4-9}$$

N being an even integer.

The magnitude squared $|X_{DFT}(f_\ell, t_k)|^2$ is then treated as the energy spectrum for the subinterval at t_k and the <u>family of energy spectra</u> for a set of t_k is considered in common usage to be the time-variant energy spectra, as sketched in Figure 2-6.

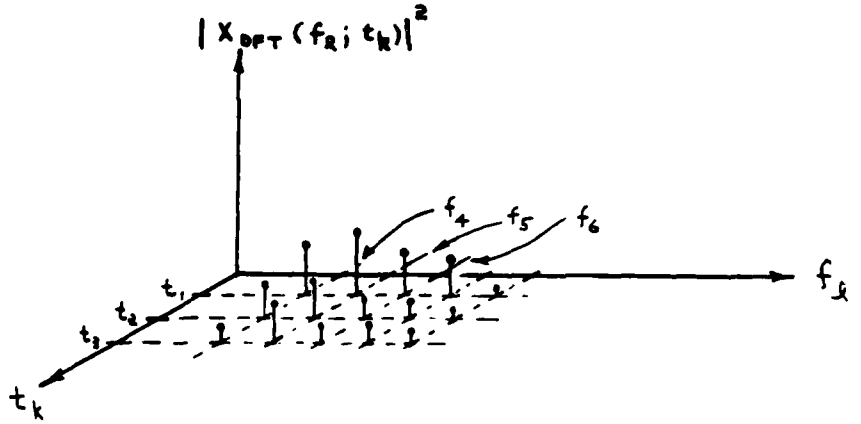

FIG. 2-6 THE FAMILY OF ENERGY SPECTRA $|X_{DFT}(f_\ell, t_k)|^2$

Although it is usual to interpret this two dimensional plot as an energy density over time and frequency, there is no justification in the open literature for this interpretation. In particular, there are no satisfying answers to the following questions:

(1) What is the relationship between the energy spectrum of the entire signal and the energy spectra of individual subintervals?

(2) What interpretation should be given to the values of $|X_{DFT}(f_\ell;\ t_k)|^2$ at arbitrary frequencies f_ℓ?

(3) At what specific frequencies, f_ℓ, should $|X_{DFT}(f_\ell;\ t_k)|^2$ be used to provide physical interpretation of a "time-variant energy spectrum?

(4) What are the effects of averaging several sets of $|X_{DFT}(f_\ell;t_k)|^2$ from different time subintervals t_k? That is, what significance can be given to the expression

$$\sum_{k=K_1}^{K_1} |X_{DFT}(f_\ell;\ t_k)|^2 \ ? \qquad (2\text{-}4\text{-}10)$$

(5) What interpretation should be given to the family of energy spectra, $|X_{DFT}(f_\ell;\ t_k)|^2$, when the signal x(t) is multiplied by a "weighting window" before it is transformed? (It is common to do this in order to attempt better resolution of sinusoids.)

This last question introduces the idea of "window weighting" with the window function w(t). The windowed DFT, $X_{WDFT}(f_\ell)$, is defined as

$$X_{WDFT}(f_\ell) = \sum_{n=0}^{N-1} w(t_n)\ x(t_n)\ e^{-j2\pi f_\ell t_n} \ , \qquad (2\text{-}4\text{-}11)$$

$$\ell = 0,\ 1,\ldots,\ N\text{-}1,$$

where w(t) is usually tapered to zero at the edge points $t=t_o$ and $t=t_{N-1}$. (The indices ℓ and n are given in (2-4-7), (2-4-8), and (2-4-9).) A detailed review of many window functions now in use is found in a paper by Frederic Harris [12].

Another common practice is to transform a sequence of overlapping partitions of the signal x(t) as shown in Figure 2-7.

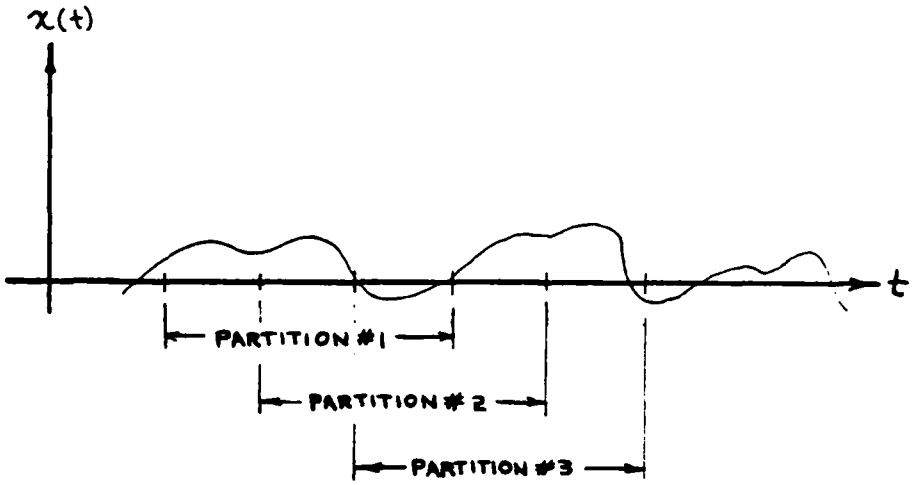

FIG. 2-7 OVERLAPPING PARTITIONS

Transforms of overlapped partitions are sometimes used with the window weighting technique to compensate for the window function's small values near the edge of the partition. For example, if the signal contains short bursts of sinusoids, the regular non-overlap processing with window weighting might de-emphasize a burst which occurs at a partition boundary.

All of these techniques have the advantage that they are easily implemented on a computer. However, the groundwork for interpreting results is for the most part lacking. The five questions posed above point out the lack of any theoretical framework and justification for the application of the DFT to time-variant energy spectral analysis. The proposed approach presented in Chapter 3 will be shown to establish this theoretical framework and in addition answer the questions posed here.

Chapter 3

A NEW APPROACH TO TIME-VARIANT ENERGY SPECTRAL ANALYSIS

This chapter presents a new concept for describing the time-frequency energy distribution of a signal. Up until this point what was meant by a time-frequency energy distribution had not been adequately explained. For our purposes, the term time-variant energy distribution will be taken to denote a discrete set of energy values indexed by specific frequencies and specific finite time intervals. This set of values can be visualized as the sampled version of a two-dimensional nonnegative function of time and frequency. Hence, the term time-frequency energy distribution will be used synonymously. Negative values of energy will not arise and the term energy density will not be used. This rules out, therefore, the occurrence of negative energy densities as encountered in Chapter 2. Secondly, the term frequency, or more precisely spectral frequency, will be used in conjunction with "shaped" sinusoidal functions of time having finite duration. This contrasts with the traditional usage which involves infinitely long sinusoids and it has the advantage of a clearer interpretation when finite-length signal observations are being analyzed. Hence, the determination of a sinusoidal signal's spectral frequency at a certain time will require the definition of that signal over a finite, nonzero-length time interval which encloses the time in question. It is clear, therefore, that the notions of time and frequency in the context of energy spectral analysis are not separable.

The meaning of the term time-frequency energy distribution as it will be developed here rests upon the physical relationship between signal energy, spectral frequency, and an associated time interval as different time intervals come under analysis. This three-fold relationship will be gradually clarified and interpreted through the use of linear vector space concepts.

3.1. The Vector Space Description of Time-Variant Energy Spectral Analysis

One of the most desirable qualities sought in a time-frequency energy distribution is the clear indication of progressive changes of the frequency distribution of energy from one moment to the next within a signal's observation interval. It is therefore natural to break up an observed signal into contiguous subintervals, each of which is analyzed sequentially. For our purposes, the signal observation interval will be denoted by $[t_A, t_B]$ while each subinterval will be defined as T seconds long and centered at a particular time t_k as shown in Figure 3-1.

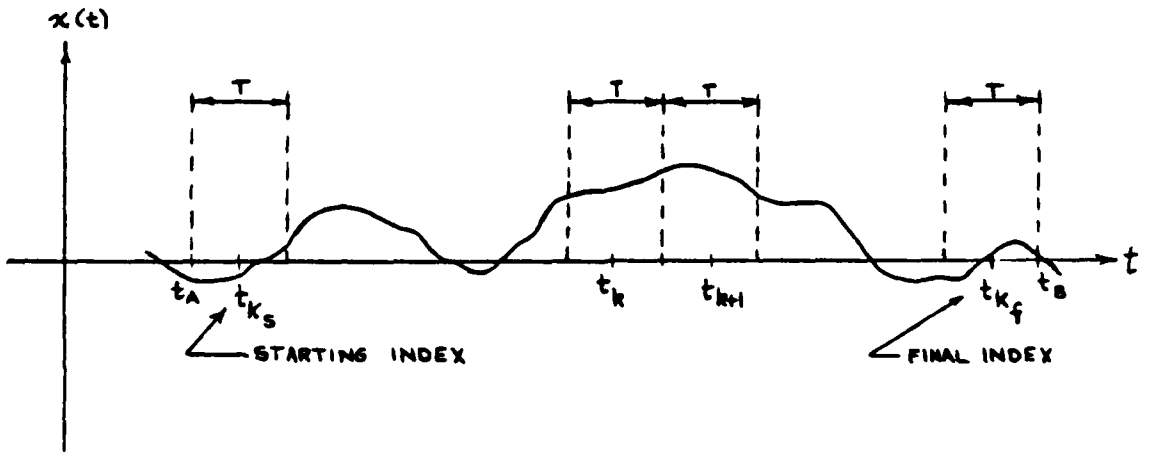

FIG. 3-1 SIGNAL OBSERVATION INTERVAL

As indicated in the figure,

$$t_{k+1} - t_k = T, \tag{3-1-1}$$

where the indices are integers given by

$$k = K_s, K_s + 1, \ldots, K_f, \tag{3-1-2}$$

It is assumed that there are N subintervals, that is,

$$K_f - K_s = N + 1. \tag{3-1-3}$$

The portion of the signal contained in the interval $[t_k - \frac{T}{2}, t_k + \frac{T}{2}]$ will be referred to as the k^{th} segment. It is important to note that the signal is assumed to be unknown outside of $[t_A, t_B]$ and all attention will be given to what is going on within this total observation interval.

The proposed approach consists in representing the signal in each subinterval by a point in a linear vector space. The location of this point and its motion in time will automatically indicate associations with various types of sinusoidal functions of specific frequencies and a convenient description of time-variant signal energy will emerge. Specifically, the entire observed signal x(t) is approximated by the function $\hat{x}(t)$ where

$$\hat{x}(t) = \sum_{k=K_s}^{K_f} \sum_{\ell=-M}^{M} c_{k\ell}\, \psi_{k\ell}(t) \tag{3-1-4}$$

and where the doubly-indexed orthonormal basis functions $\psi_{k\ell}(t)$ are given by

$$\psi_{k\ell}(t) = \begin{cases} \sqrt{w(t-t_k)}\ e^{j\omega_\ell t}\ ;\ |t-t_k| \le \frac{T}{2} \\ 0\ ;\ |t-t_k| > \frac{T}{2}\ , \end{cases} \qquad (3\text{-}1\text{-}5)$$

w(t) being known as the "window". Also the radian frequencies are given by

$$\omega_\ell = \left[\frac{2\pi Q}{T}\right] \ell, \qquad (3\text{-}1\text{-}6)$$

where Q is referred to as the "frequency spacing factor," a non-zero integer uniquely associated with the window w(t). Inspection of (3-1-4) and (3-1-5) shows that the signal in each segment is being approximated by a discrete set of basis functions, that these basis functions are non-overlapping functions of time, and that each basis function is a "shaped" or "windowed" complex cisoidal function, $e^{j\omega_\ell t}$, characterized by its particular radian frequency ω_ℓ.

It is quite significant that the <u>square root</u> of the window function, $\sqrt{w(t)}$, is the shaping tool. An illustration of one such window is given in Figure 3-2 along with the real part of a typical basis function $\psi_{k\ell}(t)$. Here the window function is the so-called "Bartlett" window, given by

$$w(t) = \begin{cases} \frac{2}{T}\left[1 - \frac{2|t|}{T}\right] ; & |t| \le \frac{T}{2} \\ 0 ; & |t| > T/2, \end{cases} \qquad (3\text{-}1\text{-}7)$$

with Q=2 as its associated frequency spacing factor.

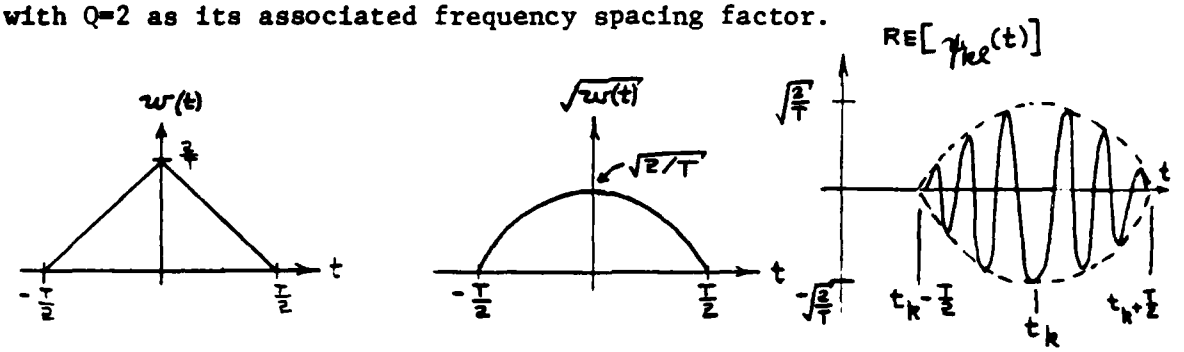

FIG. 3-2 THE BARTLETT WINDOW, ITS SQUARE ROOT, AND A TYPICAL BASIS FUNCTION

Since the basis functions defined in (3-1-5) are non-overlapping and time-limited to intervals of width T, the window function w(t) will be assumed to be time-limited to [-T/2, T/2] without loss of generality. Strictly speaking, the window function by itself need not be time-limited but the only portion of it of any consequence is the portion in the interval [-T/2, T/2]. This will be seen shortly. The assumption of a time-limited window is consistent with the basic motivation to represent the signal's frequency distribution of energy as a separate entity for each time subinterval. It is interesting to note that Gabor's choice of basis functions in (2-1-1) does not have this property which is one of the underlying reasons why the logon concept is not useful.

Introducing the Fourier Transform of the time-limited window function as $W_T(\omega)$, where

$$W_T(\omega) = \int_{-T/2}^{T/2} w(t)\, e^{-j\omega t}\, dt, \qquad (3\text{-}1\text{-}8)$$

and

$$\omega = 2\pi f, \tag{3-1-9}$$

it is required for the orthonormality of the basis functions that

$$W_T(0) = 1 \tag{3-1-10}$$

and that

$$W_T\left[n\left(\frac{2\pi Q}{T}\right)\right] = 0, \tag{3-1-11}$$

$$n = \pm 1, \pm 2, \ldots . \tag{3-1-12}$$

Of primary importance here is the requirement in (3-1-11) which states that $W_T(\omega)$ must have an infinite number of <u>equally spaced</u> zeroes, the spacing being $\frac{2\pi Q}{T}$. Although not ruling out complex window functions, in which case the procedure here would call for replacing $w(t)$ by $|w(t)|$ in (3-1-8) and $w(t - t_k)$ by $|w(t - t_k)|$ in (3-1-5), it is much easier in the computation of coefficients to be discussed later to use real window functions. Hence $w(t)$ will be assumed to be real here while the signal $x(t)$ will be allowed to be complex in general.

It is interesting to note in passing that the Bartlett window in (3-1-7) satisfies (3-1-10) and (3-1-11). In particular, for the Bartlett window,

$$W_T(\omega) = W(\omega) = \left[\frac{\sin\frac{\omega T}{4}}{\frac{\omega T}{4}}\right]^2 \tag{3-1-13}$$

and Q=2 so that (3-1-11) becomes

$$W_T\left[n\left(\frac{4\pi}{T}\right)\right] = W\left[n\left(\frac{4\pi}{T}\right)\right] = \left[\frac{\sin(n\pi)}{(n\pi)}\right]^2 = 0 \qquad (3\text{-}1\text{-}14)$$

$$n = \pm 1, \pm 2, \ldots, \qquad (3\text{-}1\text{-}15)$$

as sketched in Figure 3-3.

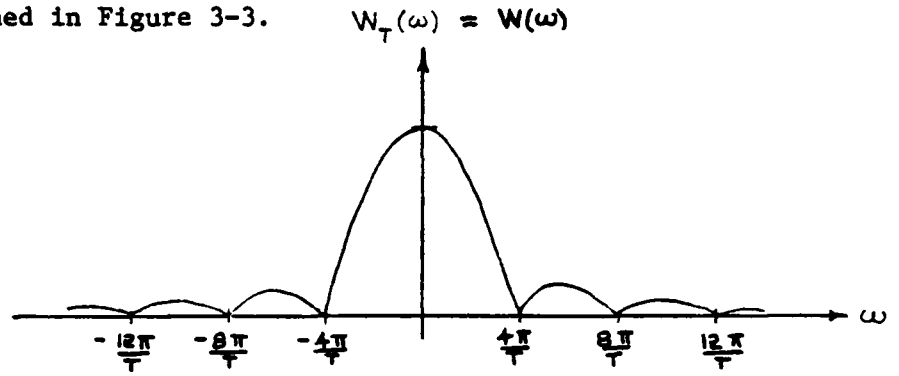

FIG. 3-3 FOURIER TRANSFORM OF THE BARTLETT WINDOW

Now in order to satisfy the orthonormality condition, it is required that

$$\int_{-\infty}^{\infty} \psi_{k\ell}(t)\, \psi^*_{mn}(t)\, dt = \delta_{km}\, \delta_{\ell n} . \qquad (3\text{-}1\text{-}16)$$

Substituting (3-1-5) into the left side of (3-1-16), there results

$$\int_{-\infty}^{\infty} \psi_{k\ell}(t)\, \psi^*_{mn}(t)\, dt = \begin{cases} \displaystyle\int_{t_k - \frac{T}{2}}^{t_k + \frac{T}{2}} w(t-t_k)\, e^{-j(\omega_n - \omega_\ell)t}\, dt; & k = m \\ 0 ; & k \neq m . \end{cases} \qquad (3\text{-}1\text{-}17)$$

Simplifying the integral in the k = m case, it is found that

$$\int_{t_k-\frac{T}{2}}^{t_k+\frac{T}{2}} w(t-t_k)\, e^{-j(\omega_n-\omega_\ell)t}\, dt = e^{-j(\omega_n-\omega_\ell)t_k} \int_{-T/2}^{T/2} w(u) e^{-j(\omega_n-\omega_\ell)u}\, du, \tag{3-1-18}$$

where

$$u = t - t_k \tag{3-1-19}$$

and

$$du = dt. \tag{3-1-20}$$

The right side of (3-1-18) is just $W_T(\omega)$ evaluated at the frequency $(\omega_n-\omega_\ell)$ and multiplied by a constant complex exponential. Specifically, (3-1-18) is

$$e^{-j(\omega_n-\omega_\ell)t_k}\ W_T(\omega_n-\omega_\ell) = e^{-j\frac{2\pi Q}{T}(n-\ell)\ t_k}\ W_T\left[\frac{2\pi Q}{T}\ (n-\ell)\right]. \tag{3-1-21}$$

Using (3-1-10) and (3-1-11), it follows that

$$e^{-j\frac{2\pi Q}{T}(n-\ell)t_k}\ W_T\left[\frac{2\pi Q}{T}(n-\ell)\right] = \delta_{\ell n}\ , \tag{3-1-22}$$

so that (3-1-17) becomes

$$\int_{-\infty}^{\infty} \psi_{k\ell}(t)\psi^*_{mn}(t)\, dt = \begin{cases} \delta_{\ell n}\ ;\ k = m \\ 0\ ;\ k \neq m \end{cases} \tag{3-1-23}$$

which satisfies the orthonormality requirement in (3-1-16). It is now evident that the equally-spaced zeroes of $W_T(\omega)$ in (3-1-11) are vitally important to ensure the orthonormality requirement. An important class of window functions which possesses this property is formed by convolving a rectangular pulse of duration $(T-\beta)$, Rect $\left[\frac{t}{T-\beta}\right]$, with a symmetric positive pulse a(t) having duration β and area $\frac{1}{T-\beta}$. This generates a time-limited window w(t) as shown in Figure 3-4. It is noted that $0 \leq \beta < T$ and that

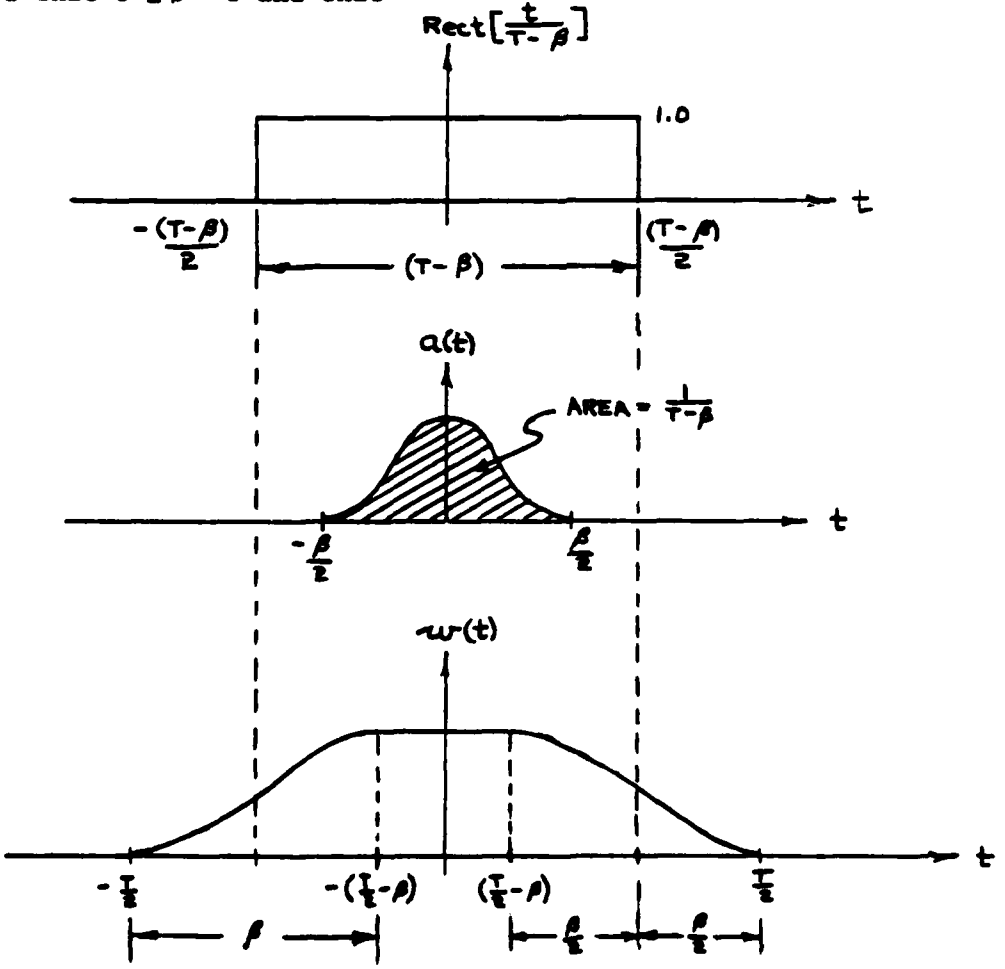

FIG. 3-4 FORMATION OF AN IMPORTANT CLASS OF WINDOWS

$$w(t) = \text{Rect}\left[\frac{t}{T-\beta}\right] \circledast a(t) \tag{3-1-24}$$

$$= \int_{-\frac{(T-\beta)}{2}}^{\frac{(T-\beta)}{2}} a(t-\tau)\, d\tau. \tag{3-1-25}$$

In addition,

$$w(o) = \int_{-\frac{(T-\beta)}{2}}^{\frac{(T-\beta)}{2}} a(\tau)\, d\tau \tag{3-1-26}$$

which evaluates to $\frac{1}{T-\beta}$ when $\beta \leq \frac{T}{2}$. The Fourier Transform of w(t), which is identical to $W_T(\omega)$ in this case, is the product of the transform of Rect $\left[\frac{t}{T-\beta}\right]$ and the transform of a(t). Specifically,

$$W_T(\omega) = W(\omega) = A(\omega) \cdot \frac{2 \sin\left[\frac{(T-\beta)}{2}\omega\right]}{\omega} \tag{3-1-27}$$

where

$$A(\omega) = \int_{-\infty}^{\infty} a(t)\, e^{-j\omega t}\, dt. \tag{3-1-28}$$

Clearly $W_T(\omega)$ has zeroes at the uniformly spaced frequencies

$$\omega = n\left[\frac{2\pi}{T-\beta}\right], \tag{3-1-29}$$

$$n = \pm 1, \pm 2, \ldots, \tag{3-1-30}$$

as well as at the zeroes of $A(\omega)$ as sketched in Figure 3-5.

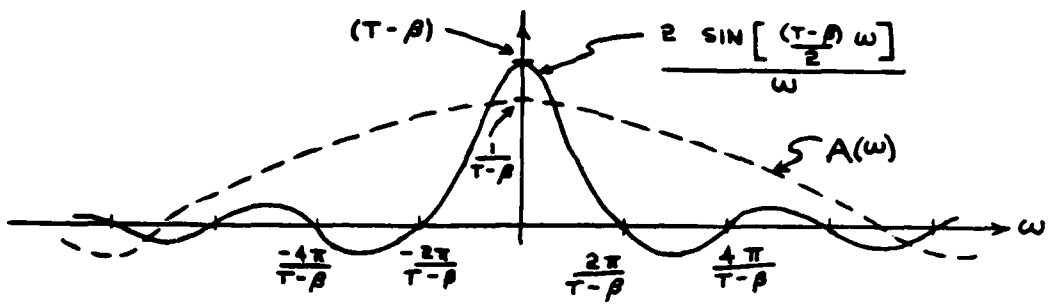

FIG. 3-5 COMPOSITION OF W(ω) AS A PRODUCT OF SOLID AND DASHED LINES

It follows from (3-1-27) and from the $(\frac{1}{T-\beta})$ area property of a(t) given in Figure 3-4 that

$$W_T(0) = 1 \qquad (3\text{-}1\text{-}31)$$

in satisfaction of the orthonormality requirement in (3-1-10). However, in order that (3-1-29) satisfy the orthonormality requirement in (3-1-11), β must be chosen so that

$$\frac{1}{T-\beta} = \frac{Q}{T} \qquad (3\text{-}1\text{-}32)$$

or

$$\beta = T\left(\frac{Q-1}{Q}\right), \qquad (3\text{-}1\text{-}33)$$

where Q is the integer "frequency spacing factor" used previously. Thus the parameter β, which controls the time duration of a(t) and the area under its curve, can be appropriately chosen to ensure the orthonormality of the basis set. The main benefit therefore from using

this class of window functions is that the frequency domain requirements for orthonormality in (3-1-10) and (3-1-11) can be restated as two time domain requirements under the control of the single, adjustable parameter β. Specifically, these time domain requirements are

$$\int_{-\beta/2}^{\beta/2} a(t)\, dt = \frac{1}{T-\beta} \qquad (3\text{-}1\text{-}34)$$

and

$$\beta = T\left(\frac{Q-1}{Q}\right) . \qquad (3\text{-}1\text{-}35)$$

In actual practice, once values for the segment width T and the frequency spacing Q have been given, β can then be determined from (3-1-35) and a suitable symmetric positive function a(t) can be chosen to have area $\frac{1}{T-\beta}$ and duration β. The specific shape of a(t) is a useful design tool and will be discussed later.

As an example of a member of the class, when Q=1, (3-1-35) requires β to vanish. Taking the limit of both sides of (3-1-34) as $\beta \to 0$ gives the requirement that

$$\lim_{\beta \to 0} \int_{-\beta/2}^{\beta/2} a(t)\, dt = \frac{1}{T} \qquad (3\text{-}1\text{-}36)$$

which can be satisfied by setting

$$a(t) = \frac{1}{T}\, \delta(t), \qquad (3\text{-}1\text{-}37)$$

which is the Dirac Delta function with area $\frac{1}{T}$.

Substituting (3-1-37) into (3-1-24), there results

$$w(t) = \frac{1}{T} \text{ Rect } \left[\frac{t}{T}\right] , \qquad (3\text{-}1\text{-}38)$$

the so-called "Rectangular" window. It is interesting to note that by setting Q=1, the smallest possible "frequency spacing" of the basis function in (3-1-5) is achieved. This spacing is $\pm\frac{2\pi}{T}$, $\pm\frac{3\pi}{T}$, $\pm\frac{4\pi}{T}$,...etc.

As another example, when Q=2, (3-1-35) requires that $\beta = \frac{T}{2}$. Examining (3-1-34) for this case, it is found that

$$\int_{-T/4}^{T/4} a(t)\, dt = \frac{2}{T} . \qquad (3\text{-}1\text{-}39)$$

There are many symmetric positive functions a(t) that will satisfy this requirement. One such function is

$$a(t) = \frac{4}{T^2} \text{ Rect } \left[\frac{t}{T/2}\right], \qquad (3\text{-}1\text{-}40)$$

sketched in Figure 3-6.

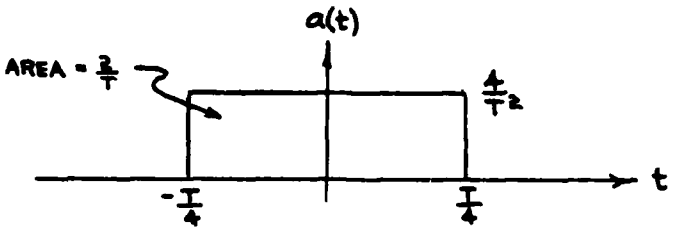

FIG. 3-6 THE FUNCTION a(t) CHOSEN IN (3-1-40)

When (3-1-40) is substituted into (3-1-25) there results

$$w(t) = \int_{-T/4}^{T/4} a(t - \tau)\, d\tau \qquad (3\text{-}1\text{-}41)$$

$$= \begin{cases} \dfrac{4}{T^2} \displaystyle\int_{t-\frac{T}{4}}^{\frac{T}{4}} dt; \; 0 \le t < \dfrac{T}{2} & (3\text{-}1\text{-}42) \\ \dfrac{4}{T^2} \displaystyle\int_{-\frac{T}{4}}^{t+\frac{T}{4}} dt; \; -\dfrac{T}{2} < t \le 0 \, , & (3\text{-}1\text{-}43) \end{cases}$$

where the integration intervals are indicated by the two shaded areas in Figure 3-7.

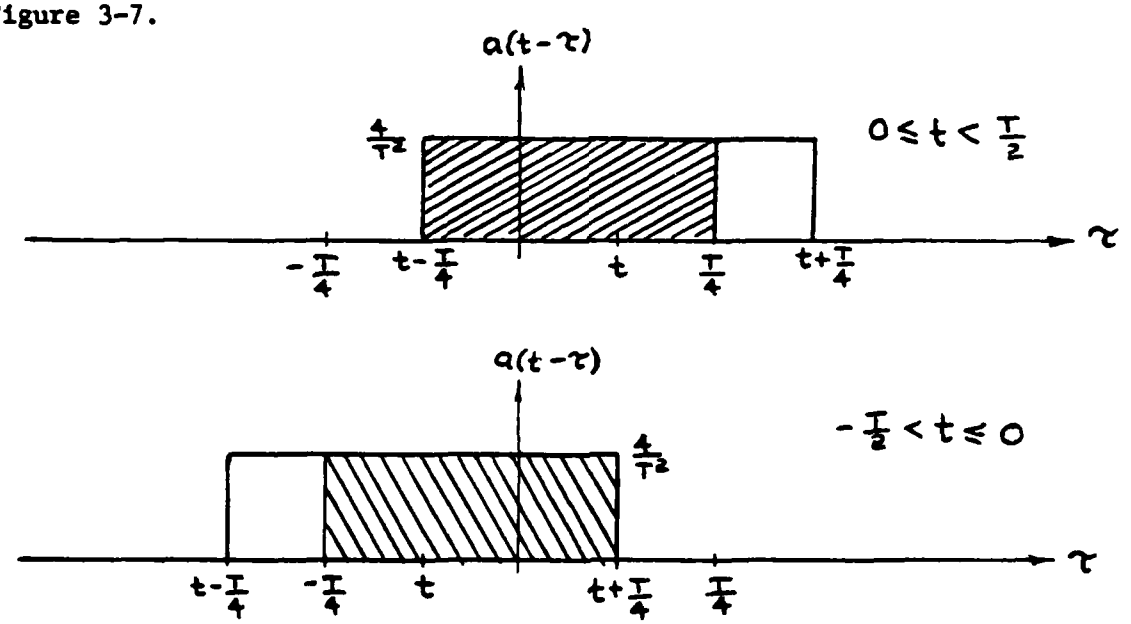

FIG. 3-7 INTEGRATION INTERVALS IN (3-1-42) AND (3-1-43)

Carrying out the integration, it follows that

$$w(t) = \begin{cases} \frac{2}{T}\left(1 - \frac{2t}{T}\right) ; \; 0 \le t < \frac{T}{2} \\ \frac{2}{T}\left(1 + \frac{2t}{T}\right) ; \; -\frac{T}{2} < t \le 0 \end{cases} \qquad (3\text{-}1\text{-}44)$$

$$= \frac{2}{T}\left(1 - \frac{2|t|}{T}\right) ; \; |t| < \frac{T}{2} \qquad (3\text{-}1\text{-}45)$$

which is recognized as just the Bartlett window from (3-1-7). Another function which satisfies (3-1-39) is

$$a(t) = \frac{2\pi}{T^2} \text{ Rect } \left[\frac{t}{T/2}\right] \cos\left(\frac{2\pi}{T} t\right), \qquad (3\text{-}1\text{-}46)$$

as sketched in Figure 3-8.

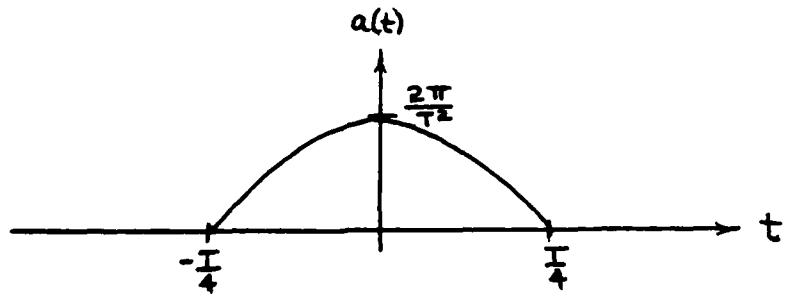

FIG. 3-8 THE FUNCTION a(t) IN (3-1-46)

When (3-1-46) is substituted into (3-1-25) there results

$$w(t) = \int_{-\frac{T}{4}}^{\frac{T}{4}} a(t - \tau)\, d\tau \qquad (3\text{-}1\text{-}47)$$

$$= \begin{cases} \frac{2\pi}{T^2} \int_{t-\frac{T}{4}}^{\frac{T}{4}} \cos\left[\frac{2\pi}{T}(t - \tau)\right] d\tau; \; 0 \le t < \frac{T}{2} \\ \frac{2\pi}{T^2} \int_{-T/4}^{t+\frac{T}{4}} \cos\left[\frac{2\pi}{T}(t - \tau)\right] d\tau; \; -\frac{T}{2} < t \le 0, \end{cases} \qquad (3\text{-}1\text{-}48)$$

where the integration intervals are indicated by the two shaded areas in Figure 3-9.

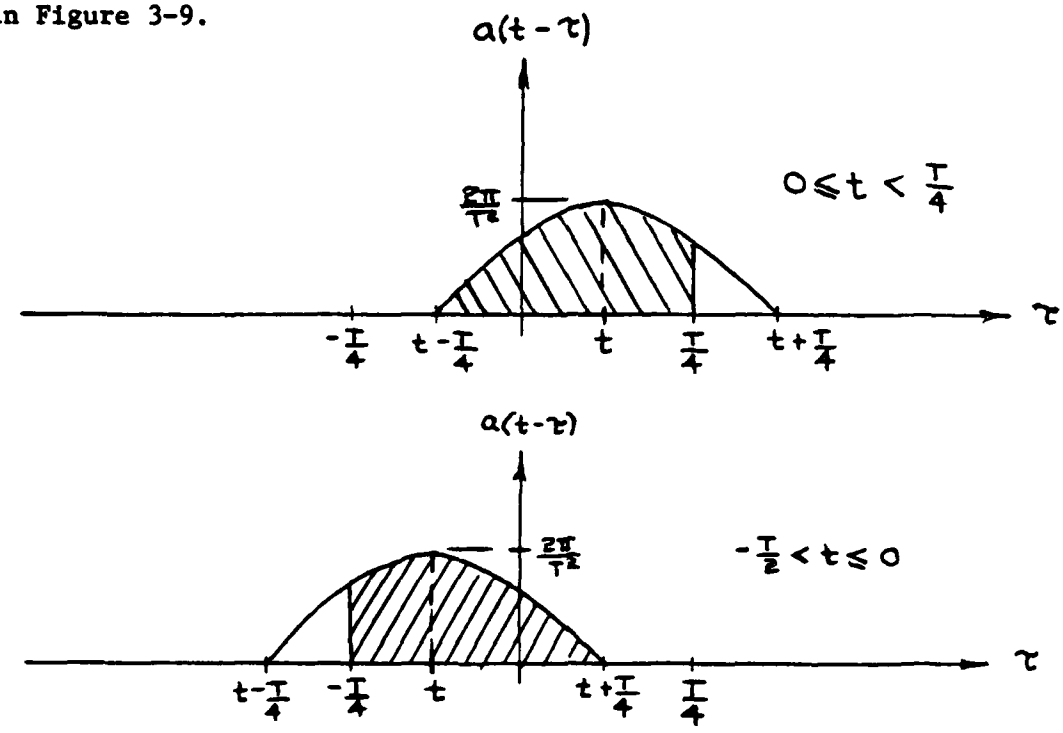

FIG. 3-9 INTEGRATION INTERVAL IN (3-1-48)

When the integration is carried out, it is found that

$$w(t) = \frac{1}{T}\left[1 + \cos\left(\frac{2\pi}{T}t\right)\right], \qquad (3\text{-}1\text{-}49)$$

which is sketched in Figure 3-10.

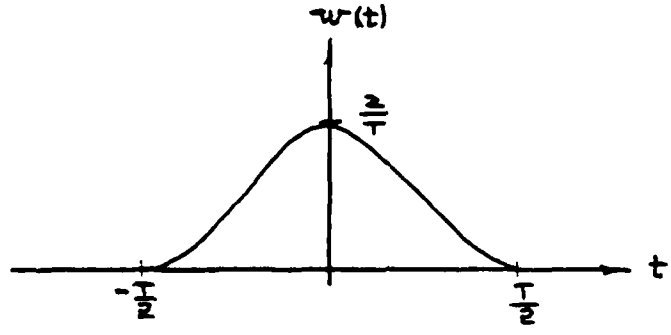

FIG. 3-10 THE "RAISED COSINE" WINDOW OF (3-1-49)

This window is known as the "Raised Cosine" or the "Hanning" window. It is interesting to note that when these windows are used, Q = 2 and the frequency spacing of the basis functions in (3-1-5) becomes $\pm\frac{4\pi}{T}$, $\pm\frac{8\pi}{T}$, $\pm\frac{12\pi}{T}$,...etc.

The frequency spacing factor is an interesting quantity. By inspection of (3-1-5) and (3-1-6), it is evident that the basis functions are shaped cisoidal functions with radian frequency ω_ℓ. The expression for ω_ℓ in (3-1-6) indicates that only integer multiples of the <u>fundamental</u> radian frequency $\frac{2\pi Q}{T}$ are allowable frequencies for the shaped cisoidal functions. Thus the larger the value for Q the larger the fundamental frequency and the larger the <u>difference</u> in frequency between each basis function.

Now that the orthonormality of the basis functions in (3-1-5) has been established and a means for their selection discussed, it is appropriate to consider the goodness of the approximation in (3-1-4). Clearly the quality of the approximation depends upon the choice of coefficients $c_{k\ell}$ and one of the most common criteria of selection is the integrated minimum mean squared error criterion. This criterion requires that the $c_{k\ell}$ be chosen in such a way that the integrated mean squared error,

$$\varepsilon = \int_{t_A}^{t_B} |x(t) - \hat{x}(t)|^2 \, dt \qquad (3\text{-}1\text{-}50)$$

be minimized. Substituting (3-1-4) into (3-1-50), there results

$$\varepsilon = \int_{t_A}^{t_B} |x(t) - \sum_{k=K_s}^{K_f} \sum_{\ell=-M}^{M} c_{k\ell}\ \psi_{k\ell}(t)|^2\ dt \qquad (3\text{-}1\text{-}51)$$

$$= \int_{t_A}^{t_B} |x(t)|^2$$

$$- 2RE\left\{ \sum_{k=K_s}^{K_f} \sum_{\ell=-M}^{M} c_{k\ell} \int_{t_A}^{t_B} x^*(t)\ \psi_{k\ell}\ (t)\ dt \right\}$$

$$+ \sum_{k=K_s}^{K_f} \sum_{\ell=-M}^{M} |c_{k\ell}|^2, \qquad (3\text{-}1\text{-}52)$$

where use was made of the orthonormality of the set $\{\psi_{k\ell}(t)\}$ to derive the last term on the right side of (3-1-52). Since the signal is assumed to be complex in general, the expansion coefficients in the approximation must also be complex in general. Thus,

$$c_{k\ell} = g_{k\ell} + j\ h_{k\ell}\ , \qquad (3\text{-}1\text{-}53)$$

where $g_{k\ell}$ is the real part and $h_{k\ell}$ the imaginary part. Making this substitution in (3-1-52) it is found that

$$\varepsilon = \int_{t_A}^{t_B} |x(t)|^2\ dt$$

$$- 2RE\left\{ \sum_{k=K_s}^{K_f} \sum_{\ell=-M}^{M} (g_{k\ell} + j\ h_{k\ell}) \int_{t_A}^{t_B} x^*(t)\ \psi_{k\ell}(t)\ dt \right\}$$

$$+ \sum_{k=K_s}^{K_f} \sum_{\ell=-M}^{M} (g_{k\ell}^2 + h_{k\ell}^2) \qquad (3\text{-}1\text{-}54)$$

$$= \int_{t_A}^{t_B} |x(t)|^2 \, dt$$

$$- 2 \sum_{k=K_s}^{K_f} \sum_{\ell=-M}^{M} g_{k\ell} \, \mathrm{RE}\left\{ \int_{t_A}^{t_B} x^*(t)\psi_{k\ell}(t) \, dt \right\}$$

$$+ 2 \sum_{k=K_s}^{K_f} \sum_{\ell=-M}^{M} h_{k\ell} \, \mathrm{IM}\left\{ \int_{t_A}^{t_B} x^*(t)\psi_{k\ell}(t) \, dt \right\}$$

$$\sum_{k=K_s}^{K_f} \sum_{\ell=-M}^{M} g_{k\ell}^2 + \sum_{k=K_s}^{K_f} \sum_{\ell=-M}^{M} h_{k\ell}^2 \quad . \qquad (3\text{-}1\text{-}55)$$

It is seen now that ε is actually a function of the two sets of variables $\{g_{k\ell}\}$ and $\{h_{k\ell}\}$ and so the minimization of a two dimensional function $\varepsilon(\{g_{k\ell}\}, \{h_{k\ell}\})$ must be performed. There are two criteria for a true minimum at some point $g_{k\ell} = g_o$ and $h_{k\ell} = h_o$. Specifically,

$$(1) \quad \left.\frac{\partial \varepsilon}{\partial g_{k\ell}}\right|_{(g_o,h_o)} = 0 = \left.\frac{\partial \varepsilon}{\partial h_{k\ell}}\right|_{(g_o,h_o)} \qquad (3\text{-}1\text{-}56)$$

and

$$(2) \quad \left[\left.\frac{\partial^2 \varepsilon}{\partial g_{k\ell}^2}\right|_{(g_o,h_o)}\right]\left[\left.\frac{\partial^2 \varepsilon}{\partial h_{k\ell}^2}\right|_{(g_o,h_o)}\right] > \left[\left.\frac{\partial^2 \varepsilon}{\partial g_{k\ell}\partial h_{k\ell}}\right|_{(g_o,h_o)}\right]^2 \qquad (3\text{-}1\text{-}57)$$

where all partial derivatives are evaluated at the point (g_o, h_o). From (3-1-55) it is seen that, for a specific k and ℓ,

$$\frac{\partial \varepsilon}{\partial g_{k\ell}} = -2RE\left\{\int_{t_A}^{t_B} x^*(t)\ \psi_{k\ell}(t)\ dt\right\} + 2g_{k\ell}, \tag{3-1-58}$$

$$\frac{\partial^2 \varepsilon}{\partial g_{k\ell}^2} = 2 \tag{3-1-59}$$

$$\frac{\partial \varepsilon}{\partial h_{k\ell}} = 2\ IM\left\{\int_{t_A}^{t_B} x^*(t)\psi_{k\ell}(t)\ dt\right\} + 2h_{k\ell}, \tag{3-1-60}$$

$$\frac{\partial^2 \varepsilon}{\partial h_{k\ell}^2} = 2, \tag{3-1-61}$$

and

$$\frac{\partial^2 \varepsilon}{\partial g_{k\ell}\partial h_{k\ell}} = 0. \tag{3-1-62}$$

Imposing the conditions in (3-1-56), it follows that

$$g_{k\ell}\Big|_{(g_o,h_o)} = RE\left\{\int_{t_A}^{t_B} x^*(t)\ \psi_{k\ell}(t)\ dt\right\} \tag{3-1-63}$$

and that

$$h_{k\ell}\Big|_{(g_o,h_o)} = -IM\left\{\int_{t_A}^{t_B} x^*(t)\ \psi_{k\ell}(t)\ dt\right\}, \tag{3-1-64}$$

or, equivalently, that

$$c_{k\ell}\Big|_{(g_o,h_o)} = g_{k\ell}\Big|_{(g_o,h_o)} + j\ h_{k\ell}\Big|_{(g_o,h_o)} \tag{3-1-65}$$

$$= \mathrm{RE}\left\{ \int_{t_A}^{t_B} x^*(t)\psi_{k\ell}(t)\, dt \right\} - j\ \mathrm{IM}\left\{ \int_{t_A}^{t_B} x^*(t)\psi_{k\ell}(t)\, dt \right\} \tag{3-1-66}$$

$$= \mathrm{RE}\left\{ \int_{t_A}^{t_B} x(t)\ \psi_{k\ell}^*(t)\, dt \right\} + j\ \mathrm{IM}\left\{ \int_{t_A}^{t_B} x(t)\psi_{k\ell}^*(t)\, dt \right\} \tag{3-1-67}$$

$$= \int_{t_A}^{t_B} x(t)\ \psi_{k\ell}^*(t)\, dt. \tag{3-1-68}$$

In addition, when (3-1-59), (3-1-61), and (3-1-62) are substituted into condition #2 in (3-1-57), it is found that the expression given in (3-1-68) is a <u>true minimum</u>. This expression is commonly known as the Fourier coefficient of x(t) relative to the orthonormal set $\{\psi_{k\ell}(t)\}$. Taking $c_{k\ell}$ to be defined in this way, that is,

$$c_{k\ell} = \int_{t_A}^{t_B} x(t)\ \psi_{k\ell}^*(t)\, dt, \tag{3-1-69}$$

it follows from (3-1-52) that the minimum error is

$$\varepsilon = \int_{t_A}^{t_B} |x(t)|^2\, dt - 2\mathrm{RE}\left\{ \sum_{k=K_s}^{K_f} \sum_{\ell=-M}^{M} c_{k\ell}\ c_{k\ell}^* \right\} + \sum_{k=K_s}^{K_f} \sum_{\ell=-M}^{M} |c_{k\ell}|^2 \tag{3-1-70}$$

$$= \int_{t_A}^{t_B} |x(t)|^2\, dt - \sum_{k=K_s}^{K_f} \sum_{\ell=-M}^{M} |c_{k\ell}|^2 \tag{3-1-71}$$

The optimum coefficient in (3-1-69) can also be written as

$$c_{k\ell} = \int_{t_k - \frac{T}{2}}^{t_k + \frac{T}{2}} x(t) \sqrt{w(t-t_k)}\, e^{-j2\frac{\pi Q}{T}\ell t}\, dt \qquad (3\text{-}1\text{-}72)$$

which is quite significant in that the coefficient for a given segment centered at $t = t_k$ is <u>completely independent of the signal outside that k^{th} segment</u>. In terms of the approximation $\hat{x}(t)$ in (3-1-4), this means that the $\hat{x}(t)$ function can be viewed as the sum of individual segment approximations. Defining the approximation of the k^{th} individual segment to be $\hat{x}_k(t)$, where

$$\hat{x}_k(t) = \sum_{\ell=-M}^{M} c_{k\ell}\, \psi_{k\ell}(t), \qquad (3\text{-}1\text{-}73)$$

$$k = K_s, K_s + 1, \ldots, K_f, \qquad (3\text{-}1\text{-}74)$$

it follows that the total approximation is

$$\hat{x}(t) = \sum_{k=K_s}^{K_f} \hat{x}_k(t). \qquad (3\text{-}1\text{-}75)$$

The fact that each $\hat{x}_k(t)$ is solely under the influence of the signal $x(t)$ in its own subinterval provides the framework within which the vector space approach is now developed.

It is recalled that the proposed approach concerned the representation of the signal $x(t)$ in each subinterval by a point in a linear vector space. This vector space is now specified as the complex vector

space of piecewise-continuous square integrable functions defined over a particular k^{th} time subinterval. The basis vectors of this space are the complex functions $\psi_{k\ell}(t)$ with k constant so that the factor $\sqrt{w(t-t_k)}$ in (3-1-5) is fixed for the vector space. All the usual vector space properties are valid here as well as the inner product. Specifically, for three vectors $\hat{p}_k(t)$, $\hat{y}_k(t)$, and $\hat{z}_k(t)$ in the space having $p_{k\ell}$, $y_{k\ell}$, and $z_{k\ell}$ as their corresponding Fourier coefficients relative to the set $\{\psi_{k\ell}(t)\}$, the following conditions are satisfied.

(1) Equality Relationships

$$\hat{y}_k(t) = \hat{z}_k(t) \rightleftarrows y_{k1} = z_{k1},\ p_{k2} = y_{k2} + z_{k2}, \ldots . \qquad (3\text{-}1\text{-}76)$$

(2) Sum Relationships

$$\hat{p}_k(t) = \hat{y}_k(t) + \hat{z}_k(t) \rightleftarrows p_{k1} = y_{k1} + z_{k1}, p_{k2} = y_{k2} + z_{k2}, \ldots . \qquad (3\text{-}1\text{-}77)$$

(3) Multiplication by Complex Scalar Relationships. Given the complex number α,

$$\hat{z}_k(t) = \alpha\hat{y}_k(t) \rightleftarrows z_{k1} = \alpha y_{k1},\ z_{k2} = \alpha y_{k2}, \ldots . \qquad (3\text{-}1\text{-}78)$$

(4) Difference Relationships

$$\hat{y}_k(t) - \hat{z}_k(t) = \hat{y}_k(t) + (-1)\ \hat{z}_k(t) . \qquad (3\text{-}1\text{-}79)$$

(5) Zero Vector or Origin Definition

$$\hat{y}_k(t) = 0 \rightleftarrows y_{k1} = 0,\ y_{k2} = 0, \ldots \ . \tag{3-1-80}$$

(6) Inner Product Definition

$$< \hat{y}_k(t),\ \hat{z}_k(t) > = \int_{t_k - \frac{T}{2}}^{t_k + \frac{T}{2}} \hat{y}_k(t)\ \hat{z}_k^*(t)\ dt \tag{3-1-81}$$

$$= \int_{t_k - \frac{T}{2}}^{t_k + \frac{T}{2}} \left[\sum_{\ell=-M}^{M} y_{k\ell}\ \psi_{k\ell}(t)\right]\left[\sum_{m=-M}^{M} z_{km}^*\ \psi_{km}^*(t)\right] dt \tag{3-1-82}$$

$$= \sum_{\ell=-M}^{M} y_{k\ell}\ z_{k\ell}^* \ . \tag{3-1-83}$$

(7) Norm or Length Definition

$$\| \hat{y}_k(t) \| = \left[<y_k(t),\ \hat{y}_k(t)>\right]^{\frac{1}{2}} \tag{3-1-84}$$

$$= \left[\int_{t_k - \frac{T}{2}}^{t_k + \frac{T}{2}} |\hat{y}_k(t)|^2\ dt\right]^{\frac{1}{2}} \tag{3-1-85}$$

$$= \left[\sum_{\ell=-M}^{M} |y_{k\ell}|^2\right]^{\frac{1}{2}} \ . \tag{3-1-86}$$

Also the norm $\| \hat{y}_k(t) - \hat{z}_k(t) \|$ is called the distance between $\hat{y}_k(t)$ and $\hat{z}_k(t)$. It is important to note that the symbol $\hat{y}_k(t)$ represents

the k^{th} segment approximation of the signal y(t) defined over $[t_A, t_B]$ and that

$$y_{k\ell} = \int_{t_A}^{t_B} y(t)\ \psi_{k\ell}^{*}(t)\ dt \qquad (3\text{-}1\text{-}87)$$

represents the corresponding Fourier coefficients.

Using the previously-discussed k^{th} segment approximation $\hat{x}_k(t)$, it follows from (3-1-84) and (3-1-73) that the norm squared of the vector $\hat{x}_k(t)$ is

$$< \hat{x}_k(t),\ \hat{x}_k(t) > = \int_{t_k - \frac{T}{2}}^{t_k + \frac{T}{2}} |x_k(t)|^2\ dt \qquad (3\text{-}1\text{-}88)$$

$$= \int_{t_k - \frac{T}{2}}^{t_k + \frac{T}{2}} \Big| \sum_{\ell=-M}^{M} c_{k\ell}\ \psi_{k\ell}(t) \Big|^2\ dt \qquad (3\text{-}1\text{-}89)$$

$$= \sum_{\ell=-M}^{M} |c_{k\ell}|^2, \qquad (3\text{-}1\text{-}90)$$

a very important result. This states that the <u>energy</u> in the k^{th} approximation, $\hat{x}_k(t)$, as seen in the right side of (3-1-88), is just the sum of its <u>squared components in the vector space</u>, or equivalently, the distance squared from the origin to the vector space <u>point</u> associated with $\hat{x}_k(t)$. This geometric interpretation arises from the fact that the basis vectors, the $\psi_{k\ell}(t)$, are orthonormal. Now, using (3-1-75), the energy in the total approximation, $\hat{x}(t)$, is expressed as

$$\int_{t_A}^{t_B} |x(t)|^2 \, dt = \int_{t_A}^{t_B} \Big| \sum_{k=K_s}^{K_f} \hat{x}_k(t) \Big|^2 \, dt \tag{3-1-91}$$

$$= \sum_{k=K_s}^{K_f} \sum_{m=K_s}^{K_f} \int_{t_A}^{t_B} \hat{x}_k(t) \, \hat{x}_m^*(t) \, dt \tag{3-1-92}$$

$$= \sum_{k=K_s}^{K_f} \int_{t_k-\frac{T}{2}}^{t_k+\frac{T}{2}} |\hat{x}_k(t)|^2 \, dt \tag{3-1-93}$$

$$= \sum_{k=K_s}^{K_f} \sum_{\ell=-M}^{M} |c_{k\ell}|^2 \, . \tag{3-1-94}$$

Thus the energy in the total approximation is the sum of the squared magnitudes of <u>all</u> the individual coefficients $c_{k\ell}$.

These squared magnitude values, the $|c_{k\ell}|^2$ are quite significant in themselves. They represent the energy in each individual <u>building block</u> of the representation, namely, each weighted basis function $c_{k\ell} \, \psi_{k\ell}(t)$. This fact is made evident by considering the energy in an arbitrary building block, that is,

$$\int_{t_A}^{t_B} |c_{k\ell} \, \psi_{k\ell}(t)|^2 \, dt = |c_{k\ell}|^2 \int_{t_A}^{t_B} |\psi_{k\ell}(t)|^2 \, dt = |c_{k\ell}|^2 \, . \tag{3-1-95}$$

But more than this, these $|c_{k\ell}|^2$ values represent a distribution of energy in time and frequency; in time by virtue of the association with the k^{th} segment of the signal, and in frequency by virtue of the association with the ℓ^{th} shaped cisoidal function, $\sqrt{w(t-t_k)} \, e^{j\omega_\ell t}$.

This is strikingly similar to the family of energy spectra produced by the conventional Discrete Fourier Transform application discussed in Section 2.4. Here, however, a theoretical justification has been given for interpreting these values as an energy distribution. In addition, the relative contributions of each shaped cisoidal building block to the energy of the total approximation can now be easily compared.

In terms of the vector space concept, the distribution of energy in time and frequency is seen in the movement of the k^{th} segment approximation of vector $\hat{x}_k(t)$ from one location to another as the index k changes. This movement produces two important pieces of information:

(1) The squared distance from the origin to the point associated with $\hat{x}_k(t)$ may change from the k^{th} time interval to the $(k+1)^{th}$ time interval, where the window function $w(t-t_k)$ in the representation remains the same except for a time shift of T seconds. This indicates a change in energy of the approximation from one subinterval to the next.

(2) As the location of the point associated with $\hat{x}_k(t)$ in the vector space changes, a quantitative indication is given of the changing influence of each basis vector $\psi_{k\ell}(t)$ upon the total approximation. This influence can be measured by the absolute value of the cosine of the angle $\theta_{k\ell}$ between the $\hat{x}_k(t)$ vector and a particular basis vector as illustrated in Figure 3-11. When the approximation vector $\hat{x}_k(t)$ points in nearly the same direction as $\psi_{k\ell}(t)$, the angle $\theta_{k\ell}$ will be very small and the point associated with $\hat{x}_k(t)$ will lie very near to the line along which $\psi_{k\ell}(t)$ lies. Consequently, the influence of $\psi_{k\ell}(t)$ is

expected to be relatively large and this fact is borne out by a measured influence value close to one. This is also true when $\hat{x}_k(t)$ points nearly in the opposite direction to $\psi_{k\ell}(t)$ as well. However, when $\hat{x}_k(t)$ points almost perpendicularly away from a particular $\psi_{k\ell}(t)$ basis vector, the influence of that basis vector will be measured to be very small as expected since $\hat{x}_k(t)$ will now be pointing almost in the same direction as some other basis vector. This other basis vector will now carry the greatest influence with $\hat{x}_k(t)$.

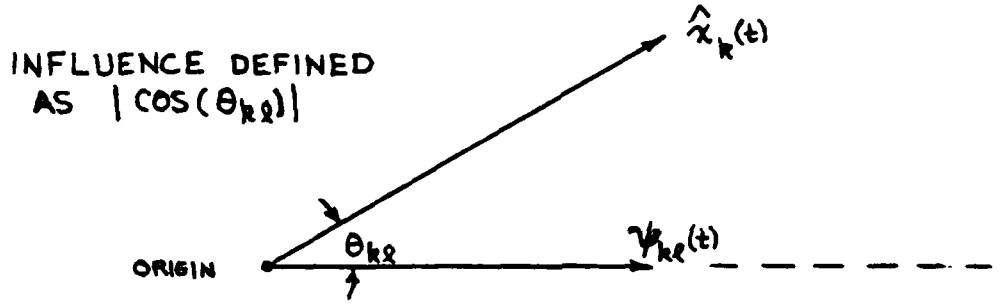

FIG. 3-11 INFLUENCE OF $\psi_{k\ell}(t)$ BASIS VECTOR

Using the energy values $|c_{k\ell}|^2$ previously discussed, the influence of a particular basis vector $\psi_{pm}(t)$ can be expressed as

$$I_{pm} = |\cos(\theta_{pm})| = \sqrt{\frac{|c_{pm}|^2}{\sum_{\ell=-M}^{M} |c_{p\ell}|^2}} \qquad (3\text{-}1\text{-}96)$$

which is just the familiar length ratio of the side adjacent to the hypotenuse in an M dimensional vector space. However, upon closer

inspection, it is recognized that I_{pm} is the magnitude of the complex correlation coefficient between the p^{th} segment approximation $\hat{x}_p(t)$ and the basis vector $\psi_{pm}(t)$. This is seen in the definition of the complex correlation coefficient ρ_{pm} which is

$$\rho_{pm} = \frac{\int_{t_A}^{t_B} \hat{x}_p(t)\ \psi_{pm}^*(t)\ dt}{\sqrt{\int_{t_A}^{t_B} |x_p(t)|^2 dt \int_{t_A}^{t_B} |\psi_{pm}(t)|^2\ dt}}$$

$$= \frac{\sum_{\ell=-M}^{M} c_{p\ell} \int_{t_A}^{t_B} \psi_{p\ell}(t)\ \psi_{pm}^*(t)\ dt}{\sqrt{\left(\sum_{\ell=-M}^{M} |c_{p\ell}|^2\right) \cdot (1)}} \qquad (3\text{-}1\text{-}97)$$

$$= \frac{c_{pm}}{\sqrt{\sum_{\ell=-M}^{M} |c_{p\ell}|^2}} \quad . \qquad (3\text{-}1\text{-}98)$$

Thus the definition of influence in (3-1-96) has a valid interpretation as a measure of how strongly related the approximation vector x(t) is to a particular basis vector.

So far a vector space representation has been described which establishes the justification for interpreting a set of squared magnitude components as a time-frequency energy distribution. The next topic concerns the question of representation error for various window functions.

3.2 Completeness of the Vector Space Representation

By completeness for the representation in shaped cisoidal functions is meant that the approximation error goes to zero as the number of basis vectors is increased without bound. Using the expression for approximation error in (3-1-71) and noting that the integer M controls the number of basis functions in the representation, it follows that the approximation error in the limit is

$$\lim_{M\to\infty} \epsilon_M = \lim_{M\to\infty} \left[\int_{t_A}^{t_B} |x(t)|^2 \, dt - \sum_{k=K_s}^{K_f} \sum_{\ell=-M}^{M} |c_{k\ell}|^2 \right] \tag{3-2-1}$$

$$= \int_{t_A}^{t_B} |x(t)|^2 \, dt - \lim_{M\to\infty} \sum_{k=K_s}^{K_f} \sum_{\ell=-M}^{M} |c_{k\ell}|^2 \, . \tag{3-2-2}$$

The behavior of the second term on the right side of (3-2-2) is now investigated. Using the definition of the coefficient $c_{k\ell}$ in (3-1-69), there results

$$\sum_{k=K_s}^{K_f} \sum_{\ell=-M}^{M} |c_{k\ell}|^2 = \sum_{k=K_s}^{K_f} \sum_{\ell=-M}^{M} \iint_{t_k-\frac{T}{2}}^{t_k+\frac{T}{2}} x(t)x^*(\tau)\psi_{k\ell}^*(t)\psi_{k\ell}(\tau)dtd\tau \tag{3-2-3}$$

$$= \sum_{k=K_s}^{K_f} \iint_{t_k-\frac{T}{2}}^{t_k+\frac{T}{2}} x(t)x^*(\tau) \sum_{\ell=-M}^{M} \psi_{k\ell}^*(t)\psi_{k\ell}(\tau) \, dtd\tau \, . \tag{3-2-4}$$

$$= \sum_{k=K_s}^{K_f} \iint_{t_k-\frac{T}{2}}^{t_k+\frac{T}{2}} x(t) \, x^*(\tau) \sqrt{w(t-t_k)w(\tau-t_k)} \sum_{\ell=-M}^{M} e^{j\frac{2\pi Q}{T}\ell(\tau-t)} dtd\tau. \tag{3-2-5}$$

Now the fact that

$$\sum_{\ell=-\infty}^{\infty} e^{j\frac{2\pi Q}{T}\ell(\tau-t)} = \frac{T}{Q}\sum_{\ell=-\infty}^{\infty}\delta(\tau-t+\frac{\ell T}{Q}) \qquad (3\text{-}2\text{-}6)$$

can be used to determine the limiting form of the right side of (3-2-2). Assuming that the summation and the integration operations can be interchanged, it is found that

$$\lim_{M\to\infty}\sum_{k=K_s}^{K_f}\sum_{\ell=-M}^{M}|c_{k\ell}|^2$$

$$= \sum_{k=K_s}^{K_f}\iint_{t_k-\frac{T}{2}}^{t_k+\frac{T}{2}} x(t)x^*(\tau)\sqrt{w(t-t_k)w(\tau-t_k)}\left[\lim_{M\to\infty}\sum_{\ell=-M}^{M} e^{j\frac{2\pi Q}{T}\ell(\tau-t)}\right]dtd\tau \qquad (3\text{-}2\text{-}7)$$

$$= \frac{T}{Q}\sum_{k=K_s}^{K_f}\iint_{t_k-\frac{T}{2}}^{t_k+\frac{T}{2}} x(t)x^*(\tau)\sqrt{w(t-t_k)w(\tau-t_k)}\sum_{\ell=-\infty}^{\infty}\delta(\tau-t+\frac{\ell T}{Q})\,dtd\tau \qquad (3\text{-}2\text{-}8)$$

$$= \frac{T}{Q}\sum_{k=K_s}^{K_f}\sum_{\ell=-\infty}^{\infty}\iint_{t_k-\frac{T}{2}}^{t_k+\frac{T}{2}} x(t)x^*(\tau)\sqrt{w(t-t_k)w(\tau-t_k)}\,\delta(\tau-t+\frac{\ell T}{Q})dtd\tau \qquad (3\text{-}2\text{-}9)$$

$$= \frac{T}{Q}\sum_{k=K_s}^{K_f}\sum_{\ell=-\infty}^{\infty}\int_{t_k-\frac{T}{2}}^{t_k+\frac{T}{2}} x(t)x^*(t-\frac{\ell T}{Q})\sqrt{w(t-t_k)w(t-t_k-\frac{\ell T}{Q})}\,dt. \qquad (3\text{-}2\text{-}10)$$

Noting that $w(t-t_k)$ is timelimited to the interval $t_k-\frac{T}{2}\le t\le t_k+\frac{T}{2}$ and that $w(t-t_k-\frac{\ell T}{Q})$ is timelimited to the interval

$$-\frac{T}{2} \le t - t_k - \frac{\ell T}{Q} \le \frac{T}{2} \tag{3-2-11}$$

or

$$t_k + \frac{T}{2}\left(\frac{2\ell}{Q} - 1\right) \le t \le t_k + \frac{T}{2}\left(\frac{2\ell}{Q} + 1\right), \tag{3-2-12}$$

it follows that the product $w(t-t_k)w(t - t_k - \frac{\ell T}{Q})$ is zero whenever $|\ell| \ge Q$. Therefore the infinite summation in (3-2-10) becomes a finite summation. Specifically,

$$\lim_{M\to\infty} \sum_{k=K_s}^{K_f} \sum_{\ell=-M}^{M} |c_{k\ell}|^2$$

$$= \frac{T}{Q} \sum_{k=K_s}^{K_f} \sum_{\ell=-(Q-1)}^{Q-1} \int_{t_k - \frac{T}{2}}^{t_k + \frac{T}{2}} x(t)x^*(t - \frac{\ell T}{Q}) \sqrt{w(t-t_k)w(t-t_k - \frac{\ell T}{Q})}\ dt . \tag{3-2-13}$$

This expression can be reduced further by separating the $\ell=0$ term from the other terms in the summation. Specifically, the right side of (3-2-13) is

$$\frac{T}{Q} \sum_{k=K_s}^{K_f} \int_{t_k - \frac{T}{2}}^{t_k + \frac{T}{2}} |x(t)|^2\, w(t-t_k)\ dt$$

$$+ \frac{T}{Q}\left[\sum_{k=K_s}^{K_f} \int_{t_k - \frac{T}{2}}^{t_k + \frac{T}{2}} x(t)x^*(t - \frac{T}{Q}) \sqrt{w(t-t_k)w(t-t_k - \frac{T}{Q}}\ dt \right.$$

$$\left. + \sum_{k=K_s}^{K_f} \int_{t_k - \frac{T}{2}}^{t_k + \frac{T}{2}} x(t)x^*(t + \frac{T}{Q}) \sqrt{w(t-t_k)w(t-t_k + \frac{T}{Q})}\ dt \right]$$

AD-A140 196 A VECTOR SPACE APPROACH TO TIME-VARIANT ENERGY SPECTRAL ANALYSIS(U) ROME AIR DEVELOPMENT CENTER GRIFFISS AFB NY J E ROACH DEC 83 RADC-TR-83-270 2/3

UNCLASSIFIED NL

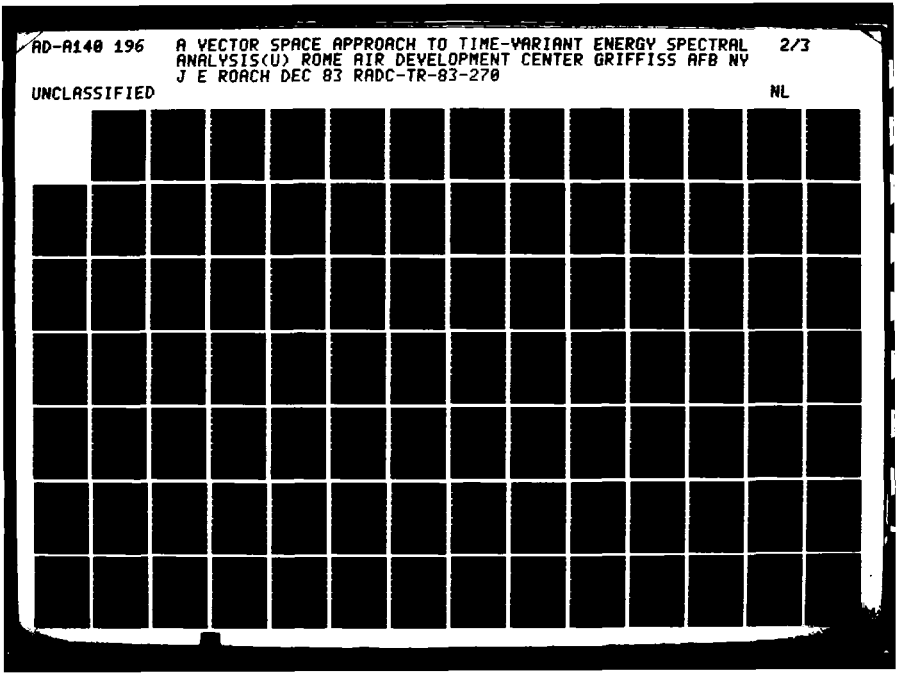

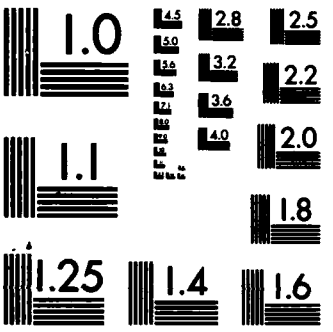

$$+\ldots+\frac{T}{Q}\left[\sum_{k=K_s}^{K_f}\int_{t_k-\frac{T}{2}}^{t_k+\frac{T}{2}} x(t)x^*(t-T+\frac{T}{Q})\sqrt{w(t-t_k w(t-t_k-T+\frac{T}{Q})}\ dt\right.$$

$$\left.+\sum_{k=K_s}^{K_f}\int_{t_k-\frac{T}{2}}^{t_k+\frac{T}{2}} x(t)x^*(t+T-\frac{T}{Q})\ \sqrt{w(t-t_k)w(t-t_k+T-\frac{T}{Q})}\ dt\right], \qquad (3\text{-}2\text{-}14)$$

3-33

where the first term results from $\ell=0$, the first braketed term results when $\ell=\pm1$, and finally the last bracketed term results when $\ell=\pm(Q-1)$. The general term above is

$$\frac{T}{Q}\left[\sum_{k=K_s}^{K_f}\int_{t_k-\frac{T}{2}}^{t_k+\frac{T}{2}} x(t)x^*(t-\frac{\ell T}{Q})\sqrt{w(t-t_k)w(t-t_k-\frac{\ell T}{Q})}\ dt\right.$$

$$\left.+\sum_{k=K_s}^{K_f}\int_{t_k-\frac{T}{2}}^{t_k+\frac{T}{2}} x(t)x^*(t+\frac{\ell T}{Q})\ \sqrt{w(t-t_k)w(t-t_k+\frac{\ell T}{Q})}\ dt\right]. \qquad (3\text{-}2\text{-}15)$$

It is now shown that this general term consists of just a quantity plus its complex conjugate. It is noted immediately that the first quantity within the bracket of (3-2-15) has the product $w(t-t_k)w(t-t_k-\frac{\ell T}{Q})$ under the square root. The two factors in this product are sketched in Figure 3-12 for ℓ a positive integer.

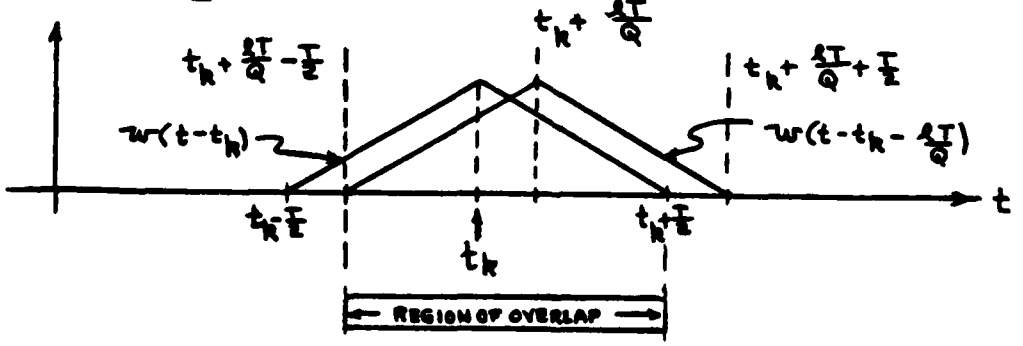

FIG. 3-12 THE PRODUCT $w(t-t_k)\,w(t-t_k-\frac{\ell T}{Q})$ FOR A TYPICAL CASE BARTLETT WINDOW

It is seen from the sketch that the region of overlap is given by

$$t_k + \frac{\ell T}{Q} - \frac{T}{2} \le t \le t_k + \frac{T}{2} \quad , \tag{3-2-16}$$

so that the first quantity within the bracket can have its integration limits changed. Specifically, the first quantity is more properly expressed as

$$\sum_{k=K_s}^{K_f} \int_{t_k - \frac{T}{2} + \frac{\ell T}{Q}}^{t_k + \frac{T}{2}} x(t)x^*(t - \tfrac{\ell T}{Q}) \sqrt{w(t-t_k)w(t-t_k - \tfrac{\ell T}{Q})}\, dt. \tag{3-2-17}$$

Similarly, the second quantity within the bracket of (3-2-15) can be expressed as

$$\sum_{k=K_s}^{K_f} \int_{t_k - \frac{T}{2}}^{t_k + \frac{T}{2} - \frac{\ell T}{Q}} x(t)x^*(t + \tfrac{\ell T}{Q}) \sqrt{w(t-t_k)w(t-t_k + \tfrac{\ell T}{Q})}\, dt, \tag{3-2-18}$$

where Figure 3-13 provides a sketch of the factors in the product $w(t-t_k)w(t-t_k+\frac{\ell T}{Q})$ and the corresponding region of overlap which justifies the change of integration limits.

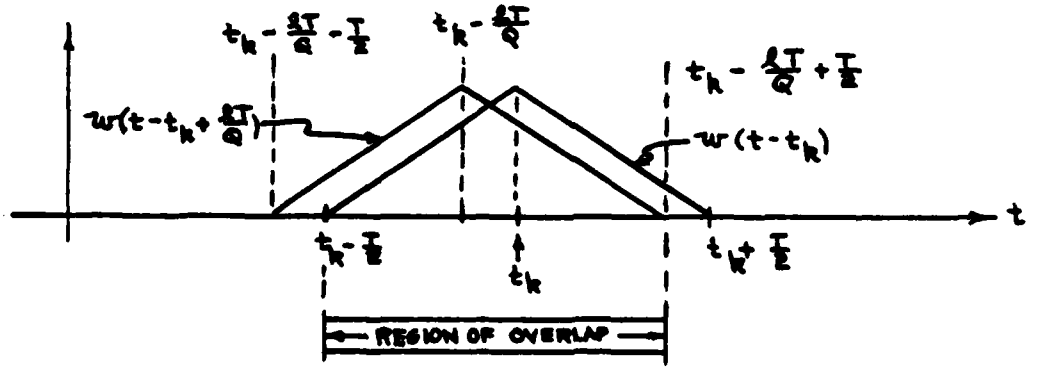

FIG. 3-13 THE PRODUCT OF $w(t-t_k)\,w(t-t_k+\frac{\ell T}{Q})$ FOR A TYPICAL CASE BARTLETT WINDOW

Now the change of variable $\tau = t + \frac{\ell T}{Q}$ can be made in (3-2-18) with the result that the second quantity in (3-2-15) is just

$$\sum_{k=K_s}^{K_f} \int_{t_k-\frac{T}{2}+\frac{\ell T}{Q}}^{t_k+\frac{T}{2}} x(\tau-\tfrac{\ell T}{Q})\, x^*(\tau)\, \sqrt{w(\tau-t_k-\tfrac{\ell T}{Q})w(\tau-t_k)}\, dt$$

$$= \left\{ \sum_{k=K_s}^{K_f} \int_{t_k-\frac{T}{2}+\frac{\ell T}{Q}}^{t_k+\frac{T}{2}} x(\tau)x^*(\tau-\tfrac{\ell T}{Q}) \sqrt{w(\tau-t_k)w(\tau-t_k-\tfrac{\ell T}{Q})}\, d\tau \right\}^*, \tag{3-2-19}$$

which is recognized as the complex conjugate of the first quantity within the bracket as expressed in (3-2-17). Therefore the general term in (3-2-15) is written as

$$\frac{2T}{Q} \mathrm{RE}\left\{ \sum_{k=K_s}^{K_f} \int_{t_k-\frac{T}{2}+\frac{\ell T}{Q}}^{t_k+\frac{T}{2}} x(t)x^*(t-\tfrac{\ell T}{Q}) \sqrt{w(t-t_k)w(t-t_k-\tfrac{\ell T}{Q})}\, dt \right\} \tag{3-2-20}$$

and the result incorporated into (3-2-14) and (3-2-13) to give

$$\lim_{M\to\infty} \sum_{k=K_s}^{K_f} \sum_{\ell=-M}^{M} |c_{k\ell}|^2$$

$$= \frac{T}{Q} \sum_{k=K_s}^{K_f} \int_{t_k-\frac{T}{2}}^{t_k+\frac{T}{2}} |x(t)|^2\, w(t-t_k)\, dt$$

$$+ \frac{2T}{Q} \sum_{k=K_s}^{K_f} \sum_{\ell=1}^{Q=1} \mathrm{RE}\left\{ \int_{t_k-\frac{T}{2}+\frac{\ell T}{Q}}^{t_k+\frac{T}{2}} x(t)x^*(t-\tfrac{\ell T}{Q}) \sqrt{w(t-t_k)w(t-t_k-\tfrac{\ell T}{Q})}\, dt \right\}. \tag{3-2-21}$$

Substituting this back into the limiting form of the approximation error in (3-2-2), it follows that

$$\lim_{M\to\infty} \epsilon_M = \sum_{k=K_s}^{K_f} \int_{t_k-\frac{T}{2}}^{t_k+\frac{T}{2}} |x(t)|^2 \left[1 - \frac{T}{Q} w(t-t_k)\right] dt$$

$$- \frac{2T}{Q} \sum_{k=K_s}^{K_f} \sum_{\ell=1}^{Q-1} RE \left\{ \int_{t_k-\frac{T}{2}+\frac{\ell T}{Q}}^{t_k+\frac{T}{2}} x(t)x^*(t-\tfrac{\ell T}{Q}) \sqrt{w(t-t_k)w(t-t_k-\tfrac{\ell T}{Q})}\, dt \right\}. \quad (3\text{-}2\text{-}22)$$

In general this approximation error reduces to zero only for the Rectangular window given in (3-1-38) for which Q was shown to be unity. Indeed, when Q=1, the second term on the right side of (3-2-22) is non-existent while the first term evaluates to zero for the Rectangular window. Thus the representation error goes to zero and the set of basis functions is complete for the Rectangular window. This holds for arbitrary, finite energy signals x(t). This important result guarantees that whatever representation accuracy is desired may be achieved by using the Rectangular-shaped cisoidal functions. This result is intuitively expected once the Rectangular window case essentially reduces to the ordinary complex Fourier Series expansion applied <u>separately</u> to each timelimited segment of the signal. If, for a finite term approximation, greater accuracy of representation is desired, all that needs to be done is to increase the number of basis functions and calculate the corresponding new coefficients using the Fourier coefficient expression in (3-1-69). The only coefficients that need to be calculated are

those associated with the newly added basis functions. Since the set of basis functions is complete, this procedure guarantees a smaller error of approximation each time it is applied. Thus the rectangular window expansion is an excellent tool for signal representation.

It is interesting to investigate the limiting form of the approximation error in (3-2-22) for <u>non-rectangular windows</u> w(t). First, however, a convenient form for the signal x(t) will be written. Introducing the Rectangular window representation for the signal x(t) as

$$x(t) = \frac{1}{\sqrt{T}} \sum_{k=K_s}^{K_f} \sum_{\ell=-\infty}^{\infty} r_{k\ell}\, e^{j\frac{2\pi}{T}\ell t}, \qquad (3\text{-}2\text{-}23)$$

where the Rectangular-windowed coefficients $r_{k\ell}$ are given by

$$r_{k\ell} = \frac{1}{\sqrt{T}} \int_{t_k-\frac{T}{2}}^{t_k+\frac{T}{2}} x(t)\, e^{-j\frac{2\pi}{T}\ell t}\, dt, \qquad (3\text{-}2\text{-}24)$$

it is possible to substitute this form for the signal x(t) into <u>any</u> expression involving the signal since this representation is complete as discussed above. Accordingly, for the purposes of this discussion, (3-2-23) will be formally substituted into (3-2-22) merely to facilitate a useful form for the non-rectangular windowed approximation error. This does not imply a contradiction since the non-rectangular windowed approximation of x(t) is just being analyzed with the particular x(t) given by (3-2-23). As will be seen, this enables a tractable expression for the approximation error in the non-rectangular case to be developed.

Substituting (3-2-23) into (3-2-22), the following simplification can be made immediately. Since the integrals in (3-2-22) are concerned with values of t in the interval

$$t_k - \frac{T}{2} \le t \le t_k + \frac{T}{2} \quad , \tag{3-2-25}$$

and since, from (3-2-23),

$$x(t) = \frac{1}{\sqrt{T}} \sum_{\ell=-\infty}^{\infty} r_{k\ell}\, e^{j\frac{2\pi}{T}\ell t} \tag{3-2-26}$$

in this interval, (3-2-26) can be used in (3-2-22). There results

$$\lim_{M\to\infty} \epsilon_M = \sum_{k=K_s}^{K_f} \int_{t_k-\frac{T}{2}}^{t_k+\frac{T}{2}} \left|\frac{1}{\sqrt{T}} \sum_{\ell=-\infty}^{\infty} r_{k\ell} e^{j\frac{2\pi}{T}\ell t}\right|^2 \left[1 - \frac{T}{Q}\, w(t-t_k)\right] dt$$

$$- \frac{2T}{Q} \sum_{k=K_s}^{K_f} \sum_{\ell=1}^{Q-1} RE \left\{ \int_{t_k-\frac{T}{2}+\frac{\ell T}{Q}}^{t_k+\frac{T}{2}} \frac{1}{T} \sum_{n=-\infty}^{\infty} \sum_{p=-\infty}^{\infty} r_{kn} r_{kp}^{*} e^{j\frac{2\pi}{T}(nt-pt+\frac{p\ell T}{Q})} \right.$$

$$\left. \cdot \sqrt{w(t-t_k)\, w(t-t_k-\frac{\ell T}{Q})}\; dt \right\}. \tag{3-2-27}$$

The first term on the right side above is more conveniently expressed as

$$\frac{1}{T} \sum_{k=K_s}^{K_f} \sum_{\ell=-\infty}^{\infty} \sum_{i=-\infty}^{\infty} r_{k\ell} r_{ki}^{*} \int_{t_k-\frac{T}{2}}^{t_k+\frac{T}{2}} e^{-j\frac{2\pi}{T}(i-\ell)t}\, dt$$

$$- \frac{1}{Q} \sum_{k=K_s}^{K_f} \sum_{\ell=-\infty}^{\infty} \sum_{i=-\infty}^{\infty} r_{k\ell} r_{ki}^{*} \int_{t_k-\frac{T}{2}}^{t_k+\frac{T}{2}} w(t-t_k)\, e^{-j\frac{2\pi}{T}(i-\ell)t}\, dt, \tag{3-2-28}$$

where interchange of summations and integration operations was assumed possible. Now the integral in the first triple summation of (3-2-28) is just

$$\int_{t_k-\frac{T}{2}}^{t_k+\frac{T}{2}} e^{-j\frac{2\pi}{T}(i-\ell)t}\,dt = T\,\mathrm{sinc}\,(i-\ell) = T\delta_{i,\ell}\,, \qquad (3\text{-}2\text{-}29)$$

so that (3-2-28) becomes

$$\sum_{k=K_s}^{K_f}\sum_{\ell=-\infty}^{\infty}|r_{k\ell}|^2 - \frac{1}{Q}\sum_{k=K_s}^{K_f}\sum_{\ell=-\infty}^{\infty}\sum_{i=-\infty}^{\infty} r_{k\ell}r_{ki}^{*}\int_{t_k-\frac{T}{2}}^{t_k+\frac{T}{2}} w(t-t_k)\,e^{-j\frac{2\pi}{T}(i-\ell)t}\,dt. \qquad (3\text{-}2\text{-}30)$$

Making the change of variable $\tau = t - t_k$, $d\tau = dt$, and noting that $w(\tau)$ has even symmetry about $\tau = 0$ by virtue of its composition in (3-1-24) by convolution of two even functions, (3-2-30) yields

$$\sum_{k=K_s}^{K_f}\sum_{\ell=-\infty}^{\infty}|r_{k\ell}|^2 - \frac{2}{Q}\sum_{k=K_s}^{K_f}\sum_{\ell=-\infty}^{\infty}\sum_{i=-\infty}^{\infty} r_{k\ell}r_{ki}^{*}\,e^{-j\frac{2\pi}{T}(i-\ell)t_k} \cdot \int_0^{T/2} w(\tau)\cos\left[\frac{2\pi}{T}(i-\ell)\tau\right]d\tau. \qquad (3\text{-}2\text{-}31)$$

The first term on the right side of (3-2-31) is the total energy in the signal as expected by careful review of the first term in (3-2-22).

The second term offsets the first term by subtracting a sum of weighted cross products of the Rectangular-windowed coefficients $r_{k\ell}r^*_{ki}$. The second term on the right side of (3-2-27) can be simplified by making the variable change

$$\tau = t - t_k - \frac{\ell T}{2Q}\ , \ d\tau = dt \tag{3-2-32}$$

which gives

$$- \frac{2T}{Q} \sum_{k=K_s}^{K_f} \sum_{\ell=1}^{Q-1} RE \left\{ \int_{t_k - \frac{T}{2} + \frac{\ell T}{Q}}^{t_k + \frac{T}{2}} \frac{1}{T} \sum_{n=-\infty}^{\infty} \sum_{p=-\infty}^{\infty} r_{kn} r^*_{kp}\ e^{j\frac{2\pi}{T}(nt - pt + \frac{p\ell T}{Q})} \right.$$

$$\left. \cdot \sqrt{w(t-t_k)w(t-t_k-\frac{\ell T}{Q})}\ dt \right.$$

$$= - \frac{2}{Q} \sum_{k=K_s}^{K_f} \sum_{\ell=1}^{Q-1} \sum_{n=-\infty}^{\infty} \sum_{p=-\infty}^{\infty} RE \left\{ r_{kn} r^*_{kp}\ e^{-j\frac{2\pi}{T}(p-r)t_k} \right.$$

$$\left. \cdot\ e^{\frac{j\pi(p+n)\ell}{Q}} \int_{-(\frac{T}{2}+\frac{\ell T}{2Q})}^{(\frac{T}{2}-\frac{\ell T}{2Q})} e^{-j\frac{2\pi}{T}(p-n)\tau} \sqrt{w(\tau+\frac{\ell T}{2Q})w(\tau-\frac{\ell T}{2Q})}\ d\tau \right\}, \tag{3-2-33}$$

where interchange of summation and integration was again assumed possible. Now the product $w(\tau+\frac{\ell T}{2Q})w(\tau-\frac{\ell T}{2Q})$ can be shown to have even symmetry about $\tau = 0$. In particular, since $w(t) = w(-t)$ for any t, then

$$w(\tau+\tfrac{T}{4}) = w(-\tau-\tfrac{T}{4}) \tag{3-2-34}$$

and

$$w(\tau - \tfrac{T}{4}) = w(-\tau + \tfrac{T}{4}) \qquad (3\text{-}2\text{-}35)$$

so that

$$w(\tau + \tfrac{T}{4})\, w(\tau - \tfrac{T}{4}) = w(-\tau - \tfrac{T}{4})\, w(-\tau + \tfrac{T}{4}) \qquad (3\text{-}2\text{-}36)$$

$$= w(-\tau + \tfrac{T}{4})\, w(-\tau - \tfrac{T}{4}), \qquad (3\text{-}2\text{-}37)$$

where the right side of (3-2-37) is the same as the right side of (3-2-36) except that the factors are re-ordered. But the right side of (3-2-37) can be expressed as

$$w(-\tau + \tfrac{T}{4})\, w(-\tau - \tfrac{T}{4}) = \left[w(t + \tfrac{T}{4})\, w(t - \tfrac{T}{4}) \right]\Big|_{t=-\tau}, \qquad (3\text{-}2\text{-}38)$$

thus showing that

$$w(\tau + \tfrac{T}{4})\, w(\tau - \tfrac{T}{4}) = \left[w(t + \tfrac{T}{4})\, w(t - \tfrac{T}{4}) \right]\Big|_{t=-\tau} \qquad (3\text{-}2\text{-}39)$$

which proves the even symmetry about $\tau = 0$. This permits the right side of (3-2-33) to be expressed as

$$-\frac{4}{Q} \sum_{k=K_s}^{K_f} \sum_{\ell=1}^{Q-1} \sum_{n=-\infty}^{\infty} \sum_{p=-\infty}^{\infty} \mathrm{RE}\, \{ r_{kn} r_{kp}^{*}\, e^{-j\frac{2\pi}{T}(p-n)t_k}$$

$$\cdot\, e^{j\frac{\pi(p+n)\ell}{Q}} \int_{t}^{(\frac{T}{2} - \frac{\ell T}{2Q})} \sqrt{w(\tau + \tfrac{\ell T}{2Q})\, w(\tau - \tfrac{\ell T}{2Q})}\, \cos\left[\frac{2\pi}{T}(p-n)\tau \right] dt \}. \qquad (3\text{-}2\text{-}40)$$

This equation represents the second term on the right side of (3-2-27) and it can be combined with (3-2-31) which represents the first term on the right side of (3-2-27) to yield a tractable form for the approximation error. Before this is done, the indices $\underline{i}$ and $\underline{\ell}$ in the triple summation in (3-2-31) are re-labeled as $\underline{p}$ and $\underline{n}$, respectively, while the indices in (3-2-40) remain unchanged. In addition, since (3-2-31) is real by virtue of its derivation from the first term on the right side of (3-2-27) it can be brought within the Real Operator, RE{.}. This gives the approximation error as

$$\lim_{M\to\infty} \varepsilon_M = \sum_{k=K_s}^{K_f} \sum_{\ell=-\infty}^{\infty} |r_{k\ell}|^2 - \frac{2}{Q} \sum_{k=K_s}^{K_f} \sum_{n=-\infty}^{\infty} \sum_{p=-\infty}^{\infty} \mathrm{RE}\left[r_{kn} r_{kp}^{*} \, e^{-j\frac{2\pi}{T}(p-n)t_k} \right.$$

$$\int_0^{T/2} w(\tau) \cos\left[\frac{2\pi}{T}(p-n)\tau\right] d\tau$$

$$\left. + 2 \sum_{\ell=1}^{Q-1} e^{j\frac{\pi(p+n)\ell}{Q}} \int_0^{(\frac{T}{2}-\frac{\ell T}{2Q})} \sqrt{w(\tau+\tfrac{\ell T}{2Q}) w(\tau-\tfrac{\ell T}{2Q})} \cos\left[\frac{2\pi}{T}(p-n)\tau\right] d\tau \right] \tag{3-2-41}$$

At this point it is noticed that the triple summation over $\underline{k}$, $\underline{n}$, and $\underline{p}$ above can be separated into two kinds of summations; one for which $n = p$ and one for which $n \neq p$. Performing this separation gives the final form for the approximation error as

$$\lim_{M\to\infty} \varepsilon_M = \sum_{\substack{k=K_s \\ n\neq p}}^{K_f} \sum_{n=-\infty}^{\infty} |r_{kn}|^2 \left\{1 - \frac{2}{Q} \int_0^{T/2} w(\tau)\, d\tau \right.$$

$$- \frac{4}{Q} \sum_{\ell=1}^{Q-1} e^{j\frac{2\pi n\ell}{Q}} \int_0^{\frac{T}{2}(1-\frac{\ell}{Q})} \sqrt{w(\tau+\frac{\ell T}{2Q})w(\tau-\frac{\ell T}{2Q})}\, d\tau\}$$

$$- \frac{2}{Q} \sum_{k=K_s}^{K_f} \sum_{\substack{n=-\infty \\ n\neq p}}^{\infty} \sum_{p=-\infty}^{\infty} RE\Bigg[r_{kn} r_{kp}^{*} e^{-j\frac{2\pi}{T}(p-n)t_k} \{ \int_0^{T/2} w(\tau)\cos[\tfrac{2\pi}{T}(p-n)\tau]d\tau$$

$$+ 2 \sum_{\ell=1}^{Q-1} e^{j\frac{\pi(p+n)\ell}{Q}} \int_0^{\frac{T}{2}(1-\frac{\ell}{Q})} \sqrt{w(\tau+\frac{\ell T}{2Q})w(\tau-\frac{\ell T}{2Q})}\, \cos[\tfrac{2\pi}{T}(p-n)\tau]d\tau \} \Bigg] \quad (3\text{-}2\text{-}42)$$

As an illustrative example, the sinusoidal "burst" signal is considered. Specifically,

$$x(t) = \begin{cases} A\cos\,[\frac{2\pi N}{T}\,t + \phi]; & |t-t_K| \leq \frac{T}{2} \\ 0\ ; & |t-t_K| > \frac{T}{2}\ , \end{cases} \quad (3\text{-}2\text{-}43)$$

where N is a positive integer, A and ϕ are arbitrary finite amplitude and phase, respectively, and t_K is a specific point in time. A sketch is given in Figure 3-14.

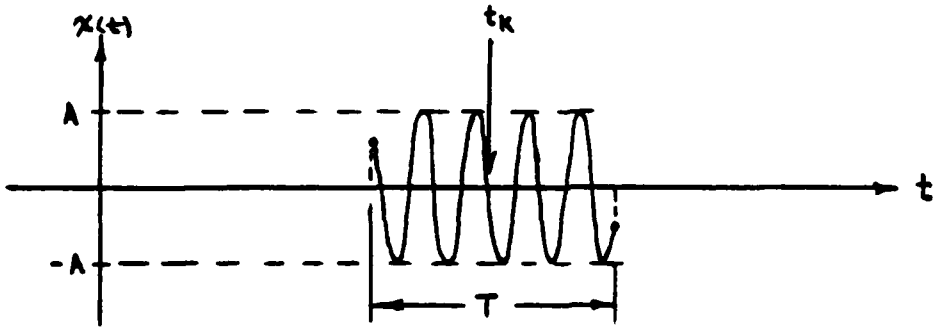

FIG. 3-14 SINUSOIDAL "BURST" CENTERED AT $t = t_K$

Assuming that t_K is the centerpoint of a particular subinterval in the Rectangular windowed expansion of x(t), the coefficients $r_{k\ell}$ in the

Rectangular window expansion are determined from (3-2-24) to be $r_{K\ell} = 0$ for $k \neq K$ and

$$r_{K\ell} = \frac{1}{\sqrt{T}} \int_{t_K - \frac{T}{2}}^{t_K + \frac{T}{2}} x(t)\, e^{-j\frac{2\pi}{T}\ell t}\, dt \qquad (3\text{-}2\text{-}44)$$

$$= \frac{A}{\sqrt{T}} \int_{t_K - \frac{T}{2}}^{t_K + \frac{T}{2}} \cos\left[\frac{2\pi N}{T} t + \phi\right] e^{-j\frac{2\pi}{T}\ell t}\, dt \qquad (3\text{-}2\text{-}45)$$

$$= \frac{A}{2\sqrt{T}} e^{j\phi} \int_{t_K - \frac{T}{2}}^{t_K + \frac{T}{2}} e^{-j\frac{2\pi}{T}(\ell - N)t}\, dt$$

$$+ \frac{A}{2\sqrt{T}} e^{-j\phi} \int_{t_K - \frac{T}{2}}^{t_K + \frac{T}{2}} e^{-j\frac{2\pi}{T}(\ell + N)t}\, dt \qquad (3\text{-}2\text{-}46)$$

$$= \frac{A}{2\sqrt{T}} e^{j\phi}\, e^{-j\frac{2\pi}{T}(\ell-N)t_K} \int_{-T/2}^{T/2} e^{-j\frac{2\pi}{T}(\ell-N)t}\, d\tau$$

$$+ \frac{A}{2\sqrt{T}} e^{-j\phi}\, e^{-j\frac{2\pi}{T}(\ell+N)t_K} \int_{-T/2}^{T/2} e^{-j\frac{2\pi}{T}(\ell+N)t}\, d\tau, \qquad (3\text{-}2\text{-}47)$$

where $\tau = t - t_K$, $d\tau = dt$. Integration yields

$$r_{K\ell} = \frac{A\sqrt{T}}{2} e^{j\phi}\, e^{-j\frac{2\pi}{T}(\ell-N)t_K}\, \text{sinc}\,(\ell-N)t$$

$$+ \frac{A\sqrt{T}}{2} e^{-j\phi}\, e^{-j\frac{2\pi}{T}(\ell+N)t_K}\, \text{sinc}(\ell+N)t \qquad (3\text{-}2\text{-}48)$$

$$= \frac{A\sqrt{T}}{2} e^{j\phi} \delta_{\ell,N} + \frac{A\sqrt{T}}{2} e^{-j\phi} \delta_{\ell,-N} \qquad (3\text{-}2\text{-}49)$$

It is noted that $r_{k\ell} = 0$ for $k \neq K$ since the signal is confined to the K^{th} subinterval. In terms of the vector space concept, the signal is represented by a vector in a two dimensional space with equal length projections along the two basis vectors

$$\psi_{K,\pm N}(t) = \frac{1}{\sqrt{T}} e^{j\frac{2\pi}{T}Nt} \qquad (3\text{-}2\text{-}50)$$

The energy in <u>each</u> component of the signal vector is

$$|r_{k,\pm N}|^2 = \frac{A^2T}{4} \qquad (3\text{-}2\text{-}51)$$

and

$$|r_{k,\ell}|^2 = 0 \text{ for } k \neq K, \ \ell \neq \pm N. \qquad (3\text{-}2\text{-}52)$$

Substituting (3-2-49) into (3-2-42), the approximation error for the window w(t) with its associated frequency spacing factor Q is found to be

$$\lim_{M\to\infty} \varepsilon_M = \frac{A^2T}{2} \{1 - \frac{2}{Q} \int_0^{T/2} w(\tau)\, d\tau$$

$$- \frac{4}{Q} \sum_{\ell=1}^{Q-1} \cos(\frac{2\pi N}{Q}\ell) \int_0^{\frac{T}{2}(1-\frac{\ell}{Q})} \sqrt{w(\tau + \frac{\ell T}{2Q}) w(\tau - \frac{\ell T}{2Q})}\, d\tau\}$$

$$- \frac{A^2T}{Q} \cos(\frac{4\pi}{T} Nt_K)\{\int_0^{T/2} w(\tau) \cos(\frac{4\pi}{T}N\tau)\, d\tau$$

$$+ 2 \sum_{\ell=1}^{Q-1} \int_0^{\frac{T}{2}(1-\frac{\ell}{Q})} \sqrt{w(\tau+\frac{\ell T}{2Q})w(\tau-\frac{\ell T}{2Q})} \cos(\frac{4\pi}{T}N\tau)\, d\tau\} \ . \tag{3-2-53}$$

This is an interesting result because it gives a tractable expression for the approximation error for an arbitrary window provided that the signal is the sinusoidal "burst" of (3-2-43). If the frequency of this sinusoid,

$$f = \frac{N}{T} \ , \tag{3-2-54}$$

were <u>not</u> an integer multiple of $\frac{1}{T}$, then the approximation error would be a complicated function of many coefficients $c_{k\ell}$ but (3-2-42) could still be used to calculate it.

When the Bartlett window, given in (3-1-7), is used in (3-2-53) along with the associated Q value of 2, the approximation error is

$$\frac{A^2T}{2}\{1 - \int_0^{T/2} w(\tau)\, d\tau - 2(-1)^N \int_0^{T/4} \sqrt{w(\tau+\frac{T}{4})w(\tau-\frac{T}{4})}\, d\tau\}$$

$$- \frac{A^2T}{2} \cos(\frac{4\pi}{T}Nt_K)\{\int_0^{T/2} w(\tau) \cos(\frac{4\pi}{T}N\tau)\, d\tau$$

$$+ 2 \int_0^{T/4} \sqrt{w(\tau+\frac{1}{4})w(\tau-\frac{1}{4})} \cos(\frac{4\pi N}{T}\tau)\, d\tau\}$$

$$= \frac{A^2T}{2}\left\{1 - \frac{2}{T}\int_0^{T/2}\left(1-\frac{2\tau}{T}\right)\,d\tau\right.$$

$$\left. - (-1)^N \frac{4}{T}\int_0^{T/4}\sqrt{\left[1 - \frac{2(\tau+\frac{T}{4})}{T}\right]\left[1 + \frac{2(\tau-\frac{T}{4})}{T}\right]}\,d\tau\right\}$$

$$-A^2 \cos\left(\frac{4\pi}{T}Nt_K\right)\left\{\int_0^{T/2}\left[1-\frac{2\tau}{T}\right]\cos\left(\frac{4\pi N}{T}\tau\right)d\tau\right. \qquad (3\text{-}2\text{-}55)$$

$$\left. + 2\int_0^{T/4}\sqrt{\left[1 - \frac{2(\tau+\frac{1}{4}T)}{T}\right]\left[1+\frac{2(\tau+\frac{1}{4}T)}{T}\right]}\cos\left(\frac{4\pi N}{T}\tau\right)\,d\tau\right\}$$

The first bracketed term above is

$$\frac{A^2T}{2}\left\{1 - \frac{2}{T}\int_0^{T/2}d\tau + \frac{4}{T^2}\int_0^{T/2}\tau\,d\tau\right.$$

$$\left. - (-1)^N \frac{8}{T^2}\int_0^{T/4}\sqrt{\left[\frac{T}{2} - (\tau+\frac{T}{4})\right]\left[\frac{T}{2}+(\tau-\frac{T}{4})\right]}\,d\tau\right\}$$

$$= \frac{A^2T}{2}\left\{1 - 1 + \frac{4}{T^2}\left(\frac{T^2}{8}\right)\right.$$

$$\left. -(-1)^N \frac{8}{T^2}\int_0^{T/4}\sqrt{\frac{T^2}{16} - \tau^2}\,d\tau\right\} \qquad (3\text{-}2\text{-}56)$$

$$= \frac{A^2T}{2}\left\{\tfrac{1}{2} -(-1)^N \frac{8}{T^2}\left[\frac{\tau}{2}\sqrt{\frac{T^2}{16} - \tau^2} + \frac{T^2}{32}\arcsin\left(\frac{4\tau}{T}\right)\right]\Bigg|_0^{T/4}\right\} \qquad (3\text{-}2\text{-}57)$$

$$= \frac{A^2T}{2} \{ \tfrac{1}{2} - (-1)^N \frac{\pi}{8} \} \qquad (3\text{-}2\text{-}58)$$

The second bracketed term in (3-2-55) will in general be a function of the value of the integer N and the centerpoint of the signal, t_K. However the first integral in this second bracketed term is evaluated as

$$\int_0^{T/2} [1 - \frac{2\tau}{T}]\cos(\frac{4\pi}{T}N\tau)\, d\tau$$

$$= \int_0^{T/2} \cos(\frac{4\pi N}{T}\tau)\, d\tau - \frac{2}{T}\int_0^{T/2} \tau \cos(\frac{4\pi N}{T}\tau)\, d\tau \qquad (3\text{-}2\text{-}59)$$

$$= \frac{T}{4N} \sin(\frac{4\pi N}{T}\tau)\Big|_0^{T/2}$$

$$- \frac{2}{T}\left[(\frac{T}{4\pi N})\tau \sin(\frac{4\pi N}{T}\tau) + (\frac{T}{4\pi N})^2 \cos(\frac{4\pi N}{T}\tau)\right]\Big|_0^{T/2} \qquad (3\text{-}2\text{-}60)$$

$$= 0. \qquad (3\text{-}2\text{-}61)$$

The second integral within the second bracketed term of (3-2-55) is plotted in Figure 3-15 The specific integral being calculated for positive integer N i.

$$2\int_0^{T/4} \sqrt{[1 - \frac{2(\tau - \frac{T}{4})}{T}][1 + \frac{2(\tau - \frac{T}{4})}{T}]}\, \cos(\frac{4\pi N}{T}\tau)\, d\tau. \qquad (3\text{-}2\text{-}62)$$

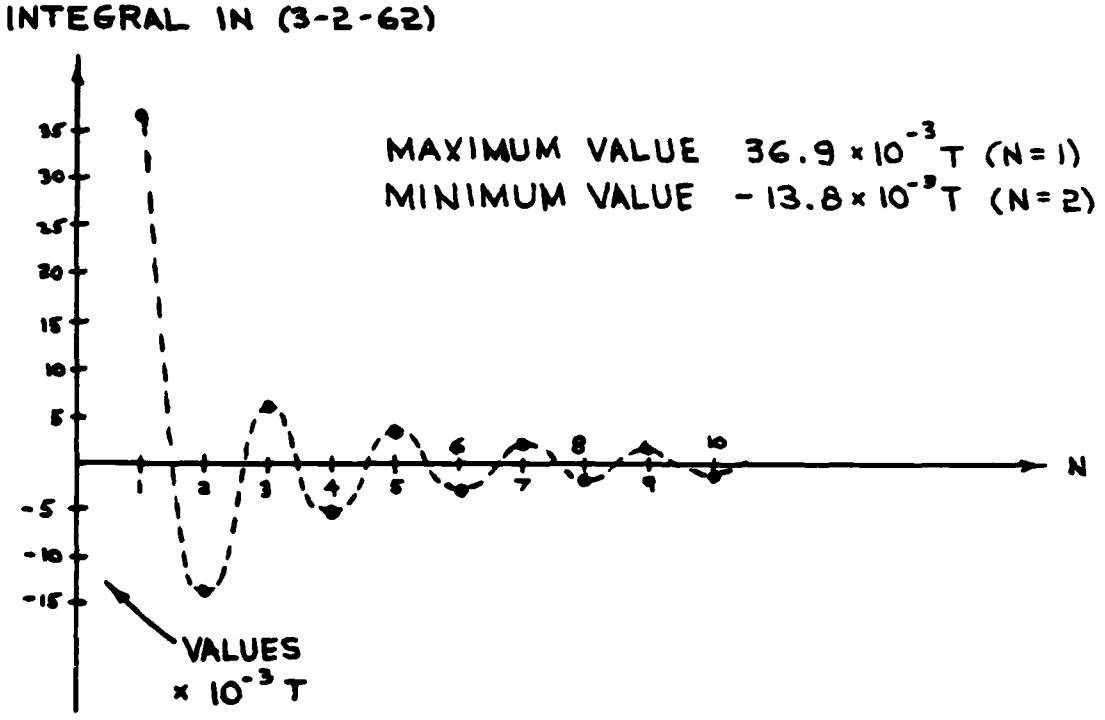

FIG. 3-15 VALUES OF INTEGRAL IN (3-2-62) FOR INTEGER N

It is noted that the dashed curve is given for comparison purposes only. In particular, for $N \geq 10$, the absolute value of the integral is less than 1.3×10^{-3}T. Thus the second bracketed term in (3-2-55) makes a relatively small offset to the first bracketed term in (3-2-55). As shown in Figure 3-15, the maximum value of the integral, 36.9×10^{-3}T, occurs when N = 1. Combining this result with the value of the first bracketed term in (3-2-55) as expressed in (3-2-58), there follows, for N = 1,

$$\lim_{M\to\infty} \varepsilon = \frac{A^2T}{2}\left[\tfrac{1}{2}+\frac{\pi}{8}-0.0738\cos\left(\frac{4\pi}{T}t_K\right)\right] \tag{3-2-63}$$

$$= \begin{cases} \frac{A^2T}{2}(0.819)\ ;\ t_K = \left(\begin{smallmatrix}\text{even}\\ \text{integer}\end{smallmatrix}\right)\cdot\frac{T}{4} \\ \\ \frac{A^2T}{2}(0.967)\ ;\ t_K = \left(\begin{smallmatrix}\text{odd}\\ \text{integer}\end{smallmatrix}\right)\cdot\frac{T}{4}\ . \end{cases} \tag{3-2-64}$$

If the percentage approximation error, P_ε , is defined as the actual approximation error in (3-2-55) divided by the total signal energy which is $\frac{A^2T}{2}$ from (3-2-51), then for N = 1,

$$81.9\% \le P_\varepsilon \le 96.7\% \tag{3-2-65}$$

Similarly, when N = 2, combining the graphical value from Figure 3-15 of $-13.8 \times 10^{-3}T$ with the first bracketed term from (3-2-58) gives the bounds on the percentage approximation error as

$$7.9\% \le P_\varepsilon \le 13.5\%. \tag{3-2-66}$$

Table 3-1 presents the bounds on the percentage approximation error for odd and even values of the integer N up to 14. It is clear from the tabular data as well as the decaying value of the integral in Figure 3-14 that P_ε approaches the limiting form in (3-2-58) of

$$P_\varepsilon = \left(\tfrac{1}{2} - (-1)^N\frac{\pi}{8}\right)\times 100\% = \begin{cases} 10.7\%, \text{ N even} \\ \\ 89.3\%, \text{ N odd} \end{cases} \tag{3-2-67}$$

as N gets larger and larger.

TABLE 3-1

BOUNDS ON PERCENTAGE ERROR, P_e, WITH BARTLETT WINDOW

EVEN N	LOWER BOUND	UPPER BOUND	ODD N	LOWER BOUND	UPPER BOUND
2	7.9%	13.5%	1	81.9%	96.7%
4	9.7	11.7	3	87.8	90.8
6	10.2	11.3	5	88.6	90.0
8	10.4	11.1	7	88.8	89.7
10	10.5	11.0	9	89.0	89.6
12	10.5	10.9	11	89.1	89.5
14	10.6	10.9	13	89.1	89.4

Since (3-2-58) is the dominant term which gives this limiting form, the term in (3-2-55) from which it was derived will be called the primary sinusoidal error term. Specifically, the primary sinusoidal error term, η_p, is defined from the left side of (3-2-55) as

$$\eta_p = \{1 - \int_0^{T/2} w(\tau)d\tau - 2(-1)^N \int_0^{T/4} \sqrt{w(\tau+\tfrac{T}{4})w(\tau-\tfrac{T}{4})}\,d\tau\}. \qquad (3\text{-}2\text{-}68)$$

Similarly, the secondary sinusoidal error term, η_s, is defined as the second bracketed term on the left side of (3-2-55), that is,

$$\eta_s = \{\int_0^{T/2} w(\tau)\cos(\tfrac{4\pi}{T}N\tau)\,d\tau$$

$$+ 2 \int_0^{T/4} \sqrt{w(\tau+\frac{T}{4})w(\tau-\frac{T}{4})}\ \cos(\frac{4\pi N}{T}\tau)d\tau\}. \qquad (3\text{-}2\text{-}69)$$

It is noted that these error terms pertain only to the representation of a sinusoidal burst by non-rectangular windows with associated frequency spacing factors of Q = 2.

It is interesting to consider why the percentage approximation error in (3-2-67) should depend so critically upon the evenness or oddness of N. It is recalled from (3-1-6) that the radian frequencies in a representation with Q = 2 are

$$\omega = 0, \pm \frac{4\pi}{T}, \pm \frac{8\pi}{T}, \ldots . \qquad (3\text{-}2\text{-}70)$$

But the radian frequency of the sinusoid under analysis here is, from (3-2-43), just $\frac{2\pi N}{T}$. Thus when N is an <u>even integer</u>, the frequency of the sinusoidal burst <u>is</u> contained in the set of frequencies while for odd integer N it is not. It should be no surprise then that the percentage approximation error is so high in (3-2-67) for N odd. This effect will always occur when the actual signal contains sinusoidal components whose frequencies are not contained in the set of frequencies of the cisoidal basis functions.

As another example of non-rectangular window approximation error, the Hanning window given in (3-1-49) is considered. Again, Q = 2 and the primary sinusoidal error term is found by substituting (3-1-49) into (3-2-68) which gives

$$\eta_p = 1 - \frac{1}{T}\int_0^{T/2} \left[1 + \cos(\frac{2\pi}{T}\tau)\right] d\tau \qquad (3\text{-}2\text{-}71)$$

$$-2(-1)^N \frac{1}{T} \int_0^{T/4} \sqrt{\{1+\cos[\tfrac{2\pi}{T}(\tau+\tfrac{T}{4})]\}\{1+\cos[\tfrac{2\pi}{T}(\tau-\tfrac{T}{4})]\}}\, d\tau \tag{3-2-71}$$

$$= 1 - \frac{1}{T}\int_0^{T/2} d\tau - \frac{1}{T}\int_0^{T/2} \cos(\tfrac{2\pi}{T}\tau)\, d\tau$$

$$- \frac{2}{T}(-1)^N \int_0^{T/4}$$

$$\sqrt{1+\cos[\tfrac{2\pi}{T}(\tau+\tfrac{T}{4})]+\cos[\tfrac{2\pi}{T}(\tau-\tfrac{T}{4})]+\cos[\tfrac{2\pi}{T}(\tau+\tfrac{T}{4})]\cos[\tfrac{2\pi}{T}(\tau-\tfrac{T}{4})]}\, d\tau. \tag{3-2-72}$$

The quantity under the square root contains the two terms

$$\cos\left[\tfrac{2\pi}{T}(\tau+\tfrac{T}{4})\right] + \cos\left[\tfrac{2\pi}{T}(\tau-\tfrac{T}{4})\right]$$

$$= 2\cos(\tfrac{2\pi}{T}\tau)\cos(\tfrac{\pi}{2}) = 0\,, \tag{3-2-73}$$

where use was made of the fact that, for any θ and ϕ,

$$\cos(\theta+\phi) + \cos(\theta-\phi) = 2\cos\theta\cos\phi. \tag{3-2-74}$$

In addition, the product term under the square root is

$$\cos\left[\tfrac{2\pi}{T}(\tau+\tfrac{T}{4})\right]\cos\left[\tfrac{2\pi}{T}(\tau-\tfrac{T}{4})\right]$$

$$= \tfrac{1}{2}\left[\cos(\tfrac{4\pi}{T}\tau) + \cos(\pi)\right], \tag{3-2-75}$$

where use was made again of the trigonometric identity in (3-2-74).

Substituting these results into (3-2-72), it follows that

$$\eta_p = 1 - \frac{1}{T}\int_0^{T/2} d\tau - \frac{1}{T}\int_0^{T/2} \cos\left(\frac{2\pi}{T}\tau\right)\, d\tau$$

$$- \frac{2}{T}(-1)^N \int_0^{T/4} \sqrt{\tfrac{1}{2}\left[1 + \cos\left(\frac{4\pi}{T}\tau\right)\right]}\, d\tau. \qquad (3\text{-}2\text{-}76)$$

Now, for any θ,

$$\cos\theta = \sqrt{\tfrac{1}{2}\,[1 + \cos 2\theta]}\,, \qquad (3\text{-}2\text{-}77)$$

so that the integral which involves the square root in (3-2-76) is

$$- \frac{2}{T}(-1)^N \int_0^{T/4} \sqrt{\tfrac{1}{2}\left[1 + \cos\left(\frac{4\pi}{T}\tau\right)\right]}\, d\tau$$

$$= - \frac{2}{T}(-1)^N \int_0^{T/4} \cos\left(\frac{2\pi}{T}\tau\right)\, d\tau \qquad (3\text{-}2\text{-}78)$$

$$= - \frac{2}{T}(-1)^N \left(\frac{T}{2\pi}\right) \sin\left(\frac{2\pi}{T}\tau\right)\Bigg|_0^{T/4} \qquad (3\text{-}2\text{-}79)$$

$$= - \frac{(-1)^N}{\pi}\,. \qquad (3\text{-}2\text{-}80)$$

Therefore

$$\eta_p = 1 - (\tfrac{1}{2}) - \frac{1}{T}\left(\frac{T}{2\pi}\right) \sin\left(\frac{2\pi}{T}\tau\right)\Bigg|_0^{T/2} - \frac{(-1)^N}{\pi} \qquad (3\text{-}2\text{-}81)$$

$$= \tfrac{1}{2} - \frac{(-1)^N}{\pi} \qquad (3\text{-}2\text{-}82)$$

$$\approx \begin{cases} 0.182; & N \text{ even} \\ 0.818; & N \text{ odd.} \end{cases} \qquad (3\text{-}2\text{-}83)$$

The secondary sinusoidal error term is found by substituting (3-1-49) into (3-2-69) which gives

$$\eta_s = \frac{1}{T}\int_0^{T/2}\left[1+\cos\left(\frac{2\pi}{T}\tau\right)\right]\cos\left(\frac{4\pi}{T}N\tau\right)\,d\tau$$
$$+\frac{2}{T}\int_0^{T/4}\sqrt{\{1+\cos[\tfrac{2\pi}{T}(\tau+\tfrac{T}{4})]\}\{1+\cos[\tfrac{2\pi}{T}(\tau-\tfrac{T}{4})]\}}\,\cos\left(\frac{4\pi N}{T}\tau\right)d\tau. \qquad (3\text{-}2\text{-}84)$$

The quantity under the square root here is identical to the quantity under the square root in (3-2-71) so that the trigonometric identities in (3-2-73), (3-2-74), and (3-2-75) can be applied again to yeild the result that

$$\sqrt{\{1+\cos[\tfrac{2\pi}{T}(\tau+\tfrac{T}{4})]\}\{1+\cos[\tfrac{2\pi}{T}(\tau-\tfrac{T}{4})]\}}$$
$$=\sqrt{\tfrac{1}{2}\left[1+\cos\left(\frac{4\pi}{T}\tau\right)\right]}. \qquad (3\text{-}2\text{-}85)$$

This can be further simplified by using (3-2-77) which gives

$$\sqrt{\tfrac{1}{2}\left[1+\cos\left(\frac{4\pi}{T}\tau\right)\right]}=\cos\left(\frac{2\pi}{T}\tau\right). \qquad (3\text{-}2\text{-}86)$$

Using these facts in (3-2-84), it is found that

$$\eta_s = \frac{1}{T}\int_0^{T/2}\left[1+\cos\left(\frac{2\pi}{T}\tau\right)\right]\cos\left(\frac{4\pi}{T}N\tau\right)\,d\tau$$
$$+\frac{2}{T}\int_0^{T/4}\cos\left(\frac{2\pi}{T}\tau\right)\cos\left(\frac{4\pi N}{T}\tau\right)\,d\tau \qquad (3\text{-}2\text{-}87)$$

$$= \frac{1}{T}\int_0^{T/4} \cos\left(\frac{4\pi N}{T}\tau\right)\, d\tau + \frac{1}{T}\int_0^{T/2} \cos\left(\frac{2\pi}{T}\tau\right) \cos\left(\frac{4\pi N}{T}\tau\right)\, d\tau$$

$$+ \frac{2}{T}\int_0^{T/4} \cos\left(\frac{2\pi}{T}\tau\right) \cos\left(\frac{4\pi N}{T}\tau\right)\, d\tau \qquad (3\text{-}2\text{-}88)$$

$$= \frac{1}{T}\left(\frac{T}{4\pi N}\right) \sin\left(\frac{4\pi N}{T}\tau\right)\Bigg|_0^{T/2}$$

$$+ \frac{1}{T}\left\{\frac{1}{2}\int_0^{T/2} \cos\left[\frac{2\pi}{T}(2N+1)\tau\right]\, d\tau + \frac{1}{2}\int_0^{T/2} \cos\left[\frac{2\pi}{T}(2N-1)\tau\right]\, d\tau\right.$$

$$\left. + \frac{2}{T}\left\{\frac{1}{2}\int_0^{T/2} \cos\left[\frac{2\pi}{T}(2N+1)\tau\right] d\tau + \frac{1}{2}\int_0^{T/4} \cos\left[\frac{2\pi}{T}(2N-1)\tau\right] d\tau\right\}\right. \qquad (3\text{-}2\text{-}89)$$

$$= \frac{1}{2T}\left\{\frac{T}{2\pi(2N+1)} \sin\left[\frac{2\pi}{T}(2N+1)\tau\right]\Bigg|_0^{T/2}\right.$$

$$\left. + \frac{T}{2\pi(2N-1)} \sin\left[\frac{2\pi}{T}(2N-1)\tau\right]\Bigg|_0^{T/2}\right\}$$

$$+ \frac{1}{T}\left\{\frac{T}{2\pi(2N+1)} \sin\left[\frac{2\pi}{T}(2N+1)\tau\right]\Bigg|_0^{T/4}\right.$$

$$\left. + \frac{T}{2\pi(2N-1)} \sin\left[\frac{2\pi}{T}(2N-1)\tau\right]\Bigg|_0^{T/4}\right\} \qquad (3\text{-}2\text{-}90)$$

$$= \frac{1}{2T}\{0\} + \frac{1}{T}\left\{\frac{(-1)^N T}{2\pi(2N+1)} + \frac{(-1)^{N+1} T}{2\pi(2N-1)}\right\} \qquad (3\text{-}2\text{-}91)$$

$$= \frac{(-1)^N}{2\pi}\left\{\frac{1}{2N+1} - \frac{1}{2N-1}\right\}\ , \qquad (3\text{-}2\text{-}92)$$

or

$$\eta_s = -\frac{(-1)^N}{\pi}\frac{1}{4N^2-1}\ . \qquad (3\text{-}2\text{-}93)$$

Since the left side of (3-2-55) can be written in terms of η_p and η_s as

$$\lim_{M\to\infty} \varepsilon_M = \frac{A^2T}{2} \{\eta_p - \cos(\frac{4\pi N}{T} t_K)\ \eta_s\}, \qquad (3\text{-}2\text{-}94)$$

the Hanning windowed approximation error is found by substituting (3-2-82) and (3-2-93) into (3-2-94). This gives

$$\lim_{M\to\infty} \varepsilon_M = \frac{A^2T}{2} \{\frac{1}{2} - \frac{(-1)^N}{\pi} + \cos(\frac{4\pi N}{T} t_K)\ \frac{(-1)^N}{\pi(4N^2-1)}\} \qquad (3\text{-}2\text{-}95)$$

$$\simeq \frac{A^2T}{2} \{\frac{1}{2} - \frac{(-1)^N}{\pi}\}\ ,\ N > 8\ . \qquad (3\text{-}2\text{-}96)$$

The contribution from η_s, which is the factor multiplying the $\cos(\frac{4\pi N}{T}\ t_K)$ term, is smaller than 1.3×10^{-3} for $N > 8$. Dividing (3-2-96) by the total signal energy, $\frac{A^2T}{2}$, and multiplying by 100%, the percentage approximation error, P_ε, is found for $N > 8$ to be

$$P_\varepsilon = \begin{cases} 18.2\%;\ N \text{ even} \\ 81.8\%;\ N \text{ odd} \end{cases} \qquad (3\text{-}2\text{-}97)$$

where use was made of (3-2-83).

Once again it is seen that the percentage approximation error is quite large for odd N, as expected. Comparing (3-2-97) with (3-2-67), a lower error is obtained for the odd N case while a higher error is obtained for the even N case by the Hanning window over the Bartlett window. This suggests that a trade-off may be made by using certain

windows; one may be willing to suffer a higher approximation error for representing sinusoids with frequencies in the set of represented frequencies (N even) so that a lower representation error may be achieved for sinusoids with frequencies outside the represented set (N odd). Or one may find that the converse of this trade-off is desirable. In any case, the evaluation of η_p and η_s provides a useful figure-of-merit by which representation error may be compared for various non-rectangular windows.

At this point it may be asked, "Why should a non-rectangular windowed expansion be used in the first place if a non-zero signal representation error will always result?" The answer is that although it is true that a non-rectangular windowed basis set is not complete in general and will not generally give zero signal representation error, energy spectral analysis is not primarily concerned with signal representation but with spectral representation. For example, a 10% or even an 89% signal representation error may be tolerable in order to get a more sharply peaked and more steeply graded appearance to the distribution of energy values over frequency. These properties greatly facilitiate the process of estimating the true frequency of a sinusoidal burst, which is of prime importance in spectral analysis. As will be seen in the following examples, the windowed expansions enjoy the benefits of sharp spectral peaks and rapid decay from those peaks. These advantages counterbalance the undesirable aspects of poor signal representation error.

The first example is the plot in Figure 3-16 of the Bartlett windowed expansion coefficients for the case of the sinusoidal burst given by

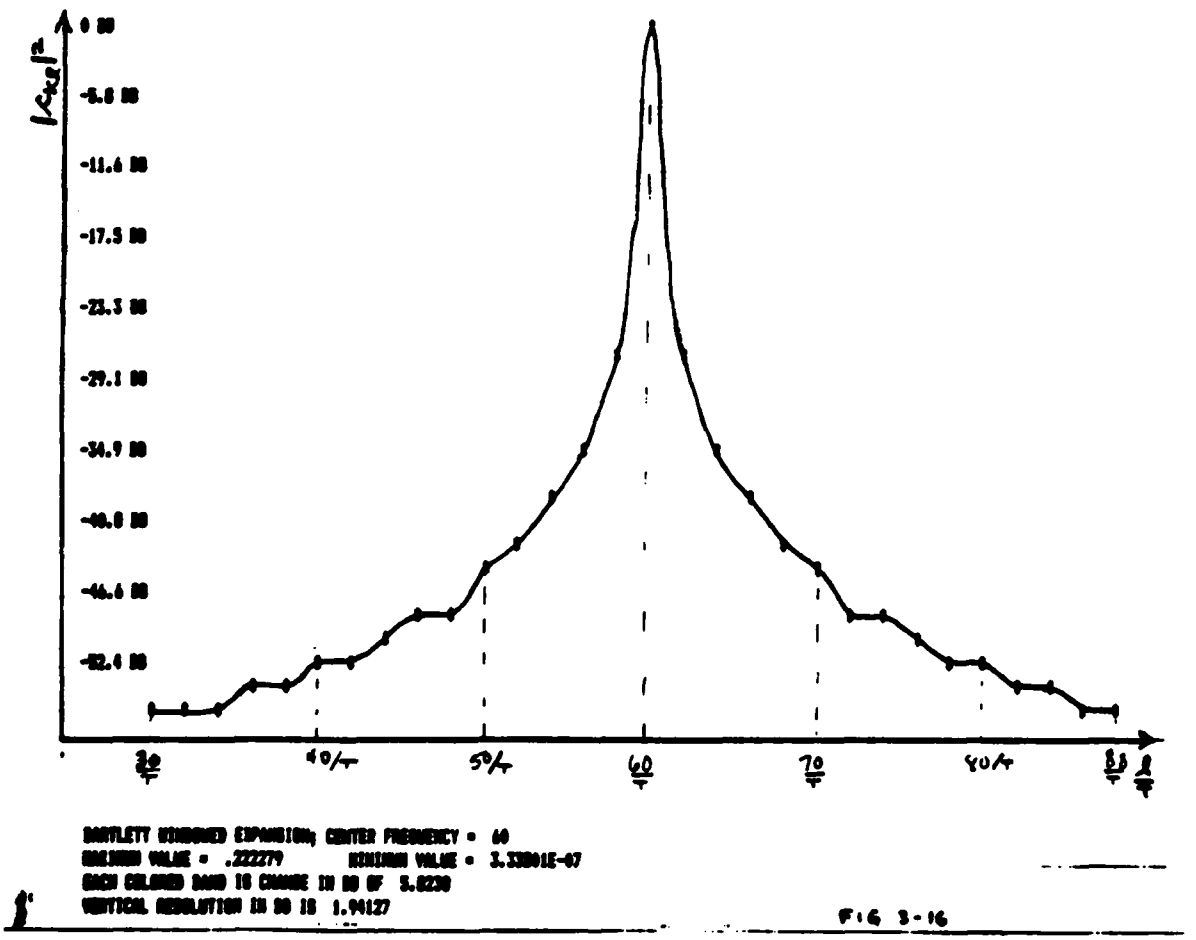

Fig. 3-16 Bartlett Energy Values for 60 Cycle Sinusoid

$$x(t) = \begin{cases} \cos\left[\frac{2\pi(60)}{T}\right]; & |t-t_K| \le \frac{T}{2} \\ 0\ ; & |t-t_K| > \frac{T}{2} \end{cases} \qquad (3\text{-}2\text{-}98)$$

Specifically, the plot shows the normalized values of the energies

$$|c_{K\ell}|^2 = \frac{2}{T}\left|\int_{t_K-\frac{T}{2}}^{t_K+\frac{T}{2}} \sqrt{1-\frac{2|t-t_K|}{T}}\cos\left[\frac{2\pi(60)}{T}\,t\right] e^{-j\frac{4\pi\ell}{T}t}\,dt\right|^2, \qquad (3\text{-}2\text{-}99)$$

which is just the squared magnitude of the expression for the coefficients in (3-1-69) with k = K and the Bartlett "windowed" basis functions

$$\psi_{K\ell}(t) = \begin{cases} \sqrt{\frac{2}{T}}\sqrt{1-\frac{2|t-t_K|}{T}}\; e^{j\frac{4\pi\ell}{T}t}\ ; & |t-t_K| \le \frac{T}{2} \\ 0\ ; & |t-t_K| > \frac{T}{2}\ . \end{cases} \qquad (3\text{-}2\text{-}100)$$

The values of $|c_{K\ell}|^2$ are normalized so that the maximum value is assigned a zero decibel level. Each value is scaled by the rule $10\log_{10}|c_{K\ell}|^2$. It is noted that the maximum energy value occurs as desired at the frequency index of

$$2\ell_{MAX} = 60 \qquad (3\text{-}2\text{-}101)$$

which corresponds to the basis set radian frequency of

$$\omega_\ell = \frac{4\pi\ell_{MAX}}{T} = \frac{2\pi(60)}{T}\ . \qquad (3\text{-}2\text{-}102)$$

Thus there are 60 complete cycles of the sinusoidal burst in the K^{th} segment and the frequency of the sinusoid is represented in the set of basis functions (N is even). In addition the centerpoint of the K^{th} segment, t_K, was chosen so that the sinusoidal burst had either a maximum or a minimum at that point. It is worthwhile to note that the second largest energy values in the plot are smaller than the maximum by about 28 dB and that the decay rate is about 7.8 dB between frequencies 10 and 20 Hz away from the center frequency of 60 Hz. The influence values $I_{k\ell}$ are also plotted for each frequency in the representation in Figure 3-17. The scale for this plot is the logarithmic rule $10 \log_{10} I_{k\ell}$ and therefore the influence values have the same shape in Figure 3-17 as the energy values in Figure 3-16. This is seen in the fact that

$$10 \log_{10} I_{k\ell} = 10 \log_{10} \sqrt{\frac{|c_{k\ell}|^2}{\sum_{p=-M}^{M} |c_{kp}|^2}} \qquad (3\text{-}2\text{-}103)$$

$$= 5 \log |c_{k\ell}|^2 - 5 \log \left(\sum_{p=-M}^{M} |c_{kp}|^2 \right) \qquad (3\text{-}2\text{-}104)$$

which is the same as the plotted energy values, $10 \log_{10} |c_{k\ell}|^2$, except for the different multiplication factor of 5 and the constant offset term, neither of which affect the relative shape of the plot. Therefore the shapes of the energy value plot and the influence value plot will always be the same. It is noted that the smooth curves are drawn

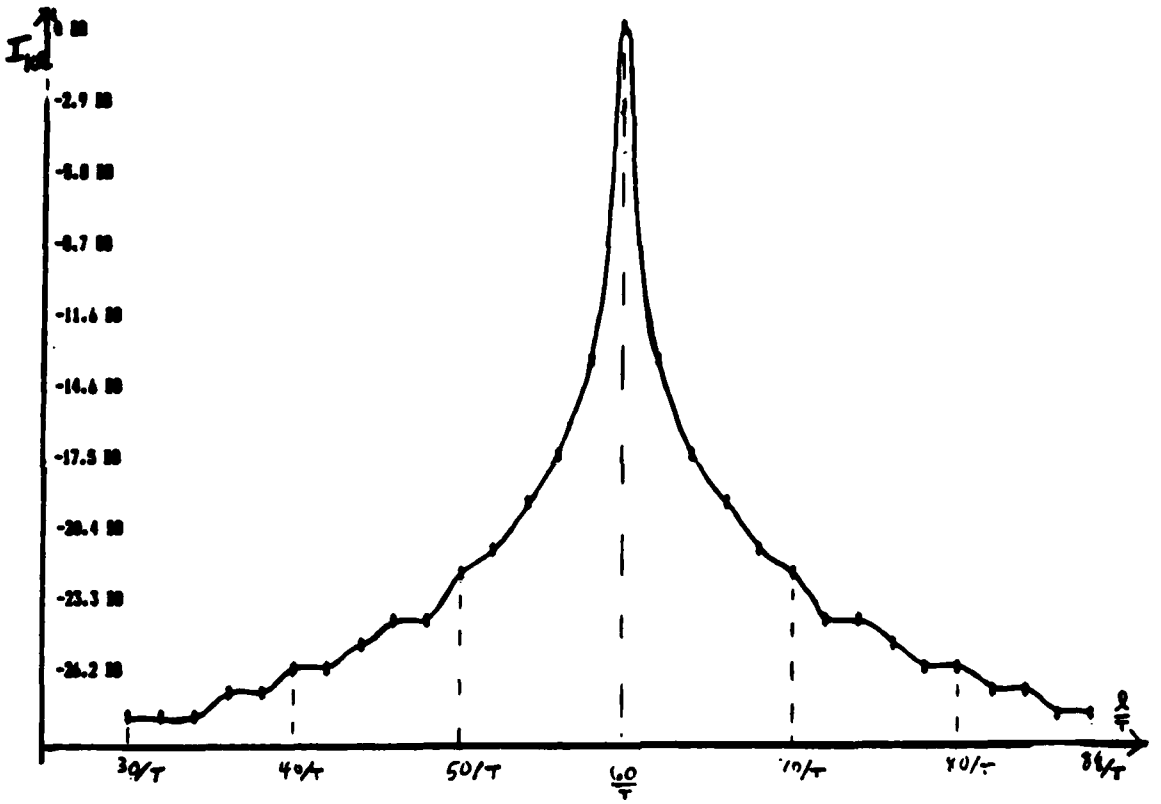

FIG 3-17

Fig. 3-17 Bartlett Influence Values for 60 Cycle Sinusoid

between the points only for ease of comparison and are not to imply a continuum of values for arbitrary frequencies.

A second example is given in Figure 3-18 in which the frequency of a sinusoidal burst is <u>not</u> contained in the set of represented frequencies of the Bartlett windowed expansion. Specifically, the signal is given by

$$x(t) = \begin{cases} \cos\left[\frac{2\pi(61)}{T}\right] \; ; \; |t-t_K| \leq \frac{T}{2} \\ \\ 0 \; ; \; |t-t_K| > \frac{T}{2} \end{cases} \qquad (3\text{-}2\text{-}105)$$

and the plotted values are almost the same as those from (3-2-99) except that the radian frequency of the cosine is $\frac{2\pi(61)}{T}$ instead of $\frac{2\pi(60)}{T}$. It is clear from the plot that there are two maxima, each of which is approximately 15.5 dB above the next lower values and that the decay rate is about 9.2 dB between frequencies of 10 and 20 Hz away from the most significant frequencies of 60 and 62 Hz. Essentially the Bartlett windowed expansion represents this 61-cycle sinusoidal burst with two equally strong <u>shaped</u> sinusoids having 60 and 62 cycles within the T second segment. Here is a case where the "Bartlett window" percentage approximation error in (3-2-67) is very near to 89.3% and yet the spectral representation is still quite good. A more precise description of spectral representation is given by the influence value plot of Figure 3-19. There it is seen that the basis functions with

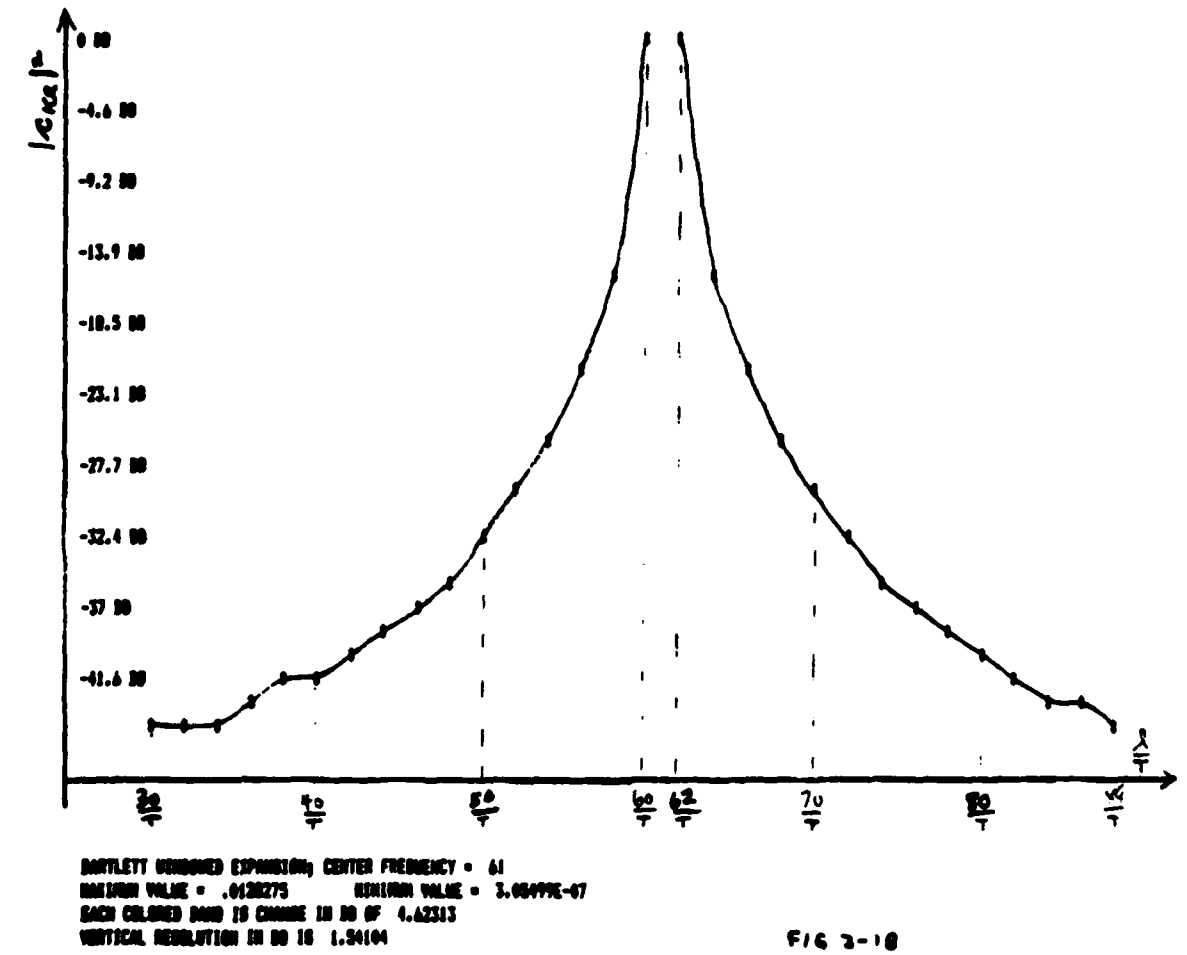

Fig. 3-18 Bartlett Energy Values for 61 Cycle Sinusoid

3-65

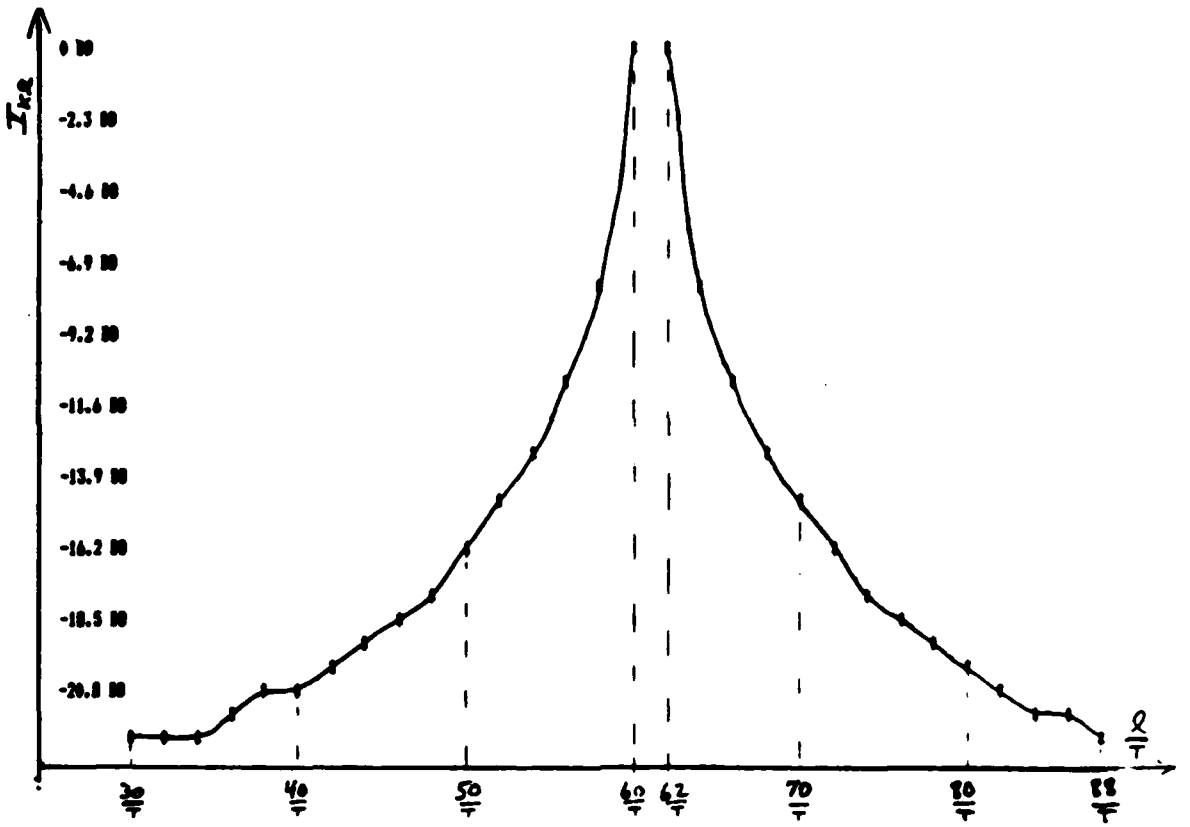

BARTLETT WINDOWED EXPANSION; CENTER FREQUENCY = 61
MAXIMUM VALUE = .490792 MINIMUM VALUE = 2.395145E-03
EACH COLORED BAND IS CHANGE IN DB OF 2.31157
VERTICAL RESOLUTION IN DB IS .770522

FIG 3-19

Fig. 3-19 Bartlett Influence Values for 61 Cycle Sinusoid

60 and 62 cycles within the K^{th} segment have the equal influence of 0.490792 upon the approximation signal (taken from the maximum value data in the block at bottom of the figure). But more significant is the fact that the next lower values of influence are more than 7 dB down from these maxima. This means that the signal is being approximated by essentially two equally weighted basis vectors. It is also important to note the high degree of symmetry about the "correct" frequency of 61 even though it is not represented in the set of plotted points. This gives the distinct impression that a sinusoid with 61 cycles in the segment is the cause of these effects. The influence values plotted for the 60 cycle case in Figure 3-17 also indicate a sharp, central maximum value with next lower values down from the maximum by about 13 dB. In each case, whether the frequency is within the set or not, the influence plots show central maxima which are clearly dominant over all other values and in addition have sharp symmetry properties which strongly imply the correct frequency of the signal. These are certainly desirable spectral characteristics.

Now it should be pointed out that the rectangular windowed expansion is superior in its spectral representation to all non-rectangular windowed expansions when the frequency of the sinusoidal burst under consideration is in the set of represented frequencies. This is evident from (3-2-44) through (3-2-52) which shows that, for integer frequency index N (that is, N cycles in the segment), the set of rectangular windowed coefficients consists of Kronecker Delta functions located at $\ell = \pm N$, the exact frequencies of the sinusoid. Thus

the indication of the true frequency of the signal is unmistakable for this case. However, when the frequency of the sinusoid is not represented in the set of basis functions, the spectral representation by the rectangular windowed expansion is not as "sharply defined" as a non-rectangular expansion such as the Bartlett. By "sharply defined" is meant the two properties of having a narrow width about the maximum value and also having a rapid decay rate or strong slope away from the peak. As an illustration, Figures 3-20 and 3-21 show the rectangular windowed expansion coefficients and associated influence values for a 60.5-cycle sinusoidal burst in the K^{th} segment. Specifically, the signal is

$$x(t) = \begin{cases} \cos\left[\frac{2\pi}{T}(60.5)t\right] ; & |t-t_K| \leq \frac{T}{2} \\ 0 ; & |t-t_K| > \frac{T}{2} \end{cases} \qquad (3\text{-}2\text{-}106)$$

It is interesting that the energy values as well as the influence values for these rectangular windowed coefficients are nicely centered in magnitude about the correct frequency index of 60.5. It should be seen here that the index ranges over all integers as expected from the rectangular windowed basis functions. The second largest values of energy each have magnitudes of about 9.0 dB smaller than the maxima at $\ell = 60$ and $\ell = 61$, and the energy decay rate between frequencies 10 and 20 Hz away from the central "point" of 60.5 Hz on the horizontal axis is about 5.7 dB. Similarly, the influence value plot in Figure 3-21 has its maxima at ℓ=60 and ℓ=61, about 4.4 dB above the next smaller values. The

decay rate is about 2.7 dB in the same region of frequencies measured before. This is not as sharply defined as the Bartlett windowed spectral representation for the same signal. This representation is given in Figures 3-22 and 3-23. The energy values in Figure 3-22 show a single maximum at ℓ=60 although there is a slight skewness to the plot indicated by the single second largest values at 62 Hz. This seems to imply that there may be a strong contribution to the signal's frequency at some idex value to the right of 60 Hz. In addition, the maximum value is more than 20 dB larger than the second largest value, in contrast to the 9.0 dB value found for the rectangular windowed coefficients in Figure 3-20. The decay rate for the Bartlett windowed expansion is also greater; about 9.3 dB of decay between frequencies 10 and 20 Hz away from the 60.5 point as compared to the rectangular windowed value of 5.7 dB. The most significant result here is that the influence values for the Bartlett windowed expansion show a single dominant basis vector of 60 Hz frequency with influence of about 10 db above the next significant basis vector with 62 Hz frequency. It is the magnitude of influence which is desirable here. On the other hand, the rectangular expansion influence values have their maxima only 4.4 dB above the next significant influence values. This shows that the Bartlett windowed expansion is more sharply defined in its spectral representation and, although it suffers from a larger spacing between its frequencies, its strong symmetry and skewness can be used to infer the presence of other frequencies outside the represented set. Thus the spectral representations of windowed expansions like the Bartlett are still quite good even though the associated approximation error may be large.

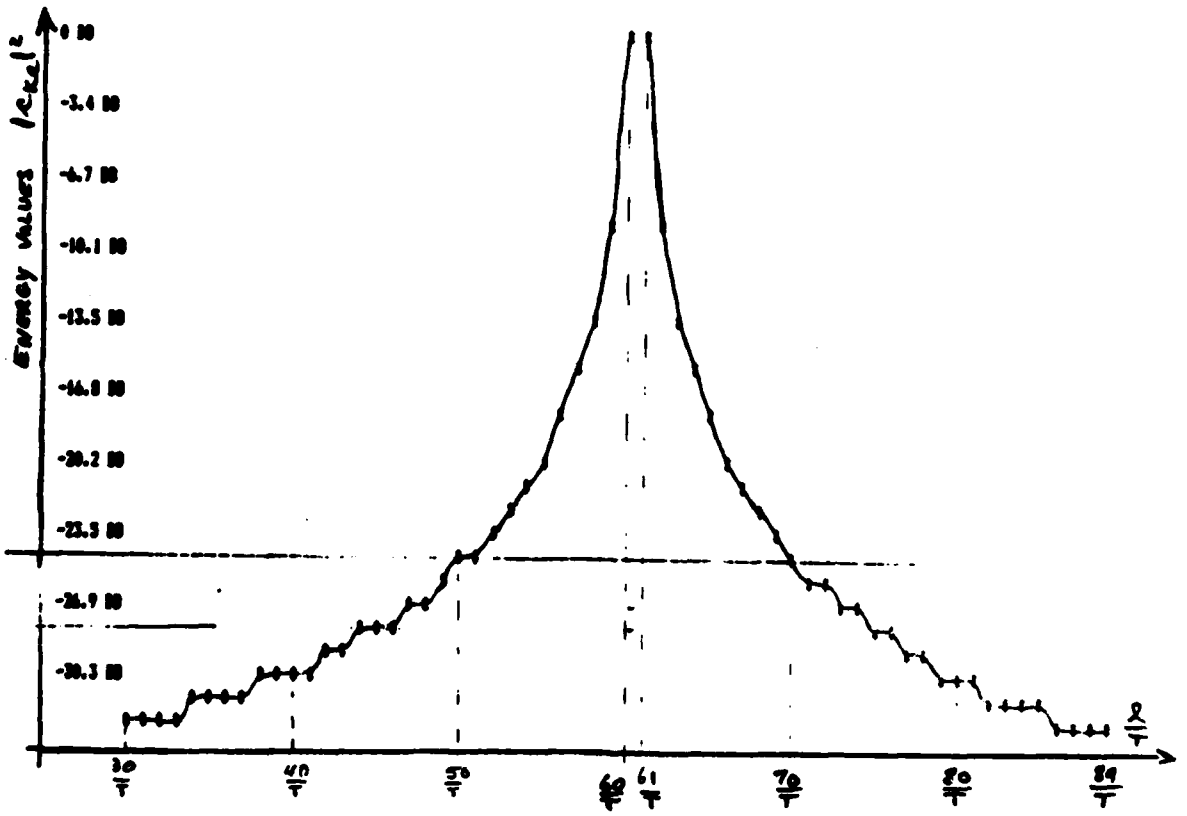

FIG 3-20

Fig. 3-20 Energy Values for Rectangular Windowed Expansion for 60.5 Cycle Sinusoid

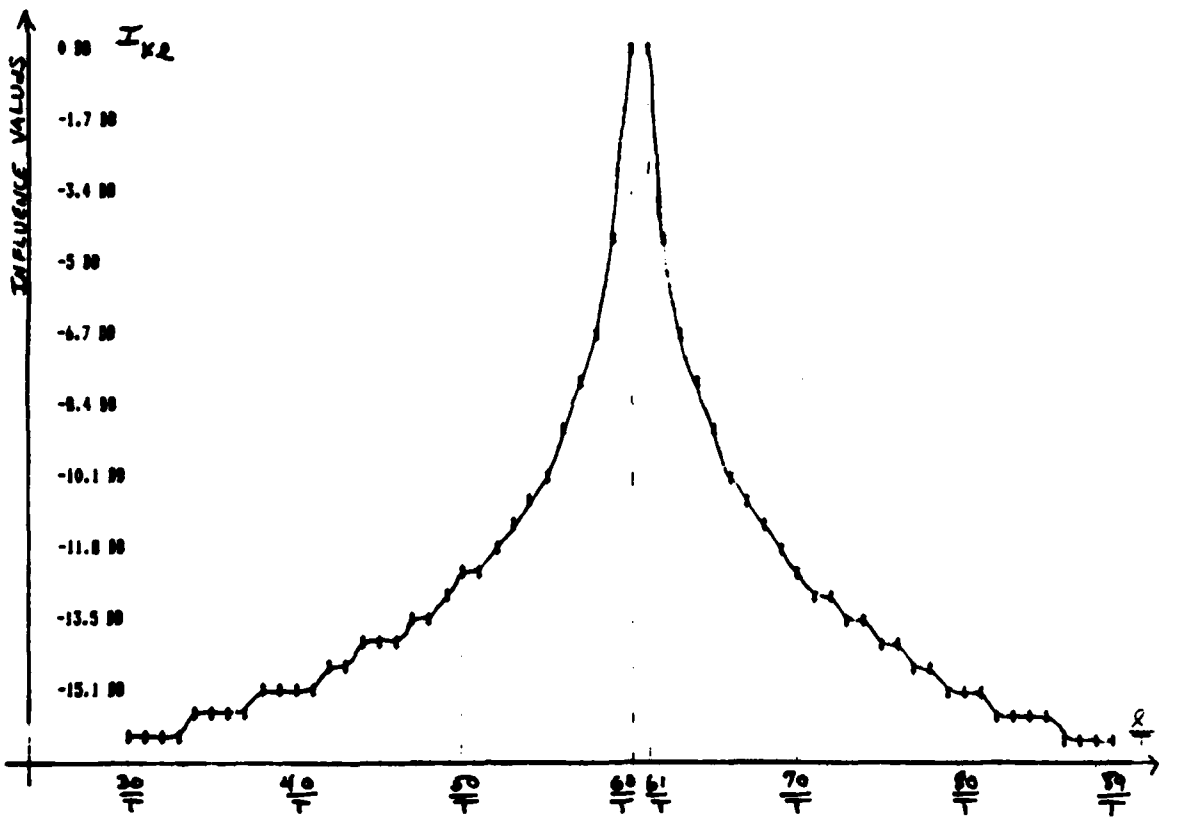

Fig. 3-21 Influence Values for Rectangular Expansion of 60.5 Cycle Sinusoid

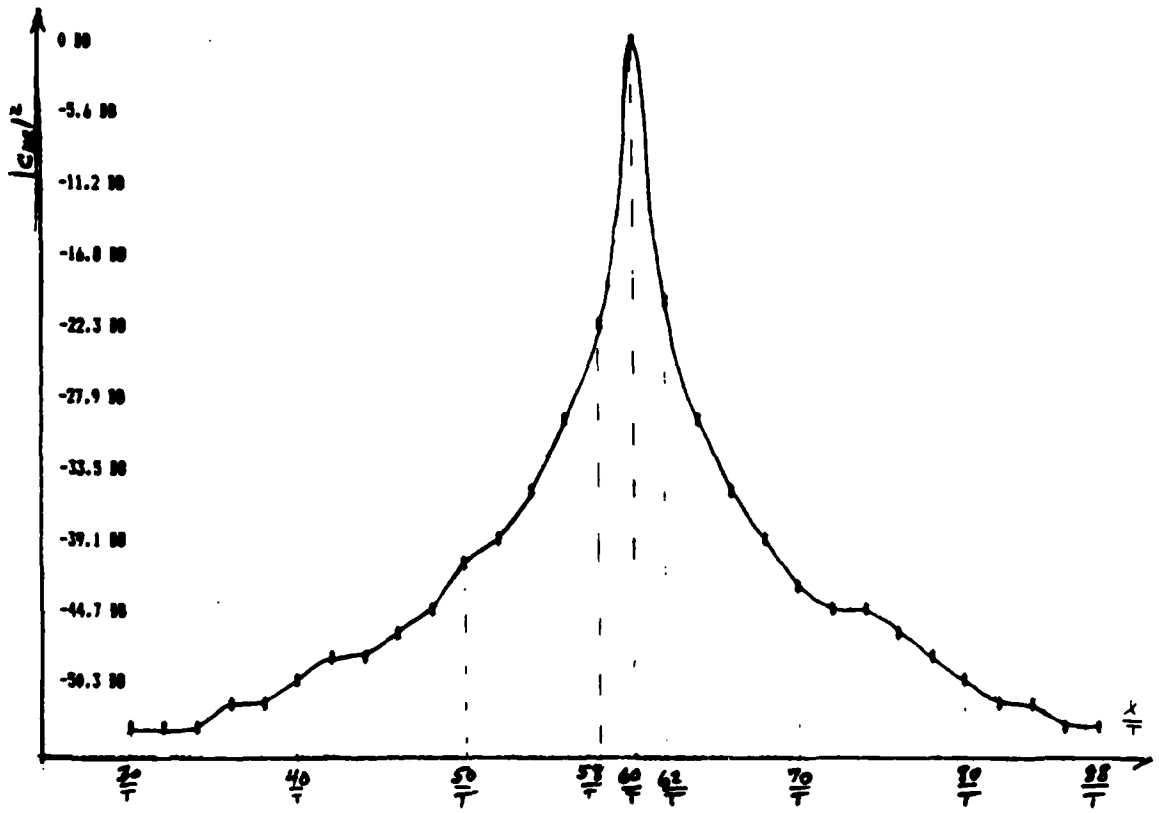

BARTLETT WINDOWED EXPANSION; CENTER FREQUENCY = 60.5
MAXIMUM VALUE = .123296 MINIMUM VALUE = 3.19072E-07
EACH COLORED BAND IS CHANGE IN DB OF 5.58706
VERTICAL RESOLUTION IN DB IS 1.86235

Fig 3-22

Fig. 3-22 Energy Values for Bartlett Expansion of 60.5 Cycle Sinusoid

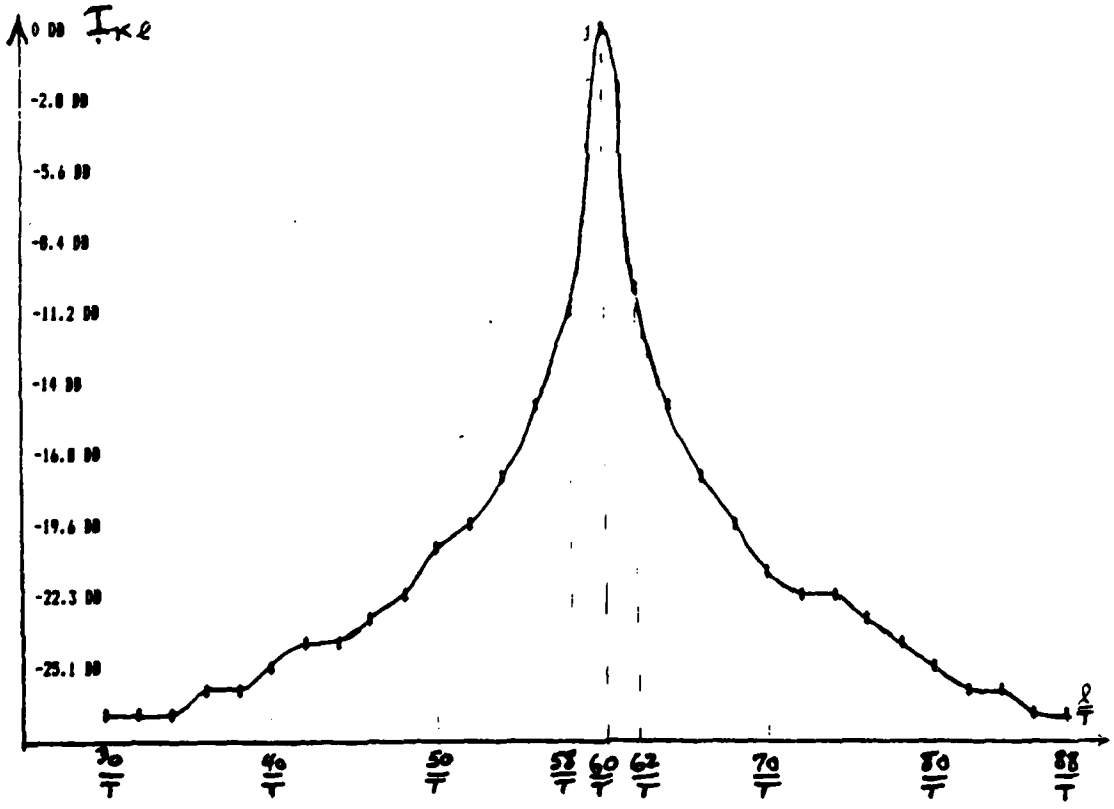

Fig. 3-23 Influence Values for Bartlett Expansion of 60.5 Cycle Sinusoid

It is worthwhile to note that the spectral characteristics of windowed expansions may be adjusted by changing the shape of the function a(t) in (3-1-24) and (3-1-25). It is recalled that this function must be symmetric about t=0 and have duration β and area $\frac{1}{T-\beta}$ where β is given by (3-1-33). The specific shape of a(t) is arbitrary within these limits. As a rule, the broader the "shoulders" of a(t), the narrower the appearance of the maximum value of its Fourier Trasnform, $A(\omega)$. It is this frequency function, $A(\omega)$, that plays an important part in the formation of $W(\omega)$, the Fourier Transform of the window w(t). This is evident in Figure 3-5 which shows that the product of the adjustable function $A(\omega)$ and a fixed function, $2 \sin [\frac{\omega}{2} (T-\beta)]/\omega$, produces $W(\omega)$. From the figure, the adjustable function $A(\omega)$ is a slowly varying "envelope" for the more rapidly varying fixed function. The adjustable function can be constructed to have a specified decay rate and "main lobe" width so that $W(\omega)$ will follow these envelope characteristics. Since the windowed expansions discussed above use the square root of the window, it is the Fourier Transform of $\sqrt{w(t)}$ that produces the spectral representation properties. In any case, the spectral characteristics desired for a windowed expansion can be achieved by judicious choice of the shape of the symmetric function of time, a(t). For most of the commonly used windows, the analytical expression for the Fourier Transform of $\sqrt{w(t)}$ does not exist so that a(t) in (3-1-25) or $A(\omega)$ in (3-1-27) must be adjusted experimentally by computer analysis to accomplish the narrow width and rapid decay specifications desired.

3.3 Relationship of the Vector Space Representation to the Conventional Discrete Fourier Transform Techniques

This section concerns the five questions posed in Section 2.4. Although the answers are implicitly connected with the preceding parts of this chapter, a detailed treatment of them is given here. Each question will be stated follows by its answer.

(1) "What is the relationship between the energy spectrum of the entire signal and the energy spectra of individual subintervals?" The Fourier energy spectrum of a signal x(t) defined over an entire observation interval $[t_A, t_B]$ is the squared magnitude $|X(\omega)|^2$ where

$$X(\omega) = \int_{t_A}^{t_B} x(t)\ e^{-j\omega t}\ dt \tag{3-3-1}$$

and

$$\omega = 2\pi f. \tag{3-3-2}$$

Using the proposed segmentation scheme of Figure 3-1, there results

$$|X(\omega)|^2 = \Big|\sum_{k=K_i}^{K_f} \int_{t_k-\frac{T}{2}}^{t_k+\frac{T}{2}} x(t)\ e^{-j\omega t}dt\Big|^2 \tag{3-3-3}$$

$$= \sum_{k=K_i}^{K_f}\Big|\int_{t_k-\frac{T}{2}}^{t_k+\frac{T}{2}} x(t)e^{-j\omega t}dt\Big|^2 + \sum_{\substack{k=K_i \\ k\neq m}}^{K_f}\sum_{m=K_i}^{K_f} \iint_{t_k-\frac{T}{2};t_m-\frac{T}{2}}^{t_k+\frac{T}{2};t_m+\frac{T}{2}} x(t)x^*(\tau)e^{-j\omega(t-\tau)}dtd\tau \tag{3-3-4}$$

This shows that the sum of the individual segment Fourier energy spectra in the first term on the right side above is not in general equal to the energy spectrum of the entire signal. On the other hand, using the proposed vector space approach, it was shown in (3-1-94) that the energy in the total approximation, $\hat{x}(t)$, is the sum of the energies of the individual basis functions in the expansion. This important result allows the comparison of contributions from each segment to the overall energy distribution. Moreover the vector space approach approximates the signal in a given segment by a vector whose length squared is the energy of the approximation for that segment. As time advances in the signal, another vector is formed to represent the signal in the next segment. Since both vectors are members of the same vector space, their relative orientation indicates the changing influence of different sinusoidal frequencies. On this basis, the frequency distribution of energy in the signal can be said to be changing with time. Thus, the vector space approach provides a clear, useful concept for time-variant spectral analysis. As a specific example, the rectangular windowed expansion reduces to a sampled version which is identical to the unwindowed Discrete Fourier Transform approach of Section 2.4.

(2) "What interpretation should be given to the values of $|X_{DFT}(f_\ell;t_k)|^2$ at arbitrary frequencies f_ℓ?" As mentioned previously in this chapter, the proposed signal expansion is valid only for the discrete radian frequencies in (3-1-6). A physical significance for energy distributed at other frequencies is not possible with this vector space approach. This is consistent with the Heisenberg Uncertainty Principle mentioned in Section 2.3 in that an arbitrarily small

frequency spacing cannot be made for the representation of arbitrarily short time signals. Thus, for the unwindowed case, $|X_{DFT}(f_\ell;t_k)|^2$ in (2-4-6) has the significance of energy only for $f_\ell = \frac{\ell}{T}$. The windowed case will be treated under Question (5) below.

(3) "At what specific frequencies, f_ℓ, should $|X_{DFT}(f_\ell;t_k)|^2$ be used to provide a physical interpretation of a 'time-variant energy spectral density'?" Although an energy density function is a convenient device for visualizing the concentration of energy in frequency, it has the disadvantage of requiring an integration operation to determine actual energy in some band of frequencies. This is a disadvantage because the energy density function must be specified for a <u>continuum</u> of frequencies, which is not possible for an arbitrary length signal segment by the Heisenberg Uncertainty Principle. In addition, the density function approach involves two steps in the calculation of energy; the first step is to calculate the density function itself and the second is to calculate the area under its curve for some given set of frequency limits. In contrast, the vector space approach requires the calculation of expansion coefficients for a <u>discrete</u> set of frequencies--a one step operation. In addition, the valuable <u>influence data</u> is produced for the small extra effort of division by a scale factor and a square root operation as indicated in (3-1-96). Therefore, the vector space approach with its discrete frequencies provides a more economical way than the density function approach for physically interpreting the change of energy with time.

(4) "What are the effects of averaging several sets of $|X_{DFT}(f_\ell;t_k)|^2$ from different time subintervals t_k? That is, what significance can be given to the expression

$$\sum_{k=K_1}^{K_2} |X_{DFT}(f_\ell;t_k)|^2 \text{ ?"} \qquad (3\text{-}3\text{-}5)$$

This expression represents a function of frequency f_ℓ associated with a number of contiguous signal segments centered at t_{K_1}, $t_{K_1+1},\ldots,t_{K_2}$. Based only upon its definition, there is no justification for its interpretation as the energy at an arbitrary frequency f_ℓ due to a sampled signal in the observation interval $[t_{K_1} - \frac{T}{2}, t_{K_2} + \frac{T}{2}]$. However, there is a sound justification for the proposed vector space view of a series of approximation vectors $\hat{x}_{K_1}(t)$, $\hat{x}_{K_2+1}(t),\ldots,\hat{x}_{K_2}(t)$. Each approximation vector has a component along a specific basis vector $\psi_{k\ell}(t)$ which is associated with the discrete frequency f_ℓ and the k^{th} time segment. The squared value of each component <u>is</u> the energy of the approximation for the frequency f_ℓ. These squared values may then be averaged from several approximation vectors to determine an <u>average energy</u> associated with frequency f_ℓ. As mentioned under Question (2) above, only certain equally spaced frequencies qualify for this interpretation. Therefore, in light of the vector space concept proposed here, the expression in (3-3-5) is recognized as the sum of the energies at f_ℓ of the approximation vectors $\hat{x}_{K_1}(t)$, $\hat{x}_{K_1+1}(t),\ldots,\hat{x}_{K_2}(t)$ provided that $X_{DFT}(f_\ell;t_k)$ is interpreted as the sampled version of the expansion coefficient

$$c_{k\ell} = \frac{1}{\sqrt{T}} \int_{t_k - \frac{T}{2}}^{t_k + \frac{T}{2}} x(t)\ e^{-j\omega_\ell t}\ dt\ . \qquad (3\text{-}3\text{-}6)$$

(5) "What interpretation should be given to the family of energy spectra, $|X_{DFT}(f_\ell;t_k)|^2$, when the signal is multiplied by a 'weighting window' before it is transformed?" Outside of the family of windowed expansions proposed here, there is no sound reason why the signal x(t) should be multiplied by an arbitrary window before a Fourier Transformation and then treated as if this process revealed the true frequency distribution of energy. It would seem that this practice would introduce error in general. The typical explanation offered is that the "windowing" process sharpens the spectral representation and facilitates estimation of sinusoidal frequencies present in the signal. Although the end result is good, the approach taken is unjustified. On the other hand, the proposed windowed expansion of a signal in (3-1-4) and (3-1-5) offers a sound vector space approach to the analysis of energy distributed in shaped cisoidal basis functions. The radian frequencies of these basis functions are limited by the rule in (3-1-7) which is

$$\omega_\ell = \frac{2\pi Q}{T}\ \ell \qquad (3\text{-}3\text{-}7)$$

This shows that for larger values of Q, a larger frequency spacing between basis functions is required. In addition, these non-rectangular windowed expansions produce sharp frequency representations which are

adjustable through the symmetric function a(t). Thus only certain frequencies and certain windows are allowed in these basis function expansions. Finally, it should be remembered that the non-rectangular windowed expansions do not in general possess the completeness property but their sharp spectral representations may make their high approximation error tolerable. The problems of energy spectral analysis, which involve many sinusoidal signals of various durations and even frequency modulated sinusoids, can often be made more manageable by taking advantage of the sharp spectral representation properties of non-rectangular windowed expansions. The application of these expansions to several realistic time-variant spectral analysis problems is the subject of Chapter 4.

Chapter 4

APPLICATION OF PROPOSED APPROACH TO TIME-VARIANT SPECTRAL ANALYSIS

In order to apply the vector space concepts of Chapter 3, rationale must be established for choosing the values of the various parameters in the signal expansion, such as the signal subinterval width, T. In addition, means of interpreting the appearance of two-dimensional plots of the energy values $|c_{k\ell}|^2$ must be established. The purpose of this chapter is to develop rationale for choosing the parameters of the expansion and rules-of-thumb for interpreting the plot of $|c_{k\ell}|^2$. Finally a realistic signal example is given as an illustration of time-variant energy spectral analysis. The computer programs used are given in the Appendix.

4.1 Types of Signal Observations

In order to efficiently use the proposed windowed expansions of Chapter 3, the type of signal observation must be clearly recognized. Four types of observations will be defined. For each type, a specific relationship exists between the observed signal and leading and trailing "edges" within the observation. These leading and trailing "edges" will be shown to have a significant effect upon the interpretation of the plotted energy values in the time-frequency plane.

As a first step, the observed signal will be denoted as x(t) but the total signal, which is only partially observed, will be denoted

as y(t). In effect, the observer knows x(t) only. In reality, however, there is a signal y(t) that accounts for both observed and unobserved data. Figure 4-1 clarifies these definitions.

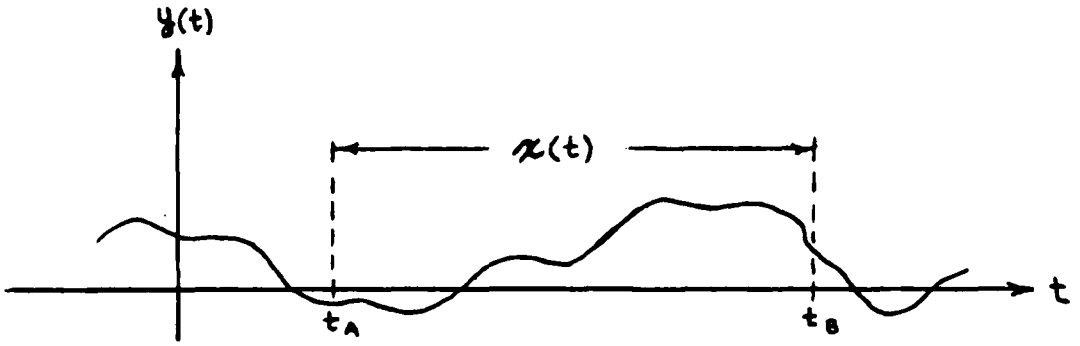

FIG. 4-1 THE OBSERVED SIGNAL, x(t), AND THE TOTAL SIGNAL y(t)

The total signal y(t) is assumed to be square integrable and to have the same smoothness properties of x(t) mentioned in Chapter 1. Again it is emphasized that x(t) is defined only during the observation interval $[t_A, t_B]$; the signal x(t) is all that is available for analysis. As in Figure 3-1 of Chapter 3, the observation interval is partitioned into N subintervals each of width T.

In order to define the four types of observations, the following terms are needed.

(1) Leading Edge point. Consider a time instant t_{LE}. If there exist a time t_1 and a time t_2 where

$$t_A \leq t_1 < t_{LE} < t_2 \leq t_B, \tag{4-1-1}$$

such that

$$\text{(a)}\quad x(t) = 0 \text{ for all } t \in [t_1, t_{LE}] \tag{4-1-2}$$

and

$$\text{(b)}\quad x(t) \neq 0 \text{ for all } t \in (t_{LE}, t_2], \tag{4-1-3}$$

then t_{LE} is a leading edge point of x(t). Figure 4-2 illustrates this idea. It is noted that $x(t_{LE}) = 0$, a characteristic of leading edge points.

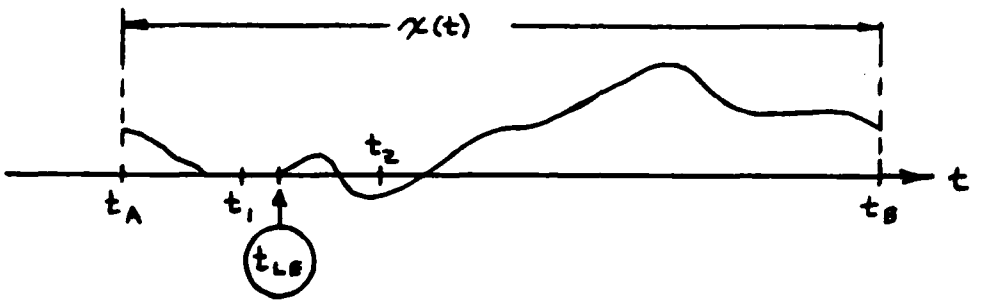

FIG. 4-2 EXAMPLE OF LEADING EDGE POINT

(2) Trailing Edge point. Consider a time instant t_{TE}. If there exist a time t_3 and a time t_4 where

$$t_A \leq t_3 < t_{TE} < t_4 \leq t_B, \tag{4-1-4}$$

such that

$$\text{(a)}\quad x(t) \neq 0 \text{ for all } t \in [t_3, t_{TE}) \tag{4-1-5}$$

and

(b) $x(t) = 0$ for all $t \in [t_{TE}, t_4]$, (4-1-6)

then t_{TE} is a trailing edge point of $x(t)$. Figure 4-3 illustrates the idea. It is noted that $x(t_{TE}) = 0$ which holds for all trailing edge points.

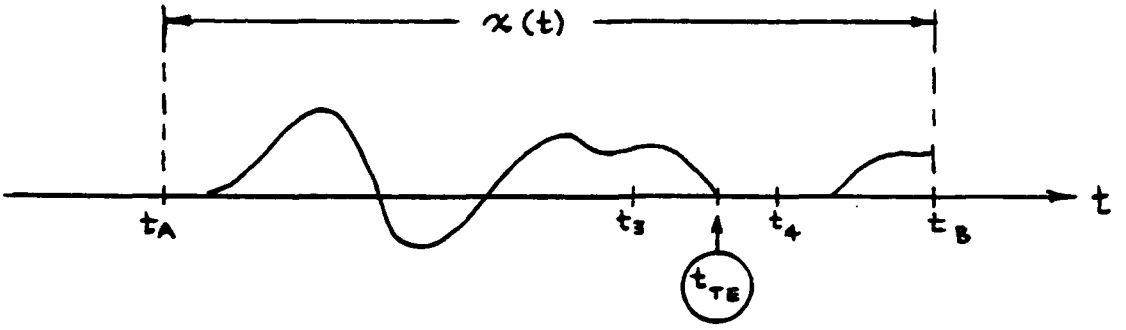

FIG. 4-3 EXAMPLE OF A TRAILING EDGE POINT

(3) Edge pair. Consider a leading edge point t_{LE} and a trailing edge point t_{TE}. If there are no leading edge points or trailing edge points in the open interval (t_{LE}, t_{TE}), and $x(t) \neq 0$ for some t in this open interval then t_{LE} and t_{TE} are said to form an edge pair. An example is given in Figure 4-4 where t_{LE_1} and t_{TE_1} constitute one edge pair and t_{LE_2} and t_{TE_2} constitute another edge pair.

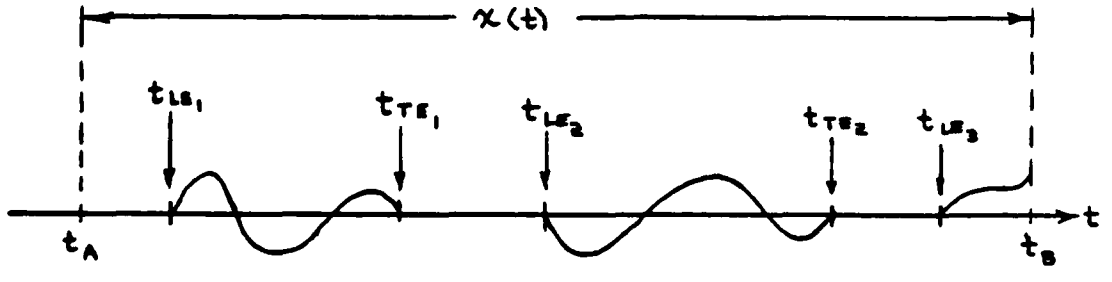

FIG. 4-4 EXAMPLE OF 2 EDGE PAIRS AND LEADING EDGE DOMINANT OBSERVATION

With this background, the four types of observations are defined.

(1) Leading Edge Dominant Observation. This is defined by the fact that $x(t_A) = 0$ and that there is one leading edge point not part of an edge pair. An example is given in Figure 4-4 above.

(2) Trailing Edge Dominant Observation. This is defined by the fact that $x(t_B) = 0$ and that there is one trailing edge point not part of an edge pair. An example is given in Figure 4-5.

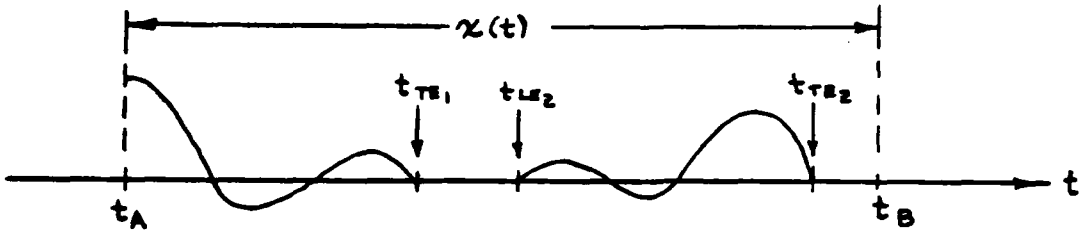

FIG. 4-5 EXAMPLE OF TRAILING EDGE DOMINANT OBSERVATION

(3) Paired Edge Observation. This situation is defined by the fact that $x(t_A) = 0 = x(t_B)$ and that all leading and trailing edge points lie in edge pairs. An example is shown in Figure 4-6.

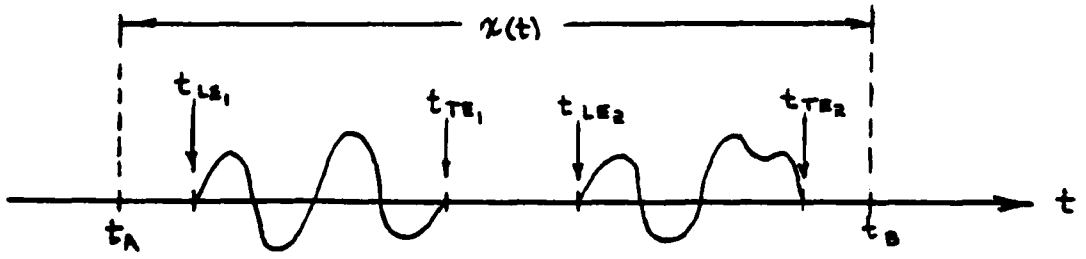

FIG. 4-6 EXAMPLE OF A PAIRED EDGE OBSERVATION

(4) Unpaired Edge Observation. This is defined by the fact that $x(t_A) \neq 0$ and $x(t_B) \neq 0$ and that leading and trailing edge points, if they exist, do not all lie in edge pairs. An example is given in Figure 4-7.

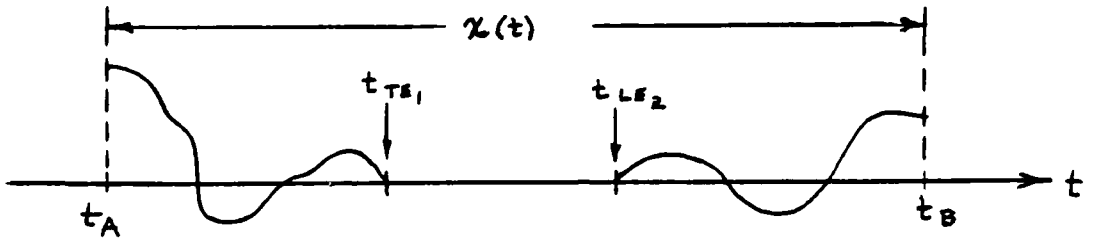

FIG. 4-7 EXAMPLE OF AN UNPAIRED EDGE OBSERVATION

Every physical, finite-length signal observation falls into one of these four categories. It is important that the type of category is recognized before time-variant spectral analysis is begun because the interpretation of the energy value plot of $|c_{k\ell}|^2$ will depend upon the presence of leading and trailing edge points.

4.2 Characteristics of the Plotted Values of Energy in the Time-Variant Frequency Plane

As an illustration of the preceding discussion, a total signal $y(t)$ is considered, where

$$y(t) = \begin{cases} A & : t_\alpha < t < t_\beta \\ A/2; & t = t_\alpha \text{ and } t = t_\beta \\ 0 & ; t < t_\alpha \text{ and } t > t_\beta . \end{cases} \qquad (4\text{-}2\text{-}1)$$

This total signal is sketched in Figure 4-8.

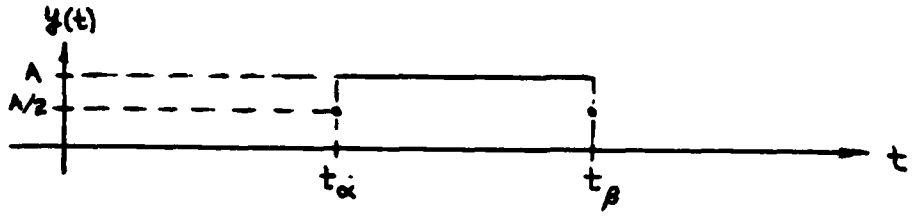

FIG. 4-8 A TOTAL SIGNAL UNDER CONSIDERATION IN (4-2-1)

For a Leading Edge Dominant Observation, the observed signal would likely appear as shown in Figure 4-9, where

$$x(t) = \begin{cases} 0 \; ; \; t_A \le t < t_\alpha \\ A/2; \; t = t_\alpha \\ A \; ; \; t_\alpha < t \le t_B \; . \end{cases} \qquad (4\text{-}2\text{-}2)$$

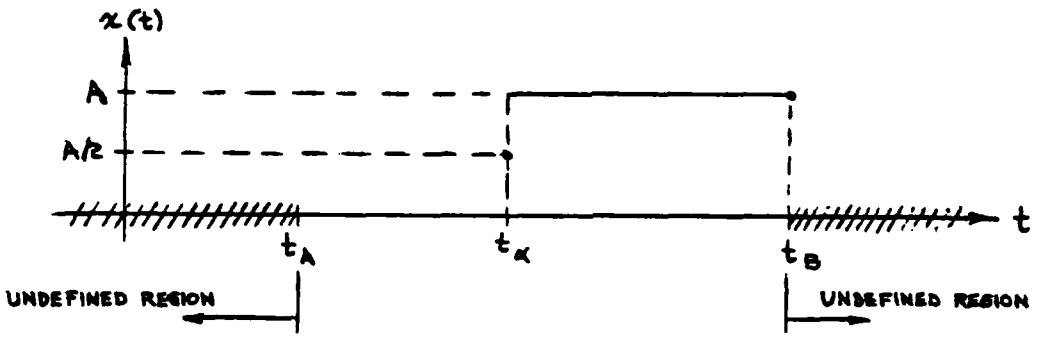

FIG. 4-9 A LEADING EDGE DOMINANT OBSERVATION

It is noted that the time instant $t = t_\alpha - \varepsilon$, with $\underline{\varepsilon}$ an infinitesimally small positive constant, is a leading edge point. The constant ε is needed to ensure that $x(t_\alpha - \varepsilon) = 0$ as required by the definition of a leading edge point. Using the procedure indicated in Figure 3-1, the observed signal is partitioned into N equi-length segments each of width T. It is required that T be such that N be an integer. Specifically,

$$N = \frac{t_B - t_A}{T} \qquad (4\text{-}2\text{-}3)$$

must be an integer. If T is chosen such that a segment boundary happens to fall exactly at the leading edge point $t = t_\alpha - \varepsilon$, then the subintervals of the observed signal appear as in Figure 4-10, where $t_B - t_A$ has been defined as 4T for convenience.

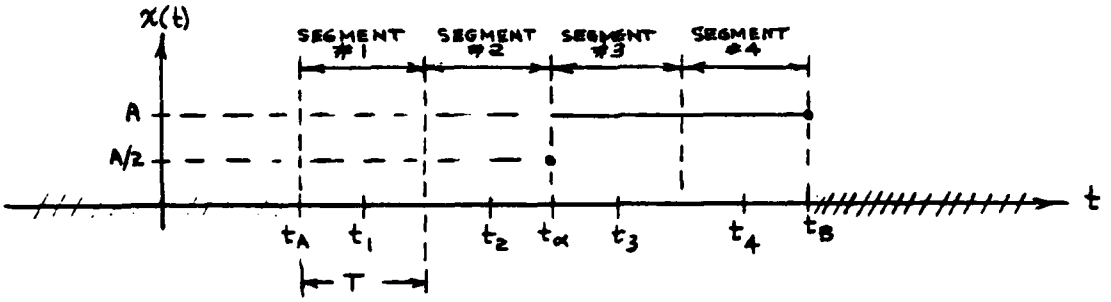

FIG. 4-10 SEGMENTION OF THE OBSERVED SIGNAL

Applying the Rectangular Windowed Expansion, the coefficients $r_{k\ell}$ are given from (3-2-24) as

$$r_{k\ell} = \frac{1}{\sqrt{T}} \int_{t_k - \frac{T}{2}}^{t_k + \frac{T}{2}} x(t)\, e^{-j\frac{2\pi}{T}\ell t}\, dt \; . \qquad (4\text{-}2\text{-}4)$$

Their magnitude squared is easily seen to be

$$|r_{k\ell}|^2 = \begin{cases} 0 \; ; \; k = 1, \; 2 \\ \frac{1}{T} \left| \int_{t_k - \frac{T}{2}}^{t_k + \frac{T}{2}} A\, e^{-j\frac{2\pi}{T}\ell t}\, dt \right|^2 \; ; \; k = 3, \; 4 \end{cases} \qquad (4\text{-}2\text{-}5)$$

More precisely,

$$|r_{k\ell}|^2 = \begin{cases} 0; & k = 1, 2 \\ \\ A^2 T \delta_{\ell,0}\ ; & k = 3, 4 \end{cases} \qquad (4\text{-}2\text{-}6)$$

This is plotted in Figure 4-11 where the appearance of the energy values nicely lends itself to the interpretation as a "DC" pulse.

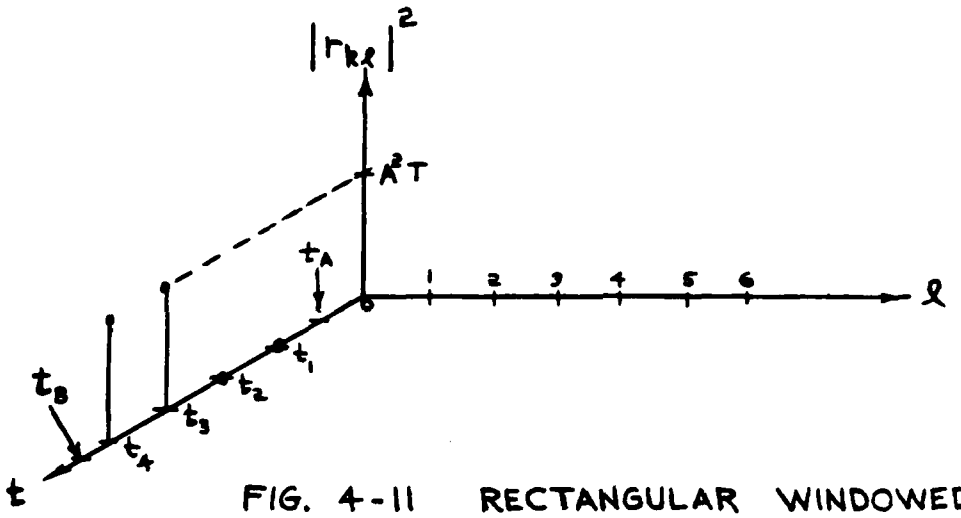

FIG. 4-11 RECTANGULAR WINDOWED EXPANSION ENERGY VALUES FOR THE OBSERVED SIGNAL IN FIG. 4-10

Applying the Bartlett Windowed Expansion from (3-1-72) with w(t) given by (3-1-7) and Q = 2, the coefficients $c_{k\ell}$ are found to be

$$c_{k\ell} = \sqrt{\frac{2}{T}} \int_{t_k - \frac{T}{2}}^{t_k + \frac{T}{2}} x(t) \sqrt{1 - \frac{2|t-t_k|}{T}}\ e^{-j\frac{4\pi\ell}{T}t}\, dt. \qquad (4\text{-}2\text{-}7)$$

It is clear again that $c_{k\ell} = 0$ for k = 1, 2. For k = 3 or 4, however, there results

$$c_{k\ell} = A\sqrt{\frac{2}{T}} \int_{t_k-\frac{T}{2}}^{t_k+\frac{T}{2}} x(t)\sqrt{1-\frac{2|t-t_k|}{T}}\, e^{-j\frac{4\pi\ell}{T}t}\, dt. \qquad (4\text{-}2\text{-}8)$$

Letting $\tau = \frac{2}{T}(t-t_k)$, $d\tau = \frac{2}{T}\,dt$, there results

$$c_{k\ell} = A\sqrt{\frac{T}{2}} \int_{-1}^{1} \sqrt{1-|\tau|}\; e^{-j\frac{4\pi\ell}{T}(\frac{T}{2}\tau + t_k)}\, d\tau \qquad (4\text{-}2\text{-}9)$$

$$= A\sqrt{\frac{T}{2}}\; e^{-j\frac{4\pi\ell}{T}t_k} \int_{-1}^{1} \sqrt{1-|\tau|}\; e^{-j2\pi\ell\tau}\, d\tau \qquad (4\text{-}2\text{-}10)$$

$$= A\sqrt{2T}\; e^{-j\frac{4\pi\ell}{T}t_k} \int_{0}^{1} \sqrt{1-\tau}\; \cos(2\pi\ell\tau)\, d\tau \qquad (4\text{-}2\text{-}11)$$

This expression is reducible to an interesting form by letting $z^2=(1-\tau)$ so that $2zdz = d\tau$. Performing the substitution, it is found that

$$c_{k\ell} = A\sqrt{8T}\; e^{-j\frac{4\pi\ell}{T}t_k} \int_{0}^{1} z^2 \cos\,[2\pi\ell(1-z^2)]\, dz. \qquad (4\text{-}2\text{-}12)$$

At this point it is useful to consider separately the case for $\ell = 0$. Setting $\ell = 0$, there results

$$c_{k,o} = A\sqrt{8T} \int_{0}^{1} z^2\, dz \qquad (4\text{-}2\text{-}13)$$

$$= A\sqrt{\frac{8}{9}T}\ . \qquad (4\text{-}2\text{-}14)$$

Therefore, the energy in the component of the Bartlett windowed expansion for $\ell = 0$ is

$$|c_{k,o}|^2 = \left(\frac{8}{9}\right) A^2 T. \qquad (4\text{-}2\text{-}15)$$

It is noted that the basis function component for $\ell = 0$ is just the square root of a triangle, as sketched in Figure 4-12.

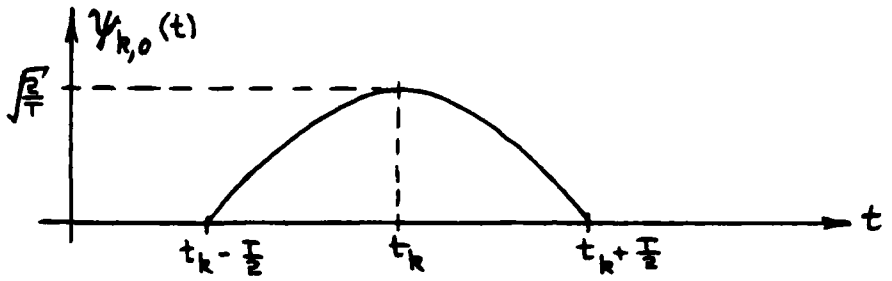

FIG. 4-12 BARTLETT WINDOWED EXPANSION BASIS FUNCTION FOR $\ell = 0$

When $\ell \neq 0$, (4-2-12) can be simplified and then integrated by parts. Specifically, the integral is

$$\int_0^1 z^2 \cos[2\pi\ell(1-z^2)dz] = \int_0^1 z^2 \cos[2\pi|\ell|z^2)dz \qquad (4\text{-}2\text{-}16)$$

$$= u.v \Big|_0^1 - \int_0^1 v\, du\,, \qquad (4\text{-}2\text{-}17)$$

where $u = z$; $du = dz$ (4-2-18)

and

$$v = \frac{1}{4\pi|\ell|} \sin(2\pi|\ell|z^2);$$

$$dv = z \cos(2\pi|\ell|z^2). \qquad (4\text{-}2\text{-}19)$$

This process gives

$$\int_0^1 z^2 \cos(2\pi|\ell|z^2)dz = \frac{1}{4\pi|\ell|} z \sin(2\pi|\ell|z^2) \Big|_0^1$$

$$- \frac{1}{4\pi|\ell|} \int_0^1 \sin(2\pi|\ell|z^2)dz \qquad (4\text{-}2\text{-}20)$$

$$= - \frac{1}{4\pi|\ell|} \int_0^1 \sin(2\pi|\ell|z^2)dz. \qquad (4\text{-}2\text{-}21)$$

Finally, when the following variable change is made, a tractable expression is produced. In particular, with

$$y = 2\sqrt{|\ell|}z, \qquad (4\text{-}2\text{-}22)$$

$$dy = 2\sqrt{|\ell|}dz\ , \qquad (4\text{-}2\text{-}23)$$

It is found that

$$\int_0^1 z^2 \cos(2\pi|\ell|z^2)dz = - \frac{1}{\pi} \frac{1}{8|\ell|^{3/2}} \int_0^{2\sqrt{|\ell|}} \sin(\frac{\pi}{2}y^2)dy \qquad (4\text{-}2\text{-}24)$$

$$= - \frac{1}{\pi} \frac{1}{8|\ell|^{3/2}} S(2\sqrt{|\ell|}), \qquad (4\text{-}2\text{-}25)$$

where S(t) is the Fresnel Sine Integral defined as

$$S(t) = \int_0^t \sin(\frac{\pi}{2} y^2)\ dy. \qquad (4\text{-}2\text{-}26)$$

Since the Fresnel Sine Integral is tabulated [17], (4-2-25) can be evaluated for $\ell \neq 0$. Inserting this result back into (4-2-12), it is found that, for $\ell \neq 0$

$$c_{k\ell} = -A\sqrt{T}\ \frac{1}{\pi\sqrt{8|\ell|^3}}\ S(2\sqrt{|\ell|}) \qquad (4\text{-}2\text{-}27)$$

so that

$$|c_{k\ell}|^2 = A^2T\ \frac{1}{\pi^2 8|\ell|^3}\ S^2(2\sqrt{|\ell|}) \ . \qquad (4\text{-}2\text{-}28)$$

Combining (4-2-15) and (4-2-28), the Bartlett windowed energy values are given by

$$|c_{k\ell}|^2 \begin{cases} \left(\frac{8}{9}\right) A^2T \ ; \ \ell = 0 \\ \left[\frac{S^2(2\sqrt{|\ell|})}{8\pi^2|\ell|^3}\right] A^2T \ ; \ \ell \neq 0 \end{cases} \qquad (4\text{-}2\text{-}29)$$

when k = 3,4. These values are listed in Table 4-1 for the 4 largest values of energy.

TABLE 4-1
BARTLETT WINDOWED ENERGY VALUES IN (4-2-29)

$\lvert\ell\rvert$	$\lvert c_{k,\ell}\rvert^2$	$10\log\left[\frac{\lvert c_{k,\ell}\rvert^2}{0.89}\right]$
0	0.89	0 dB
1	1.49×10^{-3}	-27.8 dB
2	2.39×10^{-4}	-35.7 dB
3	7.82×10^{-5}	-40.6 dB

Note: These values are the factors multiplying A^2T in (4-2-29).

It is interesting that the values listed indicate an abrupt drop in energy from $\ell = 0$ to $\ell = \pm 1$. This shows that the energy values are

essentially insignificant compared to the energy in the $\ell = 0$ component. This is a very nice spectral representation, although it is not as nice as the Rectangular windowed expansion result in (4-2-6). It is, however, tolerable in that a human observer would tend to estimate the presence of a constant signal since the $\ell = 0$ component contains the maximum energy. A sketch of (4-2-29) is given in Figure 4-13.

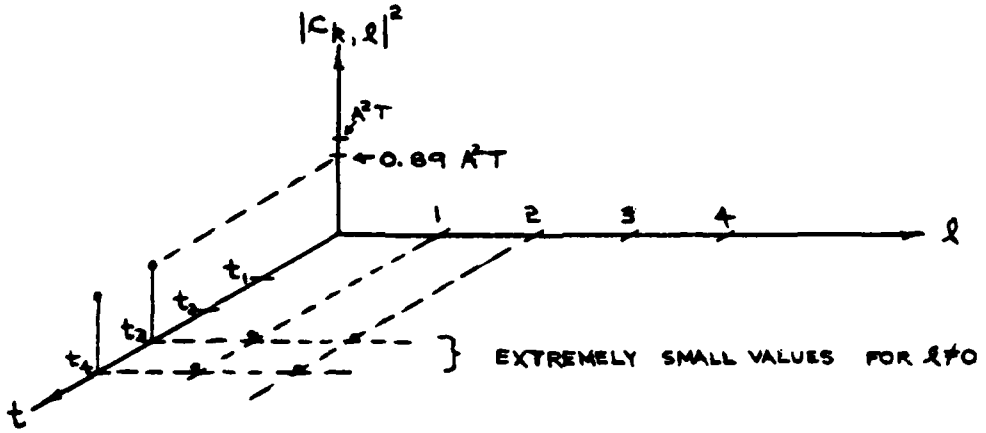

FIG. 4-13 BARTLETT WINDOWED EXPANSION ENERGY VALUES FOR THE OBSERVED SIGNAL IN FIG. 4-10

It is noted that the index ℓ in this plot does not represent the same frequencies as the index ℓ in Figure 4-11. Here the index values $\ell = 1,2,3$, for example, represent the radian frequencies of $\frac{4\pi}{T}$, $\frac{8\pi}{T}$, $\frac{12\pi}{T}$. In Figure 4-11, these index values represent the radian frequencies $\frac{2\pi}{T}$, $\frac{3\pi}{T}$, and $\frac{4\pi}{T}$.

To illustrate the effects of leading and trailing edge points, a situation is now considered in which no subinterval boundary falls on the leading edge points in Figure 4-9. The leading edge point will now lie within a segment. Specifically, a new value for N will be chosen, N = 5, and the subinterval width T will be such that

$$T = \frac{t_\alpha - t_A}{2.25} \quad , \tag{4-2-30}$$

which causes the leading edge at $t = t_\alpha - \varepsilon$ to lie one quarter of a subinterval width before the point $t = t_3$ as shown in Figure 4-14.

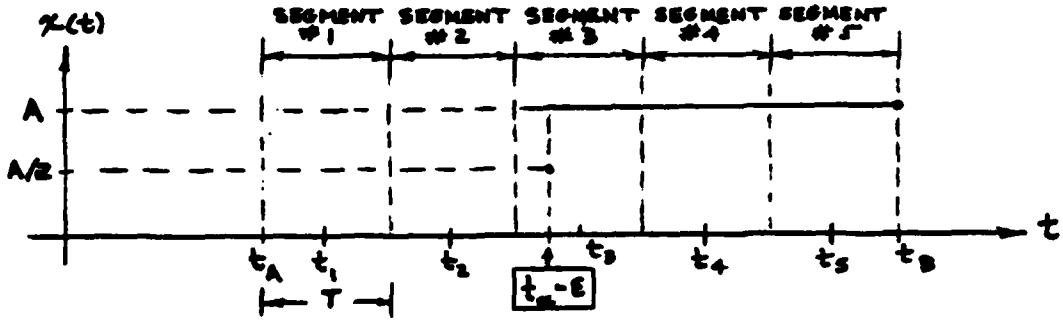

FIG. 4-14 A NEW PARTITION OF THE SIGNAL $x(t)$

The most significant result of this change will be seen in the pattern that develops for the magnitude of the energy values in the Rectangular windowed expansion. Specifically, the squared magnitude of the Rectangular windowed expansion coefficients from (4-2-4) are found to be

$$|r_{k\ell}|^2 = \begin{cases} 0 \; ; \; k = 1,2 \\ \\ A^2 T \, \delta_{\ell,o} \; ; \; k = 4,5 \end{cases} \tag{4-2-31}$$

where the case $k = 3$ is discussed shortly. These values in (4-2-31) are identical the corresponding values in (4-2-6) except for $k = 3$. When $k = 3$,

$$r_{3,\ell} = \frac{1}{\sqrt{T}} \int_{t_3 - \frac{T}{2}}^{t_3 + \frac{T}{2}} x(t) \, e^{-j\frac{2\pi}{T}\ell t} \, dt \tag{4-2-32}$$

$$= \frac{1}{\sqrt{T}} \int_{t_3 - \frac{T}{4}}^{t_3 + \frac{T}{2}} A\, e^{-j\frac{2\pi}{T}\ell t}\, dt \qquad (4\text{-}2\text{-}33)$$

$$= \frac{A}{\sqrt{T}}\, e^{-j\frac{2\pi}{T}\ell\left(t_3 + \frac{T}{8}\right)} \left(\frac{3T}{4}\right) \operatorname{sinc}\left[\frac{1}{T}\ell\left(\frac{3T}{4}\right)\right] \qquad (4\text{-}2\text{-}34)$$

$$= A\sqrt{T}\, \frac{3}{4}\, e^{-j\frac{2\pi}{T}\ell\left(t_3 + \frac{T}{8}\right)} \operatorname{sinc}\left(\frac{3}{4}\ell\right) . \qquad (4\text{-}2\text{-}35)$$

Therefore the squared magnitude is

$$|r_{3,\ell}|^2 = A^2T \left(\frac{9}{16}\right) \operatorname{sinc}^2 \left(\frac{3}{4}\ell\right) , \qquad (4\text{-}2\text{-}36)$$

which is sketched in Figure 4-15.

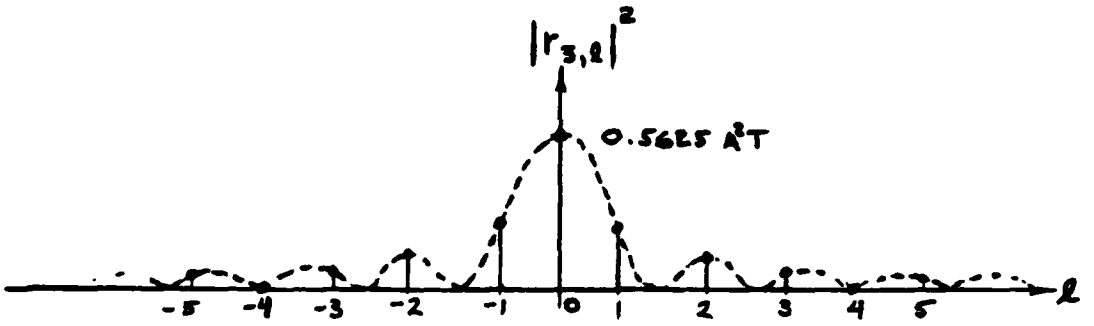

FIG. 4-15 SKETCH OF ENERGY VALUES IN (4-2-36)

It is noted that energy appears to be distributed all across the frequency axis with magnitudes which follow the envelope of the $\operatorname{sinc}^2(.)$ function sampled at integer multiples of $\frac{3}{4}$.

Applying the Bartlett Windowed Expansion from (4-2-29), it is seen that the energy values for k = 4 and 5 are given by

$$|c_{k\ell}|^2 = \begin{cases} \left(\frac{8}{9}\right) A^2T \; ; \; \ell = 0 \\ \left[\frac{S^2\left(2\sqrt{|\ell|}\right)}{8\pi^2|\ell|^3}\right] A^2T \; ; \; \ell \neq 0 \end{cases} \qquad (4\text{-}2\text{-}37)$$

and that

$$|c_{k\ell}|^2 = 0 \tag{4-2-38}$$

when k = 1 or 2. However, when k = 3, it is found from (4-2-7) that

$$c_{3,\ell} = \sqrt{\frac{2}{T}} \int_{t_3-\frac{T}{2}}^{t_3+\frac{T}{2}} x(t) \sqrt{1-\frac{2|t-t_3|}{T}}\, e^{-j\frac{4\pi}{T}\ell t}\, dt \tag{4-2-39}$$

$$= \sqrt{\frac{2}{T}} \int_{t_3-\frac{T}{4}}^{t_3+\frac{T}{2}} A\sqrt{1-\frac{2|t-t_3|}{T}}\, e^{-j\frac{4\pi}{T}\ell t}\, dt\ . \tag{4-2-40}$$

Making the variable change

$$\tau = \frac{2}{T}(t-t_3) - \frac{1}{4} \tag{4-2-41}$$

and

$$d\tau = \frac{2}{T}\, dt \tag{4-2-42}$$

there results

$$c_{3,\ell} = A\sqrt{\frac{T}{2}} \int_{-3/4}^{3/4} \sqrt{1-|\tau+\tfrac{1}{4}|}\, e^{-j\frac{4\pi}{T}\ell(\frac{T}{2})(\tau+\frac{1}{4})} \cdot e^{-j\frac{4\pi}{T}\ell t_3}\, d\tau \tag{4-2-43}$$

$$= A\sqrt{\frac{T}{2}}\, e^{-j\frac{4\pi}{T}\ell t_3}\, e^{-j\frac{\pi}{2}\ell} \int_{-3/4}^{3/4} \sqrt{1-|\tau+\tfrac{1}{4}|}\, e^{-j2\pi\ell\tau}\, d\tau\ , \tag{4-2-44}$$

so that

$$|c_{3,\ell}|^2 = \frac{A^2T}{2} \left| \int_{-3/4}^{3/4} \sqrt{1-|\tau+\tfrac{1}{4}|}\; e^{-j2\pi\ell\tau} d\tau \right|^2 . \qquad (4\text{-}2\text{-}45)$$

The integral involved here was evaluated for various integer values of ℓ by numerical integration. The results are shown in Figure 4-16 along with the logarithmically scaled values of the Rectangular expansion coefficients in (4-2-36). The Rectangular expansion energy values are indicated by the triangles while the Bartlett expansion energies are given by the asterisks. It is quite interesting that the Bartlett expansion energies of (4-2-45) actually fall below the Rectangular expansion energies at so many frequencies. The reason why there are twice as many triangles as asterisks in the plot is because the Rectangular expansion represents frequencies which are integer multiples of $\frac{2\pi}{T}$ whereas the Bartlett represents frequencies which are integer multiples of $\frac{4\pi}{T}$. The smooth curve connecting the asterisks is only for comparison purposes and is not to imply a continuum of represented points. It is noted that the Bartlett windowed expansion exceeds the fall-off rate of the Rectangular expansion for this plot. Thus the Bartlett spectral representation is quite pleasing.

In order to interpret this plot it is very important to understand why neither spectral representation produced the desirable result of a single nonzero energy component at $\ell = 0$ with the rest of the components zero. This is termed the desirable result because it would instantly suggest to the observer a square-wave pulse encountered in

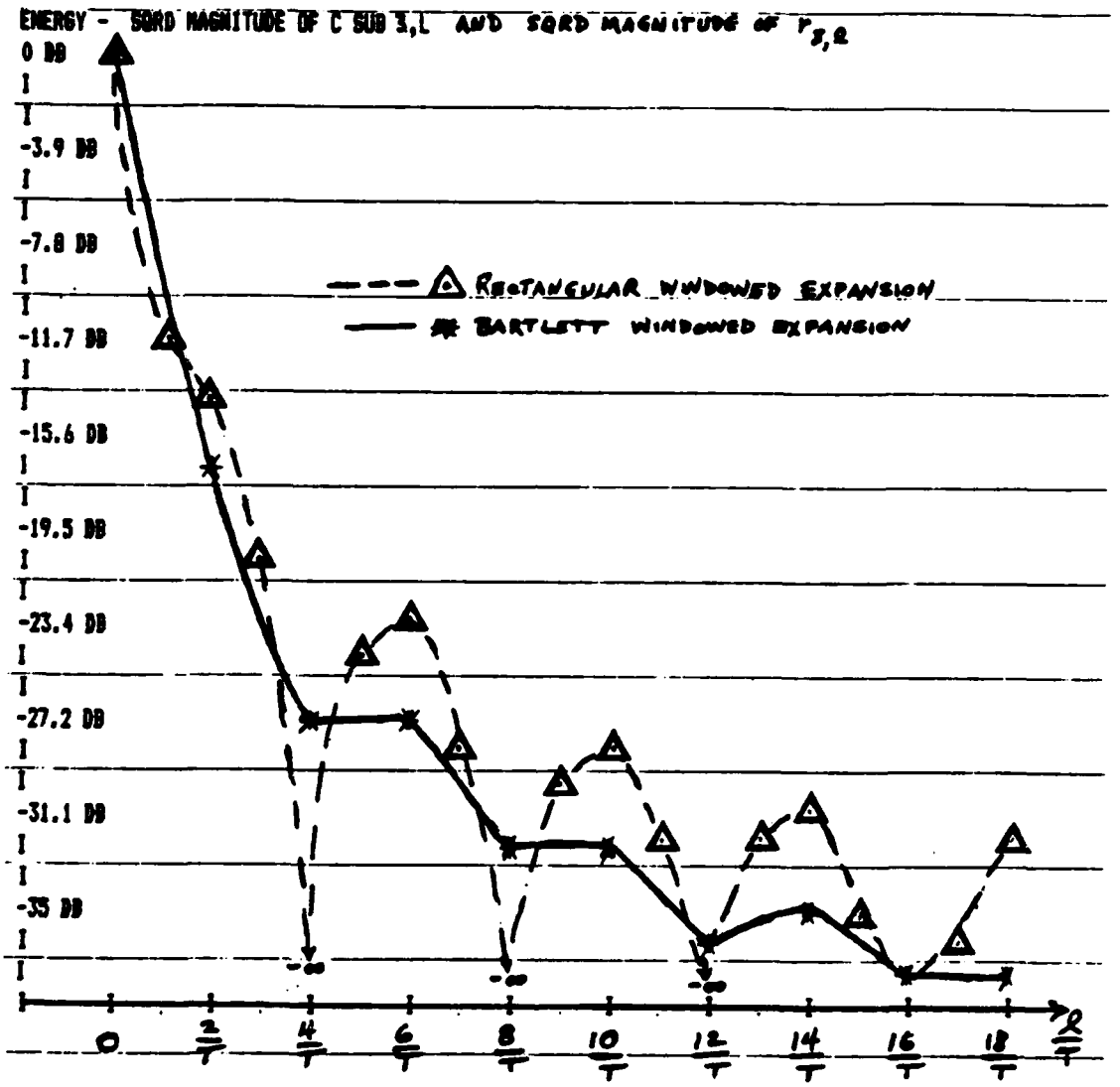

BARTLETT WINDOWED EXPANSION FOR EQUATION (4-2-45) COMPARED WITH (4-2-36)
MAXIMUM VALUE = .602397 MINIMUM VALUE = 7.71986E-05
EACH SHADED HORIZONTAL BAR HAS WIDTH IN DB OF 3.89227 LOWEST FREQUENCY = 0
VERTICAL RESOLUTION IN DB IS 1.29742 HIGHEST FREQUENCY = 18

Fig. 4-16 Comparison of Bartlett and Rectangular Windowed Expansions

the third time subinterval. Instead, a "splashing-out" of energy occurs across the entire frequency axis. The reason is simply that no basis function in either Rectangular or Bartlett expansions contains a leading edge point within the subinterval of its definition. Therefore neither expansion will represent the signal in the third subinterval with a single basis function. Furthermore, both expansions seem to need significant energy contributions from several low frequency components, the Rectangular expansion especially, in order to approximate the signal. Specifically, the Rectangular expansion needs the component at frequency 2/T to have an energy of about 13 dB below the maximum energy value at zero frequency. At the frequency of 3/T, it needs a component with an energy of about 20 dB below the maximum energy value. On the other hand, the Bartlett expansion never needs more than about a -17 dB energy value in any component, relative to its maximum at zero frequency. Thus the Bartlett windowed expansion is shown here to have a more desirable spectral representation because of its more rapid decay rate. Although these spectral representations may both be considered troublesome, at least they can be anticipated when leading edge points are noticed within a signal segment. Trailing edge points can be shown to have identical spectral representation effects as leading edge points. The lesson learned here is that the signal must be carefully scanned in the time domain to detect where leading and trailing edges may fall. Once this is done, then the basic subinterval width, T, may be chosen and any leading or trailing edge points lying on sub-

interval boundaries must be specifically accounted for in the time-frequency plot interpretation.

Another interesting investigation concerns the relationship between the subinterval width, T, and the frequency of a sinusoidal signal. The question may be asked, "What is the minimum number of cycles of a sinusoidal signal that needs to be enclosed by the basic subinterval in order to achieve a nicely 'peaked' spectral representation?" The answer depends upon the choice of window function. For simplicity the signal is given as

$$x(t) = \begin{cases} A \cos\left(\frac{2\pi\nu}{T}t\right) \; ; \; |t-t_K| \leq \frac{T}{2} \\ \\ 0 \; ; \; |t-t_K| > \frac{T}{2} \quad , \end{cases} \tag{4-2-46}$$

where the frequency parameter, ν, is not necessarily an integer. If ν <u>is</u> an integer, the Rectangular windowed expansion gives the pleasing spectral representation of the single nonzero energy value at the correct frequency index, as discussed in Chapter 3 after (3-2-49). This is due to the fact that, for integer ν, (4-2-46) is identical to the real part of the basis function $\psi_{K,\nu}(t)$ in the Rectangular expansion. For noninteger ν, the Rectangular expansion coefficients are found by substituting (4-2-46) into (3-2-24). There results

$$r_{k,\ell} = 0 \; ; \; k = K \tag{4-2-47}$$

and

$$r_{K\ell} = \frac{A}{\sqrt{T}} \int_{t_K - \frac{T}{2}}^{t_K + \frac{T}{2}} \cos\left(\frac{2\pi\nu}{T}t\right) e^{-j\frac{2\pi}{T}\ell t}\, dt \,. \tag{4-2-48}$$

The last expression can be simplified by the change of variable

$$\tau = \frac{2}{T}(t - t_K) \tag{4-2-49}$$

and

$$d\tau = \frac{2}{T}\, dt \,, \tag{4-2-50}$$

so that

$$r_{K\ell} = \frac{A\sqrt{T}}{2} \int_{-1}^{1} \cos\left(\pi\nu\tau + \frac{2\pi\nu}{T} t_K\right) e^{-j\pi\ell\tau} \cdot e^{-j\frac{2\pi}{T}\ell t_K}\, d\tau \tag{4-2-51}$$

$$= \frac{A\sqrt{T}}{4} e^{-j\frac{2\pi}{T}\ell t_K} \left\{ \int_{-1}^{1} e^{+j\left(\pi\nu\tau + \frac{2\pi\nu}{T} t_K\right)} e^{-j\pi\ell\tau}\, d\tau + \int_{-1}^{1} e^{-j\left(\pi\nu\tau + \frac{2\pi\nu}{T} t_K\right)} e^{-j\pi\ell\tau}\, d\tau \right\} \tag{4-2-52}$$

$$= \frac{A\sqrt{T}}{2} e^{-j\frac{2\pi}{T}\ell t_K} \left\{ e^{j\frac{2\pi\nu}{T} t_K} \operatorname{sinc}(\ell - \nu) + e^{-j\frac{2\pi\nu}{T} t_K} \operatorname{sinc}(\ell + \nu) \right\} . \tag{4-2-53}$$

Therefore the Rectangular windowed energy values are

$$|r_{K\ell}|^2 = \frac{A^2 T}{4} \left\{ \operatorname{sinc}^2(\ell - \nu) + \operatorname{sinc}^2(\ell + \nu) + 2\cos\left(\frac{4\pi\nu}{T} t_K\right) \left| \operatorname{sinc}(\ell - \nu) \operatorname{sinc}(\ell + \nu) \right| \right\} . \tag{4-2-54}$$

It is recalled that these values were plotted in Figure 3-18 for $\nu = 60.5$. Here it is of interest to set ν equal to small values and interpret the resulting plot of energies. Before reviewing the plots, however, it is important to note the presence in (4-2-54) of the term involving the product of two sinc functions. This "cross-product" reveals that there is a certain contribution to the energy value at a specific frequency index ℓ due to the "interaction" of the tails of two separated sinc functions. Although this term may have negligible effects for wide separations of the two sinc functions, that is, large values of ν, the effects for small values of ν are quite significant. In addition, the cosine factor which multiplies this "cross-product" term in (4-2-54) may have some noticeable effect upon the spectral representation. An example is given in Figures 4-17 and 4-18 of the Rectangular expansion energy values for $\nu = 10.25$. Figure 4-17 shows (4-2-54) for the maximum contribution from the cross product term while Figure 4-18 shows (4-2-54) for the minimum contribution from the cross product term. More precisely, Figure 4-17 corresponds to the case when

$$\frac{4\pi\nu}{T} t_K = 2n\pi, \qquad (4\text{-}2\text{-}55)$$

$$n = 0, \pm 1, \pm 2, \ldots,$$

while Figure 4-18 corresponds to

$$\frac{4\pi\nu}{T} t_K = (2n+1)\pi \qquad (4\text{-}2\text{-}56)$$

$$n = 0, \pm 1, \pm 2, \ldots .$$

The two plots appear very roughly the same although there are slight differences. In Figure 4-18, the minimum cross product case of (4-2-56), the energies for $\ell = 10$ and $\ell = 11$ are practically the same within the vertical resolution stated in the caption. In Figure 4-17, the maximum cross product case, the energies at $\ell = 10$ and $\ell = 11$ are shown at different decibel leves but the vertical resolution given in the caption is smaller than that of Figure 4-17 which may account for the difference. In fact, the only significant difference between the plots occurs at $\ell = 0$. In this case, (4-2-54) becomes

$$|r_{K,0}|^2 = \frac{A^2T}{2}\left\{\text{sinc}^2(\nu) + \cos\left(\frac{4\pi\nu}{T}t_K\right)\text{sinc}^2(\nu)\right\} \qquad (4\text{-}2\text{-}57)$$

$$= \frac{A^2T}{2}\text{sinc}^2(\nu)\left\{1 + \cos\left(\frac{4\pi\nu}{T}t_K\right)\right\}. \qquad (4\text{-}2\text{-}58)$$

When (4-2-55) holds, this reduces to

$$|r_{K,0}|^2 = A^2T\,\text{sinc}^2(\nu) \qquad (4\text{-}2\text{-}59)$$

which is shown in Figure 4-16 to be more than 16 dB down from the maximum. On the other hand, when (4-2-56) holds,

$$|r_{K,0}|^2 = 0 \qquad (4\text{-}2\text{-}60)$$

as shown in Figure 4-18. Thus the overall effect of the value of the cross product term is very slight, at least at this value for ν. Smaller values for ν will be discussed shortly, but first the Bartlett

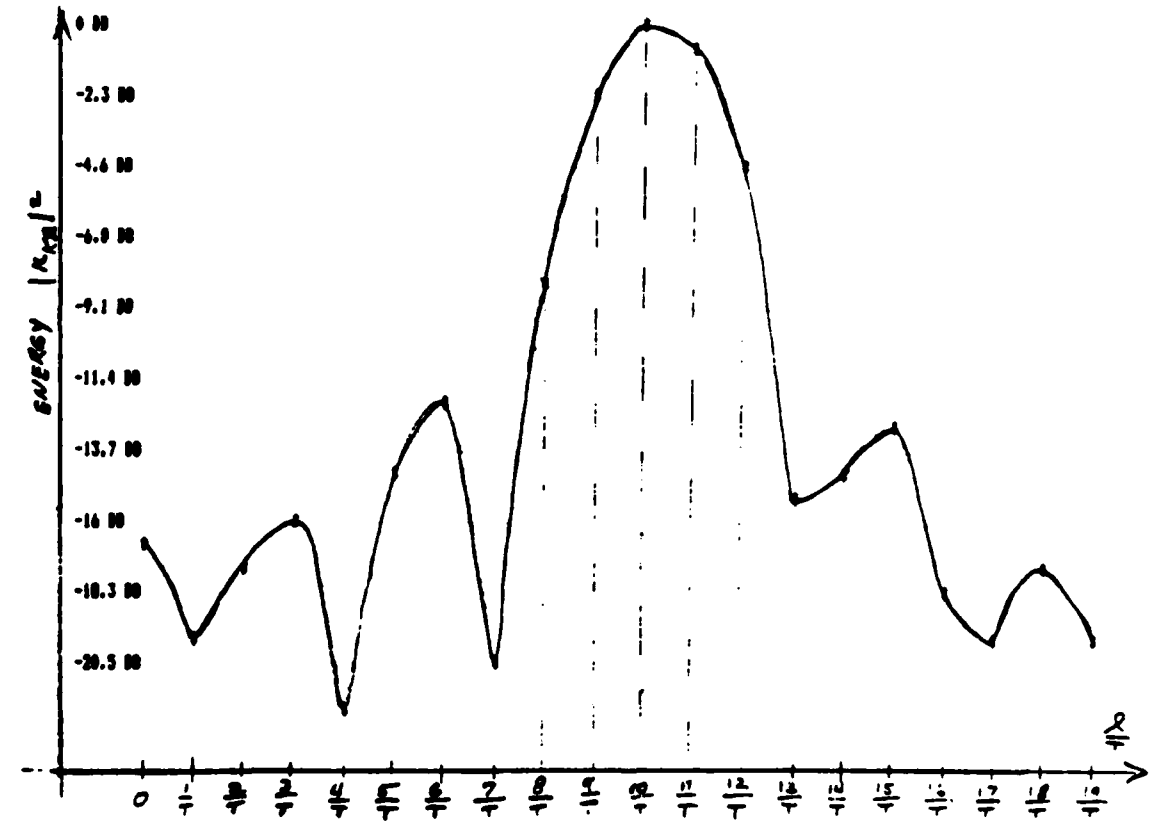

Fig. 4-17 Rectangular Windowed Expansion for ν=10.25, Maximum Cross Product Contribution

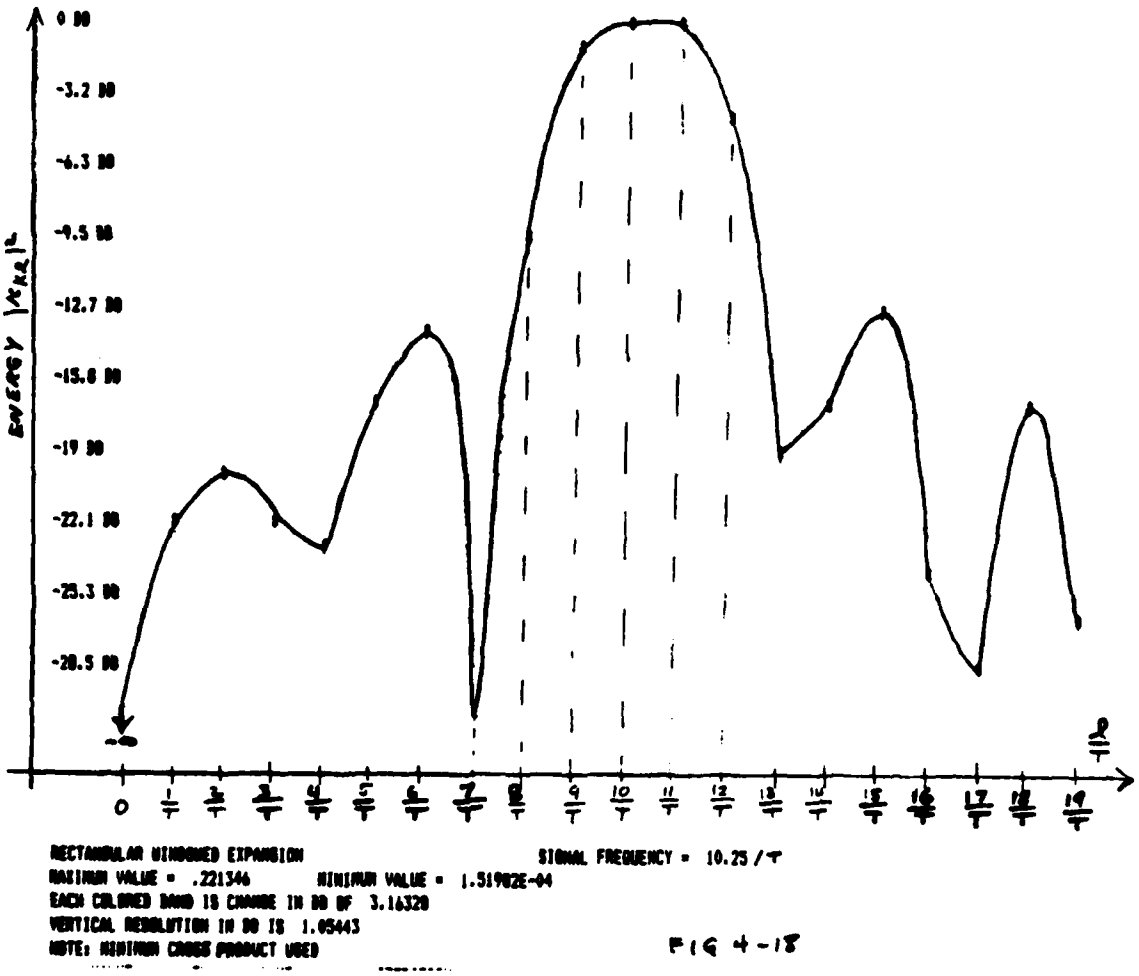

FIG 4-18

Fig. 4-18 Rectangular Windowed Expansion for ν=10.25, Minimum Cross Product Contribution

windowed expansion coefficients are plotted for the same value of ν. Using the expression for the Bartlett windowed expansion in (4-2-7) for the signal given in (4-2-46), the Bartlett coefficients are found to be

$$c_{k\ell} = \sqrt{\frac{2}{T}} \int_{t_k-\frac{T}{2}}^{t_k+\frac{T}{2}} x(t)\sqrt{1 - \frac{2|t-t_k|}{T}}\, e^{-j\frac{4\pi}{T}\ell t}\, dt \qquad (4\text{-}2\text{-}61)$$

$$= 0, \quad k \neq K \; . \qquad (4\text{-}2\text{-}62)$$

For k=K, there results

$$c_{K\ell} = A\sqrt{\frac{2}{T}} \int_{t_K-\frac{T}{2}}^{t_K+\frac{T}{2}} \cos(\frac{2\pi\nu}{T}t)\sqrt{1 - \frac{2|t-t_K|}{T}}\, e^{-j\frac{4\pi}{T}\ell t}\, dt \; . \qquad (4\text{-}2\text{-}63)$$

Making the variable change

$$\tau = \frac{2}{T}(t-t_K) \qquad (4\text{-}2\text{-}64)$$

$$d\tau = \frac{2}{T}\, dt \; , \qquad (4\text{-}2\text{-}65)$$

it is found that

$$c_{K\ell} = A\sqrt{\frac{T}{2}} \int_{-1}^{1} \cos\left[\frac{2\pi\nu}{T}\,(\frac{T}{2}\tau + t_K)\right]\sqrt{1-|\tau|}\, e^{-j\frac{4\pi}{T}\ell(\frac{T}{2}\tau)}$$

$$\cdot\; e^{-j\frac{4\pi}{T}\ell t_K}\, d\tau \qquad (4\text{-}2\text{-}66)$$

$$= \frac{A}{2}\sqrt{\frac{T}{2}}\; e^{-j\frac{4\pi}{T}\ell t_K}\left\{\int_{-1}^{1}\sqrt{1-|\tau|}\; e^{-j\pi(2\ell-\nu)\tau} e^{j\frac{2\pi}{T}\nu t_K}\, d\tau\right.$$

$$\left. + \int_{-1}^{1}\sqrt{1-|\tau|}\; e^{-j\pi(2\ell+\nu)\tau}\; e^{-j\frac{2\pi}{T}\nu t_K}\, d\tau\right\}. \qquad (4\text{-}2\text{-}67)$$

Using the notation

$$I_{\pm} = \tfrac{1}{2}\int_{-1}^{1}\sqrt{1-|\tau|}\; e^{-j\pi(2\ell\pm\nu)\tau} d\tau\,, \qquad (4\text{-}2\text{-}68)$$

$$= \int_{0}^{1}\sqrt{1-|\tau|}\,\cos\,[\pi(2\ell\pm\nu)\tau]\, d\tau\,, \qquad (4\text{-}2\text{-}69)$$

It follows that

$$c_{K\ell} = A\sqrt{\frac{T}{2}}\; e^{-j\frac{4\pi}{T}\ell t_K}\left\{e^{j\frac{2\pi}{T}\nu t_K}\; I_- + e^{-j\frac{2\pi}{T}\nu t_K}\; I_+\right\} \qquad (4\text{-}2\text{-}70)$$

and that

$$|c_{K\ell}|^2 = \frac{A^2T}{2}\left\{I_-^{\,2} + I_+^{\,2} + 2\,\cos\,(\tfrac{4\pi\nu}{T}t_K)\;|I_+I_-|\right\}. \qquad (4\text{-}2\text{-}71)$$

Again a "cross-product" term is seen here involving the product I_+I_- with the same cosine factor as in (4-2-54). Figures 4-19 and 4-20 give the logarithmically scaled values of (4-2-71) with $\nu = 10.25$ for the two cases of maximum and minimum cross product contribution, respectively. For the maximum "cross product" contribution in (4-2-71), (4-2-55) is imposed and there results

$$|c_{K\ell}|^2 = \frac{A^2T}{2}\left\{I_- + I_+\right\}^2, \qquad (4\text{-}2\text{-}72)$$

which is plotted in Figure 4-19. When the minimum "cross product" contribution condition in (4-2-56) holds, (4-2-71) becomes

$$|c_{K\ell}|^2 = \frac{A^2T}{2}\left\{I_- - I_+\right\}^2, \qquad (4\text{-}2\text{-}73)$$

which is plotted in Figure 4-20. When $\ell=0$ in (4-2-73), inspection of (4-2-69) shows that $I_-=I_+$ for all ν so that

$$|c_{K,0}|^2 = 0 \qquad (4\text{-}2\text{-}74)$$

in Figure 4-20. It is seen that Figure 4-19 and Figure 4-20 are practically identical within the vertical resolutions indicated. Thus the cross product term is not very significant for the Bartlett windowed expansion at this frequency. It is surprising, however, to compare the Bartlett windowed expansion to the Rectangular windowed expansion. Specifically, comparing Figure 4-17 with Figure 4-19, it is surprising to find a tremendous increase in spectral sharpness for the Bartlett windowed expansion. For example, although both plots have their maximum at $\ell=10$ (which is desirable since $\nu=10.25$). the Rectangular expansion energy at $\ell=12$ is only 4.6 dB down from maximum compared to about 21 dB down for the Bartlett expansion energy at $\ell=12$. On the lower frequency side of the peak, the Rectangular expansion shows an energy of about 8 dB down at $\ell=8$ compared to the Bartlett expansion energy of about 36 dB down from maximum at $\ell=8$. This indicates a

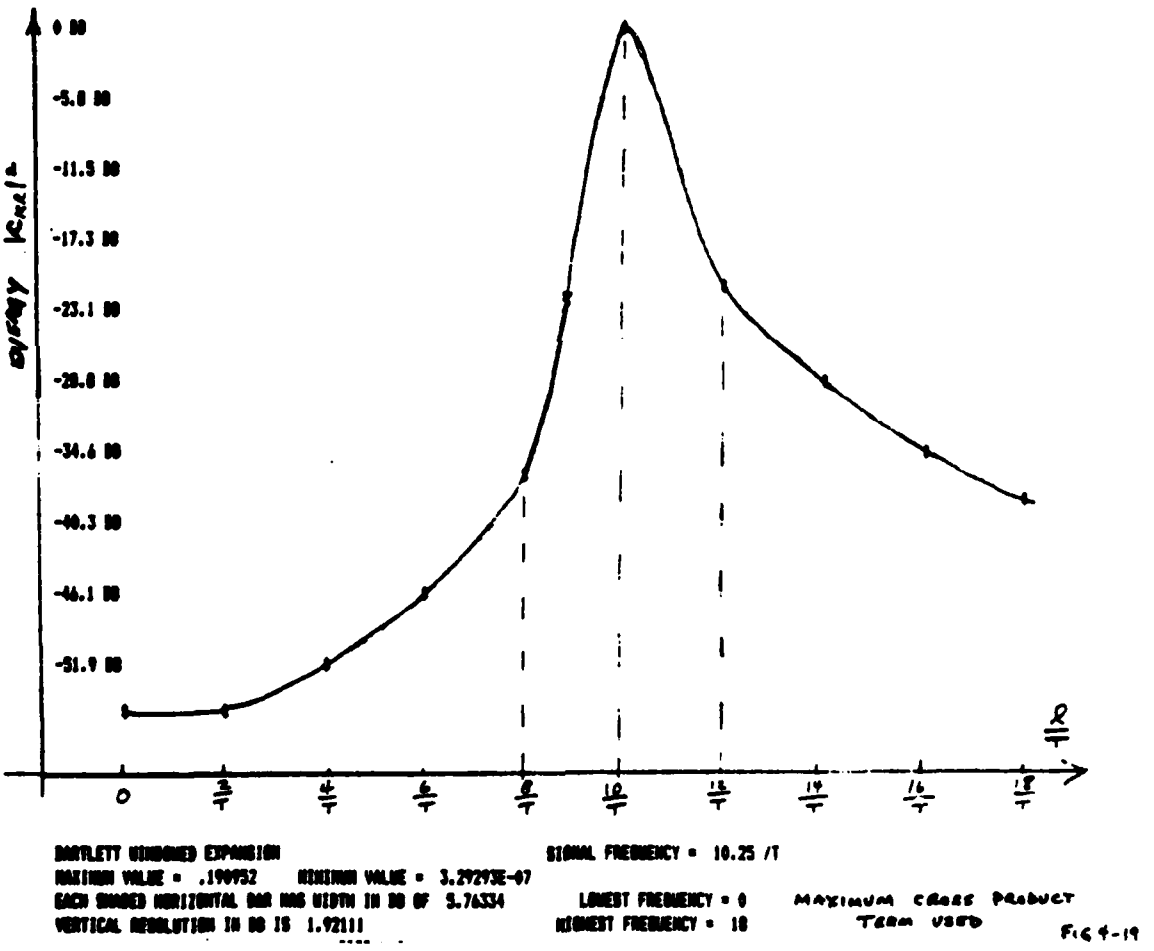

Fig. 4-19 Bartlett Windowed Expansion for ν=10.25, Maximum Cross Product Contribution

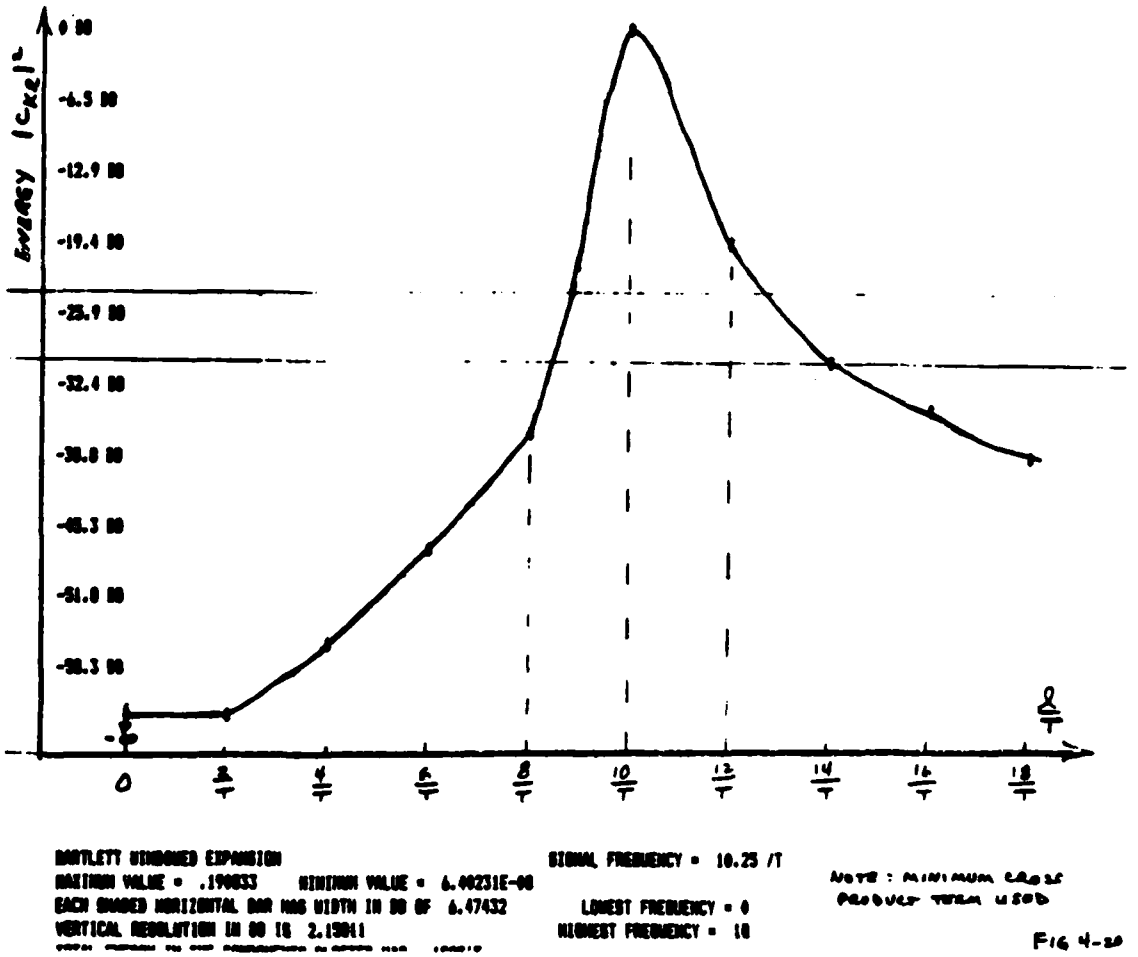

Fig. 4-20 Bartlett Windowed Expansion for ν=10.25, Minimum Cross Product Contribution

significant advantage in using the Bartlett windowed expansion for this frequency of the sinusoidal signal.

The spectral sharpness advantage of the Bartlett windowed expansion is also evident at other frequencies. Figures 4-21 and 4-22 present the Rectangular windowed energies for ν=2.5 in the two cases of maximum and minimum cross product term contribution. More precisely, Figure 4-21 presents the energy values of the Rectangular expansion in (4-2-54) for the maximum cross product contribution condition of (4-2-55) while Figure 4-22 presents the Rectangular expansion energies for the minimum cross product contribution in (4-2-56), both plots representing a sinusoidal signal with ν=2.5. The plots are somewhat similar, but there is a marked difference in the decay patterns on the high frequency side of the maxima. Figure 4-21 shows subsidiary peaks at ℓ=7,11 and 14 with magnitudes of approximately 13 dB, 17 dB, and 19 dB down from the maxima, respectively. On the other hand, Figure 4-22, the minimum cross product contribution case, indicates subsidiary peaks at ℓ=7, 10, and 13 with magnitudes of about 11 dB, 15.5 dB, and 21.2 dB down, respectively. Thus the cross term has a noticeable effect on magnitude and location of "sidelobes." The reason for this is that for low frequencies, the tail of the sinc function at the negative frequency of ν=-2.5 in (4-2-54) starts to merge with the sidelobes of the sinc function centered at the positive frequency ν=2.5. This causes the cross product term to increase in magnitude and so its effects will be seen to a greater extent. It is important to note that the presence of significantly large energies at ℓ=1 and ℓ=4 in both plots makes the

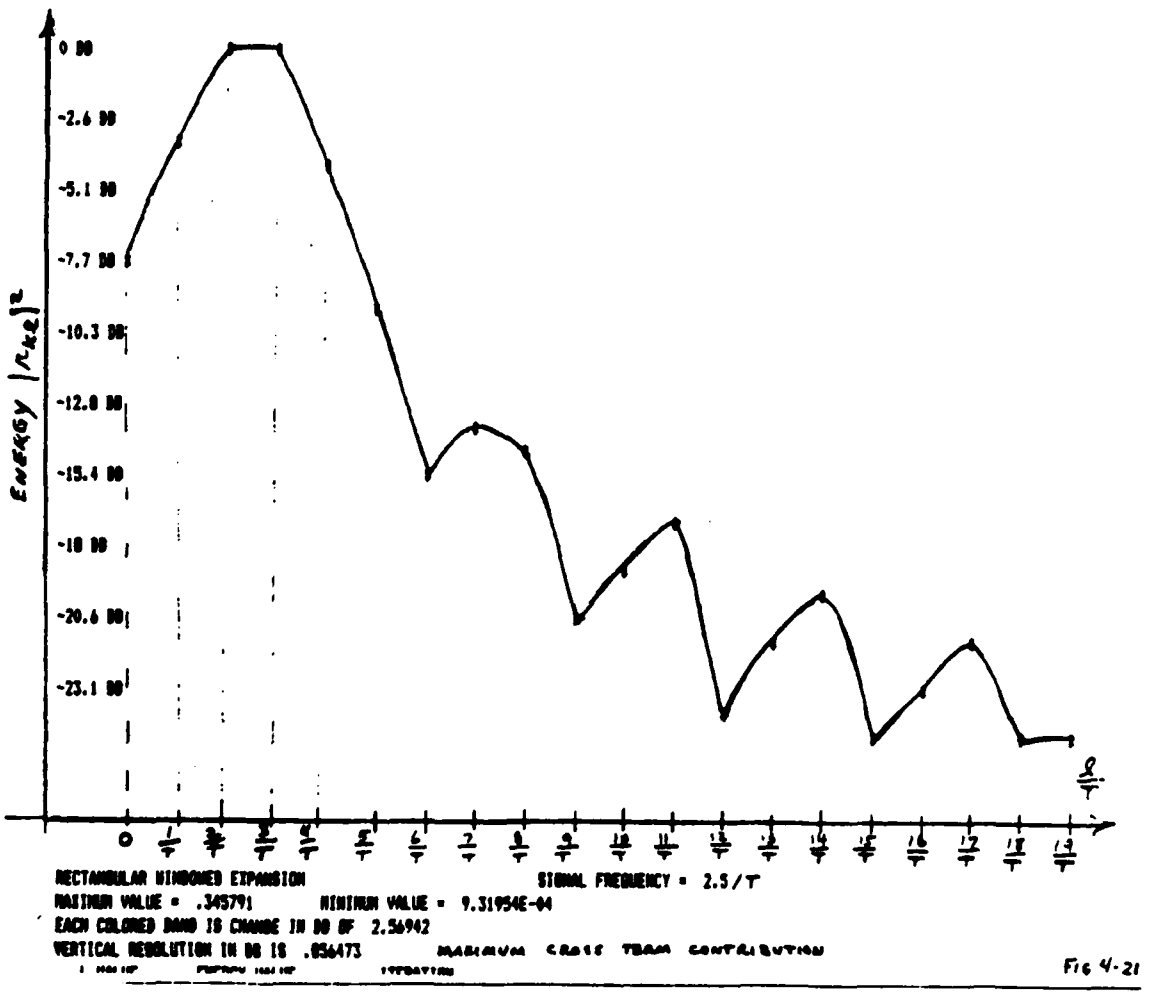

Fig. 4-21 Rectangular Windowed Expansion for ν=2.5 Maximum Cross Product Contribution

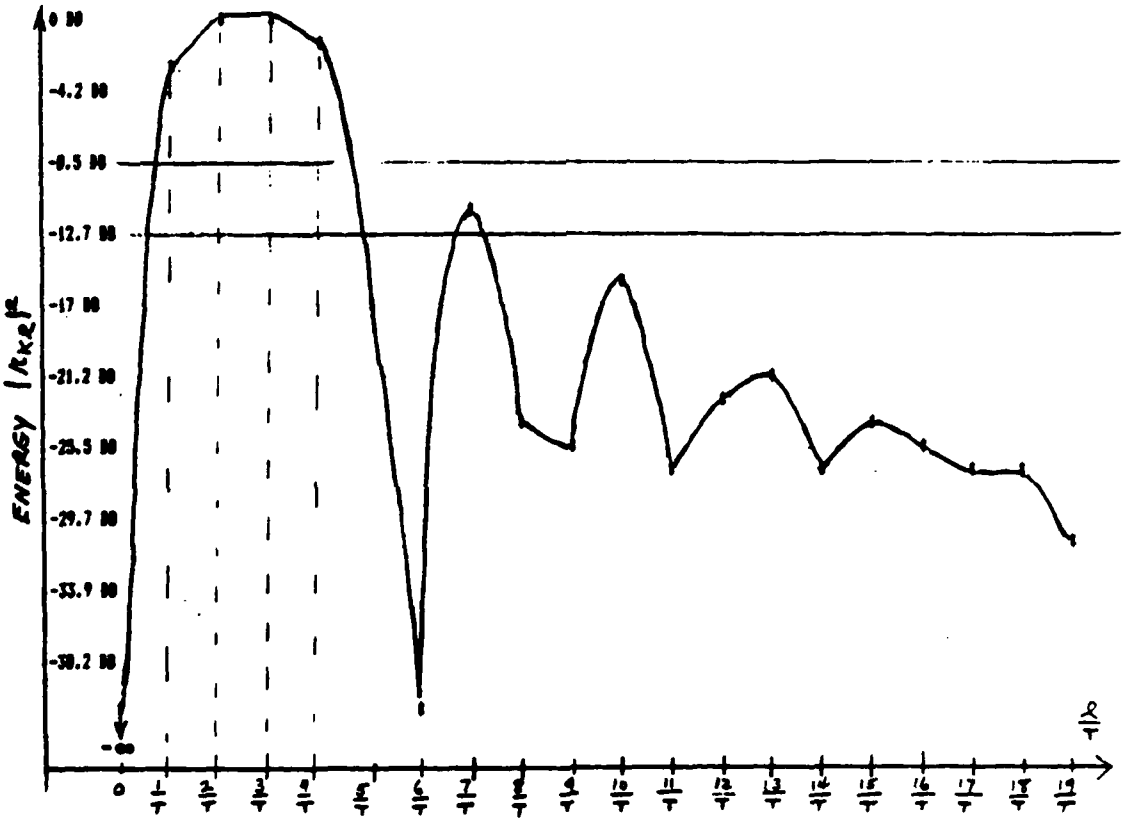

RECTANGULAR WINDOWED EXPANSION SIGNAL FREQUENCY = 2.5/T
MAXIMUM VALUE = .172462 MINIMUM VALUE = 9.87249E-06
EACH COLORED BAND IS CHANGE IN DB OF 4.24227
VERTICAL RESOLUTION IN DB IS 1.41409
NOTE: MINIMUM CROSS PRODUCT USED

Fig 4-22

Fig. 4-22 Rectangular Windowed Expansion for ν=2.5 Minimum Cross Product Contribution

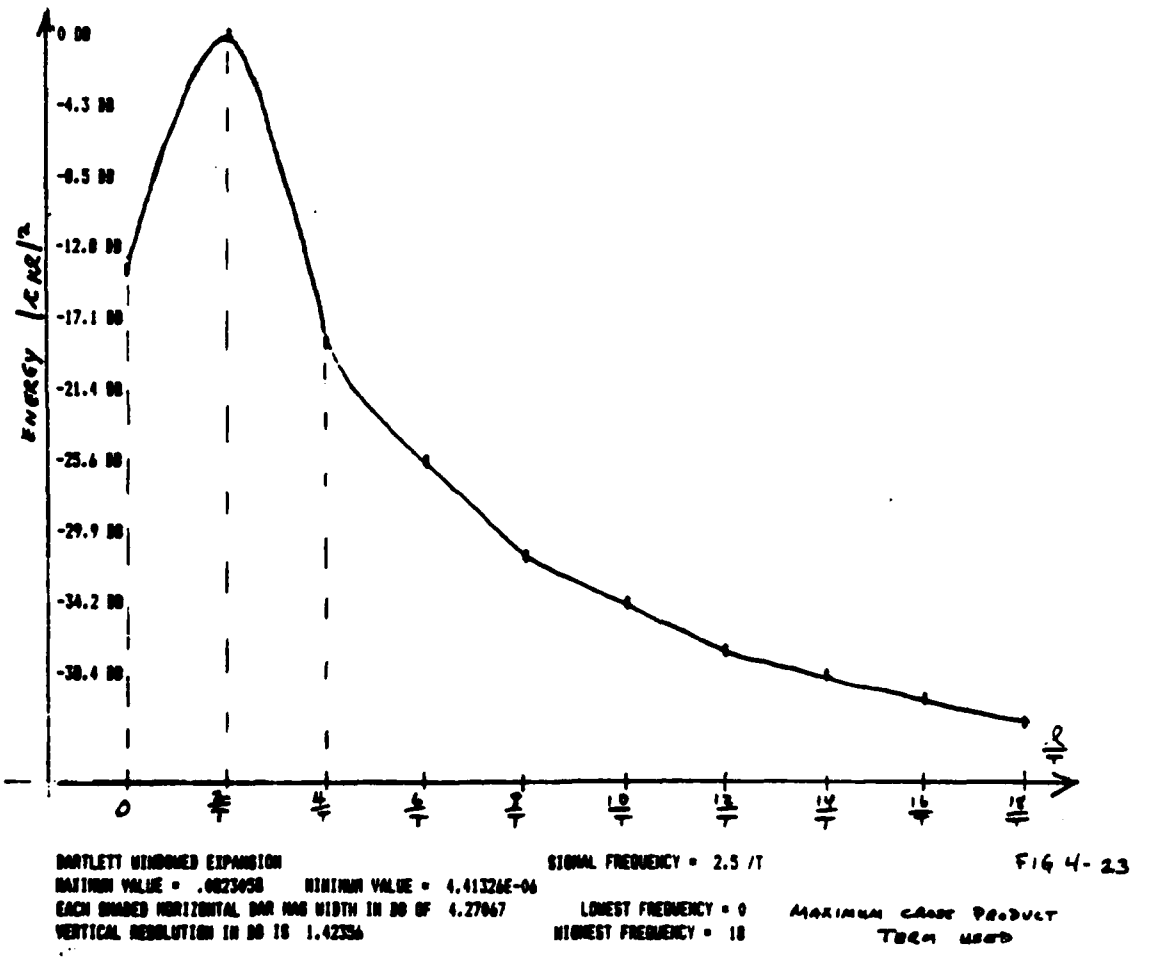

Fig. 4-23 Bartlett Windowed Expansion for ν=2.5 Maximum Cross Product Contribution

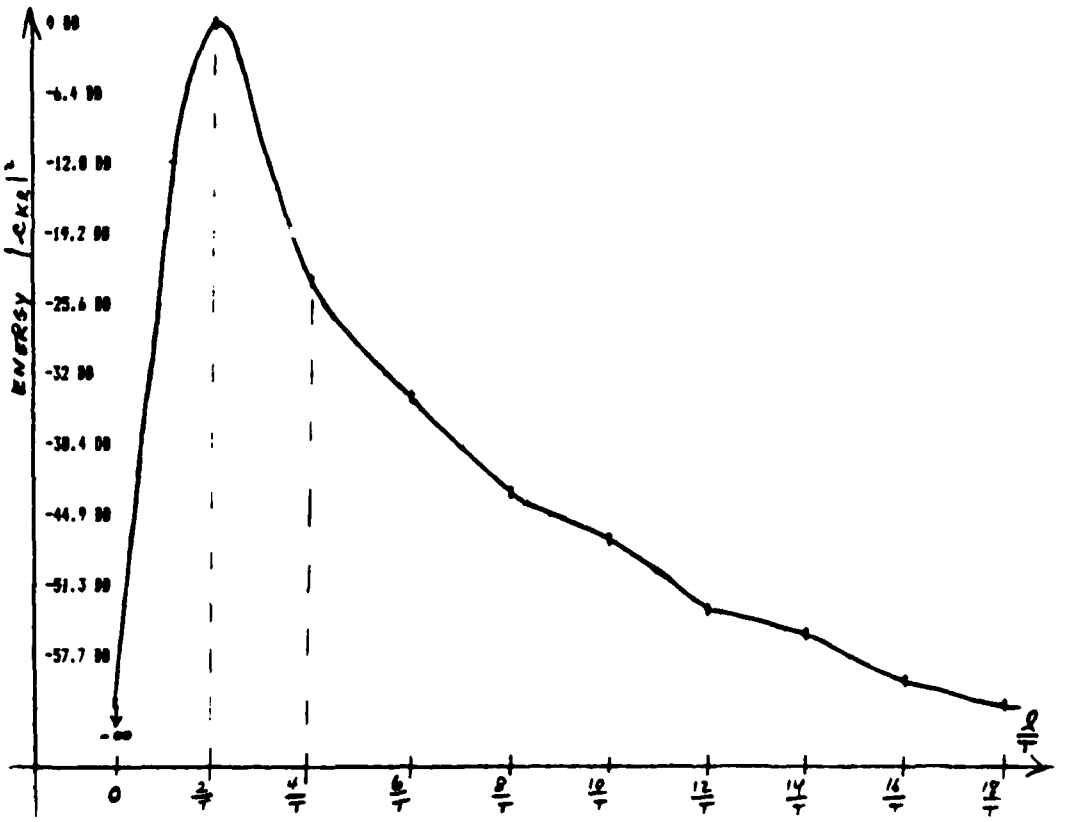

Fig. 4-24 Bartlett Windowed Expansion for ν=2.5 Minimum Cross Product Contribution

Rectangular expansion's spectral representation somewhat undesirable. In fact, once the signal's frequency becomes smaller than 10, the Rectangular expansion begins to produce a troublesome spectral representation. It is interesting at this point to review the Bartlett expansion plots for the same signal frequency of ν=2.5. Figure 4-23 presents the Bartlett expansion energies for the maximum cross product term while Figure 4-24 presents these energies for the minimum cross product term contribution. The difference between these Bartlett spectral representations and the Rectangular spectral representations is quite pronounced now. For example, comparing the maximum cross product term plots in Figure 4-21 and Figure 4-23, it is readily apparent that the Bartlett windowed expansion is sharper and has a more rapid decay rate than the Rectangular windowed expansion. In particular, the Bartlett expansion energies at ℓ=0 and ℓ=4 are down about 14 dB and 18 dB, respectively, from the maximum whereas the Rectangular expansion energies are down only 7.7 dB and 4.3 dB from their maximum value at the same frequencies. In addition the energy values have decreased by about 41 dB from ℓ=2 to ℓ=18 in the Bartlett expansion of Figure 4-23 compared to only about 24.8 dB over the same frequency band in the Rectangular expansion of Figure 4-21. The difference is even more pronounced for the minimum cross product term cases of Figure 4-22 and Figure 4-24. At ℓ=4, the Bartlett expansion of Figure 4-24 is down about 24.5 dB from maximum whereas the Rectangular is down about only 1.4 dB from maximum at ℓ=4! Furthermore the decay rate of the Bartlett expansion in Figure 4-24 is about 62 dB from ℓ=2

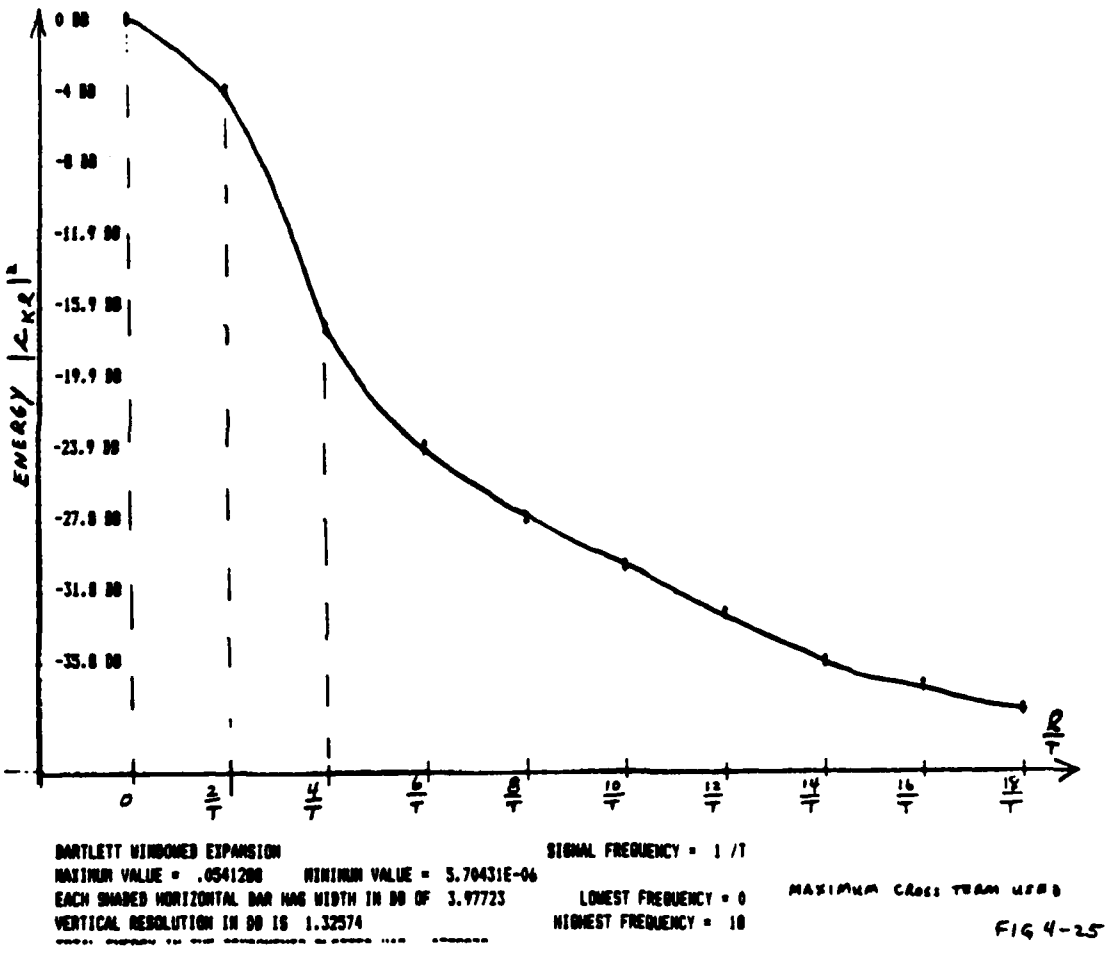

Fig. 4-25 Bartlett Windowed Expansion for ν=1.0 Maximum Cross Product Contribution

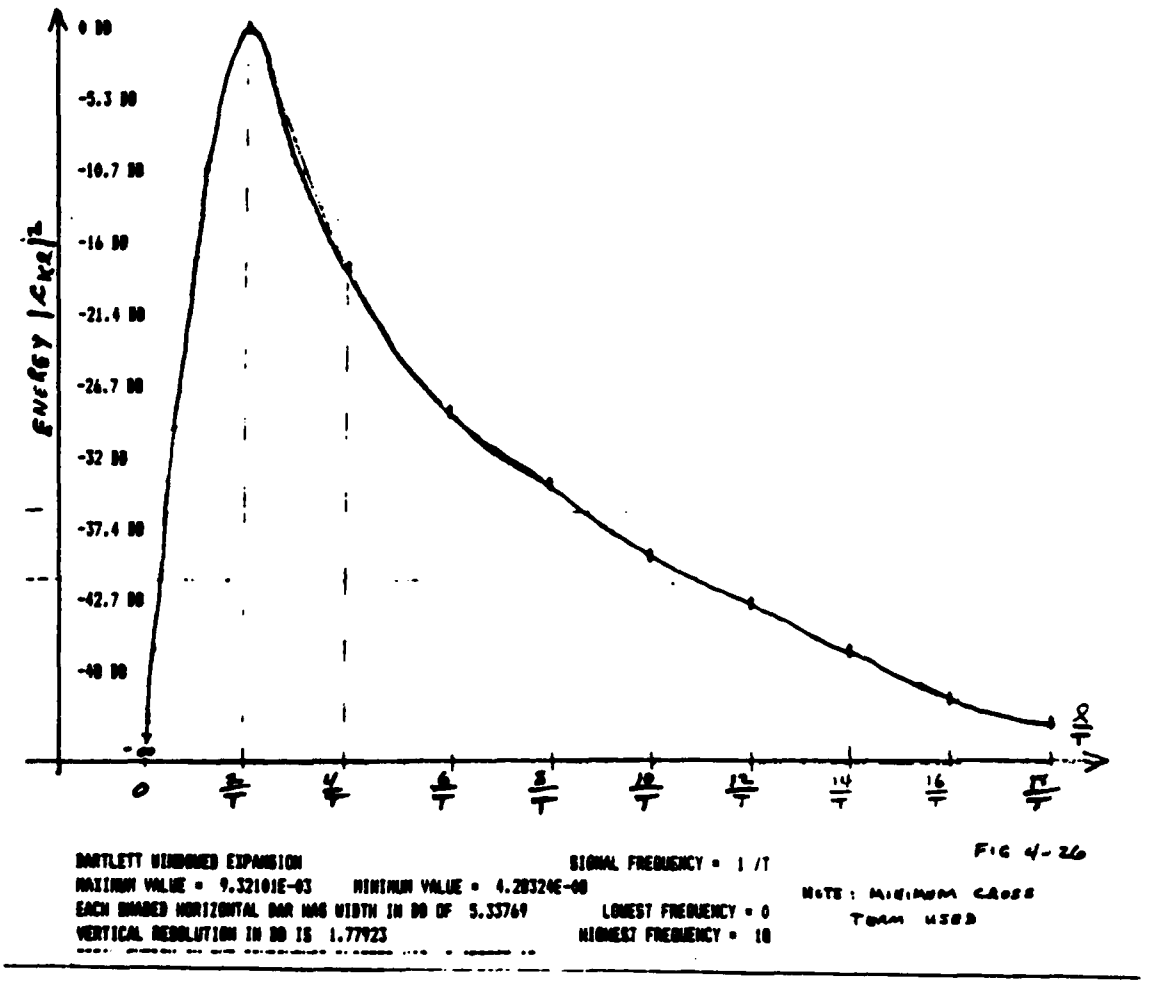

Fig. 4-26 Bartlett Windowed Expansion for ν=1.0, Minimum Cross Product Contribution

to ℓ=18 compared to about only 31 dB for the Rectangular expansion over the same frequency band. (The deep null at ℓ=6 in Figure 4-22 cannot be interpreted as the indication of decay rate from ℓ=2 to ℓ=18.) These facts show that the Bartlett expansion is far superior in spectral representation to the Rectangular expansion when the basic subinterval contains only 2.5 cycles of the sinusoidal signal. Even though the signal is not represented in the set of basis functions of either expansion, the Bartlett expansion still gives a tolerable spectral representation. Of course when there are an integer number of cycles of the sinusoid in the basic subinterval, the Rectangular expansion produces an ideal spectral representation, as mentioned before. However, the Bartlett expansion is still useful even for these cases of integer ν. For example, when ν=1, the smallest frequency for which the Rectangular expansion gives an ideal spectral representation, the Bartlett expansion is still somewhat tolerable, as shown in Figures 4-25 and 4-26. In Figure 4-25, the maximum cross term case is plotted while in Figure 4-26 the minimum cross term case is given. In Figure 4-25 the maximum value occurs at ℓ=0 and the next significant value is at ℓ=2, 4 dB down from this maximum. The decay rate is quite rapid, having decreased about 38 dB from ℓ=0 to ℓ=18. Thus it is likely that an observer would estimate the presence of a sinusoid with frequency between zero and 2/T in the signal. On the other hand, the minimum cross product term case for ν=1 plotted in Figure 4-26 has a pronounced peak at ℓ=2 because the cross product term causes the Bartlett energy value to vanish at ℓ=0 in accordance with (4-2-74). Again the decay rate is quite

pleasing, being about 51 dB from ℓ=2 to ℓ=18. It is likely that here the observer would estimate the sinusoidal signal's frequency to be 2/T, off from the true frequency by 1/T Hz. This may be troublesome but at least the spectral representation is fairly sharp.

As a final example in this series, the Rectangular expansions are given for ν=0.5, the maximum cross product term being used in Figure 4-27 and the minimum cross product term being used in Figure 4-28. In both cases the spectral representations are not very desirable, especially in the minimum cross product term case of Figure 4-28. In that plot the energy peaks at ℓ=2 and the decay rate is about 29 dB from the ℓ=2 to ℓ=19 values. Similarly, Figure 4-27, the maximum cross product term case, shows only a little better representation with the maximum value at ℓ=0, off by only 0.5/T Hz from the correct frequency. The value of energy at ℓ=1 is only 1 dB down from this peak which is acceptable. Additionally, the decay rate is about 30.6 dB from ℓ=0 to ℓ=19 which is about the same as that for Figure 4-28. Thus the Rectangular expansion for ν=0.5 is not very safe to use in general, mainly because of the dominant effect of the cross product term. It is interesting to compare the Bartlett expansion energies for ν=0.5, plotted in Figures 4-29 and 4-30. Figure 4-29 gives the maximum cross product term contribution while Figure 4-30 gives the minimum cross product term contribution. The result in Figure 4-30 is not very desirable because the maximum occurs for ℓ=2, off by 1.5/T Hz from the correct frequency. The result in Figure 4-29 is much more acceptable, with a maximum value at zero frequency and a rapid decay rate of about 47 dB from ℓ=0 to ℓ=18. Despite these drawbacks, the

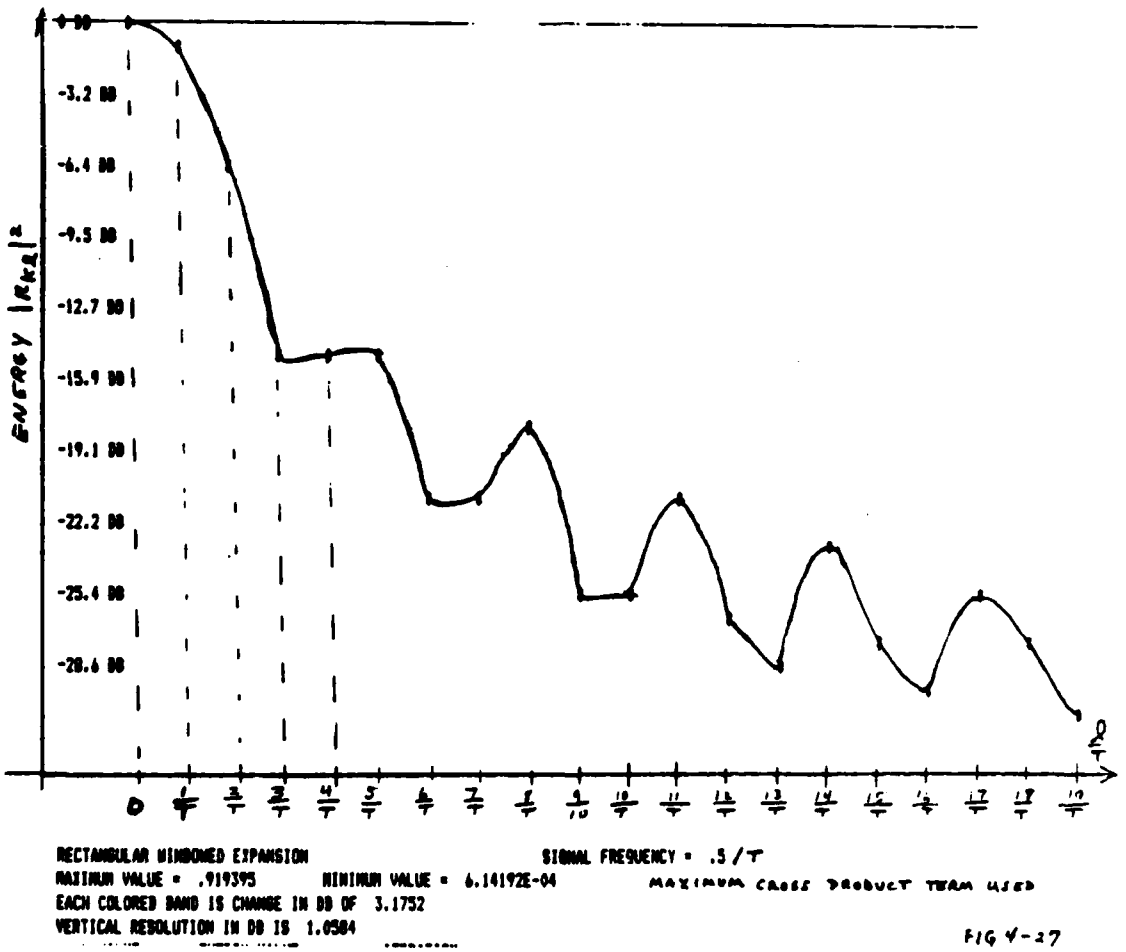

Fig. 4-27 Rectangular Windowed Expansion for ν=0.5, Maximum Cross Product Contribution

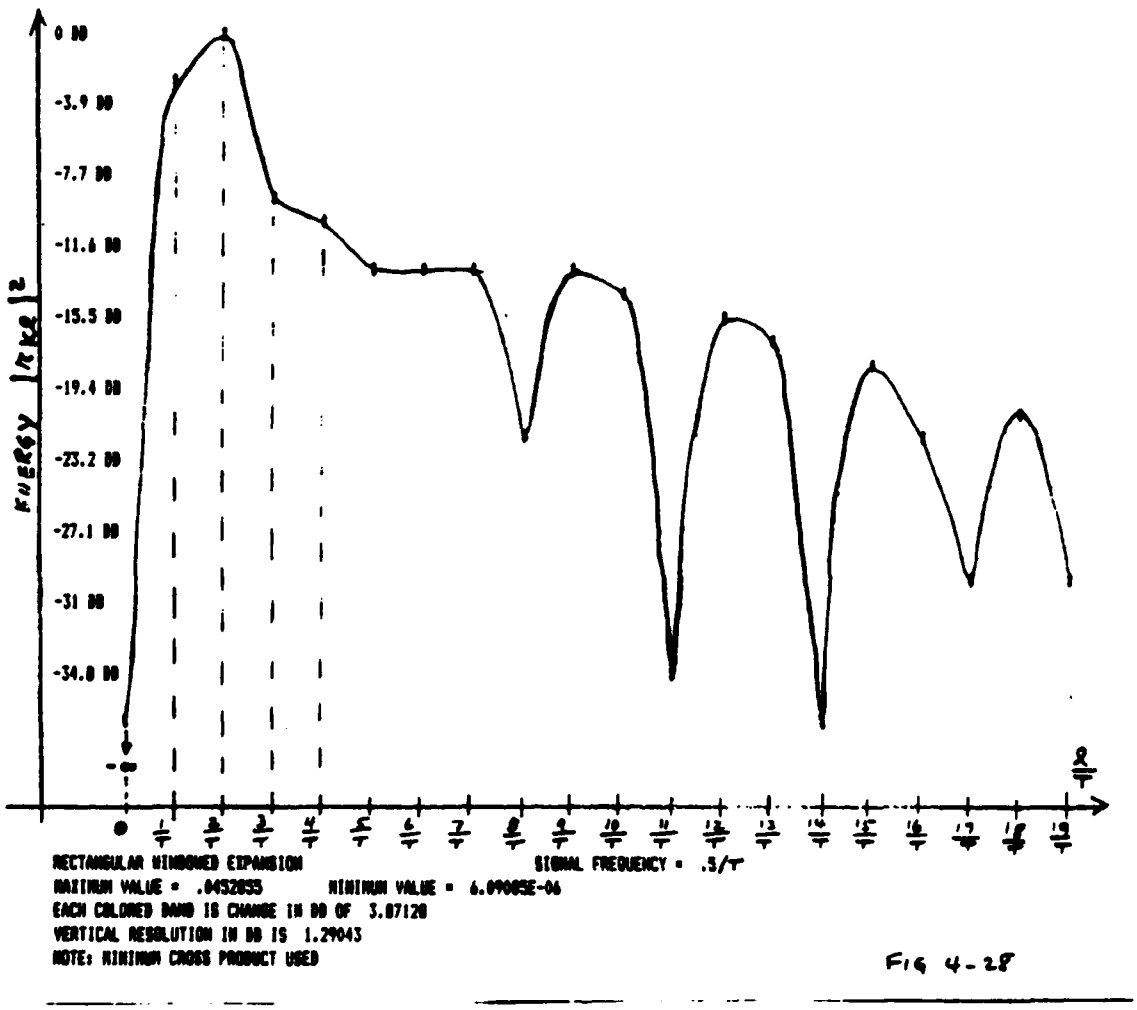

Fig. 4-28 Rectangular Windowed Expansion for ν=0.5, Minimum Cross Product Contribution

Bartlett windowed expansion has important advantages to offer over the Rectangular windowed expansion. First, the sharpness of spectral representation is quite evident and is certainly noteworthy for non-integer values of ν down to about ν=2.5. For lower non-integer values of ν, both Bartlett and Rectangular spectral representations become unacceptably "contaminated" by the cross product term. Secondly, the increased frequency spacing of the Bartlett energy values over the Rectangular energy values seems to enable a smoother, more rapid decay of the spectral plot away from the maximum. Thirdly, the cross product term itself appears to be more attenuated and confined to a narrower frequency band for the Bartlett spectral representation. This last point is evident from the comparison of plots in the ν=0.5 case. In conclusion, it should be evident that the desirable spectral characteristics of the Bartlett windowed expansion for an integer number of sinusoidal cycles as well as a non-integer number of cycles in the basic subinterval make it a useful windowed expansion. This provides greater flexibility for the choice of the basic subinterval width, T. Using only spectral sharpness as the criterion for choosing T, the Bartlett windowed expansion is acceptable with as few cycles as 2.5 in the subinterval. On the other hand, if T is adjustable so that an integer number of cycles can be contained within the basic subinterval, the Rectangular expansion is superior. In the final analysis, the choice of T depends upon knowledge of local time characteristics in the signal, that is, the number of cycles per second in a given time interval. This can be estimated roughly by the number of zero crossings.

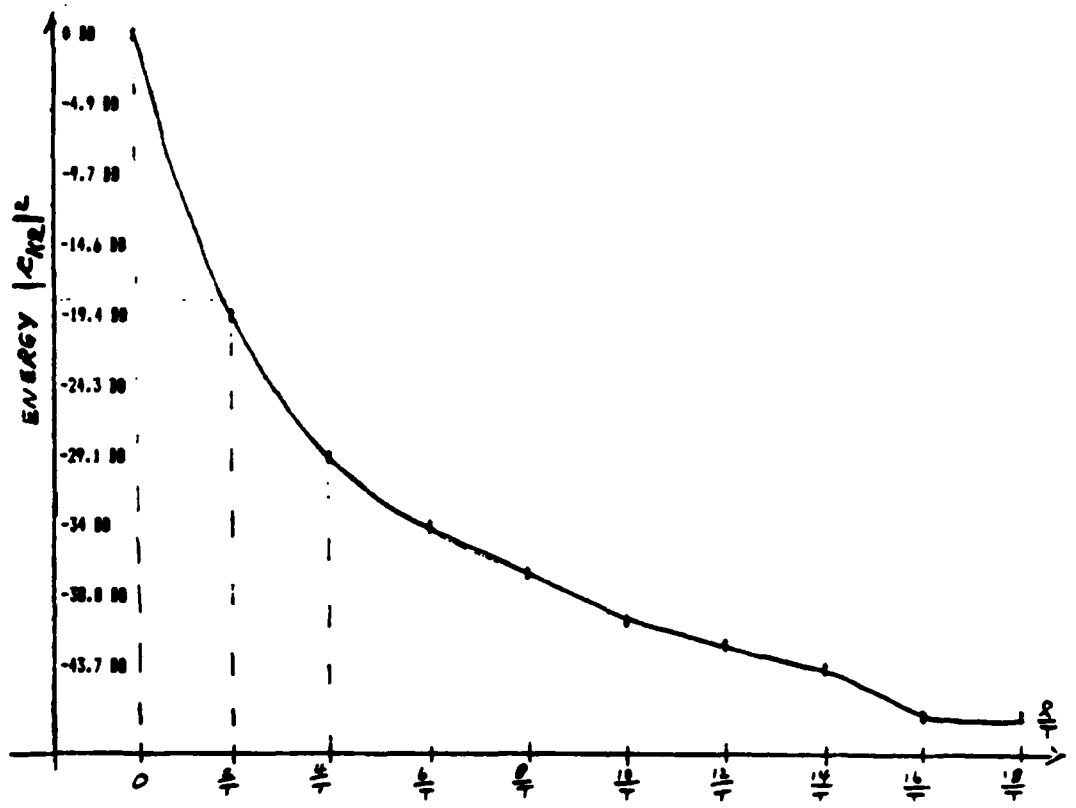

Fig. 4-29 Bartlett Windowed Expansion for ν=0.5, Maximum Cross Product Contribution

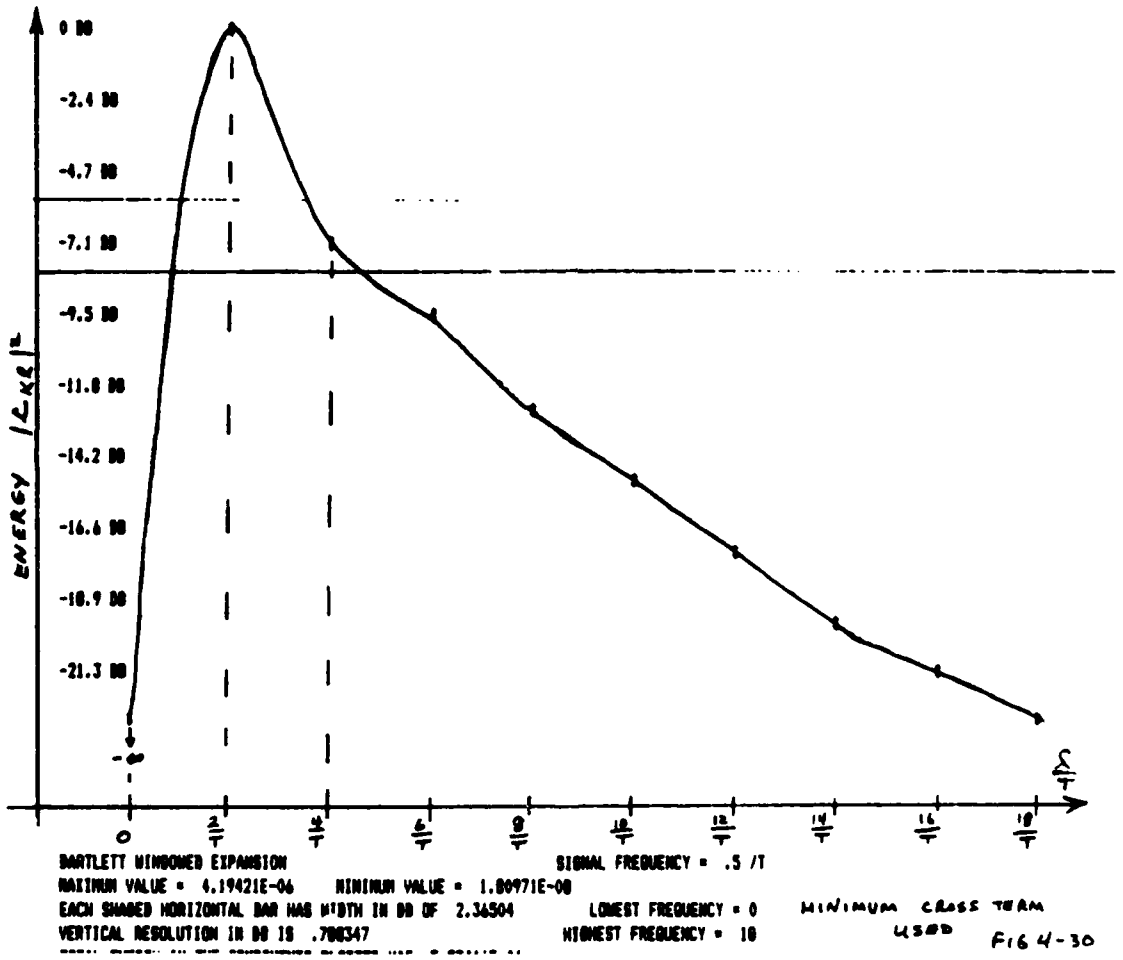

Fig. 4-30 Bartlett Windowed Expansion for ν=0.5, Minimum Cross Product Contribution

Secondly, it should be remembered that the smaller the value of T chosen, the larger will be the frequency spacing in Hertz in the energy distribution plot. Finally it should be realized that the windowed signal expansions express the signal in the given subinterval by a linear combination of shaped cisoidal functions so that interpretations of energy versus frequency plots must include a reference to the shape or amplitude modulation of the basic building block of the expansion.

4.3 Example of Time-Variant Energy Spectral Analysis

This section discusses the analysis of an FM-tone modulated signal. Specifically,

$$x(t) = \begin{cases} A \cos [2\pi\nu_c t + \beta \sin (2\pi\nu_m t)]; \; t_A \leq t < t_B \\ \\ \text{unknown} \; ; \; t < t_A \text{ and } t > t_B \; , \end{cases} \tag{4-3-1}$$

where β is known as the modulation index defined by

$$\beta = \frac{A_m \nu_d}{\nu_m} \quad . \tag{4-3-2}$$

In this context, the modulating signal is

$$m(t) = A_m \cos (2\pi\nu_m t) \; , \tag{4-3-3}$$

The carrier frequency in Hertz is ν_c, and the signal x(t) is another form of the more general expression

$$x(t) = \begin{cases} A \cos \left[2\pi\nu_c t + 2\pi\nu_d \int_o^t m(\tau)\, d\tau\right]; \; t_A \le t \le t_B \\ \\ \text{unknown}; \; t < t_A \text{ and } t > t_B. \end{cases} \qquad (4\text{-}3\text{-}4)$$

Within the observation interval $[t_A, t_B]$, the instantaneous frequency, ν_{INST}, is found by differentiating the phase of $x(t)$ and then dividing by 2π. Specifically,

$$\nu_{INST} = \nu_c + \beta\, \nu_m \cos\,(2\pi\nu_m t)\ , \qquad (4\text{-}3\text{-}5)$$

which is sketched as a function of time in Figure 4-31. It is seen from the sketch that β and ν_m control the extent of the maximum deviation of ν_{INST} away from ν_c. Also ν_m directly controls the rate of change with time of the sinusoidally varying instantaneous frequency.

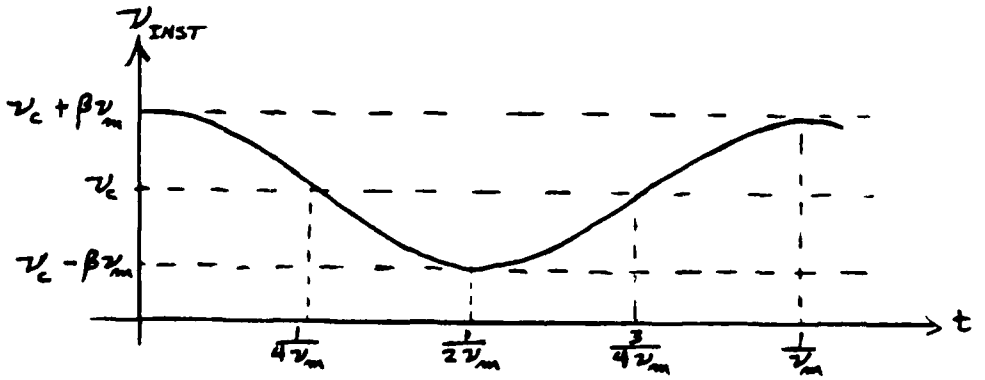

FIG. 4-31 INSTANTANEOUS FREQUENCY FUNCTION OF (4-3-5)

A sketch of the signal corresponding to this instantaneous frequency function is given in Figure 4-31.

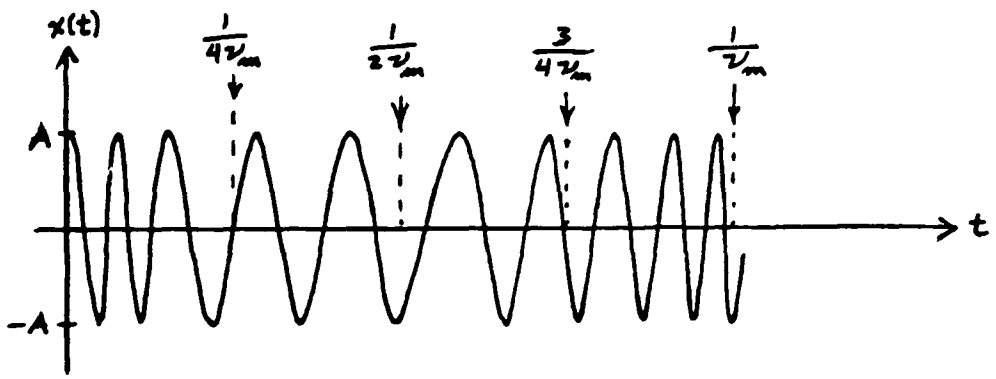

FIG. 4-32 AN FM TONE-MODULATED SIGNAL

The Bartlett windowed expansion will be determined first. The Bartlett windowed coefficients from (4-2-7) are

$$c_{k\ell} = \sqrt{\frac{2}{T}} \int_{t_k - \frac{T}{2}}^{t_k + \frac{T}{2}} x(t) \sqrt{1 - \frac{2|t-t_k|}{T}}\, e^{-j\frac{4\pi\ell}{T}}\, dt. \qquad (4\text{-}3\text{-}6)$$

Making the change of variable

$$\tau = \frac{2}{T}\ (t-t_k) \qquad (4\text{-}3\text{-}7)$$

$$d\tau = \frac{2}{T}\, dt, \qquad (4\text{-}3\text{-}8)$$

there results

$$c_{k\ell} = \sqrt{\frac{T}{2}} \int_{-1}^{1} x(\tfrac{T}{2}\tau + t_k)\ \sqrt{1-|\tau|}\ e^{-j\frac{4\pi}{T}\ell(\frac{T}{2}\tau + t_k)}\, d\tau \qquad (4\text{-}3\text{-}9)$$

For simplicity, let

$$T = NT_c \qquad (4\text{-}3\text{-}10)$$

AD-A140 196 A VECTOR SPACE APPROACH TO TIME-VARIANT ENERGY SPECTRAL ANALYSIS(U) ROME AIR DEVELOPMENT CENTER GRIFFISS AFB NY J E ROACH DEC 83 RADC-TR-83-270 3/3

UNCLASSIFIED NL

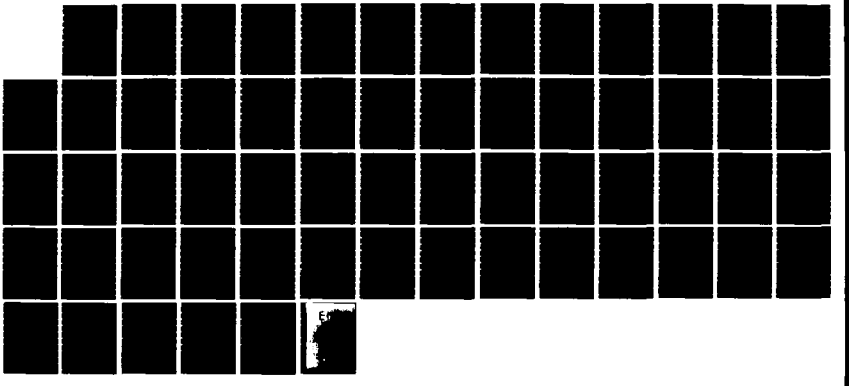

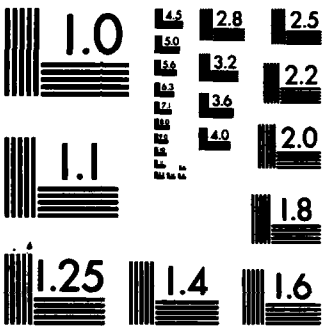

where

$$T_c = \frac{1}{\nu_c} \tag{4-3-11}$$

and N is a positive integer. This assumption means that the basic subinterval is exactly as long as N cycles of the carrier frequency. It follows that

$$x\left(\frac{T}{2}\tau + t_k\right) = x\left(\frac{N}{2\nu_c}\tau + t_k\right) \tag{4-3-12}$$

$$= A\cos\left\{2\pi\nu_c\left(\frac{N}{2\nu_c}\tau + t_k\right) + \beta\sin\left[2\pi\nu_m\left(\frac{N}{2\nu_c}\tau + t_k\right)\right]\right\} \tag{4-3-13}$$

$$= A\cos\left\{\pi N\tau + 2\pi\nu_c t_k + \beta\sin\left[\pi\left(\frac{\nu_m}{\nu_c}\right)N\tau + 2\pi\nu_m t_k\right]\right\}. \tag{4-3-14}$$

Substituting this for $x\left(\frac{T}{2}\tau + t_k\right)$ in (4-3-9), there results

$$c_{k\ell} = A\sqrt{\frac{T}{2}}\; e^{-j\frac{4\pi}{T}\ell t_k}\int_{-1}^{1}\cos\left\{\pi N\tau + 2\pi\nu_c t_k + \beta\sin\left[\pi\left(\frac{\nu_m}{\nu_c}\right)N\tau + 2\pi\nu_m t_k\right]\right\}\sqrt{1-|\tau|}\; e^{-j2\pi\ell\tau}\,d\tau\,. \tag{4-3-15}$$

Notation is simplified by the following expressions. Letting

$$\phi_{c_k} = 2\pi\nu_c t_k\,, \tag{4-3-16}$$

$$\phi_{m_k} = 2\pi\nu_m t_k\,, \tag{4-3-17}$$

and

$$R = \frac{\nu_m}{\nu_c} , \tag{4-3-18}$$

where R is not necessarily an integer, it follows that

$$c_{k\ell} = A\sqrt{\frac{T}{2}}\ e^{-j\frac{4\pi}{T}\ell t_k} \int_{-1}^{1} \cos\ \{\pi N\tau + \phi_{c_k} + \beta \sin[\pi RN\tau + \phi_{m_k}]\}$$

$$\cdot \sqrt{1-|\tau|}\ e^{-j2\pi\ell\tau}\, d\tau \tag{4-3-19}$$

and so the Bartlett windowed energy values are found to be

$$|c_{k\ell}|^2 = \frac{A^2T}{2} \left|\int_{-1}^{1} \cos\{\pi N\tau + \phi_{c_k} + \beta \sin\ [\pi RN\tau + \phi_{m_k}]\}\right.$$

$$\left. \cdot \sqrt{1-|\tau|}\ e^{-j2\pi\ell\tau}\, d\tau\right|^2 . \tag{4-3-20}$$

Without loss of generality, the observation interval $[t_A, t_B]$ will be defined as

$$t_A = 0 \tag{4-3-21}$$

and

$$t_B = 12T \tag{4-3-22}$$

so that, using (4-3-10), the centerpoints of the subintervals are

$$t_1 = \frac{T}{2} = \frac{N}{2\nu_c}$$

$$t_2 = \frac{3T}{2} = \frac{3N}{2\nu_c}$$

$$\vdots \qquad \vdots$$

$$t_{12} = \frac{23T}{2} = \frac{23N}{2\nu_c} \quad . \tag{4-3-23}$$

Substituting (4-3-23) into (4-3-16), it follows that

$$\phi_{c_1} = 2\pi\nu_c t_1 = \pi N$$

$$\phi_{c_2} = 2\pi\nu_c t_2 = 3\pi N$$

$$\vdots \qquad \vdots$$

$$\phi_{c_{12}} = 2\pi\nu_c t_{12} = 23\pi N. \tag{4-3-24}$$

Similarly, substituting (4-3-23) into (4-3-17) and using (4-3-18), there results

$$\phi_{m_1} = 2\pi\nu_m t_1 = \pi RN$$

$$\phi_{m_2} = 2\pi\nu_m t_2 = 3\pi RN$$

$$\vdots \qquad \vdots$$

$$\phi_{m_{12}} = 2\pi\nu_m t_{12} = 23\pi RN \ . \tag{4-3-25}$$

As an example, the Bartlett energy values for the first subinterval centered at $t_1 = \frac{T}{2}$ are given by

$$|c_{1,\ell}|^2 = \frac{A^2T}{2} \left| \int_{-1}^{1} \cos \{\pi N\tau + \pi N + \beta \sin [\pi RN\tau + \pi RN]\} \sqrt{1-|\tau|}\ e^{-j2\pi\ell\tau}\, d\tau \right|^2 \qquad (4\text{-}3\text{-}26)$$

and the Bartlett energy values for the second subinterval are given by

$$|c_{2,\ell}|^2 = \frac{A^2T}{2} \left| \int_{-1}^{1} \cos \{\pi N\tau + 3\pi N + \beta \sin [\pi RN\tau + 3\pi RN]\} \sqrt{1-|\tau|}\ e^{-j2\pi\ell\tau}\, d\tau \right|^2 . \qquad (4\text{-}3\text{-}27)$$

When

$$\left.\begin{aligned} N &= 14 \\ \beta &= 48 \\ \text{and} \\ R &= \frac{1}{(12)(14)} \end{aligned}\right\} \qquad (4\text{-}3\text{-}28)$$

the instantaneous frequency function in (4-3-5) and in Figure 3-30 has the appearance shown in Figure 3-32.

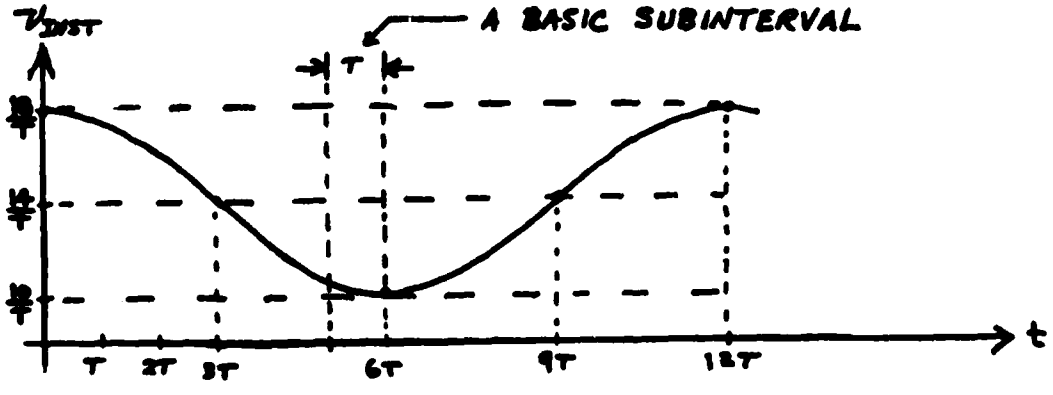

FIG. 3-32 INSTANTANEOUS FREQUENCY FOR THE CHOICE OF PARAMETERS IN (4-3-28)

For this case, the centerpoints in (4-3-23) for each subinterval and their corresponding instantaneous frequencies are given in Table 4-2.

Table 4-2

Centerpoints of Subintervals and Corresponding Instantaneous Frequencies

Centerpoint	Instantaneous Frequency
t_1	17.864/T
t_2	16.828/T
t_3	15.035/T
t_4	12.965/T
t_5	11.172/T
t_6	10.136/T
t_7	10.136/T
t_8	11.172/T
t_9	12.965/T
t_{10}	15.035/T
t_{11}	16.828/T
t_{12}	17.864/T

The graphs of the Bartlett expansion energy values for the first three subintervals are given in Figures 4-33, 4-34, and 4-35. A condensed plot of these energy values for the first eight subintervals is given in Figure 4-36. In Figure 4-36, the dashed line represents the instantaneous

frequency and the vertical axes indicate values of energy greater than -10 dB down from the maximum of all subinterval energy values. Thus a "global" scaling is used in Figure 4-36. It is interesting to note that the significant values of energy follow the instantaneous frequency quite well. An important feature is that the magnitude of the energy values decreases when the rate of change of instantaneous frequency increases. For example, from the first subinterval centered at $t=t_1$ to the next subinterval at $t=t_2$, the maximum energy value decreases by about 6 dB. The maximum energy value continues to stay near this lower level for the third through the fifth subintervals as the instantaneous frequency changes from 17/T to 11/T. Then, in the sixth and seventh subintervals the maximum value becomes large again, essentially equal in magnitude to the maximum of the first subinterval. Thus when the instantaneous frequency changes to about (1.5/T) Hz or more during a particular subinterval, the peak value decreases by about 6 dB from the maximum value of the "steady" tone case. Conversely, when the instantaneous frequency is relatively "steady," the frequency distribution of energy shows a strong peak at or near the instantaneous frequency. In terms of Figure 4-36, a rule of thumb for definition of "steady" is the condition in which the instantaneous frequency changes by less than 1/T Hz over the subinterval being considered. Subintervals 1, 6, and 7 would qualify for "steady" tone cases. The basic fact being presented here is that each windowed expansion coefficient involves the average of the product of the signal and a shaped cisoidal function. Thus instantaneous information is being "smoothed" out over the basic subinterval. As a final

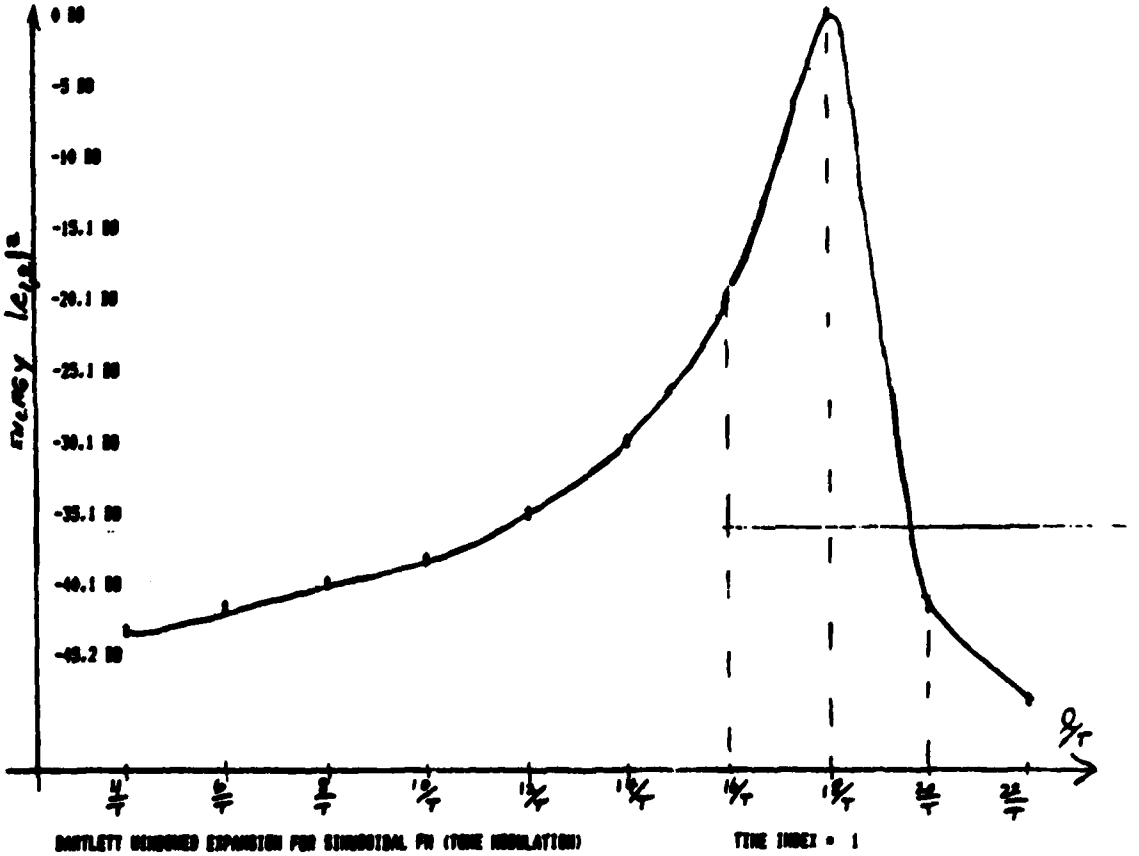

Fig. 4-33 Bartlett Windowed Expansion for First Subinterval

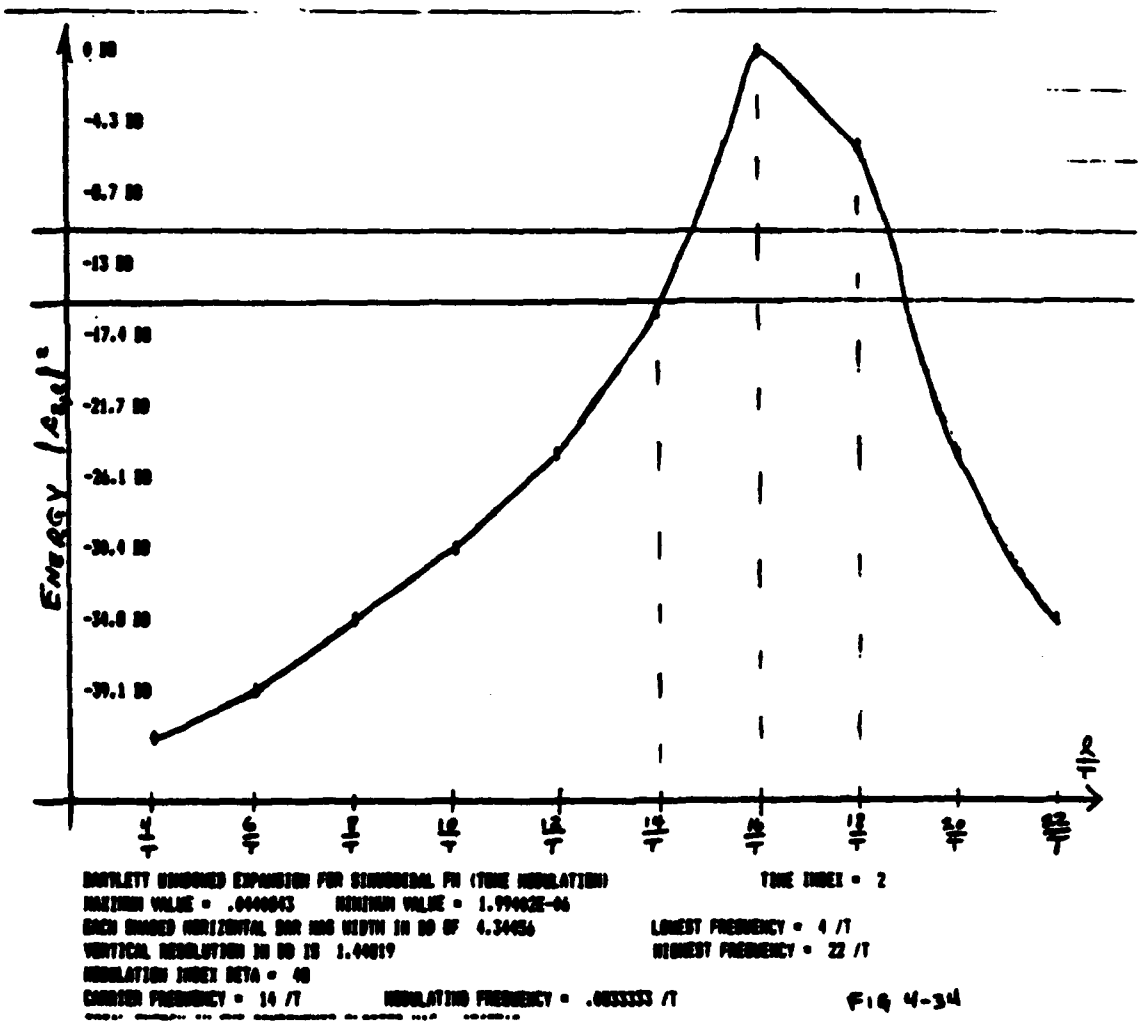

Fig. 4-34 Bartlett Windowed Expansion for Second Subinterval

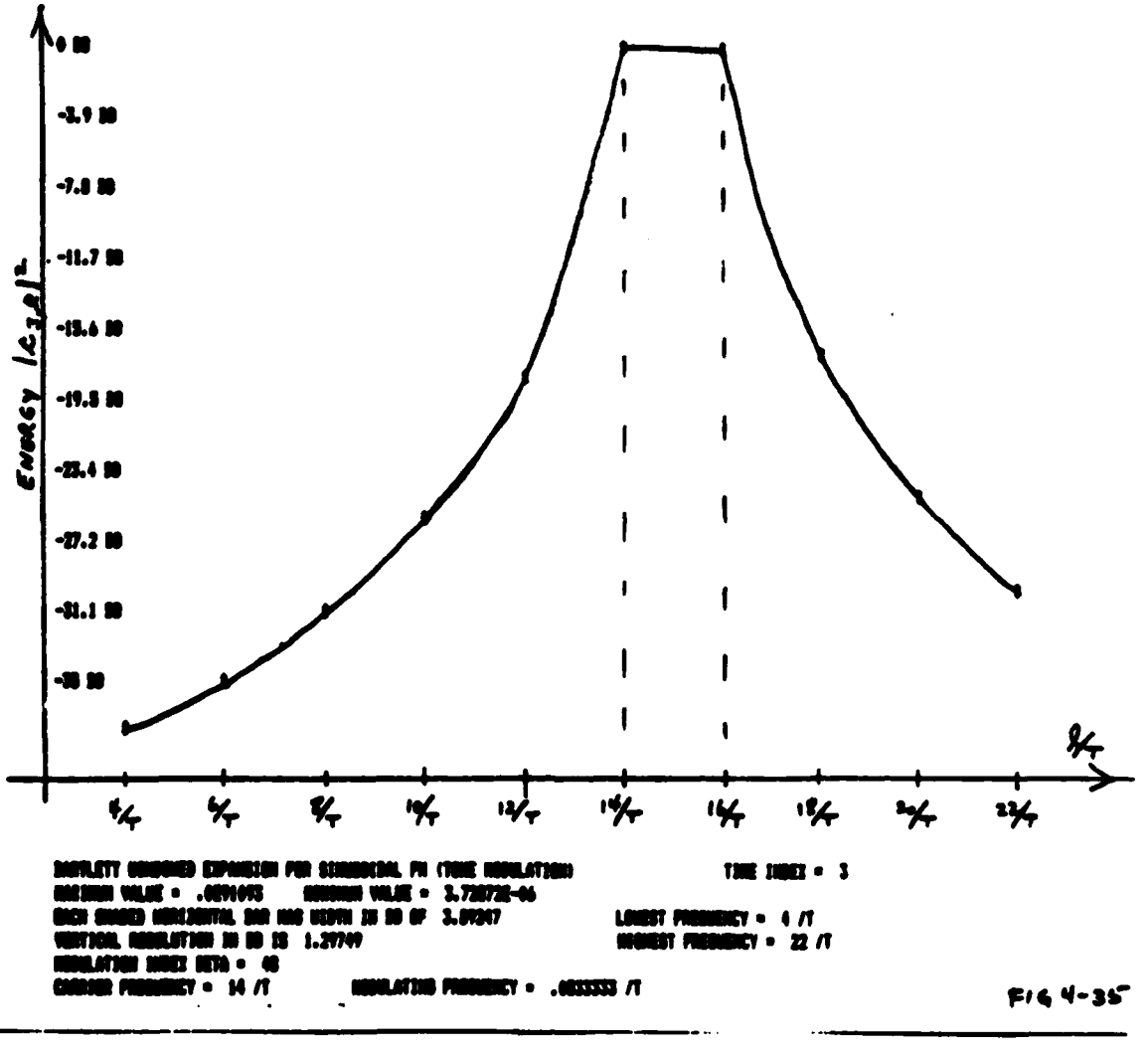

Fig. 4-35 Bartlett Windowed Expansion for Third Subinterval

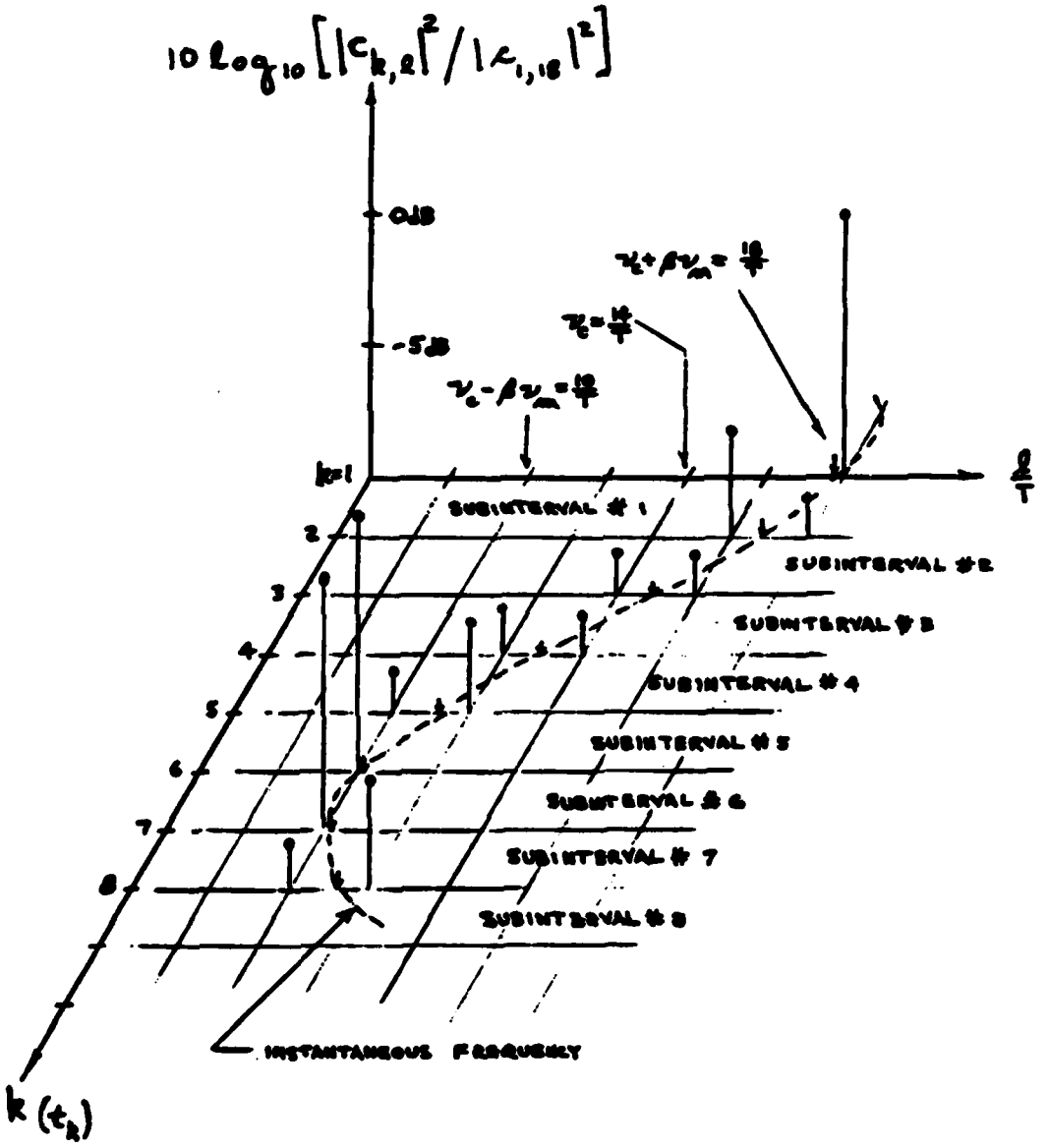

Fig. 4-36 Bartlett Expansion Energy Values for Sinusoidal FM Signal

comment on Figure 4-36, it should be noted that a basic pattern is shown in the first 6 subintervals; the pattern repeats itself in a mirror image fashion in subintervals 7 through 12.

The Rectangular windowed expansion is now presented for the sinusoidally modulated FM signal. From (4-2-4), the expansion coefficients are

$$r_{k\ell} = \frac{1}{\sqrt{T}} \int_{t_k - \frac{T}{2}}^{t_k + \frac{T}{2}} x(t)\, e^{-j\frac{2\pi}{T}\ell t}\, dt \ . \qquad (4\text{-}3\text{-}29)$$

Making the change of variable

$$\tau = \frac{2}{T}\,(t - t_k) \qquad (4\text{-}3\text{-}30)$$

and

$$d\tau = \frac{2}{T}\, dt \ , \qquad (4\text{-}3\text{-}31)$$

there results

$$r_{k\ell} = \frac{\sqrt{T}}{2}\, e^{-j\frac{2\pi}{T}\ell t_k} \int_{-1}^{1} x(\tfrac{T}{2}\tau + t_k)\, e^{-j\pi\ell\tau}\, d\tau \qquad (4\text{-}3\text{-}32)$$

and

$$|r_{k\ell}|^2 = \frac{T}{4}\, \left| \int_{-1}^{1} x(\tfrac{T}{2}\tau + t_k)\, e^{-j\pi\ell\tau} d\tau \right|^2 \qquad (4\text{-}3\text{-}33)$$

Substituting $x(\frac{T}{2}\tau + t_k)$ from (4-3-9) and using the simplifications of (4-3-16), (4-3-17), and (4-3-18), it follows that

$$|r_{k\ell}|^2 = \frac{A^2T}{4} \left| \int_{-1}^{1} \cos \{\pi N\tau + \phi_{c_k} + \beta \sin [\pi RN\tau + \phi_{m_k}]\} \right.$$

$$\left. \cdot\ e^{-j\pi\ell\tau} d\tau \right|^2. \qquad (4\text{-}3\text{-}34)$$

These energy values are plotted in Figures 4-37, 4-38, and 4-39 for k=1, 2, and 3, respectively. The same parameter values of the Bartlett windowed expansion case in (4-3-28) were used here. Thus the first three subintervals produce energy values which are shown in the three figures mentioned. In addition, a condensed plot of the first eight subintervals is given in Figure 4-40. In this condensed plot it is seen that the peak values of the energy "track" the instantaneous frequency quite well. In fact, because of the smaller frequency spacing of the Rectangular windowed expansion, the condensed plot of Figure 4-40 seems to give a better "track" than the condensed plot of Figure 4-36. Upon close examination, several interesting differences between the Rectangular and Bartlett expansions emerge. First, when the energy plots for the first subinterval (k=1) are compared, i.e., Figure 4-37 of the Rectangular expansion with Figure 4-33 of the Bartlett expansion, it is seen that the Bartlett expansion has the sharper spectral representation. This is shown by comparing energy values at similar frequencies. Specifically, the Bartlett energy value at ℓ=16 is 20.1 dB below the maximum while the corresponding Rectangular energy value is 18.4 dB below

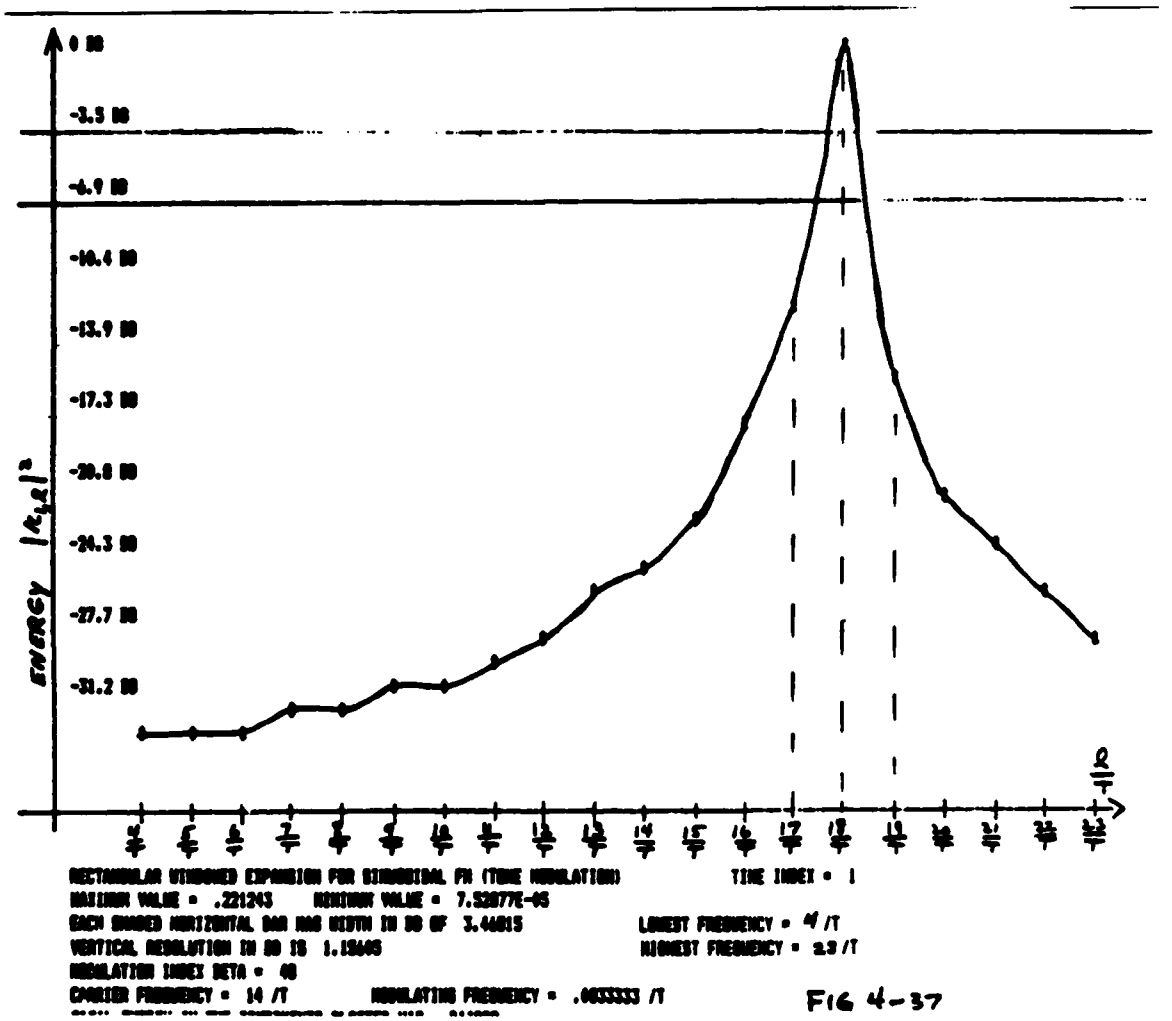

FIG 4-37

Fig. 4-37 Rectangular Expansion for First Subinterval

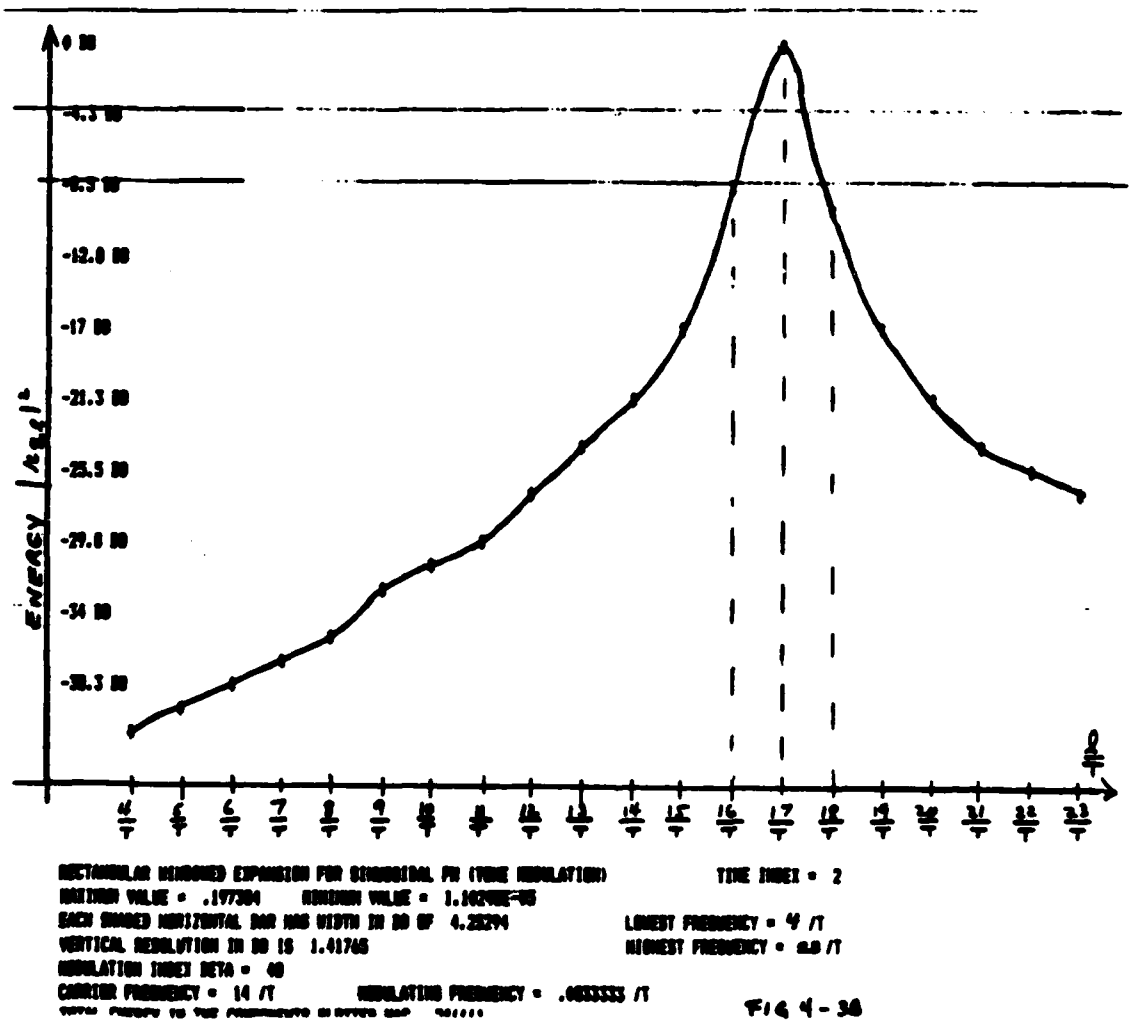

Fig. 4-38 Rectangular Expansion for Second Subinterval

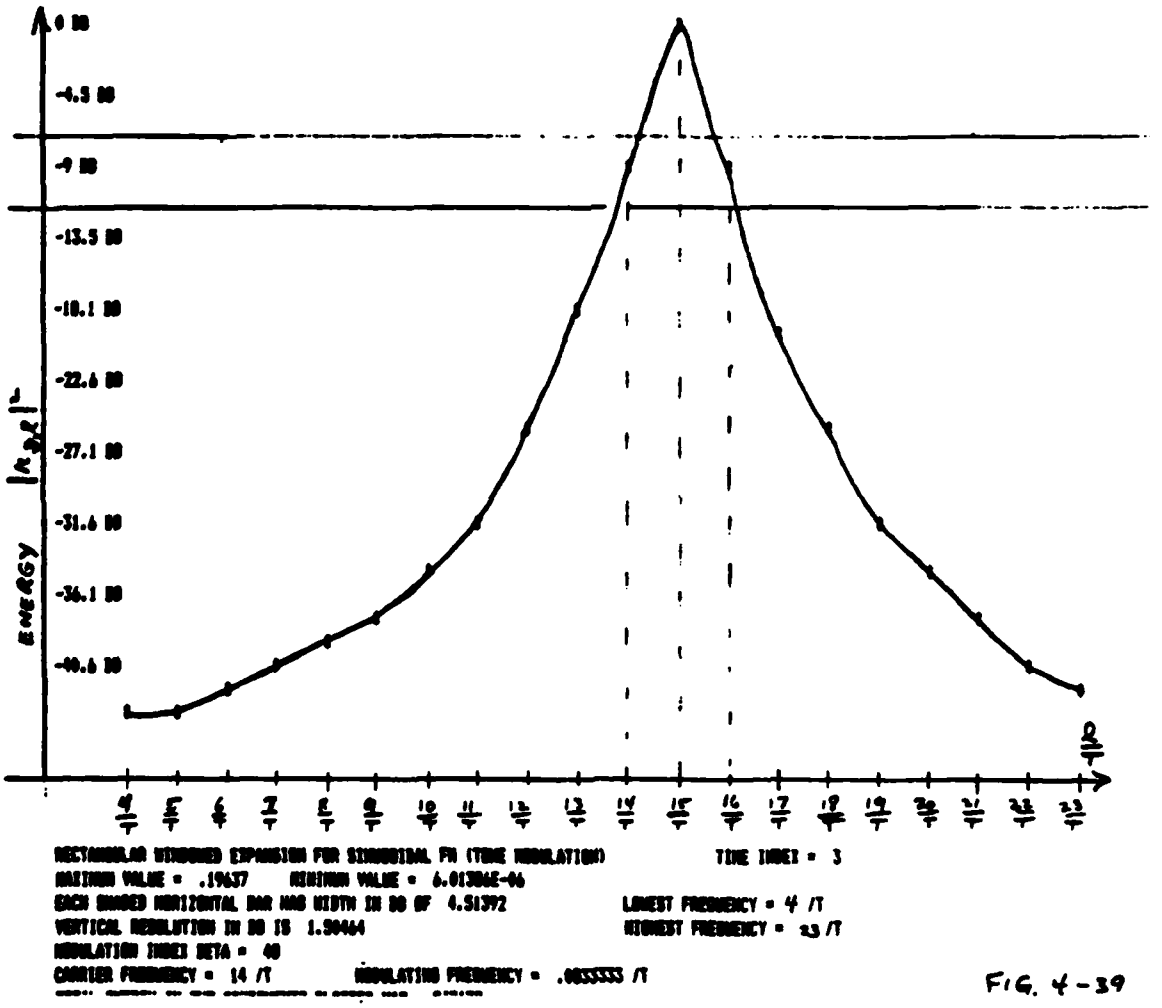

Fig. 4-39 Rectangular Expansion for Third Subinterval

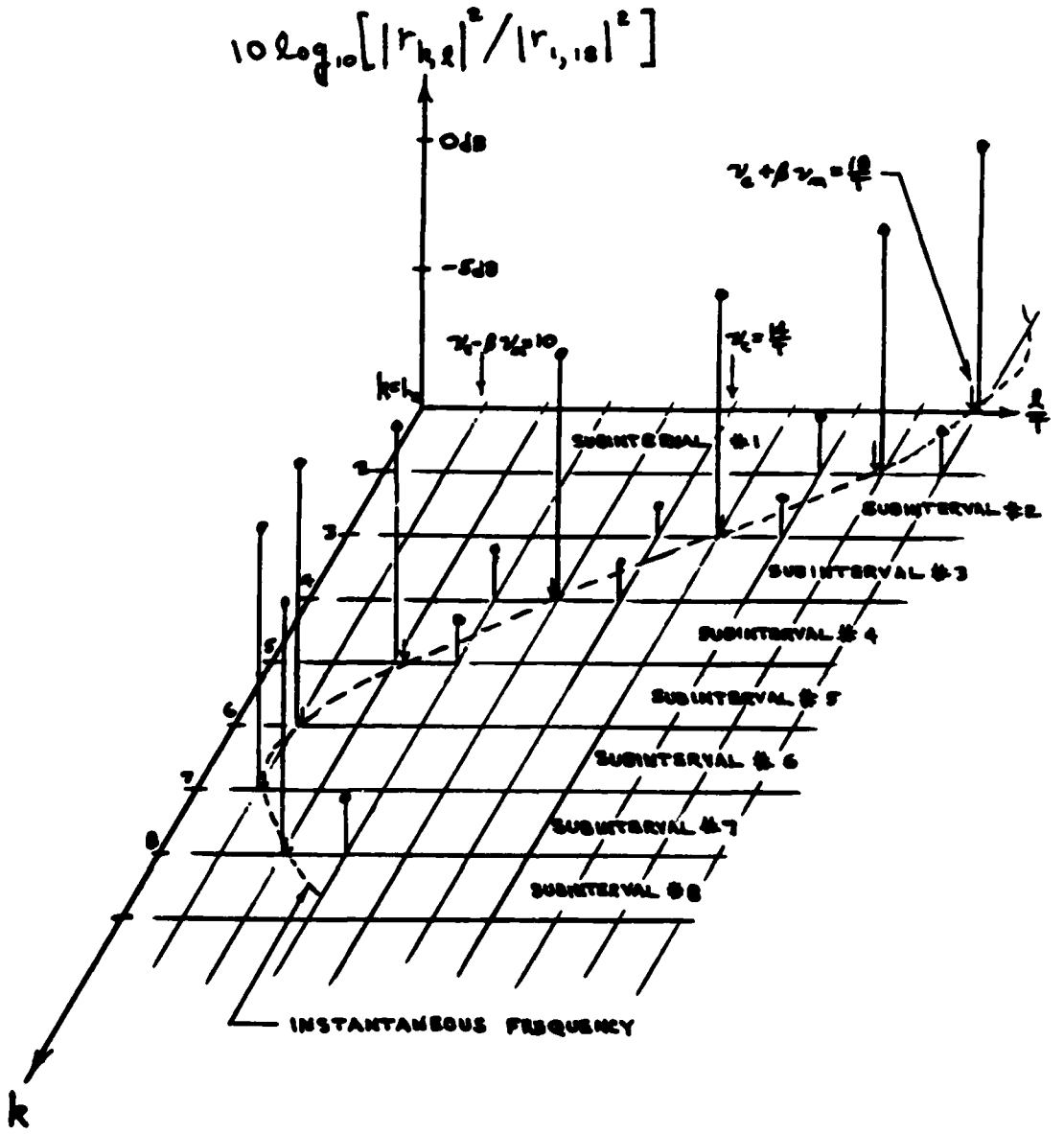

Fig. 4-40 Rectangular Windowed Expansion Values for Sinusoidal FM Signal

its maximum. A similar trend is seen at other frequency indexes also. It is noted that the instantaneous frequency is fairly constant during this first time subinterval, beginning at t=0 with the value of (18/T) Hz and ending with the value of (17.46/T) Hz at t=T. Now for the second subinterval (k=2), the Rectangular expansion of Figure 4-38 is compared to the Bartlett expansion of Figure 4-34. The instantaneous frequency at the centerpoint $t=t_2$ is (16.828/T) Hz from Table 4-2 and the Rectangular expansion appears to have the better spectral representation with its peak at (17/T) Hz. But more importantly, the Rectangular expansion plot has a slightly more desirable decay rate. At the frequency (14/T) Hz, for instance, the Rectangular windowed energy is down 21.3 dB from its maximum while the corresponding Bartlett windowed energy is only down 16 dB from its maximum. On the high frequency side of the peak, however, both expansions decay quite rapidly. In particular, at 20/T Hz, the Bartlett energy is about 24.6 dB below its maximum and the Rectangular energy is about 21.3 dB below maximum. The instantaneous frequency decreases from its value of 17.46/T Hz at the beginning of the second subinterval to a value of 16/T Hz at the end of this subinterval, a change of almost 1.5/T Hz. Finally, in the third subinterval, the Rectangular expansion of Figure 4-35 is compared to the Bartlett expansion of Figure 4-39. The Rectangular energy plot is clearly more desirable here with its sharp spectral peak at 15/T Hz. From Table 4-2 the instantaneous frequency at the third subinterval centerpoint ($t=t_3$) is 15.035/T Hz. The Bartlett energy plot is tolerable with maxima at

14/T Hz and 16/T Hz, although its energy at 12/T Hz is only 18.2 dB down from maximum compared to about 25.6 dB down from maximum for the Rectangular expansion at the same frequency. Thus the Bartlett expansion has a slower decay characteristic than the Rectangular expansion for this case. It should be noted that, for the third subinterval, the instantaneous frequency changes by 2/T Hz, starting with the value of 16/T Hz at the beginning and ending with the value of 14/T Hz which is the carrier frequency. Figure 3-32 is helpful in considering these values of instantaneous frequency.

The analysis performed here indicates that there are advantages and disadvantages for using any windowed expansion. The Rectangular expansion is more sensitive to changes of instantaneous frequency than the Bartlett expansion and provides more precision for estimating instantaneous frequency with its smaller frequency spacing. Also the Rectangular expansion is complete for arbitrary finite-energy signals while other windowed expansions are in general not complete. On the other hand, the Bartlett windowed expansion provides a sharper spectral representation than the Rectangular expansion when the instantaneous frequency is fairly constant within the subinterval being considered. This sharp spectral representation entails a rapid numerical decay from maximum as well as a monotonically smooth fall-off on both sides of the peak.

4.4 Example of the Resolution of Two Sinusoidal Signals

Since non-rectangular windowed expansions like the Bartlett are expected to offer sharper spectral representations when the signal instantaneous frequency is fairly constant, it is natural to expect these properties to provide good resolution for two or more sinusoidal signals. In this context, resolution means the process of estimating the true frequency and energy of a sinusoidal signal in the presence of other sinusoidal signals. In this section, two sinusoidal signals are assumed to occupy the same subinterval of width T. The energy values for both the Bartlett and Rectangular windowed expansions are calculated and an interesting comparison results.

The signal under consideration is given by

$$x(t) = \begin{cases} A\left\{\cos\left(\frac{2\pi}{T}\nu t\right) + \xi\cos\left[\frac{2\pi}{T}(\nu-\Delta)t\right]\right\}; & |t-t_K| \leq \frac{T}{2} \\ 0; & |t-t_K| \geq \frac{T}{2}\,, \end{cases} \tag{4-4-1}$$

where

$$0 < \xi \leq 1$$

and

$$0 \leq \Delta \leq \nu \quad .$$

The parameter ξ represents the ratio of the amplitude of the weaker sinusoid which has frequency $(\nu - \Delta)/T$ Hz to that of the stronger sinusoid which has frequency ν/T Hz. The parameter Δ is the frequency separation factor between the two sinusoids. Using (4-3-9), the

Bartlett windowed expansion coefficients are given by

$$c_{k\ell} = \sqrt{\frac{T}{2}}\, e^{-j\frac{4\pi}{T}\ell t_k} \int_{-1}^{1} x(\tfrac{T}{2}\tau + t_k)\, \sqrt{1-|\tau|}\; e^{-j2\pi\ell\tau}\, d\tau \,. \tag{4-4-2}$$

Substituting the signal from (4-4-1) into this expression, there results

$$c_{k\ell} = 0;\ k \neq K \tag{4-4-3}$$

and

$$c_{K\ell} = A\sqrt{\frac{T}{2}}\, e^{-j\frac{4\pi}{T}\ell t_K} \int_{-1}^{1} \cos[\tfrac{2\pi\nu}{T}(\tfrac{T}{2}\tau + t_K)]\, \sqrt{1-|\tau|}\; e^{-j2\pi\ell\tau} d\tau \tag{4-4-4}$$

$$+ A\xi\sqrt{\frac{T}{2}}\, e^{-j\frac{4\pi\ell}{T}t_K} \int_{-1}^{1} \cos[\tfrac{2\pi}{T}(\nu-\Delta)(\tfrac{T}{2}\tau + t_K)]\sqrt{1-|\tau|}\; e^{-j2\pi\ell\tau} d\tau$$

$$= A\sqrt{\frac{T}{2}}\; e^{-j\frac{4\pi\ell}{T}t_K}\, [\, I_1 + \xi\, I_\Delta\,] \tag{4-4-5}$$

where

$$I_1 = \int_{-1}^{1} \cos[\pi\nu\tau + \tfrac{2\pi}{T}\nu\, t_K]\, \sqrt{1-|\tau|}\; e^{-j2\pi\ell\tau}\, d\tau \tag{4-4-6}$$

and

$$I_\Delta = \int_{-1}^{1} \cos[\pi(\nu-\Delta)\tau + \tfrac{2\pi}{T}(\nu-\Delta)t_K]\, \sqrt{1-|\tau|}\; e^{-j2\pi\ell\tau}\, d\tau \,. \tag{4-4-7}$$

Therefore,

$$|c_{K\ell}|^2 = \frac{A^2T}{2}\, |\, I_1 + \xi\, I_\Delta\,|^2 \,. \tag{4-4-8}$$

Choosing t_K=0 for simplicity, the values of $|c_{K\ell}|^2$ are plotted in Figures 4-41 and 4-42 for the cases when ξ = 1/10 and ξ = 1/16, respectively. In both figures, the sinusoidal frequency

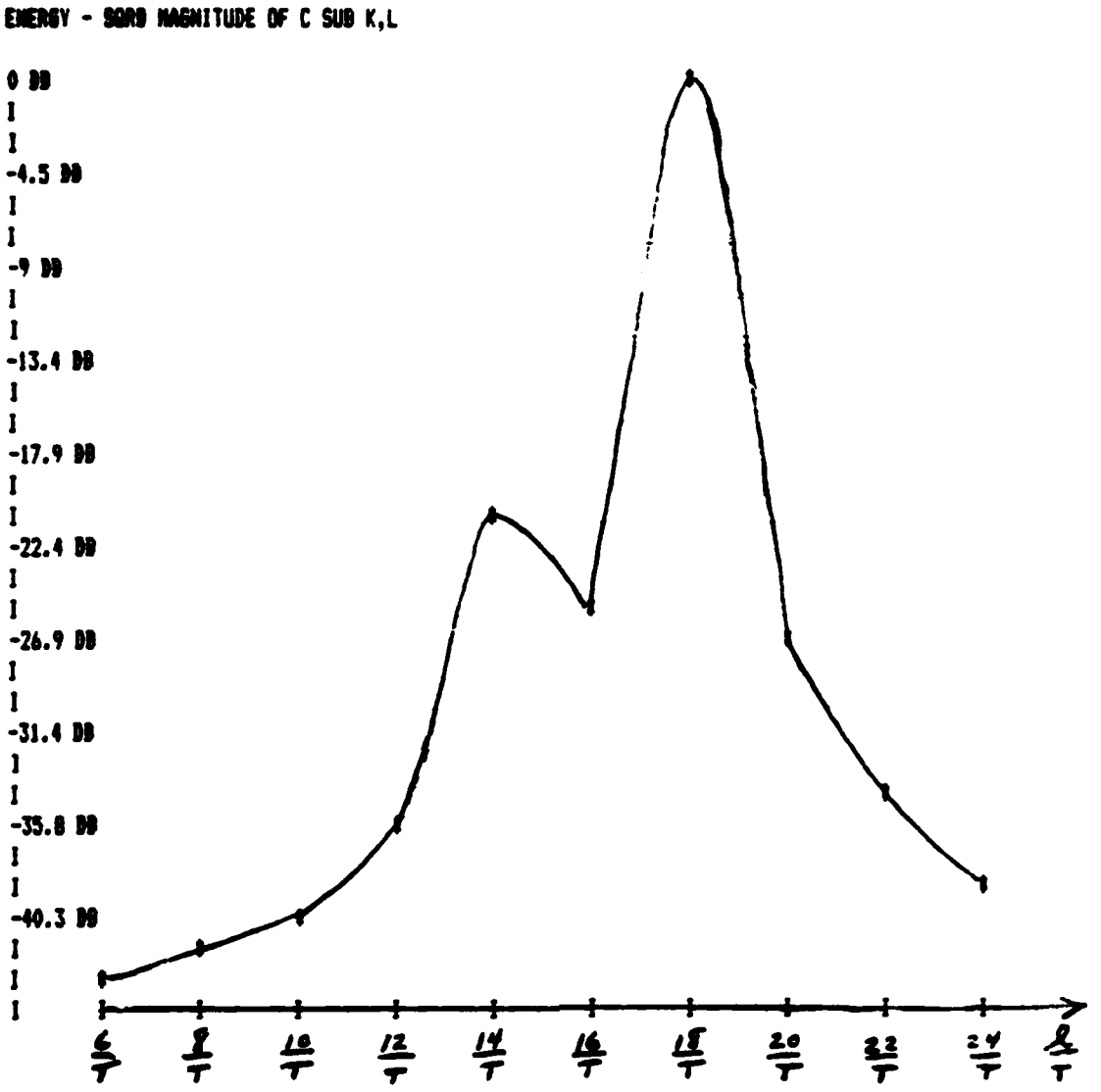

BARTLETT WINDOWED EXPANSION FOR TWO SINUSOIDS
MAXIMUM VALUE = .220941 MINIMUM VALUE = 7.30611E-06
EACH SHADED HORIZONTAL BAR HAS WIDTH IN DB OF 4.48059 LOWEST FREQUENCY = 6
VERTICAL RESOLUTION IN DB IS 1.49353 HIGHEST FREQUENCY = 24
SINUSOIDAL FREQUENCIES WERE 16 /T AND 14 /T
THE RATIO OF AMPLITUDE OF THE 14 /T HZ SINE TO THE 16 /T HZ SINE IS .1

Figure 4-41 Bartlett Windowed Expansion for Two Sinusoids with $\xi = 1/10$

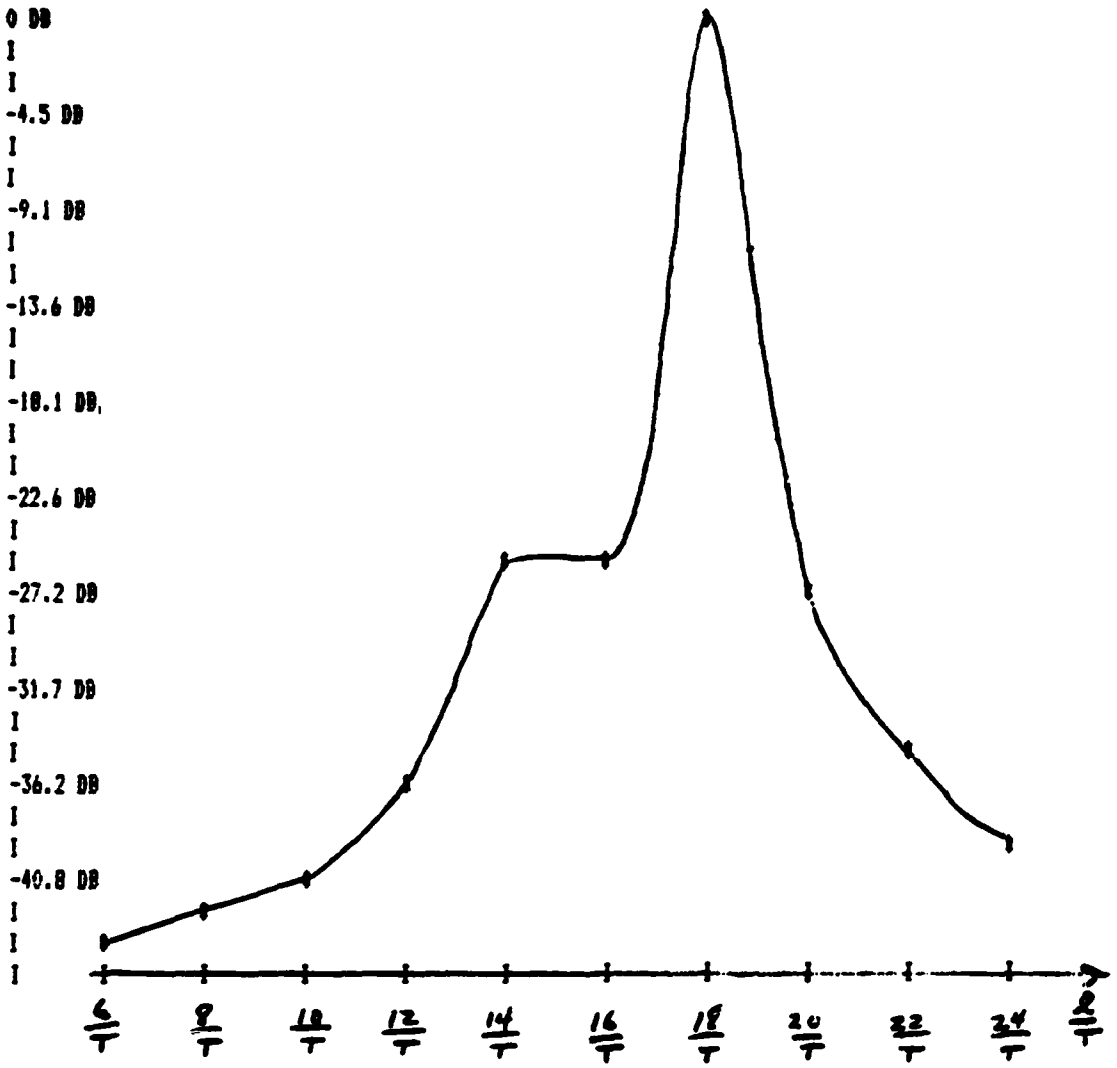

BARTLETT WINDOWED EXPANSION FOR TWO SINUSOIDS
MAXIMUM VALUE = .221229 MINIMUM VALUE = 6.55602E-06
EACH SHADED HORIZONTAL BAR HAS WIDTH IN DB OF 4.5282 LOWEST FREQUENCY = 6
VERTICAL RESOLUTION IN DB IS 1.5094 HIGHEST FREQUENCY = 24
SINUSOIDAL FREQUENCIES WERE 18 /T AND 14 /T
THE RATIO OF AMPLITUDE OF THE 14 /T HZ SINE TO THE 18 /T HZ SINE IS .0625

Figure 4-42 Bartlett Windowed Expansion for Two Sinusoids with $\xi = 1/16$

parameters were chosen as

$$\nu = 18 \qquad (4\text{-}4\text{-}9)$$

and

$$\Delta = 4. \qquad (4\text{-}4\text{-}10)$$

This choice of parameters indicates that a dominant 18/T Hz sinusoidal burst and a weaker 14/T Hz sinusoidal burst are present in the same subinterval and that the lower frequency sinusoid has an amplitude which is smaller by the given factor ξ. It is interesting that the weaker sinusoidal burst is barely detectable when $\xi = 1/16 = 0.0625$ in Figure 4-42. In terms of the energy of each sinusoidal burst alone, the weaker sinusoid has an energy of $A^2\xi^2T/2$ while the stronger sinusoid has an energy of $A^2T/2$. Thus the ratio of their energies is ξ^2 and the rule $10\log_{10}(\xi^2)$ gives -20.0 dB for $\xi = 1/10$ in Figure 4-41 and -24.1 dB for $\xi = 1/16$ in Figure 4-42. It is noted that even though the frequencies involved here are contained in the set of represented frequencies of the Bartlett windowed expansion, the spectral properties exhibited are not ideal. For example, the graphs indicate energy at other frequencies than the those in the signal and the weaker sinusoid is almost hidden from view when $\xi = 1/16$. The reason for this is that the Bartlett windowed basis functions are shaped sinusoidal bursts with the general shape sketched in Figure 3-2. In contrast, the Rectangular windowed expansion gives the ideal spectral representation for this case. To show this fact, the expression for the signal in (4-4-1) is substituted into the expression for the Rectangular windowed energies in (4-3-33) to give

$$|r_{k\ell}|^2 = 0;\ k \neq K \tag{4-4-11}$$

and

$$|r_{K\ell}|^2 = \frac{T}{4}\Big| \int_{-1}^{1} \{A \cos[\frac{2\pi}{T} \nu(\frac{T}{2}\tau + t_K) + A\xi \cos[\frac{2\pi}{T}(\nu-\Delta)(\frac{T}{2}\tau + t_K)]\}\ e^{-j\pi\ell\tau}\ d\tau\Big|^2 . \tag{4-4-12}$$

Setting t_K=0 for simplicity, it follows that

$$|r_{K\ell}|^2 = \frac{A^2T}{4}\Big|\int_{-1}^{1} \cos(\pi\nu\tau)\ e^{-j\pi\ell\tau}\ d\tau + \xi \int_{-1}^{1}\cos[\pi(\nu-\Delta)\tau]\ e^{-j\pi\ell\tau}\ d\tau\Big|^2 \tag{4-4-13}$$

$$= \frac{A^2T}{4}\Big[\int_{0}^{1} \cos[\pi(\ell-\nu)\tau]\ d\tau + \int_{0}^{1} \cos[\pi(\ell+\nu)\tau]\ d\tau + \xi \int_{0}^{1} \cos[\pi(\ell-\nu+\Delta)\tau\ ]\ d\tau + \xi\int_{0}^{1} \cos[\pi(\ell+\nu-\Delta)\tau]\ d\tau\Big]^2 \tag{4-4-14}$$

$$= \frac{A^2T}{4}\ [\ \mathrm{sinc}(\ell-\nu) + \mathrm{sinc}(\ell+\nu) + \xi\ \mathrm{sinc}(\ell-\nu+\Delta) + \xi\ \mathrm{sinc}(\ell+\nu-\Delta)]^2 . \tag{4-4-15}$$

When ν and Δ are both integers, there results

$$|r_{K\ell}|^2 = \frac{A^2T}{4}\ [\ \delta_{\ell,\nu} + \delta_{\ell,-\nu} + \xi\delta_{\ell,(\nu-\Delta)} + \xi\delta_{\ell,-(\nu-\Delta)}\ ]^2 . \tag{4-4-16}$$

This is expected since the two sinusoidal bursts are identical,

except for a scale factor, to the two corresponding basis functions in the Rectangular windowed expansion. Thus the ideal spectral representation is achieved here.

Now the Bartlett windowed energies of (4-4-8) are compared to the Rectangular windowed energies of (4-4-15) when the two sinusoidal frequencies in the signal are non-integers. Specifically,

$$\nu = 18.5 \tag{4-4-17}$$

and

$$\Delta = 4 \tag{4-4-18}$$

so that

$$\nu - \Delta = 14.5 \tag{4-4-19}$$

Figure 4-43 presents the Bartlett windowed energy values for $\xi = 1/10$ and Figure 4-44 presents these energy values for $\xi = 1/16$. Although neither plot clearly indicates the correct frequencies involved in the signal, the two peaks are relatively close to the correct locations. The Rectangular windowed energies for the same parameter values are given in Figure 4-45 in which $\xi = 1/10$ and in Figure 4-46 in which $\xi = 1/16$. Again it is evident that neither plot gives the ideal spectral representation. But the spectral representation for the case $\xi = 1/16$ in Figure 4-46 is sharper than the corresponding Bartlett case in Figure 4-44. In Figure 4-44, the smaller peak at $\ell = 14$ is just barely seen whereas the peak at $\ell = 14$ in Figure 4-46 is easily detected. In fact, comparing Figure 4-45 with Figure 4-43, it is seen that the deeper "valley" at $\ell = 15$ in the Rectangular windowed energy plot makes the peak at

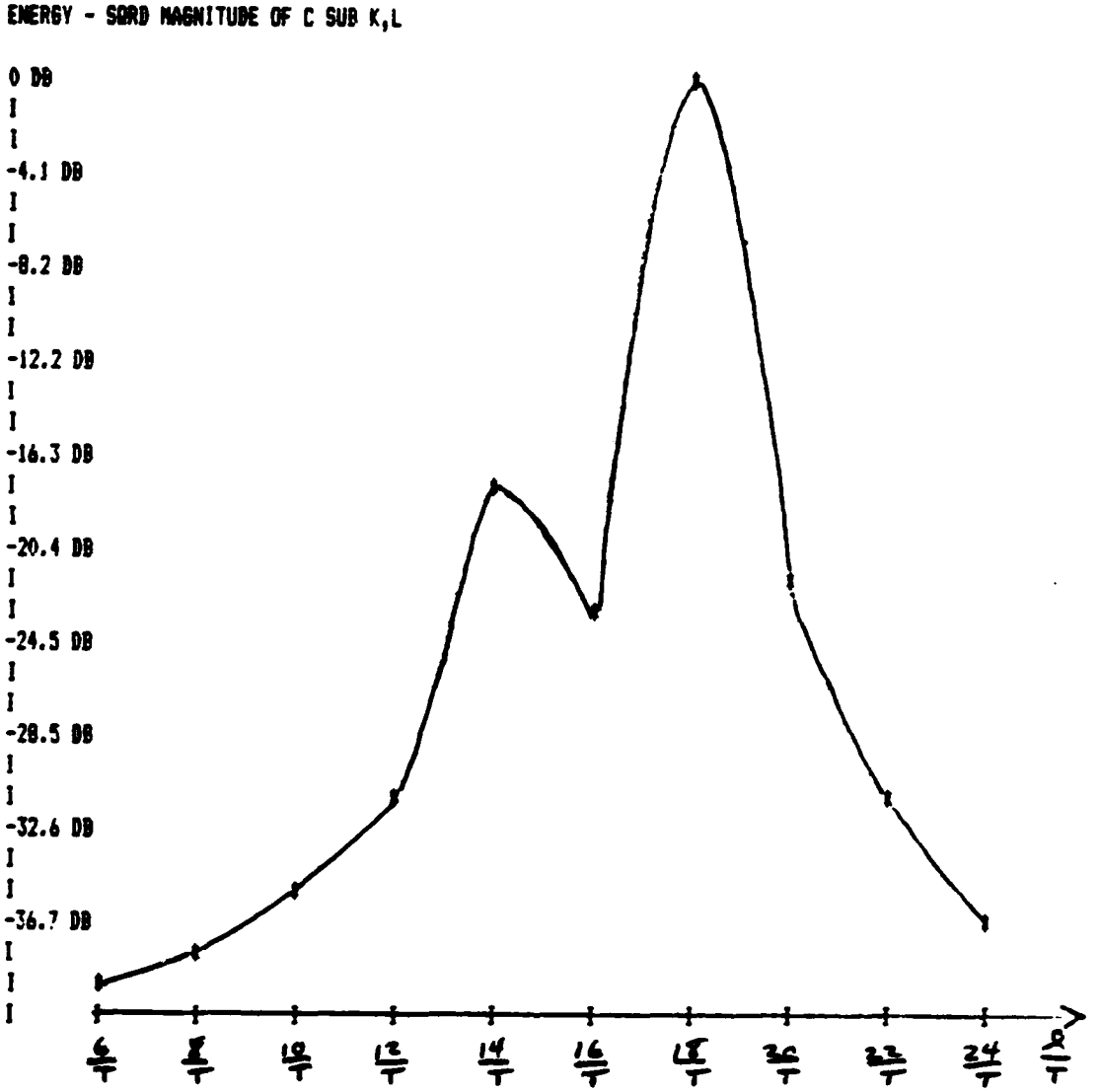

BARTLETT WINDOWED EXPANSION FOR TWO SINUSOIDS
MAXIMUM VALUE = .122815 MINIMUM VALUE = 1.03133E-05
EACH SHADED HORIZONTAL BAR HAS WIDTH IN DB OF 4.07585 LOWEST FREQUENCY = 6
VERTICAL RESOLUTION IN DB IS 1.35862 HIGHEST FREQUENCY = 24
SINUSOIDAL FREQUENCIES WERE 18.5 /T AND 14.5 /T
THE RATIO OF AMPLITUDE OF THE 14.5 /T HZ SINE TO THE 18.5 /T HZ SINE IS .1

Figure 4-43 Bartlett Windowed Expansion for 18.5/T Hz and 14.5/T Hz Sinusoids with ξ = 1/10

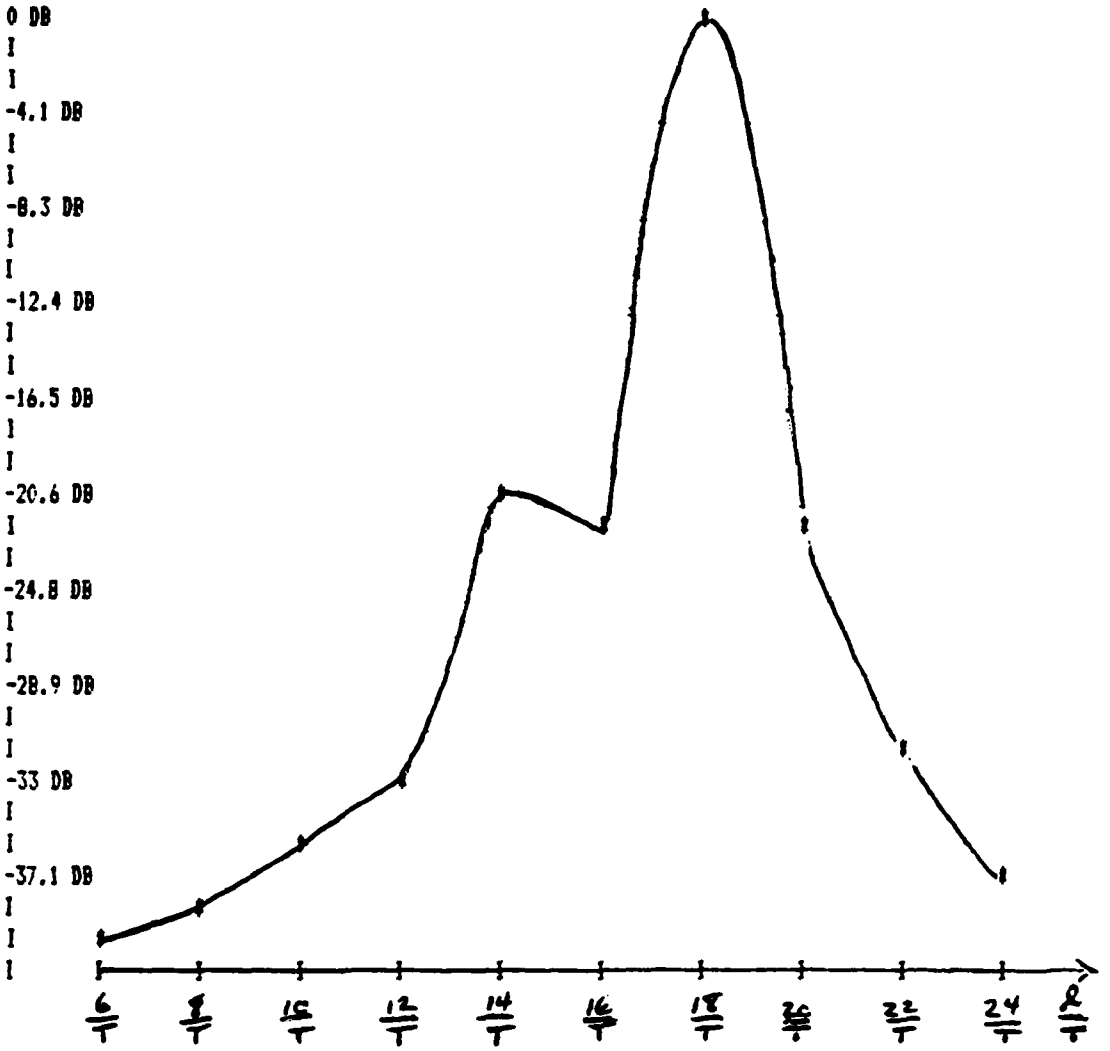

BARTLETT WINDOWED EXPANSION FOR TWO SINUSOIDS
MAXIMUM VALUE = .123046 MINIMUM VALUE = 9.22401E-06
EACH SHADED HORIZONTAL BAR HAS WIDTH IN DB OF 4.12515 LOWEST FREQUENCY = 6
VERTICAL RESOLUTION IN DB IS 1.37505 HIGHEST FREQUENCY = 24
SINUSOIDAL FREQUENCIES WERE 18.5 /T AND 14.5 /T
THE RATIO OF AMPLITUDE OF THE 14.5 /T HZ SINE TO THE 18.5 /T HZ SINE IS .0625

Figure 4-44 Bartlett Windowed Expansion for 18.5/T Hz and 14.5/T Hz Sinusoids with $\xi = 1/16$

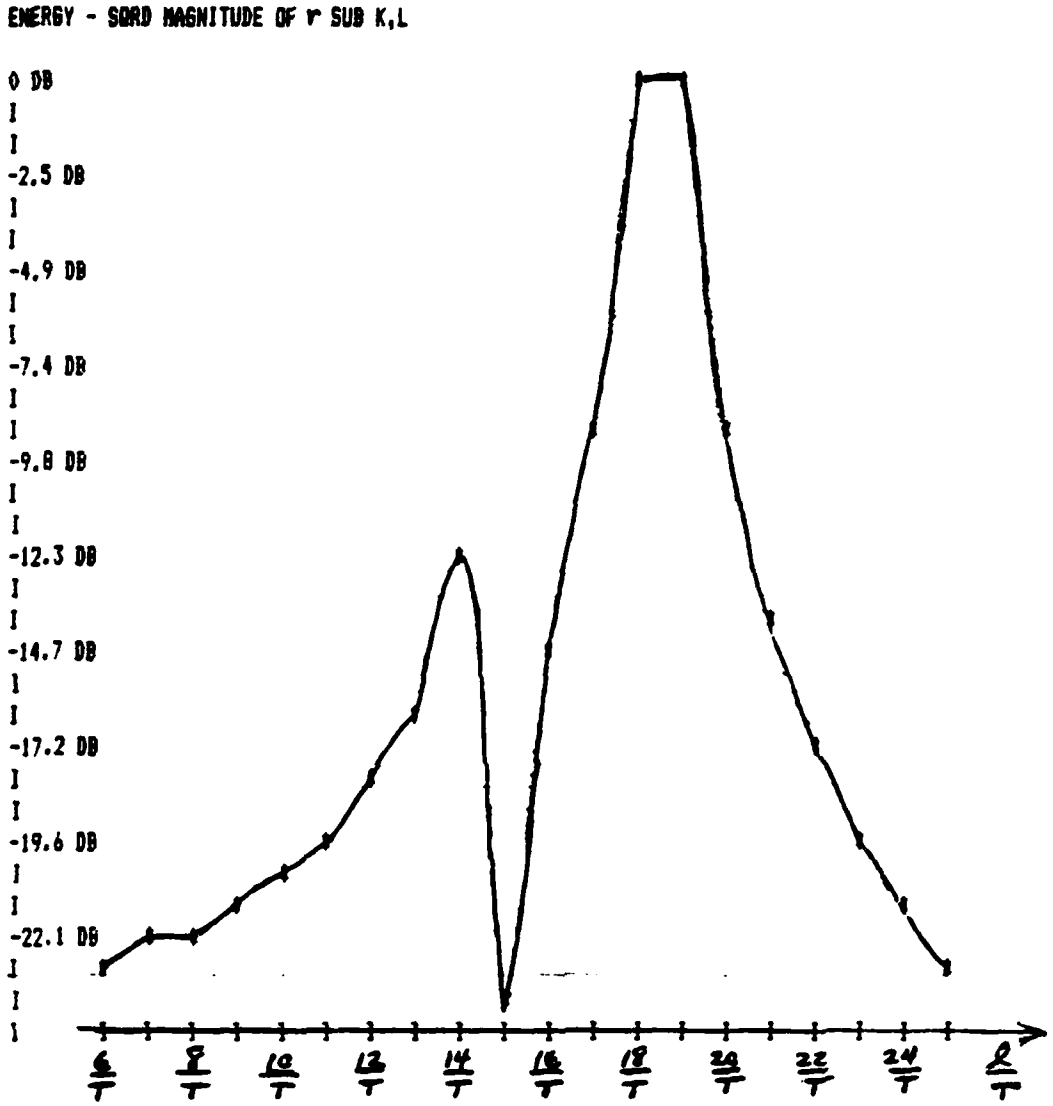

RECTANGULAR WINDOWED EXPANSION FOR TWO SINUSOIDS
MAXIMUM VALUE = .101514 MINIMUM VALUE = 3.5843E-04
EACH SHADED HORIZONTAL BAR HAS WIDTH IN DB OF 2.45212 LOWEST FREQUENCY = 6
VERTICAL RESOLUTION IN DB IS .817374 HIGHEST FREQUENCY = 25
SINUSOIDAL FREQUENCIES WERE 18.5 /T AND 14.5 /T
THE RATIO OF AMPLITUDE OF THE 14.5 /T HZ SINE TO THE 18.5 /T HZ SINE IS .1

Figure 4-45 Rectangular Windowed Expansion for 18.5/T Hz and 14.5/T Hz Sinusoids with ξ = 1/10

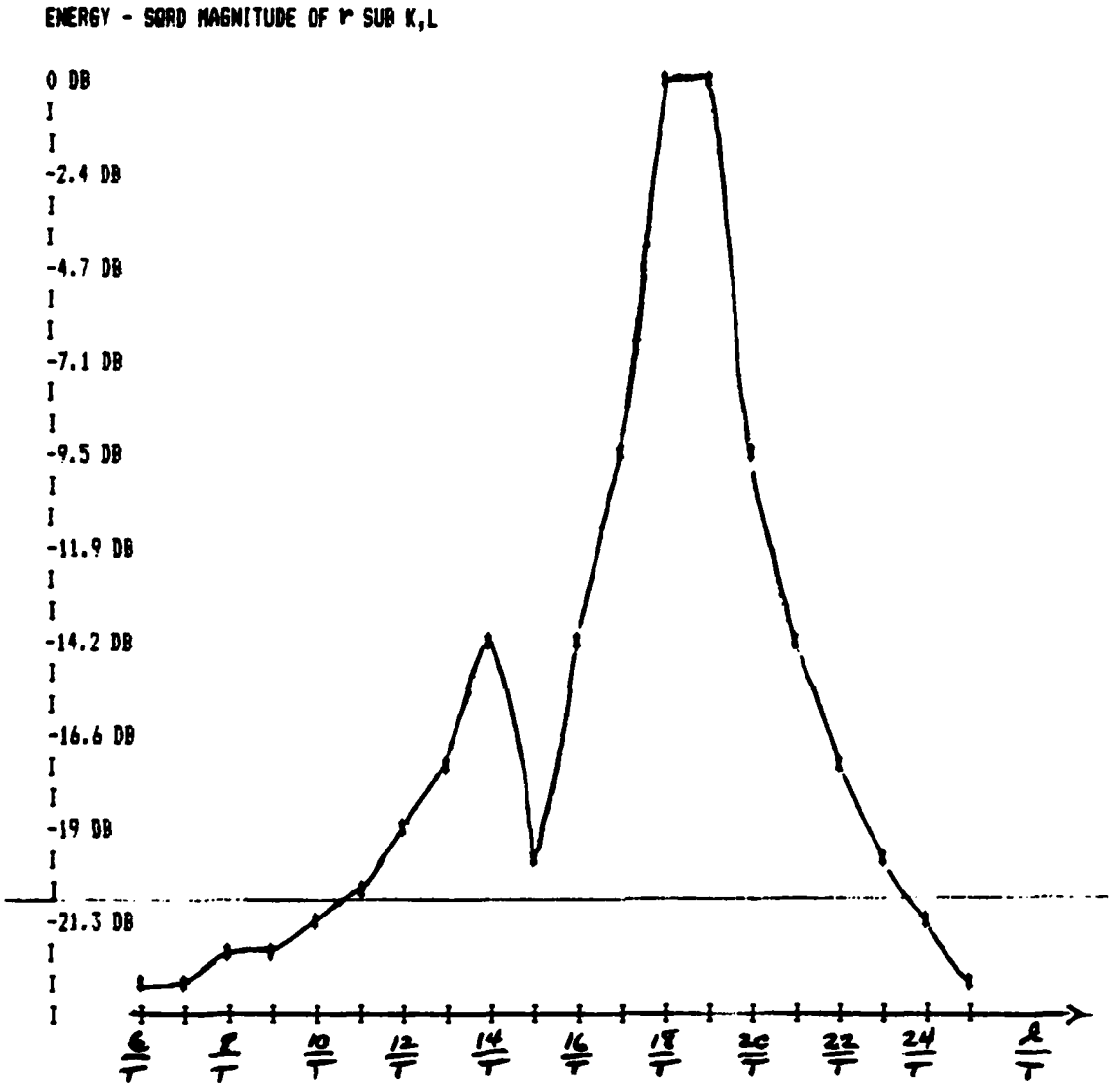

RECTANGULAR WINDOWED EXPANSION FOR TWO SINUSOIDS
MAXIMUM VALUE = .102486 MINIMUM VALUE = 4.36141E-04
EACH SHADED HORIZONTAL BAR HAS WIDTH IN DB OF 2.37104 LOWEST FREQUENCY = 6
VERTICAL RESOLUTION IN DB IS .790346 HIGHEST FREQUENCY = 25
SINUSOIDAL FREQUENCIES WERE 18.5 /T AND 14.5 /T
THE RATIO OF AMPLITUDE OF THE 14.5 /T HZ SINE TO THE 18.5 /T HZ SINE IS .0625

Figure 4-46 Rectangular Windowed Expansion for 18.5/T Hz and 14.5/T Hz Sinusoids with $\xi = 1/16$

$\ell = 14$ much more prominent. The Bartlett windowed energy plot does not present such a deep "valley" and is therefore less desirable for the resolution problem in this case. It should be noted that the "valley" effect is made possible by the interference of the "tails" of two neighboring sinc functions in (4-4-15). As a final example, the Bartlett and Rectangular windowed energies are compared for the case when

$$\nu = 18.5 \tag{4-4-20}$$

and

$$\Delta = 5 \tag{4-4-21}$$

so that

$$\nu - \Delta = 13.5 \quad . \tag{4-4-22}$$

Figure 4-47 and Figure 4-48 present the Bartlett windowed energies for $\xi = 1/10$ and $\xi = 1/16$, respectively, while Figure 4-49 and Figure 4-50 present the Rectangular windowed energies for $\xi = 1/10$ and $\xi = 1/16$, respectively. In the latter two plots, the deep "valleys" occur on the lower frequency side of the weaker sinusoid's frequency of 13.5/T Hz and not <u>between</u> the two correct frequencies as in Figures 4-45 and 4-46 for which $\Delta = 4$. This makes the task of resolution more difficult for the Rectangular windowed expansion in this case. Again, this is caused by the degree of overlap of the tails of two neighboring sinc functions in (4-4-15). It is surprising, however, that the Bartlett windowed energy values plotted in Figures 4-47 and 4-48 with $\Delta = 5$ exhibit practically the same characteristics

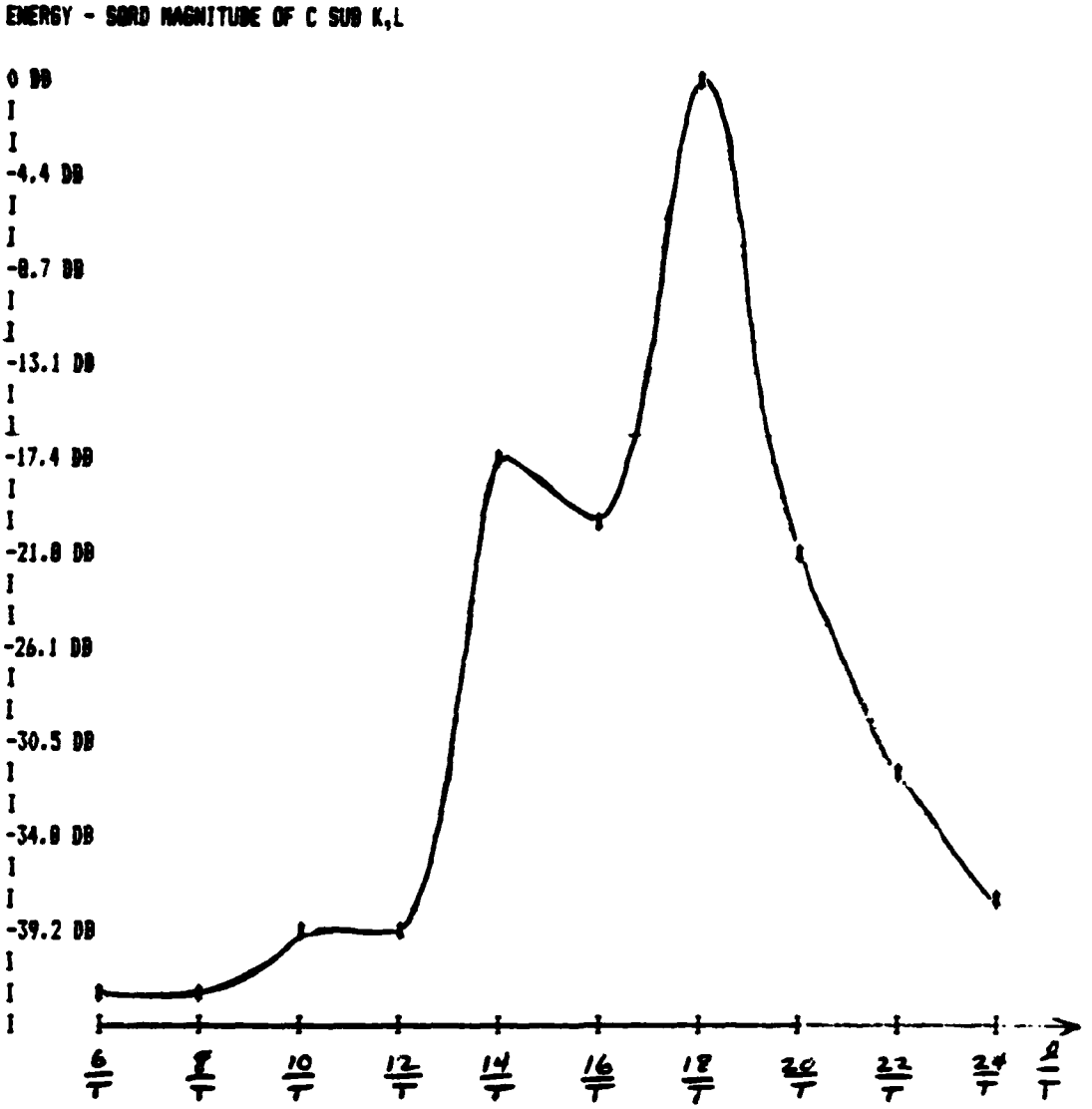

BARTLETT WINDOWED EXPANSION FOR TWO SINUSOIDS
MAXIMUM VALUE = .124112 MINIMUM VALUE = 5.47451E-06
EACH SHADED HORIZONTAL BAR HAS WIDTH IN DB OF 4.35547 LOWEST FREQUENCY = 6
VERTICAL RESOLUTION IN DB IS 1.45182 HIGHEST FREQUENCY = 24
SINUSOIDAL FREQUENCIES WERE 18.5 /T AND 13.5 /T
THE RATIO OF AMPLITUDE OF THE 13.5 /T HZ SINE TO THE 18.5 /T HZ SINE IS .1

Figure 4-47 Bartlett Windowed Expansion for 18.5/T Hz and 13.5/T Hz Sinusoids with $\xi = 1/10$

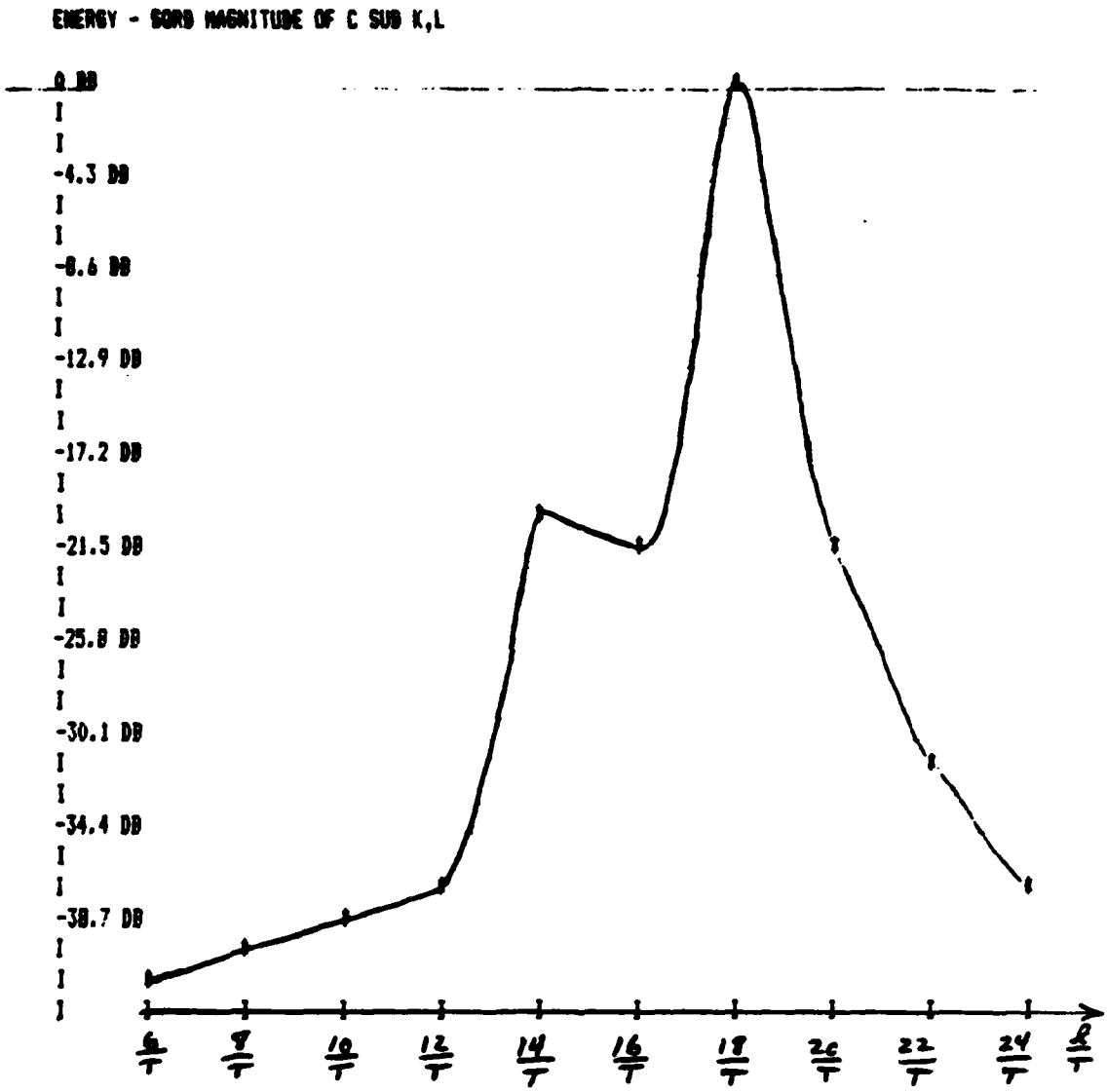

BARTLETT WINDOWED EXPANSION FOR TWO SINUSOIDS
MAXIMUM VALUE = .123857 MINIMUM VALUE = 6.21162E-06
EACH SHADED HORIZONTAL BAR HAS WIDTH IN DB OF 4.29971 LOWEST FREQUENCY = 6
VERTICAL RESOLUTION IN DB IS 1.43324 HIGHEST FREQUENCY = 24
SINUSOIDAL FREQUENCIES WERE 18.5 /T AND 13.5 /T
THE RATIO OF AMPLITUDE OF THE 13.5 /T HZ SINE TO THE 18.5 /T HZ SINE IS .0625

Figure 4-48 Bartlett Windowed Expansion for 18.5/T Hz and 13.5/T Hz Sinusoids with $\xi = 1/16$

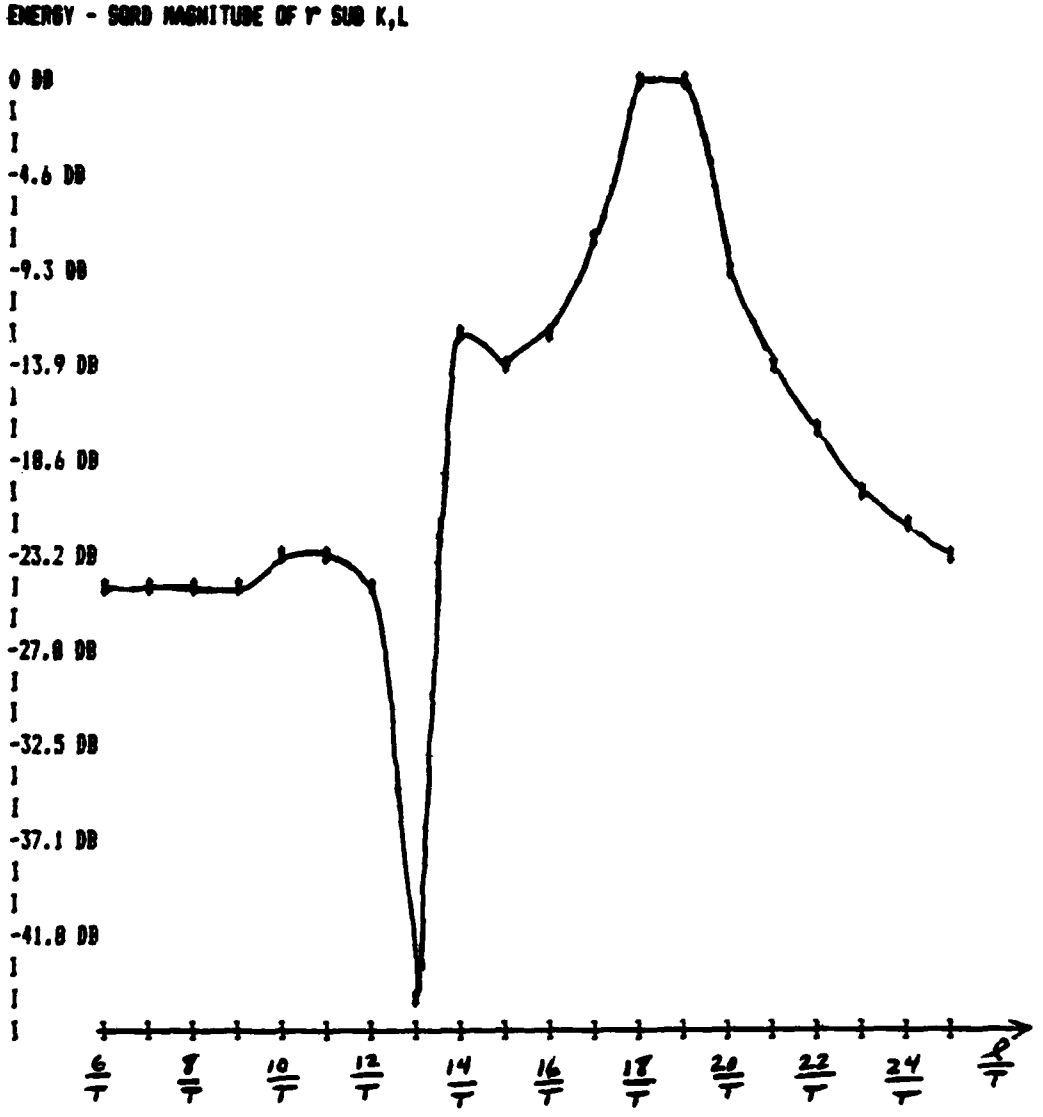

RECTANGULAR WINDOWED EXPANSION FOR TWO SINUSOIDS
MAXIMUM VALUE = .106082 MINIMUM VALUE = 2.42807E-06
EACH SHADED HORIZONTAL BAR HAS WIDTH IN EB OF 4.64038 LOWEST FREQUENCY = 6
VERTICAL RESOLUTION IN DB IS 1.54679 HIGHEST FREQUENCY = 25
SINUSOIDAL FREQUENCIES WERE 18.5 /T AND 13.5 /T
THE RATIO OF AMPLITUDE OF THE 13.5 /T HZ SINE TO THE 18.5 /T HZ SINE IS .1

Figure 4-49 Rectangular Windowed Expansion for 18.5/T Hz and 13.5/T Hz Sinusoids with $\xi = 1/10$

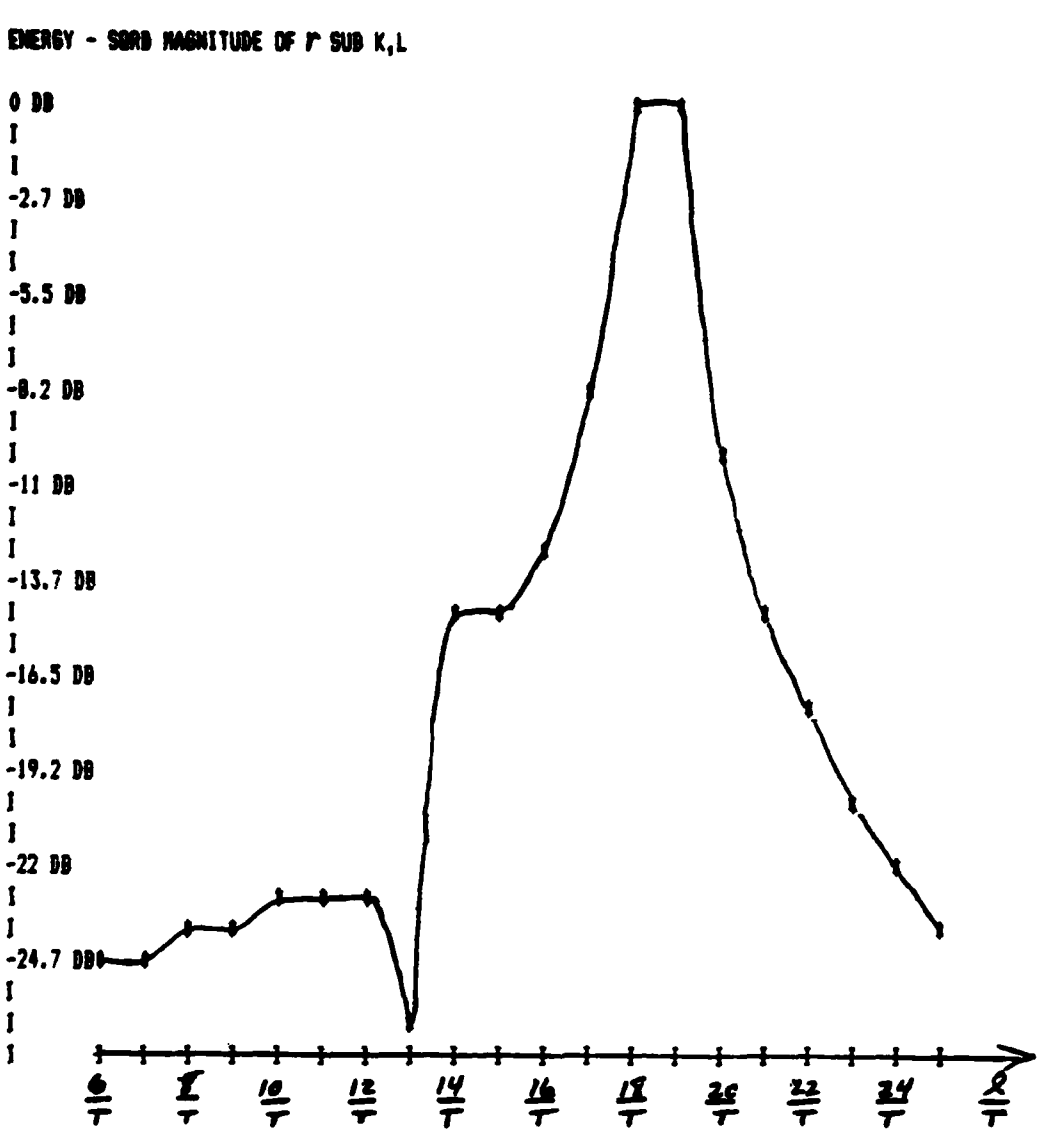

RECTANGULAR WINDOWED EXPANSION FOR TWO SINUSOIDS
MAXIMUM VALUE = .105342 MINIMUM VALUE = 1.8824E-04
EACH SHADED HORIZONTAL BAR HAS WIDTH IN DB OF 2.74789 LOWEST FREQUENCY = 6
VERTICAL RESOLUTION IN DB IS .915964 HIGHEST FREQUENCY = 25
SINUSOIDAL FREQUENCIES WERE 18.5 /T AND 13.5 /T
THE RATIO OF AMPLITUDE OF THE 13.5 /T HZ SINE TO THE 18.5 /T HZ SINE IS .0625

Figure 4-50 Rectangular Windowed Expansion for 18.5/T Hz and 13.5/T Hz Sinusoids with $\xi = 1/16$

as the Bartlett windowed energies of Figure 4-43 and Figure 4-44 for which $\Delta = 4$. Thus an increase of the frequency separation factor has produced a noticeable difference in appearance for the Rectangular energy plot but not for the Bartlett energy plot. This indicates that the tails of the sinc functions in the Rectangular windowed expansion are much more significant in value compared to the corresponding properties of the Bartlett windowed expansion. The Bartlett properties referred to are the rapid decay effects noted previously in Chapter 3 and in Section 4.2.

In conclusion, it must be stated that neither Rectangular nor Bartlett windowed expansion is clearly superior for the resolution problem in all of its aspects. But it is important to understand the spectral characteristics of various windowed expansions so that maximum benefit can be derived from their different advantages. In the resolution problem, the closer frequency spacing of the Rectangular windowed expansion must be carefully weighed against the benefits of a more rapid decay from maximum offered by the Bartlett windowed expansion. In addition, maximum use must be made of knowledge gained by a careful inspection of the signal by eye. Such knowledge consists of the dominant shapes of envelopes within the signal and characteristic durations of these shapes. These observations influence the choice of window and the choice of subinterval length, T, respectively.

CHAPTER 5

SUMMARY AND RECOMMENDATIONS FOR FUTURE RESEARCH

This research presents a sound approach to time-variant energy spectral analysis using vector space concepts. Chapter 1 briefly describes the motivation for the time-frequency description of signals along with some basic definitions. Chapter 2 contains a survey of previous concepts proposed for joint time-frequency signal analysis. Several important problems with these concepts involve their interpretation and implementation. The conventional Finite Fourier Transform approach is presented and a number of new questions are raised which have not been answered in the open literature. Chapter 3 introduces the vector space approach to time-variant energy spectral analysis. The essential points covered involve the segmentation of the observed signal into contiguous signal "pieces", the representation of each signal "piece" by a vector in a specific vector space, and the interpretation of the components of this vector as time progresses. A useful family of windowed signal expansions is presented which provides theoretical justification for using weighting windows with the Finite Fourier Transform. The questions posed in Chapter 2 are fully answered, providing a foundation for use of the Discrete Fourier Transform for "piece-wise" energy spectral analysis. Chapter 4 establishes some ground rules for applying the proposed vector space approach. A realistic example is also given of the joint time-frequency energy spectral analysis of an FM tone-modulated signal. The appendix lists the computer programs used in Chapters 3 and 4.

A number of interesting aspects of time-variant energy spectral analysis remain for further study.

(1) The spectral representation effects of windowed signal expansions on noisy signals is an important area of study. Strengths and weaknesses of various windows may be revealed when specific noise-like signals are added to the signal whose time-variant energy is being analyzed.

(2) The windowed expansions may be optimized for specific purposes through adjustment of the function a(t) discussed in (3-1-24). The desired placement of deep nulls in the spectral representation of sinusoids may be conveniently achieved by adjustment of the shape of a(t).

(3) The problems of signal detection and signal parameter estimation in noise might be attacked more fruitfully using the proposed vector space concept of signal representation. In general this may involve windowed expansions of random signals as well as noise.

(4) The general area of bi-orthonormal signal expansions such as Bastiaans' [2] approach should be more thorougly investigated to determine usefulness for representing special large time-bandwidth product signals.

Appendix

All integrals in the text were evaluaced by the numerical integration method known as Filon's Method [18]. This method involves interpolation of the integrand at a number of equally spaced points. The number of interpolation points is chosen based upon the number of cycles of the sinusoidal part of the integrand contained within the integration interval. Specifically, two types of integrals are numerically integrated, I_c and I_s, defined by

$$I_c = \int_{t_A}^{t_B} g(t) \cos(\xi t)\, dt \qquad \text{(A-1)}$$

and

$$I_s = \int_{t_A}^{t_B} g(t) \sin(\xi t)\, dt, \qquad \text{(A-2)}$$

ξ being a constant for the integration process. In this notation, g(t) is assumed to be non-sinusoidal. Tranter [18] shows that Filon's method is just a modified form of Simpson's Rule. Programs were written in BASIC and used on a Radio Shack TRS-80 computer. Graphs were plotted on an Epson MX-80 printer with 132 character capability. The computer had 48K of core memory and was used in conjunction with an Aerocomp disk drive. Computer programs are now listed by corresponding figure number.

```
20 REM BARTLETT EXPANSION OF SINGLE SINUSOIDAL TONE
25 REM FILON INTEGRATION METHOD USED
40 DIM A(123),C(123)
60 PI=3.14159265358979324
80 P2=2*PI
100 INPUT "HOW MANY POINTS TO BE PLOTTED";NQ
120 IM=-1.0E21
140 MM=1.0E21
160 F2=0.4342945
180 SM=0
190 INPUT "WHAT IS THE SINUSOIDAL FREQUENCY OF THE SIGNAL";F9
260 FOR J=0 TO 123
280 C(J)=0
300 NEXT J
320 I=0
340 LPRINT "FREQUENCY          ENERGY VALUE"
360 BE=.6863352186
380 GA=1.312884582
420 FOR Q=0 TO (NQ-1)
425 S0=(2*Q)-F9
430 S1=(2*Q)+F9
440 FOR F1=0 TO 1
460 IF S0=0 AND F1=0 THEN 480:ELSE 505
480 A1=0.666666666667
500 GOTO 1300
505 IF F1=0 THEN A0=8*ABS(S0):ELSE A0=8*ABS(S1)
512 IF A0<8 THEN 514:ELSE 520
514 H=0.125
515 A0=8
516 GOTO 540
520 H=1/A0
540 NI=INT(A0/2)
560 AR=0
580 R1=0
600 R0=0
620 FOR N=1 TO NI
640 AR=AR+H
660 IF F1=0 THEN GOSUB 1120:ELSE GOSUB 1240
680 R1=R1+Z
700 AR=AR+H
720 IF F1=0 THEN GOSUB 1120:ELSE GOSUB 1240
740 R0=R0+Z
760 NEXT N
780 R0=R0-(Z/2)
800 AR=0
820 IF F1=0 THEN GOSUB 1120:ELSE GOSUB 1240
840 R0=R0+(Z/2)
940 IF F1=1 THEN 1000
960 A1=((R0*BE)+(R1*GA))*H
980 GOTO 1300
1000 B1=((R0*BE)+(R1*GA))*H
1020 C(I)=(A1*A1)+(B1*B1)+(2*ABS(A1*B1))
1100 GOTO 1300
```

FIGURES 3-16 THROUGH 3-19 AND 3-22, 3-23

```
1120 GOSUB 1180
1140 Z=Z1*COS(S0*PI*AR)
1160 RETURN
1180 IF AR>1 THEN AR=1
1200 Z1=SQR(1-(ABS(AR)))
1220 RETURN
1240 GOSUB 1180
1260 Z=Z1*COS(S1*PI*AR)
1280 RETURN
1300 NEXT F1
1302 C(I)=C(I)/2
1303 IF C(I)=0 THEN 1308
1304 IF C(I)>=XM THEN XM=C(I)
1306 IF C(I)<=MM THEN MM=C(I)
1308 LPRINT 280;"                    ";C(I)
1320 SM=SM+C(I)
1340 I=I+1
1360 NEXT Q
1370 IF C(0)=0 THEN C(0)=MM
1380 FOR I=0 TO (NQ-1)
1400 A(I)=10*F2*LOG(C(I))
1420 NEXT I
1440 MX=10*F2*LOG(XM)
1460 MM=10*F2*LOG(MM)
1480 REM BEGINNING OF THE HORIZONTAL GRAPHING MODULE
1500 SP=INT(124/NQ)
1520 RC=(MX-MM)/30
1540 LPRINT CHR$(15)
1560 LPRINT "0 DB    ";
1580 FOR N=0 TO 29
1600 QU=MX-(RC*N)
1620 QL=QU-RC
1640 IF N=29 THEN QL=-200
1660 PL=0
1680 LQ=0
1700 OP=-1
1720 IF N=0 THEN 1900
1740 IF N=3*(INT(N/3)) THEN 1760:ELSE 1840
1760 DB=(-1)*INT(((RC*N)+.05)*10)/10
1780 LPRINT DB;"DB";
1800 IF DB)(-10) THEN LPRINT CHR$(32);
1820 IF DB=INT(DB) THEN LQ=2:ELSE 1900
1840 FOR L=1 TO LQ
1860 LPRINT CHR$(32);
1880 NEXT L
1900 FOR J=0 TO (NQ-1)
1920 IF A(J)<=QU AND A(J)>QL THEN PL=SP*J:ELSE 2060
1940 IF (PL-OP)=1 THEN 2020
1960 FOR K=0 TO (PL-OP-2)
1980 LPRINT CHR$(32);
2000 NEXT K
```

```
2020 LPRINT "*";
2040 QP=PL
2060 NEXT J
2080 LPRINT
2100 NEXT N
2120 FOR K=1 TO 5
2140 LPRINT
2160 NEXT K
2180 LPRINT "BARTLETT WINDOWED EXPANSION                    SIGNAL FREQUENCY = ";F9;"/T"
2200 LPRINT "MAXIMUM VALUE = ";XM;"    MINIMUM VALUE = ";NM
2220 LPRINT "EACH SHADED HORIZONTAL BAR HAS WIDTH IN DB OF ";RC#3;"       LOWEST FREQUENCY = 0"
2240 LPRINT "VERTICAL RESOLUTION IN DB IS ";RC;"                  HIGHEST FREQUENCY = ";2#(NO-1)
2260 LPRINT "TOTAL ENERGY IN THE COMPONENTS PLOTTED WAS ";SM
2280 END
```

FIGURES 3-20, 3-21

```
5 REM RECTANGULAR EXPANSION OF SINGLE SINUSOID
7 REM FILON'S INTEGRATION METHOD IS NOT USED
10 DIM A(123),C(123)
20 PI=3.141592
30 NI=1.0E21
40 XI=-1.0E21
45 INPUT "HOW MANY POINTS TO BE PLOTTED";NN
47 F1=0.434294482
50 INPUT "WHAT IS THE FREQUENCY INDEX NUMBER";TT
52 SM=0
53 LG=1
59 LPRINT "   L VALUE       ENERGY VALUE          ITERATION"
60 I=0
70 FOR J=0 TO (NN-1)
80 TL=ABS(J+TT)
90 AR=TL
100 GOSUB 250
110 QN=Q
120 IF J=0 THEN QP=QN:GOTO 170
125 TU=ABS(J-TT)
127 IF TU=0 THEN QP=1:GOTO 170
130 AR=TU
150 GOSUB 250
160 QP=Q
170 A(I)=((QP#QP)+(QN#QN)+(2#ABS(QP#QN)))/4
190 C(I)=F1#10#LOG(A(I))
200 IF A(I)>=XI THEN XI=A(I)
210 IF A(I)<=NI THEN NI=A(I)
215 SM=SM+ABS(A(I))
217 LPRINT "     ";J;"         ";A(I);"           ";I+1
220 I=I+1
230 NEXT J
234 MX=F1#10#LOG(XI)
236 MN=F1#10#LOG(NI)
240 GOTO 290
```

```
250 AR=(SIN(AR))/AR
260 Q=ABS(AR)
270 RETURN
275 REM HORIZONTAL GRAPHING MODULE
280 PRINT "MAXIMUM OF GRAPH =",MX," MINIMUM OF GRAPH =",MN
290 REM BEGINNING OF HORIZONTAL GRAPHING MODULE
300 REM MX,MN ARE THE ASSUMED MAXIMUM AND MINIMUM, RESPECTIVELY
310 REM NH IS THE NUMBER OF POINTS PLOTTED
320 SP=INT(124/NH)
330 RC=(MX-MN)/30
340 LPRINT CHR$(15)
350 LPRINT "0 DB    ";
360 FOR N=0 TO 29
370 QU=MX-(RC*N)
380 QL=QU-RC
390 IF N=29 THEN QL=-200
400 PL=0
410 LQ=0
420 OP=-1
430 IF N=0 THEN 450
431 IF N=3*(INT(N/3)) THEN 432:ELSE 442
432 DB=(-1)*INT(((RC*N)+.05)*10)/10
433 LPRINT DB;"DB";
434 IF DB)(-10) THEN LPRINT CHR$(32);
435 IF DB=INT(DB) THEN LQ=2:ELSE 450
442 FOR L=1 TO LQ
443 LPRINT CHR$(32);
444 NEXT L
450 FOR J=0 TO (NH-1)
470 IF C(J)<=QU AND C(J)>QL THEN PL=SP*J:ELSE 540
480 IF (PL-OP)=1 THEN 520
490 FOR K=0 TO (PL-OP-2)
500 LPRINT CHR$(32);
510 NEXT K
520 LPRINT "*";
530 OP=PL
540 NEXT J
550 LPRINT
560 NEXT N
570 FOR N=1 TO 5
580 LPRINT
590 NEXT N
600 LPRINT "RECTANGULAR WINDOWED EXPANSION                    SIGNAL FREQUENCY = ";TT
610 LPRINT "MAXIMUM VALUE = ";XI;"      MINIMUM VALUE = ";NI
620 LPRINT "EACH COLORED BAND IS CHANGE IN DB OF ";RC*3
630 LPRINT "VERTICAL RESOLUTION IN DB IS ";RC
640 IF LG=1 THEN END
650 REM INFLUENCE MEASUREMENT MODULE
660 XI=-1.0E21
670 NI=1.0E21
680 LPRINT "     FREQUENCY        INFLUENCE"
690 FOR J=0 TO (NH-1)
700 C(J)=SQR(A(J)/SM)
710 IF C(J)>=XI THEN XI=C(J)
```

```
720 IF C(J)<=NI THEN NI=C(J)
730 LPRINT "     ";2#(T2-W+J);"              ";C(J)
740 NEXT J
750 LPRINT "TOTAL ENERGY IN THE COMPONENTS PLOTTED WAS ";SM
760 LG=1
770 FOR I=0 TO (NM-1)
780 C(I)=10#F18108LOG(C(I))
790 NEXT I
800 MX=F18108LOG(XI)
810 MN=F18108LOG(NI)
820 GOTO 320


20 REM FILON INTEGRATION OF (4-2-45)        ASSOCIATED WITH FIGURE - 4 -16
40 DIM A(90),C(90)
60 PI=3.14159265358979324
80 P2=2#PI
100 INPUT "HOW MANY POINTS TO BE PLOTTED";NQ
120 XM=-1.0E21
140 NM=1.0E21
160 F2=0.4342945
180 SM=0
260 FOR J=0 TO 90
280 C(J)=0
300 NEXT J
320 I=0
340 LPRINT "FREQUENCY          ENERGY VALUE"
350 REM FILON'S THETA = PI/16 (THERE ARE 32 INTERPOLATION POINTS PER CYCLE OF THE SINUSOID)
360 BE=.6717506078
380 GA=1.328200019
400 AA=3.345886673E-04
420 FOR Q=0 TO (NQ-1)
422 TH=P2#Q
425 IF Q>0 THEN GOTO 435
430 C(I)=1.204793974
432 GOTO 1302
435 H=(1/(32#Q))
437 NI=INT(24#Q)
440 FOR FI=0 TO I
560 AR=-0.75
580 R1=0
600 R0=0
620 FOR N=1 TO NI
640 AR=AR+H
660 IF FI=0 THEN GOSUB 1120:ELSE GOSUB 1240
680 R1=R1+Z
700 AR=AR+H
720 IF FI=0 THEN GOSUB 1120:ELSE GOSUB 1240
740 R0=R0+Z
760 NEXT N
780 R0=R0-(Z/2)
800 AR=-0.75
820 IF FI=0 THEN GOSUB 1120:ELSE GOSUB 1240
```

```
840 RO=RO+(Z/2)
860 AR=-0.75
880 IF F1=0 THEN GOSUB 1240:ELSE GOSUB 1120
900 Y=Z
920 AR=0.75
940 IF F1=0 THEN GOTO 960
950 GOSUB 1120
955 AO=AA!(Y-Z)
958 GOTO 980
960 GOSUB 1240
970 AO=AA!(Z-Y)
975 C(I)=((RO!BE)+(R1!GA)+AO)!H
976 GOTO 1300
980 C(I)=((((RO!BE)+(R1!GA)+AO)!H)[2)+((C(I))[2)
1100 GOTO 1300
1120 GOSUB 1180
1140 Z=Z1!COS(TH!AR)
1160 RETURN
1180 IF AR>0.75 THEN AR=0.75
1200 Z1=SQR(1-(ABS(AR+0.25)))
1220 RETURN
1240 GOSUB 1180
1260 Z=Z1!SIN(TH!AR)
1280 RETURN
1300 NEXT F1
1302 C(I)=C(I)/2
1304 IF C(I)>=XN THEN XN=C(I)
1306 IF C(I)<=NN THEN NN=C(I)
1308 LPRINT 28Q;"                    ";C(I)
1320 SN=SN+C(I)
1340 I=I+1
1360 NEXT Q
1380 FOR I=0 TO (NQ-1)
1400 A(I)=10!F2!LOG(C(I))
1420 NEXT I
1440 MX=10!F2!LOG(XN)
1460 MN=10!F2!LOG(NN)
1480 REM BEGINNING OF THE HORIZONTAL GRAPHING MODULE
1485 LPRINT CHR$(15)
1487 LPRINT
1488 LPRINT
1490 LPRINT"                    ENERGY -  SQRD MAGNITUDE OF C SUB K,L"
1500 SP=INT(90/NQ)
1520 RC=(MX-MN)/30
1560 LPRINT "                    0 DB    ";
1580 FOR N=0 TO 29
1590 IF N>0 THEN LPRINT "                    ";
1600 QU=MX-(RC!N)
1620 QL=QU-RC
1640 IF N=29 THEN QL=-200
1660 PL=0
1680 LQ=7
1700 QP=-1
```

```
1720 IF N=0 THEN 1900
1740 IF N=3*(INT(N/3)) THEN 1760:ELSE 1750
1750 LPRINT "I";
1755 GOTO 1840
1760 BB=(-1)*INT((10*M)+.05)*10)/10
1780 LPRINT BB;"DB";
1800 IF BB>(-10) THEN LPRINT CHR$(32);
1820 IF BB=INT(BB) THEN LB=2:ELSE 1900
1840 FOR L=1 TO LB
1860 LPRINT CHR$(32);
1880 NEXT L
1900 FOR J=0 TO (NQ-1)
1920 IF A(J)<=QU AND A(J)>QL THEN PL=SP*J:ELSE 2060
1940 IF (PL-OP)=1 THEN 2020
1960 FOR K=0 TO (PL-OP-2)
1980 LPRINT CHR$(32);
2000 NEXT K
2020 LPRINT "*";
2040 OP=PL
2060 NEXT J
2080 LPRINT
2100 NEXT N
2105 LPRINT "                    I     I";
2107 FOR J=1 TO NQ-1
2109 FOR K=1 TO SP-1
2111 LPRINT CHR$(32);
2113 NEXT K
2115 LPRINT "I";
2117 NEXT J
2120 FOR K=1 TO 5
2140 LPRINT
2160 NEXT K
2180 LPRINT "  BARTLETT WINDOWED EXPANSION FOR EQUATION (4-2-45)"
2200 LPRINT "  MAXIMUM VALUE = ";XM;"    MINIMUM VALUE = ";MN
2220 LPRINT "  EACH SHADED HORIZONTAL BAR HAS WIDTH IN DB OF ";RC3;"  LOWEST FREQUENCY = 0"
2240 LPRINT "  VERTICAL RESOLUTION IN DB IS ";RC;"    HIGHEST FREQUENCY = ";2*(NQ-1)
2260 LPRINT "  TOTAL ENERGY IN THE COMPONENTS PLOTTED WAS ";SM
2280 END
```

ASSOCIATED WITH FIGURES 4-45, 4-46, 4-49, AND 4-50

```
20 REM TWO SINUSOIDS IN THE SAME SUBINTERVAL - RECTANGULAR WINDOWED EXPANSION
40 DIM A(90),C(90)
60 PI=3.14159265358979324
80 P2=2*PI
100 INPUT "HOW MANY POINTS TO BE PLOTTED";NQ
110 N2=INT(NQ/2)
```

```
120 XM=-1.0E21
140 MM=1.0E21
160 F2=0.4342945
180 SM=0
190 INPUT"WHAT IS THE FREQUENCY OF THE 1ST SINE";F0
200 INPUT"WHAT IS THE FREQUENCY OFFSET OF THE 2ND SINE";U0
220 INPUT"RATIO OF 2ND SINE AMPLITUDE TO 1ST SINE AMPLITUDE";K0
240 BI=INT((F0-(U0/2)))
250 S0=(F0-U0)
260 FOR J=0 TO 90
280 C(J)=0
300 NEXT J
320 I=0
340 LPRINT "FREQUENCY          ENERGY VALUE"
420 FOR Q=(BI-N2) TO (BI+N2-1)
440 AR=Q+F0
460 GOSUB 1040
480 R=Z
500 AR=ABS(Q-F0)
510 GOSUB 1040
520 R=R+Z
540 AR=Q+S0
560 GOSUB 1040
580 R=R+(K0*Z)
600 AR=ABS(Q-S0)
620 GOSUB 1040
640 R=R+(K0*Z)
660 C(I)=(R*R)/4
740 IF C(I)>=XM THEN XM=C(I)
760 IF C(I)<=MM THEN MM=C(I)
780 LPRINT Q;"                 ";C(I)
785 I=I+1
790 NEXT Q
800 GOTO 1380
1040 IF AR<>0 THEN GOTO 1100
1060 Z=1
1080 GOTO 1200
1100 AR=AR*PI
1120 Z=(SIN(AR))/AR
1200 RETURN
1380 FOR I=0 TO (N0-1)
1400 A(I)=10*F2*LOG(C(I))
1420 NEXT I
1440 MX=10*F2*LOG(XM)
1460 MM=10*F2*LOG(MM)
1480 REM BEGINNING OF THE HORIZONTAL GRAPHING MODULE
1490 LPRINT "                  ENERGY - DOWN MAGNITUDE OF C SUB K,L"
1500 SP=INT(90/N0)
1520 RC=(MX-MM)/30
1540 LPRINT CHR$(15)
1560 LPRINT "                  0 DB    ";
1580 FOR N=0 TO 29
1590 IF N>0 THEN LPRINT "                    ";
```

```
1600 OU=MX-(RC$N)
1620 OL=OU-RC
1640 IF N=29 THEN OL=-200
1660 PL=0
1680 LQ=7
1700 OP=-1
1720 IF N=0 THEN 1900
1740 IF N=3$(INT(N/3)) THEN 1760:ELSE 1750
1750 LPRINT "I";
1755 GOTO 1840
1760 DB=(-1)$INT(((RC$N)+.05)$10)/10
1780 LPRINT DB;"DB";
1800 IF DB>(-10) THEN LPRINT CHR$(32);
1820 IF DB=INT(DB) THEN LQ=2:ELSE 1900
1840 FOR L=1 TO LQ
1860 LPRINT CHR$(32);
1880 NEXT L
1900 FOR J=0 TO (NQ-1)
1920 IF A(J)<=OU AND A(J)>OL THEN PL=SP$J:ELSE 2060
1940 IF (PL-OP)=1 THEN 2020
1960 FOR K=0 TO (PL-OP-2)
1980 LPRINT CHR$(32);
2000 NEXT K
2020 LPRINT "$";
2040 OP=PL
2060 NEXT J
2080 LPRINT
2100 NEXT N
2105 LPRINT "                    I      I";
2107 FOR J=1 TO NQ-1
2109 FOR K=1 TO SP-1
2111 LPRINT CHR$(32);
2113 NEXT K
2115 LPRINT "I";
2117 NEXT J
2120 FOR K=1 TO 5
2140 LPRINT
2160 NEXT K
2180 LPRINT "  RECTANGULAR WINDOWED EXPANSION FOR TWO SINUSOIDS"
2200 LPRINT "  MAXIMUM VALUE = ";XM;"     MINIMUM VALUE = ";MM
2220 LPRINT "  EACH SHADED HORIZONTAL BAR HAS WIDTH IN DB OF ";RC$3;"      LOWEST FREQUENCY = ";DI-N2
2240 LPRINT "  VERTICAL RESOLUTION IN DB IS ";RC;"                HIGHEST FREQUENCY = ";DI+N2-1
2260 LPRINT "  SINUSOIDAL FREQUENCIES WERE ";F0;"/T     AND ";(F0-U0);"/T"
2270 LPRINT "  THE RATIO OF AMPLITUDE OF THE ";(F0-U0);"/T HZ SINE TO THE ";F0;"/T HZ SINE IS ";K0
2275 LPRINT "  TOTAL ENERGY IN THE COMPONENTS PLOTTED WAS ";SM
2280 END
```

```
20 REM TWO SINUSOIDS IN SAME DATA WINDOW
40 DIM A(90),C(90)
60 PI=3.14159265358979324
80 P2=2$PI
```

ASSOCIATED WITH FIGURES 4-41, 4-42, 4-43, 4-44, 4-47, AND 4-48

```
100 INPUT "HOW MANY POINTS TO BE PLOTTED";NO
110 N2=INT(NO/2)
120 XN=-1.0E21
140 NN=1.0E21
160 F2=0.4342945
180 SN=0
190 INPUT"WHAT IS THE FREQUENCY OF THE 1ST SINE";F0
200 INPUT"WHAT IS THE FREQUENCY OFFSET OF THE 2ND SINE";U0
220 INPUT"RATIO OF 2ND SINE AMPLITUDE TO 1ST SINE AMPLITUDE";K0
240 DI=INT((F0-(U0/2))/2)
250 S0=(F0-U0)
260 FOR J=0 TO 90
280 C(J)=0
300 NEXT J
320 I=0
340 LPRINT "FREQUENCY          ENERGY VALUE"
360 BE=0.6863352186
380 GA=1.312884582
420 FOR Q=(DI-N2) TO (DI+N2-1)
424 T1=PI*((2*Q)+F0)
426 T2=PI*((2*Q)+S0)
428 T3=PI*((2*Q)-F0)
430 T4=PI*((2*Q)-S0)
440 A0=B*(ABS((2*Q)+F0))
445 H=1/A0
450 N1=A0/2
460 FOR F1=0 TO 1
580 AR=0
600 R1=0
620 R0=0
640 FOR N=1 TO N1
660 AR=AR+H
680 IF F1=0 THEN GOSUB 1040:ELSE GOSUB 1160
700 R1=R1+Z
720 AR=AR+H
740 IF F1=0 THEN GOSUB 1040:ELSE GOSUB 1160
760 R0=R0+Z
780 NEXT N
800 R0=R0-(Z/2)
820 AR=0
840 IF F1=0 THEN GOSUB 1040:ELSE GOSUB 1160
860 R0=R0+(Z/2)
1000 C(I)=(((R0*BE)+(R1*GA))*H)+C(I)
1020 GOTO 1220
1040 GOSUB 1100
1060 Z=Z1*((COS(T1*AR))+(K0*(COS(T2*AR))))
1080 RETURN
1100 IF AR>1 THEN AR=1
1120 Z1=SQR(1-(ABS(AR)))
1140 RETURN
1160 GOSUB 1100
1180 Z=Z1*((COS(T3*AR))+(K0*(COS(T4*AR))))
1200 RETURN
```

```
1220 NEXT F1
1240 C(I)=((C(I))[2)/2
1260 IF C(I)>=XM THEN XM=C(I)
1280 IF C(I)<=MM THEN MM=C(I)
1300 LPRINT 28Q;"              ";C(I)
1320 SM=SM+C(I)
1340 I=I+1
1360 NEXT Q
1380 FOR I=0 TO (NQ-1)
1400 A(I)=10@F28LOG(C(I))
1420 NEXT I
1440 MX=10@F28LOG(XM)
1460 MM=10@F28LOG(MM)
1480 REM BEGINNING OF THE HORIZONTAL GRAPHING MODULE
1490 LPRINT "                    ENERGY - SQRD MAGNITUDE OF C SUB K,L"
1500 SP=INT(90/NQ)
1520 RC=(MX-MM)/30
1540 LPRINT CHR$(15)
1560 LPRINT "                    0 DB    ";
1580 FOR N=0 TO 29
1590 IF N>0 THEN LPRINT "                    ";
1600 QU=MX-(RC@N)
1620 QL=QU-RC
1640 IF N=29 THEN QL=-200
1660 PL=0
1680 LQ=7
1700 OP=-1
1720 IF N=0 THEN 1900
1740 IF N=3@(INT(N/3)) THEN 1760;ELSE 1750
1750 LPRINT "I";
1755 GOTO 1840
1760 DB=(-1)@INT(((RC@N)+.05)@10)/10
1780 LPRINT DB;"DB";
1800 IF DB>(-10) THEN LPRINT CHR@(32);
1820 IF DB=INT(DB) THEN LQ=2;ELSE 1900
1840 FOR L=1 TO LQ
1860 LPRINT CHR$(32);
1880 NEXT L
1900 FOR J=0 TO (NQ-1)
1920 IF A(J)<=QU AND A(J)>QL THEN PL=SP@J;ELSE 2060
1940 IF (PL-OP)=1 THEN 2020
1960 FOR K=0 TO (PL-OP-2)
1980 LPRINT CHR$(32);
2000 NEXT K
2020 LPRINT "@";
2040 OP=PL
2060 NEXT J
2080 LPRINT
2100 NEXT N
2105 LPRINT "                    I      I";
2107 FOR J=1 TO NQ-1
2109 FOR K=1 TO SP-1
2111 LPRINT CHR@(32);
```

```
2113 NEXT K
2115 LPRINT "I";
2117 NEXT J
2120 FOR K=1 TO 5
2140 LPRINT
2160 NEXT K
2180 LPRINT "  BARTLETT WINDOWED EXPANSION FOR TWO SINUSOIDS"
2200 LPRINT "  MAXIMUM VALUE = ";IN;"     MINIMUM VALUE = ";MM
2220 LPRINT "  EACH SHADED HORIZONTAL BAR HAS WIDTH IN DB OF ";RC*3;"      LOWEST FREQUENCY = ";2*(DI-N2)
2240 LPRINT "  VERTICAL RESOLUTION IN DB IS ";RC;"                HIGHEST FREQUENCY = ";2*(DI+N2-1)
2260 LPRINT "  SINUSOIDAL FREQUENCIES WERE ";F0;"/T      AND ";(F0-U0);"/T"
2270 LPRINT "  THE RATIO OF AMPLITUDE OF THE ";(F0-U0);"/T HZ SINE TO THE ";F0;"/T HZ SINE IS ";K0
2275 LPRINT "  TOTAL ENERGY IN THE COMPONENTS PLOTTED WAS ";SM
2280 END
```

Associated with Fig. 4-33 through 4-36 inclusive

```
20 REM SINUSOIDAL FM TONE MODULATION WITH BARTLETT EXPANSION
40 REM FILON INTEGRATION METHOD USED
60 DIM A(123),C(123)
80 PI=3.14159265358979324
100 P8=PI/8
120 P2=2*PI
140 INPUT"HOW MANY POINTS TO BE PLOTTED";N0
160 IN=-1.0E21
180 MM=1.0E21
200 F2=0.4342945
220 SM=0
240 N2=INT(N0/2)
250 INPUT"WHAT IS THE TIME INDEX";Y
260 INPUT"WHAT IS THE MODULATION INDEX BETA";B9
280 INPUT"RATIO OF MODULATION TO CARRIER FREQUENCY";R9
300 INPUT"NUMBER OF CARRIER CYCLES IN THE DATA WINDOW";N9
320 N8=INT(N9/2)
340 FOR J=0 TO 123
360 C(J)=0
380 NEXT J
400 I=0
420 LPRINT "FREQUENCY          ENERGY VALUE"
430 REM FB=1+(BETA)*R
440 FB=1+(B9*R9)
445 BE=0.735220407
450 B0=1.252878002
455 REM F7=N8*(1+(BETA)*R)
460 F7=N9*FB
470 T2=((2*Y)-1)*P1*R9*N9
480 T4=((2*Y)-1)*P1*N9
490 S2=P1*R9*N9
520 FOR B=(N8-N2) TO (N8+N2-1)
530 W=(48*(ABS((2*B)+F7)))^(-1)
532 IF W<=0.25 THEN GOTO 538
534 W=0.25
536 N1=B
```

```
537 GOTO 539
538 N1=INT(4*(ABS((2*Q)+F7)))
539 PRINT "N1 = ";N1
540 FOR F1=0 TO 1
550 REM F1 CONTROLS THE REAL (=0) OR IMAGINARY (=1) INTEGRALS
551 REM J CONTROLS THE PLUS (=0) OR MINUS (=1) ARGUMENTS
560 FOR J=0 TO 1
580 T1=P2*(Q+(((-1)^J)*(N9/2)))
860 AR=-1
880 R1=0
900 R0=0
920 FOR N=1 TO N1
940 AR=AR+H
960 IF F1=0 THEN GOSUB 1320:ELSE GOSUB 1460
980 R1=R1+Z
1000 AR=AR+H
1020 IF F1=0 THEN GOSUB 1320:ELSE GOSUB 1460
1040 R0=R0+Z
1060 NEXT N
1080 R0=R0-(Z/2)
1100 AR=-1
1120 IF F1=0 THEN GOSUB 1320:ELSE GOSUB 1460
1140 R0=R0+(Z/2)
1160 IF F1=1 THEN 1200
1180 C(I)=(((R0*BE)+(R1*GO))*H)+C(I)
1190 GOTO 1540
1200 IF J=1 THEN 1260
1220 T3=C(I)*C(I)
1240 C(I)=0
1260 C(I)=(((R0*BE)+(R1*GO))*H)+C(I)
1280 IF J=1 THEN C(I)=(C(I)*C(I))+T3
1300 GOTO 1540
1320 GOSUB 1400
1330 REM T4=PHI SUB C AND T2=PHI SUB N
1340 Z2=((-1)^J)*((B9*SIN((S2*AR)+T2))+T4)
1360 Z=Z1*COS((T1*AR)+Z2)
1380 RETURN
1400 IF AR>1 THEN AR=1
1420 Z1=SQR(1-(ABS(AR)))
1440 RETURN
1460 GOSUB 1400
1480 Z2=((-1)^J)*((B9*SIN((S2*AR)+T2))+T4)
1500 Z=Z1*SIN((T1*AR)+Z2)
1520 RETURN
1540 NEXT J
1560 NEXT F1
1580 C(I)=C(I)/8
1600 IF C(I)>=XM THEN XM=C(I)
1620 IF C(I)<=NM THEN NM=C(I)
1640 LPRINT 2*Q;"                ";C(I)
1660 SM=SM+C(I)
1680 I=I+1
1700 NEXT Q
```

```
1720 FOR I=0 TO (NO-1)
1740 A(I)=10*F2*LOG(C(I))
1760 NEXT I
1780 MX=10*F2*LOG(XM)
1800 MN=10*F2*LOG(NM)
1820 REM BEGINNING OF THE HORIZONTAL GRAPHING MODULE
1840 SP=INT(124/NO)
1860 RC=(MX-MN)/30
1880 LPRINT CHR$(15)
1900 LPRINT "0 DB    ";
1920 FOR N=0 TO 29
1940 OU=MX-(RC*N)
1960 OL=OU-RC
1980 IF N=29 THEN OL=-200
2000 PL=0
2020 LO=6
2040 OP=-1
2060 IF N=0 THEN 2240
2080 IF N=3*(INT(N/3)) THEN 2100:ELSE 2180
2100 DB=(-1)*INT(((RC*N)+.05)*10)/10
2120 LPRINT DB;"DB";
2140 IF DB)(-10) THEN LPRINT CHR$(32);
2160 IF DB=INT(DB) THEN LO=2:ELSE 2240
2180 FOR L=1 TO LO
2200 LPRINT CHR$(32);
2220 NEXT L
2240 FOR J=0 TO (NO-1)
2260 IF A(J)<=OU AND A(J)>OL THEN PL=SP*J:ELSE 2400
2280 IF (PL-OP)=1 THEN 2360
2300 FOR K=0 TO (PL-OP-2)
2320 LPRINT CHR$(32);
2340 NEXT K
2360 LPRINT "*";
2380 OP=PL
2400 NEXT J
2420 LPRINT
2440 NEXT N
2460 FOR K=1 TO 5
2480 LPRINT
2500 NEXT K
2520 LPRINT "BARTLETT WINDOWED EXPANSION FOR SINUSOIDAL FM (TONE MODULATION)                TIME INDE
2540 LPRINT "MAXIMUM VALUE = ";XM;"    MINIMUM VALUE = ";NM
2560 LPRINT "EACH SHADED HORIZONTAL BAR HAS WIDTH IN DB OF ";RC*3;"          LOWEST FREQUENCY = ";2
2580 LPRINT "VERTICAL RESOLUTION IN DB IS ";RC;"                            HIGHEST FREQUENCY = ";2*
2605 LPRINT "MODULATION INDEX BETA = ";B9
2610 LPRINT "CARRIER FREQUENCY = ";N9;"/T";"          MODULATING FREQUENCY = ";N9*R9;"/T"
2615 LPRINT "TOTAL ENERGY IN THE COMPONENTS PLOTTED WAS ";SM
2620 END
```

ASSOCIATED WITH FIGURES 4-37 THROUGH 4-40

```
20 REM SINUSOIDAL FM TONE MODULATION WITH RECTANGULAR WINDOWED EXPANSION
40 REM FILON INTEGRATION METHOD USED
60 DIM A(123),C(123)
80 PI=3.14159265358979324
100 P8=PI/8
120 P2=2*PI
140 INPUT"HOW MANY POINTS TO BE PLOTTED";NO
160 XM=-1.0E21
180 NM=1.0E21
200 F2=0.4342945
220 SM=0
240 N2=INT(NO/2)
250 INPUT"WHAT IS THE TIME INDEX";Y
260 INPUT"WHAT IS THE MODULATION INDEX BETA";B9
280 INPUT"RATIO OF MODULATION TO CARRIER FREQUENCY";R9
300 INPUT"NUMBER OF CARRIER CYCLES IN THE DATA WINDOW";N9
320 N8=INT(N9/2)
340 FOR J=0 TO 123
360 C(J)=0
380 NEXT J
400 I=0
420 LPRINT "FREQUENCY          ENERGY VALUE"
430 REM F8=1+(BETA)*R
440 F8=1+(B9*R9)
442 REM FILON'S THETA IS PI/4 HERE
445 BE=0.735220407
450 GO=1.252878002
455 REM F7=N9*(1+(BETA)*R)
460 F7=N9*F8
470 T2=((2*Y)-1)*PI*R9*N9
480 T4=((2*Y)-1)*PI*N9
490 S2=PI*R9*N9
520 FOR Q=(N9-N2) TO (N9+N2-1)
530 H=(4*(ABS(Q+F7)))[(-1)
532 IF H<=0.25 THEN GOTO 538
534 H=0.25
536 N1=8
537 GOTO 539
538 N1=INT(4*(ABS(Q+F7)))
539 PRINT "N1 = ";N1
540 FOR F1=0 TO 1
550 REM F1 CONTROLS THE REAL (=0) OR IMAGINARY (=1) INTEGRALS
551 REM J CONTROLS THE PLUS (=0) OR MINUS (=1) ARGUMENTS
560 FOR J=0 TO 1
580 T1=PI*(Q+(((-1)[J)*N9))
860 AR=-1
880 R1=0
900 R0=0
920 FOR N=1 TO N1
940 AR=AR+H
```

```
960 IF F1=0 THEN GOSUB 1320:ELSE GOSUB 1460
980 R1=R1+Z
1000 AR=AR+H
1020 IF F1=0 THEN GOSUB 1320:ELSE GOSUB 1460
1040 R0=R0+Z
1060 NEXT N
1080 R0=R0-(Z/2)
1100 AR=-1
1120 IF F1=0 THEN GOSUB 1320:ELSE GOSUB 1460
1140 R0=R0+(Z/2)
1160 IF F1=1 THEN 1200
1180 C(I)=(((R0*BE)+(R1*GO))*H)+C(I)
1190 GOTO 1540
1200 IF J=1 THEN 1260
1220 T3=C(I)*C(I)
1240 C(I)=0
1260 C(I)=(((R0*BE)+(R1*GO))*H)+C(I)
1280 IF J=1 THEN C(I)=(C(I)*C(I))+T3
1300 GOTO 1540
1320 Z1=1
1330 REM T4=PHI SUB C AND T2=PHI SUB M
1340 Z2=((-1)[J)*((B9*SIN((S2*AR)+T2))+T4)
1360 Z=Z1*COS((T1*AR)+Z2)
1380 RETURN
1460 Z1=1
1480 Z2=((-1)[J)*((B9*SIN((S2*AR)+T2))+T4)
1500 Z=Z1*SIN((T1*AR)+Z2)
1520 RETURN
1540 NEXT J
1560 NEXT F1
1580 C(I)=C(I)/16
1600 IF C(I)>=XM THEN XM=C(I)
1620 IF C(I)<=NM THEN NM=C(I)
1640 LPRINT Q;"                 ";C(I)
1660 SM=SM+C(I)
1680 I=I+1
1700 NEXT Q
1720 FOR I=0 TO (NO-1)
1740 A(I)=10*F2*LOG(C(I))
1760 NEXT I
1780 MX=10*F2*LOG(XM)
1800 MN=10*F2*LOG(NM)
1820 REM BEGINNING OF THE HORIZONTAL GRAPHING MODULE
1840 SP=INT(124/NO)
1860 P=(MX-MN)/30
1880 LPRINT CHR$(15)
1900 LPRINT "0 DB    ";
1920 FOR N=0 TO 29
1940 GU=MX-(RC*N)
1960 GL=GU-RC
1980 IF N=29 THEN GL=-200
2000 PL=0
```

```
2020 LQ=8
2040 OP=-1
2060 IF N=0 THEN 2240
2080 IF N=3*(INT(N/3)) THEN 2100:ELSE 2180
2100 DB=(-1)*INT(((RC*N)+.05)*10)/10
2120 LPRINT DB;"DB";
2140 IF DB)(-10) THEN LPRINT CHR$(32);
2160 IF DB=INT(DB) THEN LQ=2:ELSE 2240
2180 FOR L=1 TO LQ
2200 LPRINT CHR$(32);
2220 NEXT L
2240 FOR J=0 TO (N0-1)
2260 IF A(J)<=QU AND A(J)>QL THEN PL=SP*J:ELSE 2400
2280 IF (PL-OP)=1 THEN 2360
2300 FOR K=0 TO (PL-OP-2)
2320 LPRINT CHR$(32);
2340 NEXT K
2360 LPRINT "*";
2380 OP=PL
2400 NEXT J
2420 LPRINT
2440 NEXT N
2460 FOR K=1 TO 5
2480 LPRINT
2500 NEXT K
2520 LPRINT "RECTANGULAR WINDOWED EXPANSION FOR SINUSOIDAL FN (TONE MODULATION)              TIME INDEX
2540 LPRINT "MAXIMUM VALUE = ";XM;"     MINIMUM VALUE = ";NM
2560 LPRINT "EACH SHADED HORIZONTAL BAR HAS WIDTH IN DB OF ";RC*3;"          LOWEST FREQUENCY = ";(N9
2580 LPRINT "VERTICAL RESOLUTION IN DB IS ";RC;"                            HIGHEST FREQUENCY = ";(N9+
2605 LPRINT "MODULATION INDEX BETA = ";B9
2610 LPRINT "CARRIER FREQUENCY = ";N9;"/T";"          MODULATING FREQUENCY = ";N9*R9;"/T"
2615 LPRINT "TOTAL ENERGY IN THE COMPONENTS PLOTTED WAS ";SM
2620 END
```

References

[1] Gabor, D., "Theory of Communication," Journal of the Institute for Electrical Engineers, pp. 429-457, November, 1946.

[2] Bastiaans, M., "Gabor's Expansion of a Signal into Gaussian Elementary Signals," Proceedings of the IEEE, Vol. 68, April 1980, pp. 538-539.

[3] Lerner, R., "Representation of Signals," Chapter 10 in Lectures on Communication System Theory, E. Baghdady, ed., McGraw-Hill, New York, 1961.

[4] Page, C.H., "Instantaneous Power Spectra," Journal of Applied Physics, Vol. 23, January 1952, pp. 103-106.

[5] Levin, M.J., "Instantaneous Spectra and Ambiguity Functions," IEEE Transactions on Information Theory, Vol. IT-10, January 1964, pp. 95-97.

[6] Rihaczek, A.W., "Signal Energy Distribution in Time and Frequency," IEEE Transactions on Information Theory, Vol. IT-14, May 1968, pp. 369-374.

[7] Claasen, T.A.C.M., and Mecklenbräuker, W.F.G., "The Wigner Distribution--A Tool for Time-Frequency Signal Analysis, Part I: Continuous-Time Signals," Philips Journal of Research, Vol. 35 No. 3, 1980, pp. 217-250.

[8] ------, "The Wigner Distrubution--A Tool for Time-Frequency Signal Analysis, Part II: Discrete-Time Signals," Philips Journal of Research, Vol. 35, Nos. 4/5, 1980, pp. 276-300.

[9] ------, "The Wigner Distribution--A Tool for Time-Frequency Signal Analysis, Part III: Relations with Other Time-Frequency Signal Trasnformations," Philips Journal of Research, Vol. 35, No. 6, 1980, pp. 372-389.

[10] deBriujn, N.G., "A Theory of Generalized Functions, with Applications to Wigner Distribution and Weyl Correspondence," Nieuw Archief voor Wiskunde (3), Vol. XXI, 1973, pp. 205-280.

[11] Kincaid, T.G., "Dynamic Bandwidth," Technical Report to Office of Naval Research, Contract No. N00014-71-C-0229, General Electric Company, Automation and Control Laboratory, Schenectady, New York, October 1976.

[12] Harris, F.J., "On the Use of Windows for Harmonic Analysis with the Discrete Fourier Transform," Proceedings of the IEEE, Vol. 66, January 1978, pp. 51-83.

[13] Feller, W., An Introduction to Probability Theory and Its Applications, Volume I, John Wiley, New York, 1957.

[14] Kaplan, W., Operational Methods for Linear Systems, Addison-Wesley, Reading, Meassachusetts, 1962, pp. 190-191.

[15] Protter, M.H. and Morrey, C.B., Jr., Modern Mathematical Analysis, Addison-Wesley, Reading Massachusetts, 1964, p. 438.

[16] Davis, Philips J., Interpolation and Approximation, Dover, New York, 1975.

[17] Abramowitz, M., and Stegun, I., Handbook of Mathematical Functions with Formulas, Graphs, and Mathematical Tables, National Bureau of Standards, Applied Mathematics Series 55, Washington, D.C., 1964.

[18] Tranter, C.J., Integral Transforms in Mathematical Physics, John Wiley, New York, 1951, pp. 67-72.

BIOGRAPHICAL DATA

Name:	James Edward Roach
Date and Place of Birth:	22 November 1946
	Rochester, New York
Elementary Schools:	St. Thomas Acquinas School,
	Buffalo, New York
High School:	Canisius High School,
	Buffalo, New York
College:	Canisius College,
	Buffalo, New York,
	B.S., Physics, 1968
Graduate Work:	Syracuse University
	Syracuse, New York,
	M.S., Electrical Engineering, 1972

MISSION
of
Rome Air Development Center

RADC plans and executes research, development, test and selected acquisition programs in support of Command, Control Communications and Intelligence (C^3I) activities. Technical and engineering support within areas of technical competence is provided to ESD Program Offices (POs) and other ESD elements. The principal technical mission areas are communications, electromagnetic guidance and control, surveillance of ground and aerospace objects, intelligence data collection and handling, information system technology, ionospheric propagation, solid state sciences, microwave physics and electronic reliability, maintainability and compatibility.

END

FILMED

5-84

DTIC